

“They say that the definition of madness is doing the same thing over and over again and expecting different results.”

University of Alberta

UNIAXIAL COMPACTION OF PHARMACEUTICAL POWDERS

by

Abouzar Shamsaddini Shahrabak

A thesis submitted to the Faculty of Graduate Studies and Research in
partial fulfillment of the requirements for the degree of

Master of Science

Department of Mechanical Engineering

©Abouzar Shamsaddini Shahrabak
Spring 2013
Edmonton, Alberta

Permission is hereby granted to the University of Alberta Libraries to reproduce single copies of this thesis and to lend or sell such copies for private, scholarly or scientific research purposes only. Where the thesis is converted to, or otherwise made available in digital form, the University of Alberta will advise potential users of the thesis of these terms.

The author reserves all other publication and other rights in association with the copyright in the thesis and, except as herein before provided, neither the thesis nor any substantial portion thereof may be printed or otherwise reproduced in any material form whatsoever without the author's prior written permission.

Abstract

A thorough understanding and precise characterization of powdered excipients and drugs are of great importance to enhance the quality of the final product. Powder compression is a common method to evaluate their properties and behavior. It is essential to understand the elastic, viscoelastic and plastic response of powder to the compression force. A new instrument, the University of Alberta Density Tester, was developed for this purpose. It can be used to measure the *Compressed Bulk Density* of pharmaceutical powders along with other parameters. A measurement method using low-pressure compaction was implemented. This type of powder characterization method has several advantages. A very small amount of sample is needed which is important when dealing with expensive or scarce samples. Secondly, poorly compactable powders can be analyzed accurately. The importance of the former is evident as powder characterization using traditional methods are restricted by the high amount of sample required. The latter allows analysis of respirable samples where interparticle forces rather than inertial forces become dominant for the compaction behavior. For the same reasons the applicability of the conventional methods like tapped density measurements is questionable. Another advantage of this technique is that the developed instrument is very sensitive and shows significant response to any changes in the testing conditions even if the changes are very slight. Experimental results were fitted to two empirical models, the Heckel and Kawakita models, to evaluate mechanistic behavior of the powders under different levels of compaction. In this study, a novel mod-

ulated compaction technique was developed that helps in the interpretation of different compaction stages. *Modulated Compression Profiles* differentiate between elastic and plastic behavior of powders under compression which may lead to further development or refinement of compression models that can provide a better understanding of the different compression mechanisms.

Acknowledgements

This thesis has greatly benefitted from the efforts and support of many people who have been instrumental throughout my work. I would like to highlight the following acknowledgment in particular;

First and foremost, I owe my sincerest gratitude to my advisor, Dr. Reinhard Vehring, for his friendship, advice, intellectual guidance, scientific integrity, commitment to learning, steadfast support and overall positive influence. I am grateful to Dr. Vehring for his open door policy and answers to my myriad of questions.

Special thanks go out to Dr. Jason Olfert and Dr. Raimar Löbenberg for their time and encouragement and serving on my defence committee and providing valuable suggestion to the completion of this work.

Much appreciation is extended to Dr. Warren Finlay for his support and allowing me to access the facilities in his lab and whom I have had the wonderful opportunity of learning from and who have consistently demonstrated such high commitment to the field.

Thanks go out to the faculties, staffs and students that I had a pleasure of working with at the University of Alberta. Special thanks go out to the machine shop technical staffs, IT technicians and an electronic technologist of the department of Mechanical Engineering, specially Daniel Mooney, Roger Marchand, David Dubyc and Rick Conrad for their suggestion, assistance and excellent work in building the experimental setup.

I also wish to take this opportunity to thank all of my colleagues, past and present. It has been my immense pleasure to have worked along with some of the finest research students in our group. In particular, Mohammed Boraey,

James Ivey, Susan Hoe, Sadaf Matinkhoo, Paul Finlay, Mehdi Azhdarzadeh. Surely there are many others whose presence and friendship helped me retain some semblance of sane and a balanced life. I am thanking them all for their friendship and conversation, scientific or otherwise.

Finally I would like to thank the people who are not directly related to my research but I would have never taken upon this journey without their involvement. I owe immeasurable amount of gratitude to my dad for always believing in me, supporting me at every junction of life, being a wonderful advisor for my life and being a living example of dedication and hard work. I am thankful for my mom for dedicating her life for my well being and being the epitome of perfection. I am thankful for my siblings for always being there for me and being responsible for all good things in my life. I dedicate this thesis to you and the rest of the family for your love, and endless encouragement and support with no reservation.

Contents

1	Introduction	1
2	Powders and Their Characteristics	4
2.1	Introduction	4
2.2	Powders, Definitions	4
2.3	Powder Behaviour	5
2.4	Fluidization	6
2.4.1	Geldart Classification	7
2.5	Flowability	9
2.5.1	Angle of Repose	10
2.5.2	Flow through an Orifice	11
2.5.3	Shear Cells	12
3	The Compaction of Pharmaceutical Powders	13
3.1	Introduction	13
3.2	Interparticulate Bonding	17
3.2.1	Solid Bridges	19
3.2.2	Intermolecular Forces, Distance Attraction forces	20
3.2.3	Mechanical Interlocking	23
3.3	Consolidation	24
3.3.1	Decompression	26
3.4	Elasticity and Plasticity	26
3.5	Material Compaction Behaviour	30
3.6	ParticleDensity	30
3.6.1	True Density	30
3.6.2	Apparent Particle Density	31
3.6.3	Aerodynamic/Hydrodynamic Particle Density	31
3.6.4	Bulk Density	31
3.6.5	Compressed Bulk Density	33

4	Uniaxial Powder Compaction	35
4.1	Introduction	35
4.2	Porosity of Packed Bed	37
4.3	Porosity-Pressure Function in Compaction	38
4.4	Porosity-Pressure Equations, Compaction Data Analysis . . .	38
4.4.1	Heckel Equation	40
4.4.2	Kawakita Equation	44
4.5	On the Hausner Ratio and Compressibility Index	47
5	Experimentation	49
5.1	Introduction	49
5.2	Experimental Consideration	50
5.3	Instrumentation	50
5.4	UAlberta Density Tester	51
5.5	Instrumentation	52
5.6	Data Acquisition Using NI LabVIEW	59
5.7	Measurement	60
5.8	Errors and Uncertainties	62
5.8.1	Sources of Error	63
5.8.2	Error Propagation	64
6	Low-Pressure Compaction, Results and Discussion	70
6.1	Introduction	70
6.2	Applicability of Tapped Density Measurement	70
6.3	Method	71
6.4	Materials	74
6.5	Compaction Data Analysis	77
6.6	Compact Porosity	79
6.7	Moisture Content Influences on CBD	81
6.8	Data Fitting	83
6.8.1	Heckel's Profile	84
6.8.2	Kawakita's profile	86
6.9	Hausner Ratio and Compressibility Index	88
6.10	Compressibility and Compaction Factor	90
6.11	Compression Speed	92
6.12	Modulated Compression Profile	94
7	Conclusion	105

A	SolidWorks Drawings	117
A.1	Tolerances and Fits	117
B	LabVIEW Code	164
C	Instrument Implementation, Code Compilation and Control	188
C.1	Sample Preparation	188
C.2	Cavity Position Calibration	189
C.3	Instrument Startup	190
C.4	Troubleshooting and Important Remarks	191
C.4.1	Restoring Loadcell Calibration Data	192
C.5	Code Compilation	193
C.5.1	Compressed Bulk Density Measurement	193
C.6	Actuator's Harmonic Advancement, Modulated Compaction Profile	195
C.6.1	Sawtooth Mode	195
C.6.2	Triangle Wave Mode	197
C.6.3	Sinusoidal Mode	198
C.6.4	Step Mode	200
C.7	Assembling and Disassembling	200
D	List of the Compression Models	202
E	Scanning Electron Microscopy (SEM) Images	204

List of Tables

2.1	Flow properties and the corresponding angle of repose	11
3.1	Density definitions	34
4.1	Scale of flowability	47
5.1	Uncertainties associated with systematic errors involved in UAl- berta density tester	64
5.2	Uncertainties associated with random errors involved in UAl- berta density tester	65
6.1	Materials used for compression test	75
6.2	Hausner Ratio and Carr Index for different samples	89
6.3	Different wave functions of actuator movement	96
A.1	Tollerances and fits in UAlberta density tester instrument . .	118
D.1	Various equations describing the compaction of powders, V_0 =initial apparent volume of powder, V = volume of powder under the applied pressure P , V_∞ =net volume of powder, $c_1 \dots c_{37}$ = con- stants, E_0 =initial porosity, P_m = mean pressure, V_1 = pressure at 1 MPa	203

List of Figures

2.1	Characteristics of powder behavior in various fluidization regimes	7
2.2	Left: Geldart powder classification diagram, Right: Simplified model of forces acting on particle in bed of particulate material with gas flowing upward	9
2.3	Schematic diagram of (a) angle of repose and (b) segregation of powder during angle of repose measurement	10
3.1	Tablet formation in tablet machine (schematic)	14
3.2	Mechanism of Compaction	16
3.3	Events occurring during the compression process	25
3.4	Schematic of reversible and irreversible compression	27
3.5	Compressional cycle of an ideal elastic body	28
3.6	Compressed cycle of a body with constant yield stress in shear	29
4.1	Schematic of the force being transmitted through powder bed	36
4.2	Schematic representation of the compaction behavior according to the Heckel equation	41
4.3	Schematic of Heckel compaction profile	42
4.4	Different types of compression profile distinguished by the Heckle equation	43
4.5	Graphical representation of Kawakita's equation	46
4.6	A schematic description of a typical compression pressure curve and interpretation of the Kawakita parameters	46
5.1	Schematic of the UAlberta Density Tester	53
5.2	PI Actuator and Step Motor	53
5.3	FuTeK loadcell and USB Interface	54
5.4	Sample pan	54
5.5	Thorlabs Translation Stages and Base plate	55
5.6	Apparatus front view photo	56

5.7	Apparatus side view photo	57
5.8	Apparatus back view photo	58
5.9	LabVIEW front panel 1	59
5.10	LabVIEW front panel 2	60
5.11	LabVIEW output, measurement data	61
5.12	Distinction between systematic and random errors	63
6.1	Compressed bulk density profile for Crystalline Leucine	73
6.2	Density profile for some samples, open Circle=Crystalline Trehalose; closed square= Crystalline L-Leucine; close triangle= Dextromethorphan; open triangle=flowable L-Leucine	78
6.3	Plots of Porosity versus compaction pressure	79
6.4	Effect of ambient humidity on spray-dried Leucine (open symbols) and crystalline Leucine (closed symbols), (red=dry condition, blue=humid condition)	82
6.5	Effect of humidity on CBD for crystalline Trehalose (red=dry condition, blue=humid condition)	83
6.6	A schematic illustration of three different types of Heckel's profile	84
6.7	Heckel compression profile for four samples in the pressure range of 0-1 MPa	85
6.8	Plot of strain versus compression pressure for four different samples: line= compaction curve when C, Kawakita parameter, was determined at the poured pressure, dashed line = compaction curve when C, Kawakita parameter was determined at the initial volume recorded at the pressure of 5N	87
6.9	Sample history causes large variability at low pressure and wide range of HR and CI for the same powder	89
6.10	Compressibility of four different samples as a function of axial pressure, axis is in log scale for the left graph	90
6.11	Schematic of powder cohesivity	91
6.12	Compaction profiles at different compaction rate	93
6.13	Schematic of the modulated compression profile, harmonic (sinusoidal) and triangle wave	95
6.14	Modulated compression profile differentiating the elastic and plastic region of the powder bed, Triangular wave mode is used	97

6.15	Modulated compression and Heckel profiles for microcrystalline Cellulose representing three different regions in the compression mechanism	99
6.16	Modulated compression and Heckel profiles for flowable Leucine representing different regions in the compression mechanism	100
6.17	Modulated compression and Heckel profiles for crystalline Leucine representing different regions in the compression mechanism	101
6.18	Modulated compression and Heckel profiles for micronized Paracetamol representing different regions in the compression mechanism	102
6.19	Modulated compression and Heckel profiles for crystalline Trehalose representing different regions in the compression mechanism	103
E.1	SEM images of Microcrystalline Cellulose	204
E.2	SEM images of Dextromethorphan	205
E.3	SEM images of Ibuprofen	205
E.4	SEM images of Micronized Paracetamol	205
E.5	SEM images of Crystalline Leucine	206
E.6	SEM images of Crystalline Flowable Leucine	206
E.7	SEM images of NaCl	206
E.8	SEM images of Crystalline Trehalose	207
E.9	SEM images of Magnesium Stearate	207
E.10	SEM images of Talc	207
E.11	SEM images of Spray Dried L-leucine/Trehalose	208

Nomenclature

a	Distance between two particles
A_H	Hamaker constant,
b	Diameter of the base of the powder cone
C	Volumetric shrinkage
CI	Compressibility Index
D_p	Drag force
d_a	Aerodynamic diameter
d_f	Feret diameter
d	Particle diameter
D	Relative density
D_c	Diameter of the compact (tablet)
E	Powder porosity
E_0	Initial porosity of the powder bed
E_P	Porosity of the powder bed at pressure P
F_e	Electrostatic force
F_{VdW}	Van der Waals force
F_c	Capillary force
F_{DMT}	Derjaguin-Muller-Toporov pull of force
F_{JKR}	Johnson-Kendall-Roberts pull of force
F_U	Sum of the forces exerted on a powder column
F_L	Force exerted on the lower punch
F_D	Die-wall friction force
G_p	Gravitational force exerted on a particles
H_c	Compact height
h_w	Lifshitz-Van der Waals constant
h	height of the powder cone
HR	Hausner Ratio
K	Heckel's constant
m	mass of powder
P	Compaction Pressure
q_1	Electrostatic charge of the first particle
S	Yield stress
U	Gas velocity
Y	Yield pressure
V_0	Initial volume of the powder bed

V	Volume of the powder bed at pressure P
V_b	Initial bulk volume of the powder bed
V_t	Tapped volume of a powder bed
<i>Greek Symbols</i>	
ϵ_0	Vacuum permittivity
θ	Angle of repose
φ	Effective interparticle force
λ	Surface tension
γ	Surface energy
ν	Poisson ratio
τ	Radial force
σ	Axial force
μ	Coefficient of friction
ρ	density
δ	specific volume
ρ_T	Ture density
ρ_a	Apparent density
ρ_p	Particle density
ρ_b	Powder bulk density
ρ_A	Air density
ρ_0	Initial powder bulk density
ρ_P	Powder bulk density at pressure P
ρ_t	Tapped density

Chapter 1

Introduction

The solid form of pharmaceutical products is the preferred physical form in the pharmaceutical industry. For instance, it is used in the production of capsules, granules, and tablets. The solid form is also used in the form of powder for formulation into different dosage forms such as respiratory drugs. Due to many reasons such as, being cost effective in manufacturing drugs, storage convenience and providing various easy means of administering powders to the patients, this dosage form is very advantageous. The importance of this dosage form calls for efficient and reliable techniques for the manufacturing of such drugs. However manufacturing of these products is often accompanied by complexities such that the pharmaceutical industry needs to focus on understanding, monitoring and control of the manufacturing process to identify those issues, e.g., looking at the flowability of powders under test.

Various methods have been introduced to evaluate and predict the mechanical properties of samples. During manufacturing of the solid form, drugs and excipients are subjected to mechanical stresses, e.g. during discharging from a hopper, grinding, mixing, fluidization, compression, and coating. Therefore, it is of great importance for the manufacturers to understand the reaction of solids to mechanical stresses during processing. However, mechanical testing of small particles is not straightforward.

Scientist should have a thorough understanding of the physical and chemical properties of pharmaceutical ingredients to make rational formulation decisions. Density is one of the intrinsic properties for pharmaceutical materials that should be determined. Knowledge of density is required to determine the exact amount of binders, excipients or other ingredients needed to produce a

strong and intact tablet while still providing unique release characteristics for different purposes.

There are different types of density based on the way they are measured. Two main categories are present in this regard. The first is considering individual particles and the second describes the powder in bulk. The density of an individual particle as it is explained in chapter 3.6, due to its random shape and surface structure varies based on the measurement method used. The volume of the particle may contain internal and external pores, thus categorizes particle densities based on the volume included in the total volume. For instance the volume for true density measurement includes internal pores and pycnometry methods that are based on the Archimedes principle by using different displacing fluid is used.

Tapped density measurement is one of the common techniques used to determine the bulk density of powders. According the United States Pharmacopeia, tapped density is an indirect measurement of compressibility and flowability of powders. The specification about this technique is stated in both European and United States Pharmacopeia [2012, 2010]. Compressed bulk density testing is another technique to characterize powders that is simply conducted by the compression of a volume of powder that is confined within a die with a known volume.

Compression of powder has been a very useful approach in determining physical characteristics of a material. The compaction of pharmaceutical powders, which is described by the volume reduction of a powder bed when it is subjected to varying levels of mechanical force, consists of simultaneous processes of compression and consolidation, [Klevan et al., 2010]. According to Alderborn and Nystrom [1996], compression is the reduction in the volume of a powder bed due to application of stress or vibration while consolidation is the transformation of a powder into a coherent specimen of defined shape by compression. The relationship between these two processes has become a centre of attention in the pharmaceutical industry for different purposes. A variety of methods and techniques along with numerical methods have been published to better evaluate the functionality of powders. Among those, the assessment of the degree to which a powder consolidates as a function of pressure is common in pharmaceutical sciences as such success of robust formulation mainly relies

on better understanding of the properties of the powder components and their behavior to the applied pressure.

Compression test on powders are not limited to the measurement of compressed bulk density. The porosity of the powder bed undergoes significant changes during different phases of compression, such as particle rearrangement, and different strain hardening mechanisms. During compression these stages may overlap each other. This makes it difficult to point out distinct regions where only one compaction mechanism occurs. Various studies, Duberg and Nystrom [1986], Higuchi et al. [1953], Ramsey [1996] have investigated the changes in porosity and volume of the compact during compression. In addition to that, numerous empirical methods, Heckel [1961b], Sonnergaard [2001], Zhao et al. [2006], Kawakita and Tsutsumi [1965] were proposed to model the compaction of powders and attempted to correlate different stages of compression with the experimental results. Differentiating between elastic and plastic response of particulate material subjected to a compression force is important as it can help categorize powders based on their consolidation level, which may be influenced by different factors such as ambient humidity, particle size, compression rate and so on.

Tapped density is known to be very material consuming, which is a major drawback especially for expensive powders. Another disadvantage of this technique is its low resolution in determining the exact volume of the bulk. This provides the motivation to develop a more efficient and sensitive method such as the one presented in this thesis.

This thesis is organized as follows. Chapter 2 provides background information about powders and their characteristics. Chapter 3 presents a review of powder compaction and related topics followed in Chapter 4 by the discussion about the new technique in determining compression parameters and the relationship between compression, density and porosity. Chapter 5 and 6 cover the experimental technique, results and discussion.

Chapter 2

Powders and Their Characteristics

2.1 Introduction

Powders are important in industries dealing with food (corn starch), or pharmaceuticals (medicines in solid dosage form), etc. Their application has increased to the point that, about one half of all of chemical products and one third of all chemical raw materials are in the powder state [Nedderman, 1992, Rietema, 1991, Huang, 2009].

Powder handling is a series of steps that are necessary to transform raw materials into a desirable and applicable product form. These processes include, fluidization, mixing, separation, storage, transportation, agglomeration, compaction, etc. It is not within the scope of this thesis to address the full underlying knowledge about powders but there are some fundamental concepts in particle characterization that will be discussed here. The followings briefly review some of the important theories about powders and their properties correlating to powder behavior.

2.2 Powders, Definitions

Powders appear to be ill-defined substance that scientific literature doesn't always define it well. According to some literature, a powder, or granular material, or particulate matter can be defined as a collection of many small individual solid particles that is in close contact with each other [Nedderman, 1992, Rietema, 1991]. This definition seems to be inadequate. According to

some researchers, powders comprise discrete solid particles that do not fill the whole powder volume, the remaining interstitial spaces are filled with gas [Rietema et al., 1980, Puri, 2001]. Because of their two-phase nature the powder possesses a relatively lower density, called bulk density, than the individual particles [Rietema, 1991]. Even this definition of powder still is inadequate, as a criterion concerning the maximum particle size should also be given.

So, what exactly are powders? Based on the aforementioned definitions it is more accurate to integrate the interstitial gas into the definition of powder, or granular, or particulate materials.

Generally powder is a dispersed two-phase system consisting of a dispersed phase of solid particles of various diameters and gas as a continuous phase [Huang, 2009, Puri, 2001, Sayyar Roudsari, 2007]. However the continuous phase and the dispersed phase can be changed as the powder state changes [Huang, 2009]. The presence of gas within the system of dispersed solid makes it possible for powder to behave like a solid, a gas, or a liquid [Huang, 2009, Sayyar Roudsari, 2007, Rietema, 1984].

2.3 Powder Behaviour

The following are the three characteristics of powders [Huang, 2009, Sayyar Roudsari, 2007, Rietema, 1984]:

Powder is not a solid, although it has the capability to withstand some deformation when it is subjected to some pressure.

Powder is not a liquid, although it has the capability to flow under certain circumstances.

Powder is not a gas, although it has the capability to be compressed and expanded to some degree [Rietema, 1984].

Powders usually show different behavior in comparison to liquids, solids or gases [Rietema, 1991].

Even though powders have often been characterized by the nature of solid

particles based on their physical and chemical composition and their particle-size distribution, it is important to fully realize the interaction of the gas phase with the solid phase. Powder mostly cannot be treated as a single continuum [Rietema et al., 1980].

The interaction between the continuous and dispersed phase is also important, which is one of the main reasons that different powders show different behavior. If the gas possess a high viscosity or adsorption rate, the interaction between solid and gas phase would be stronger therefore powder will expand more. Consequently higher expansion is accompanied with improved flowability of the powder which can be characterized by lower apparent viscosity and lower yield values, thus, the higher the gas viscosity the lower the powder viscosity [Rietema, 1991].

There are two mechanisms that can control the behavior of powder;

- The interaction between particles in the dispersed phase such as friction and cohesion as a result of close contact between solid particles
- Another one is the effect of interstitial or surrounding gas properties on the mechanics of dry solids that is twofold; one hydrodynamic or aerodynamic interaction which is mainly controlled by dynamic viscosity of the gas and the elasticity of the solid state, and the other is a physico-chemical interaction via gas adsorption to the solid surface [Rietema et al., 1980]. The latter affects the resistance to breakage. Thus the properties of the suspended gas have to be taken into account, or controlled.

2.4 Fluidization

Fluidization at its simplest is powder bed expansion as a result of pressure drop due to fluid drag or in the other word, fluidization is the result of a balance between fluid dynamic forces on one hand and gravitational and interparticle forces from the other hand. When a powder bed is subjected to the upward gas flow, with increasing gas velocity, the drag force exerted by the passing fluid will balance the gravitational force applied on powders. Thus powders become less stressed and will suspend in fluidizing gas. The term fluidization is used because the powder in this situation behaves with some characteristics

of a fluid, e.g., it has horizontal surface in a tilted surface. The interaction

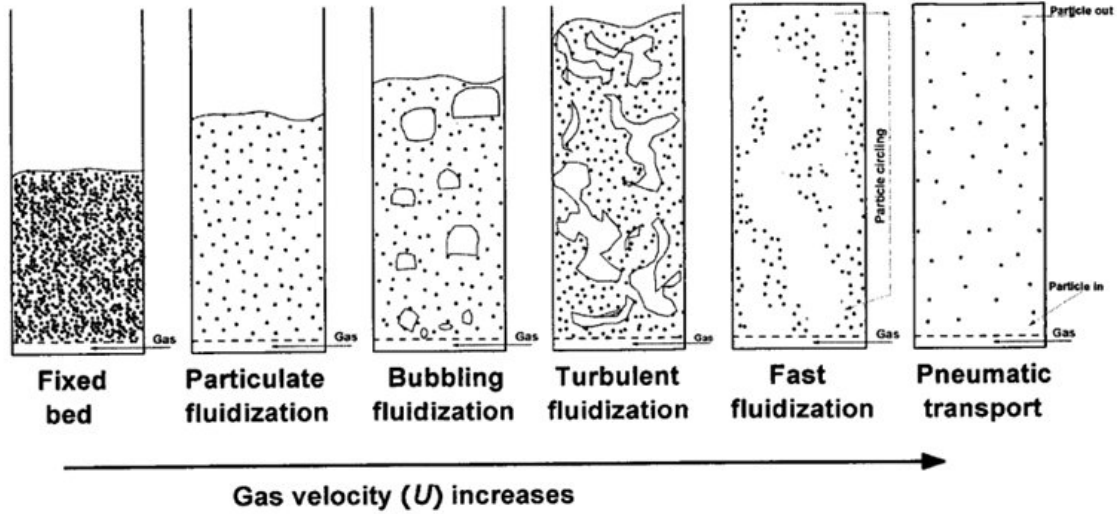


Figure 2.1: Characteristics of powder behavior in various fluidization regimes, [Huang, 2009]

of solid-gas phase is different for different powders and will be compromised by changing flowrate and leads the powder state to move from fixed bed to fluidization. Figure 2.1 shows the classification of powder bed when fluidized by different levels of flowrate.

Fluidization is considered as the preferred method when powders and the gas need to be brought into good contact so that results in extensive solid mixing and facilitates solid handling.

2.4.1 Geldart Classification

A comprehensive classification has been published by Geldart [1973] in order to describe the fluidization behavior of powders. Geldart classified gas-solid fluidization into four groups characterized by taking the two most important properties into account; density difference between the solid and fluidizing gas, and mean particle size.

Group A comprises powders with small mean sizes that are within the range of 25–40 μm to about 150–200 μm . This group is called aeratable powder, which can be fluidized well and experiences a dense phase expansion after minimum fluidization and prior to the commencement of bubbling. Powder

bed collapses very slowly when the supply gas interrupted. Group B are sand-like powders that are in the mean size ranges of 150–200 μm to about 700–900 μm . These powders easily reach the bubbling phase as the flowrate reaches the minimum fluidization velocity. In this group, bed collapses rapidly when the supply gas is cut off. Powders larger than group B are categorized in group D and they require gas with much higher velocities to be fluidized.

Group C powder or cohesive powders are the finest group of powder with the mean size smaller than 25 μm . The fluidization of this type of powder is extremely difficult and usually accompanied by the formation of channels within the powder bed through which the up-flowing gas passes without fluidizing the fine particles. The difficulty in fluidizing this group of powders is due to the cohesivity of the particles. Cohesive powder may be defined as a powder in which interparticle forces are greater than the aerodynamic drag that the fluid can exert on the particle [Huang, 2009, Geldart, 1973, Baerns, 1966, Antony et al., 2004].

In order to separate a particle from its surrounding and to suspend it in gas the following relation must be valid:

$$D_p = G_p + \psi \quad (2.1)$$

Where D_p , G_p and ψ are drag, gravitational and effective interparticle forces, respectively [Huang, 2009].

Left figure in Figure 2.2 shows the plot of particle classification based on mean particle size against the density difference of solid and fluid phase in a powder bed. Right figure is a schematic of forces that are applied on particles by the fluidizing fluid.

Powders in group C has been paid a great deal of attention in some industries such as the pharmaceutical industry due to its special characteristics. These powders have high contact areas that lead to a better quality final product. Generally, as the particle size decreases, its mechanical strength increases, and the underlying reason for this behavior can be correlated to the reduction in the probability of the presence of crack and defect in the crystal structure.

Consequently, particle size may also affect the volume reduction and compressibility of powders. With the same token, fragmentation of large particles

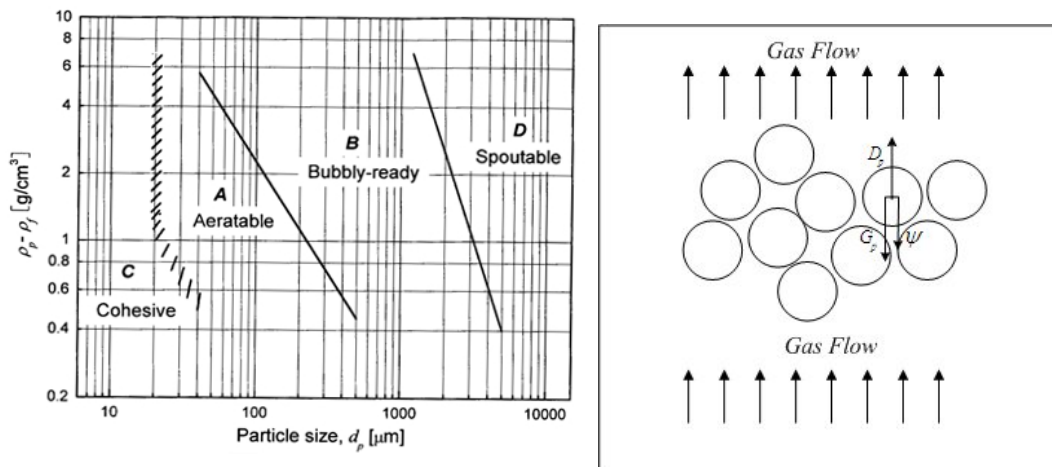


Figure 2.2: Left: Geldart powder classification diagram [Geldart, 1973], Right: Simplified model of forces acting on particle in bed of particulate material with gas flowing upward

that occurs at high compaction pressure during tableting, results in the formation of many smaller particles that helps in further filling of the voids between particles within the powder bed and consequently results in a large number of contact sites between particles at which strong bonds can be formed.

2.5 Flowability

Flowability is one of the parameters of pharmaceutical powders that is critical for the production of a pharmaceutical dosage form [Staniforth and Aulton, 2002]. Flowability of powder is the ability of powder to flow under certain conditions. However, this parameter is strongly affected by the physical properties of particles (such as shape, size, compressibility), the property of the bulk powder (such as size distribution, compaction) and processing environment (such as storage, handling, humidity). Flowability is also functionally dependent on the interparticle attraction [Alderborn and Nystrom, 1996, Li et al., 2004].

There are complexities and challenges in measuring such an abstract but very important characteristic as powder flowability. Thus, various empirical techniques and description methods have been purposed that are not always accurate and consistent or may not be easy to interpret. Carr Index [Carr,

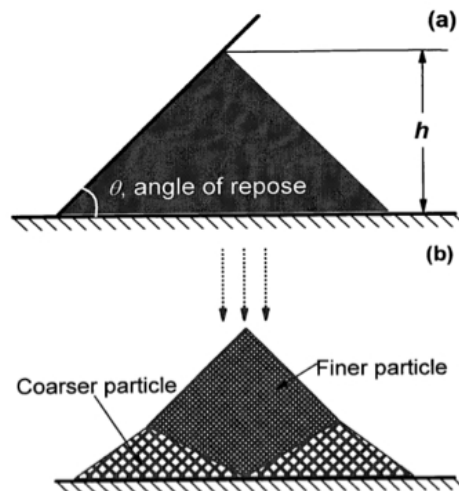
1965] or Hausner ratio [Abdullah and Geldart, 1999, Grey and Beddow, 1969] which will be discussed later in Chapter 4.5, are two common ways of describing flowability. Angle of repose measurements, determination of powder flowrate through an orifice, and shear-cell methods are the most frequent methods to characterize this property of powders [Pharmacopeia, 2011a]. Each of these methods reveals something different about the flow behavior of powder but more than one is typically needed and which of those should be selected depends on their correlation with manufacturing experience and their cost [Rios, 2006].

The following paragraphs will briefly describe the mentioned techniques in more details.

2.5.1 Angle of Repose

The angle of repose is a characteristic related to inter-particulate friction or resistance to movement between particles. According to Pharmacopeia [2011a] angle of repose is the constant, three dimensional angle (relative to the horizontal base) assumed by a cone like pile of material, formed by passing powder through a vertical funnel.

This method is fast, but strongly depends on the methods used to form the cone and has its own experimental difficulties such as segregation of materials and consolidation or aeration of the powder as the cone is being formed [Rios, 2006]. Segregation occurs when powder is piled up due to the further travel of coarser particles down the slope, as shown in Figure 2.3 [Huang, 2009].



$$\tan(\theta) = \frac{h}{0.5 * b} \quad (2.2)$$

Flow Properties	Angle of Repose(degrees)
Excellent	25 – 30
Good	31 – 35
Fair-aid not needed	36 – 40
Passable-may hang up	41 – 45
Poor-must agitate, vibrate	46 – 55
Very poor	55 – 65
Very, very poor	> 66

Table 2.1: Flow properties and the corresponding angle of repose [Pharmacopeia, 2011b]

Figure 2.3: Schematic diagram of (a) angle of repose and (b) segregation of powder during angle of repose measurement

In the above equation, θ is the angle of repose, b is the diameter of the base of the pile and h is the height of the cone of the powder as it is illustrated in Figure 3a.

Table 2.1 represents the range of angle of reposes for different flow properties of powder. This table is a useful classification for pharmaceutical manufacturing purposes. e.g., literature has it that powders with the angle of repose greater than 50 are rarely acceptable for manufacturing purposes.

Angle of repose is an extrinsic property of powder and is very much dependent upon the method used to form the powder cone.

2.5.2 Flow through an Orifice

This method is only practical for powders that have some capability to flow such that the flow rate through an orifice can be determined. It is measured as the mass rate or volume rate of a powder flowing from a container. There is no reference table provided because the flowrate of powders depends on many factors. The technique is likely sensitive to moisture content of the flowing powder and its specific behavior due to changes in electrostatic charges, shapes or sizes.

2.5.3 Shear Cells

Shear tests are basically correlate the normal and shear stresses in solids that is determined experimentally under different load. The shear cell methodology has been used extensively in the study of pharmaceutical materials in order to characterize flow properties of solid material along with other useful parameters. Jenikes shear cell is the most well known type of this method in which powder is poured into a cylindrical cavity that is split horizontally then the upper part is pushed in a linear direction and the force to shear the powder bed by moving the upper part is determined. An annular cell can also be used that needs less amount of sample but the powder bed is not sheared uniformly. In another type, a powder is sheared when sandwiched between two rough surfaces.

A comprehensive discussion about these three mentioned methods does not fall within the scope of this thesis, as they are applicable for samples that are available in a large amount and are not practical for small sample masses. The Hausner Ratio and Compressibility Index parameters will be discussed in detail in Chapter 4.5 to show their usefulness in addressing the flow behavior along with compressibility of powder.

In this thesis the main focus will be on using the powder compression technique for powders with different shape, size, and cohesivity that have different flow properties.

Chapter 3

The Compaction of Pharmaceutical Powders

3.1 Introduction

Several studies have shown that powder compression is a very good method for characterizing the physical properties of powders. This technique is broadly used in diverse fields such as material science, ceramics production, food industry, and pharmaceutical industry.

Compressibility and compactibility of pharmaceutical powders are important properties with which mechanical properties of powders can be characterized. This is important in design of solid dosage form in the pharmaceutical industry. There have been many studies investigating this phenomenon, however, the parameters, which control the compaction behavior of pharmaceutical powders, and which were monitored in these studies vary widely from study to study. A list of those parameters includes the relationship between the measurement of punch forces and strain rate of the compact, die wall friction, axial and radial load transmission, temperature changes, etc. [Hardman et al., 1973].

The two aforementioned terms, compressibility and compactibility should be well understood when dealing with powder compaction characteristics. Compressibility is the ability of powders to reduce their volume as a result of compression while compactibility is the ability of powders to turn into strong and well intact compacts, such as tablets.

Powder compaction is defined as a volume reduction of a powder as a result of applied axial compression force. As the compression pressure on the powder bed that is confined within a container increases, the particles are forced to move to closer proximity and to fill out the voids within the bulk. This will lead to the formation of bonds between particles, which enable the particles to cohere into porous specimen with more or less well-defined shape. For a powder to be suitable for compaction, it must possess two essential properties, flowability and compressibility.

Flowability is important, firstly, because powders should flow easily from a hopper and, secondly, the process should not result in excess air, or entrapped air in the compact that would lead to the formation of a poorly formed compact. A typical tablet machine, as shown schematically in Figure 3.1, comprises of a lower and upper punch and a die. Powder is fed into a cavity and compressed by the upper punch while the lower one is stationary. Then powder is compacted to form a tablet. The lower punch is then used to eject the tablet from the die.

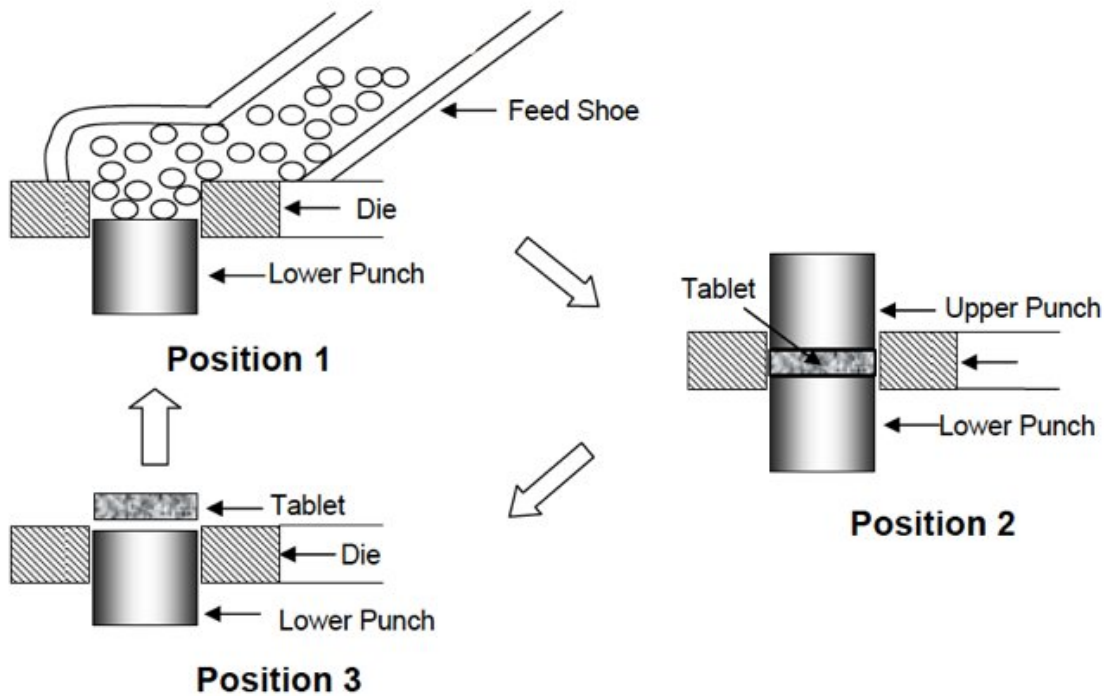


Figure 3.1: Tablet formation in tablet machine (schematic), [Sayyar Roudsari, 2007, Derjaguin et al., 1975]

The powder compression is a complex process that involves several sub-processes, including particle rearrangement, elastic and plastic particle deformation, particle fracture, interparticle bonding, and both interparticle and particle-die wall friction. The entire process of powder compression from the powder filling to the final step, the tablet ejection, falls into several steps:

First, powder flows into the cavity and loose packing configuration is obtained. Then the upper punch starts to descend while the lower punch is held still to attain close packing. Any increases in compressive pressure at this point will result in elastic distortion of the particle structure. When the elastic behavior reaches its upper limit, the yield point, plastic deformation in the powder bulk occurs and permanent particle deformation begins and lasts until the end point of the upper punch advancement. This going beyond the yield strength of the material is a very crucial step in the formation of a strong tablet. At the final stage when the pressure is released from the bulk, a noticeable relaxation, uniaxial expansion occurs in the tablet. Thereafter, the lower punch is used to eject the tablet from the die [Ramsey, 1996, Johnson et al., 1971].

As a result of compression a reduction in volume occurs by various mechanisms and different types of bonds may be established depending on the applied pressure and the properties of the powder. The relationship that exists between the applied pressure and the change in height or volume of the bulk explains very little about the complexities of the process. It does not determine whether this process is useful in producing a coherent compact or not. However many studies have tried to rectify this situation and they categorized the aforementioned process into three groups.

Figure 3.2 describes the volume reduction in a compression process. At first the porosity, which is the volume of the voids within the poured bulk, is relatively high. When the compression pressure is low, during the initial stage of compression, rearrangement of the particles occur which leads to air removal from the compact and tighter packing (A). At this stage, some compression energy is dissipated to overcome the friction between the particles. The amount is dependent on the friction coefficient of inter-particulate friction [Coffin-Beach and Hollenbeck, 1983, Rowlings et al., 1995]. This is the stage in which arches formed by fine particles collapse [Sayyar Roudsari, 2007,

Derjaguin et al., 1975]. These fragile arches are created when the presence of smaller particle in a loose system of powder increases the contact area per unit volume and, consequently, results in a stronger compact.

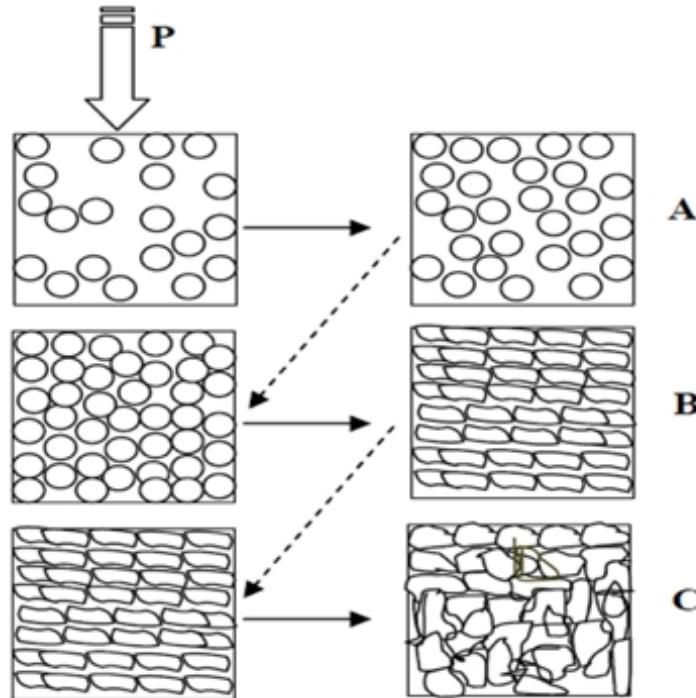


Figure 3.2: Mechanism of Compaction, [Sayyar Roudsari, 2007, Derjaguin et al., 1975]

If the poured bulk at the initial stage of compression is considered as a porous solid, the compression phase up to the end of the rearrangement step can be considered as a plastic phase. The shape of the particles at the rearrangement stage plays a very important role, because powder with spherical shape undergoes rearrangement more easily than those with irregular shape [Mattsson, 2000, York, 1978].

At higher pressures, powder fills the voids and elastic or plastic deformation of particles occurs that leads to an increase in the surface area of the contact point between two adjoining particles and leads to particle interlocking (B) [Duberg and Nystrom, 1986]. In the case of brittle material, the surface structure of the particles may become compromised and particle fragmentation, i.e. the breakage of particles into smaller ones, takes place, part (C). This results in a further reduction in volume as the small fractured particles tend to flow

into voids. Consequently, this results in further increase in the area of interparticle contact that leads to the increase in the bulk density of the powder bed [Sayyar Roudsari, 2007]. The flowability of the powders is a factor that influences this step [Derjaguin et al., 1975]. As the brittle material undergo compression, fractured particles tend to fill up the small empty voids within the powder bed and due to irregular shape of particle, interlocking occurs which will be discussed in more details in the following section.

3.2 Interparticulate Bonding

What holds particles together in a tablet?

The formation of strong tablet by compaction of particulate materials depends on their deformation and bonding characteristics.

Interparticle bonding results in the reduction of powder surface [Ramsey, 1996]. There are several factors that need to be addressed in order to define interparticulate attraction, such as particles physical properties, interparticular and intermolecular distances. However, within a particle, external forces might also be involved in the creation of attraction forces while the influence of gravity force as such, strongly depends on the powder particle size.

Generally speaking, there are three types of interparticulate attraction mechanisms that are involved in a system of particulate matter, electrostatic such as chemical bonding, molecular, and interfacial interaction. Each of these three forces involves several bonding mechanisms and the strength of these forces depends on the powder characteristics, preparation, and on ambient conditions.

The meaning of electrostatic forces at its simplest is the interaction of charged particles or charged surfaces, being active over a distance, i.e., particles 1 and 2 with their respective electrostatic charges of q_1 and q_2 , which are at a distance a from each other, interact with force, F_e , based on coulomb law:

$$F_e = \frac{q_1 q_2}{4\pi\epsilon_0 a^2} \quad (3.1)$$

Where ϵ_0 is the vacuum permittivity.

The direction of the force depends on the particles charge, i.e., repulsive if both charges have the same sign and attractive if both possess the opposite sign.

In a powder bed, where particles are in close proximity of each other the resulting forces due to the presence of a tertiary particle can be relatively high. The lesser the distance between the particles, the higher the attractive force and the lesser chance of having flowable powder. The aforementioned statement relies on the relationship between the attractive force and the weight of particles [Alderborn and Nystrom, 1996].

This type of force can be divided further into different kinds based on the situation applied on a powder, e.g., triboelectrostatic charges which are due to the rapid movement of particles in a mixer, or permanent electrostatic charge that is an immobile charge on a particle surface, and is a consequence of the surface structure and can result in having different charges at each surface. A comprehensive discussion of these types of attraction mechanisms are beyond the scope of this thesis and the review by Alderborn and Nystrom [1996] is brought to the attention of the interested reader.

To form a molecular interaction, a short interatomic distance and a certain arrangement between the particle surfaces is required. These forces are not the chemical attraction or valence bonds that link atoms in compounds. They are forces of longer range that pull molecules of a substance together [Derjaguin, 1960]. There are only very few interactions of this kind between particles as it is unlikely to have functional groups which are by coincidence in a suitable opposite position to cause interparticle linkage by this mechanism. Hence, this force is very weak and a small mechanical stress can break this linkage and cause the powder to flow. These are secondary bond or Van der Waals attractions. Van der Waals forces are named after the Dutch Scientist Johannes D. Van der Waals. They include attraction between atoms, molecules and surfaces as well as other intermolecular forces.

Generally during compaction of powders, bonding mechanisms can be classified into five types:

- Solid bridges (due to melting, crystallization and chemical reaction)
- Mechanical interlocking (shape related bonds)
- Distance attraction forces (intermolecular forces)
- Bonding due to the movable liquids (capillary and surface tension)
- Non-freely-movable binder bridges (viscous binders)

Even though the effect of liquid in enhancing the strength of tablet, due to its influence on the compressibility of the powder, has been shown (to be discussed in detail in Chapter 6.7), the first three are considered to be the most important bonding mechanisms that contribute to the compaction process of pharmaceutical powders [De Boer et al., 1978].

3.2.1 Solid Bridges

Solid bridges are categorized as an interfacial force that occurs when material undergoes solidification as a result of fusion between particles. Solid bridge formation can be aggravated by heat, the presence of liquid, or increase in the applied load. When the particles in a system of powder get into very close proximity of each other, at a separation of less than 50 nm, as a result of extensive compaction pressure a process is evolved that is known as cold welding. During this phenomenon the free surface energy of particles causes the formation of very strong attractive force. This force is similar to the force that acts at a molecular level during the formation of single particles. Another phenomenon that could happen as a result of high compression force is the creation of fusion bonding. This idea relies on the fact that the surface of all particles possesses irregularities that during compression would be the points of contact that transmit the load. Consequently, a significant amount of friction heat would be generated which leads to melting of the contact point. This would result in formation of bond upon solidification and increase the mechanical strength.

These forces are believed to be one of the main reasons for the increase in the mechanical strength of the compact as it undergoes compression. This agrees with what some researchers have published [Tabor et al., 2001], i.e.,

that compaction of powder occurs when particles are in true contact of each other. Based on the theory of friction, true contact occurs when there is no interface between two adjoined particles as such they can be called as one single particle. This theory strongly agrees with what Sir Isaac Newton proposed, i.e. two homogenous hard bodies that are fully in contact, stick together very strongly.

As a result of that the interparticular interfaces of the contact areas within a powder bed may disappear by recrystallization, melting or self diffusion of atoms between surfaces and particles fuse and grow together [Ahlneck and Alderborn, 1989]; however, several factors are involved. Because a fracture of the solid bridge must occur, these aggregates cannot be separated by mechanical or other treatment into their original particles. Solid bridges are relatively strong bonds where a true physical contact, contact at an atomic level, is established between adjoined particles in comparison to the intermolecular forces that are weaker bonds that act over distances [Alderborn and Nystrom, 1996].

3.2.2 Intermolecular Forces, Distance Attraction forces

Cohesion mechanisms between solid particles in gaseous atmosphere are the forces of interest in study of the dry powder aerosols. Cohesion forces between smooth spray dried particles can be derived from Van der Waals forces, electrostatics forces and in presence of humidity from capillary forces.

Intermolecular forces are the compilation of interparticle attraction based on physical attraction between solid particles [Ramsey, 1996]. Two of the important types of intermolecular forces that arise when pharmaceutical powders are brought to close proximity as a result of compression are Van der Waals force [Luangtana-Anan and Fell, 1990] and Hydrogen bonding [Alderborn and Nystrom, 1996].

Van der Waals forces are known to be the most important distance attraction forces holding particles together. They have their origin in the forces between their constituent molecules. This is dependent on the distance between particles and this intermolecular force is always present in a system of powder between molecules due to the electrical nature of intermolecular attraction. There are three types of Van der Waals forces which are; London

dispersion, dipole-dipole (Keesom) and induced dipole-dipole (Debye) forces that can be either attractive or repulsive being effective from a large distance from ($> 100 \text{ \AA}$) down to inter-atomic spacing (about 2 \AA). Debye force occurs between a permanent dipole and an induced dipole. Generally, it is the material properties that accounts for how well the molecule can produce induced dipole when put near the permanent dipole molecule. In Keesom force, two molecules with permanent dipole attract each other. London-dispersion attraction force talks about the interaction between two dipoles that are induced by some outer molecules possessing permanent dipole. The magnitude of Van der Waals force is depended on the size and distance of two particles participating in contact. In the other word, the magnitude of this force becomes negligible when compared with the gravitational force as the particle size exceeds a certain value.

Hydrogen bonding as previously pointed out is of major concern when dealing with direct compression of pharmaceutical powders. It is considered as a strong dipole-dipole interaction with some electrostatic properties [Derjaguin, 1960]. In the presence of liquid or a humid environment, the condensed liquid between particles and inner pores result in the creation of liquid bridges. In this case the capillary forces are dominant. However, in the absence of humidity, Van der Waals force is known to be the most effective interparticle force [Alderborn and Nystrom, 1996, Derjaguin, 1960].

Van der Waals attraction forces arise due to dipole-dipole interactions between atoms and molecules of adjacent surfaces and depend on material properties. Van der Waals forces are short-range and it can be neglected for a separation distance of $a > 0.5 \text{ nm}$, i.e., this force is only noticeable when particles can come sufficiently close together. The distance of 0.4 nm is often used for calculation for particles that are in contact. Van der Waals force for two ideally flat, rigid and spherical particles having a diameter of d can be calculated by the following formula:

$$F_{VdW} = \frac{h_w d}{32\pi a^2} \quad (3.2)$$

The distance between two particles (a) in a settled powder bed is assumed to be 4 \AA (0.4 nm). h_w is the Lifshitz-Van der Waals constant and is related to the Hamaker constant (A_H) of the particle material by:

$$h_w = \frac{4\pi}{3} A_H \quad (3.3)$$

If you know the electromagnetic properties of material you can find Hamaker constant. The Van der Waals equation after replacing h_w with Hamaker constant is:

$$F_{VdW} = \frac{A_H}{24a^2} d \quad (3.4)$$

In case of having particles with different particle sizes, the particle diameter d is calculated by:

$$d = \frac{2d_1d_2}{d_1 + d_2} \quad (3.5)$$

Where d_1 and d_2 are the diameters for two perfectly spherical particles.

Capillary attraction force between two particles occurs in presence of humidity due to the *Kelvin Effect*. The high surface tension of water gives strong attraction between two particles and creates bridge that holds them together. According to the Kelvin effect, the vapor concentration on the surfaces with sharp curvature is higher than that when it is next to the flat surface [Finlay, 2001]. The total capillary force of this bridge is given by the following formula:

$$F_c = \pi \lambda d \quad (3.6)$$

Where λ is the surface tension of the liquid (the surface tension of the water is 72.7 mJ/m^2).

Cohesion between Real Particles

The Van der Waals, capillary forces and electrostatic forces are directly proportional to the particle size [Hinds, 1982]. There are some other factors that are overlooked in consideration of these models. The validity of these models for pharmaceutical particles is limited due to the fact that the surface of all real pharmaceutical particles are covered with a certain degree of asperities or irregularities that reduces the cohesion force between them. The cohesion between particles is affected by surface characteristics and ambient condition. Van der Waals force calculated for idealized smooth geometries do not consider surface roughness or deformation of the contact area and cannot be used for

real particles [Finlay, 2001]. From the other side, the contact area of two particles adjoining together in a humid environment undergoes plastic deformation as a result of capillary condensation of humidity. Thus, the intensity of the cohesion forces depends on the properties of the contact zone [Weiler et al., 2010].

Two models have been proposed to describe the force needed to separate two real spherical particles with the diameter of d_1 and d_2 : *Johnson-Kendall-Roberts* (F_{JKR}) [Johnson et al., 1971] and *Derjaguin-Muller-Toporov* (F_{DMT}) [Derjaguin et al., 1975].

$$F_{JKR} = \frac{3}{2}\pi\gamma d_r \quad (3.7)$$

$$F_{DMT} = 2\pi\gamma d_r \quad (3.8)$$

$$d_r = \frac{d_1 d_2}{d_1 + d_2} \quad (3.9)$$

Where γ is the surface energy of solid particle. The literature showed that the pull of force for real organic and spherical particles is 1-3 orders of magnitude higher compared Van der Waals cohesion [Weiler et al., 2010]. In case of having two particles with the same diameter, the pull of force of the DMT model is equivalent to the capillary force. JFK model is appropriate for large, soft spheres and the DMT model for small, hard spheres. The surface energies of different solids can be determined experimentally using atomic force microscopy, inverse gas chromatography or contact angle measurement, which is beyond the scope of this thesis.

3.2.3 Mechanical Interlocking

Mechanical interlocking is the term that is used to describe the hooking and twisting together of the packed material [Alderborn and Nystrom, 1996]. This bonding mechanism is based on the particle morphology, i.e., it is dependent on the shape and surface structure of the particles.

Relatively high compression pressure on materials with low compact strength and long disintegration time are required to produce a strong compact with this bonding mechanism. If this bonding was a major contributor to overall bond strength, it would not explain the ability of particles with regular or

spherical shapes to form strong intact tablets [Ramsey, 1996].

Particle size plays a significant role in cohesivity of powders. Powder with the size of smaller than a critical value possesses a relatively high interparticle force in regard to the gravitational and drag force that causes the powder to experience cohesiveness and poor flow properties [Huang, 2009]. Van der Waals force and capillary force of a liquid bridge are the most significant attraction forces for particles with the size of smaller than $10\ \mu m$.

The dominance of any type of these forces that contribute to the interparticle attraction is varied in certain circumstances, however; the forces of primary concern are Van der Waals, electrostatic and interfacial forces.

3.3 Consolidation

Consolidation is defined as the mechanical strength of a compact as a result of particle/particle interaction. Particle rearrangement, elastic and plastic deformation during consolidation can result in large areas of true contact between particles, in which the stronger this particle-particle bond the more intact tablet is formed.

The compression event has been divided into a series of time periods, Figure 3.3 , by Jones [1981], as follows:

- Consolidation time, time to reach maximum force
- Dwell time, time at a maximum force
- Contact time, time for compression and decompression excluding ejection time
- Ejection time, time during which ejection occurs (not shown in the figure)
- Residence time, time during which the formed compact is within the die

The degree of volume reduction in particulate materials depends on the mechanical properties of the particles and the type of the compaction mechanism involved. For example, it will be shown in chapter 6 that the particle size

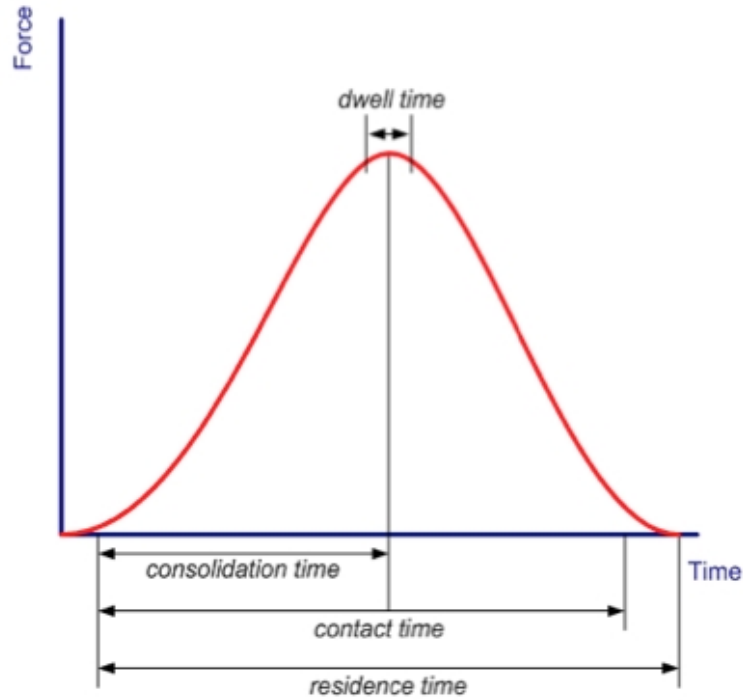


Figure 3.3: Events occurring during the compression process [Odeku, 2007]

and the compression speed influence the volume reduction rate. Smaller particles have a lower tendency to undergo fragmentation [Alderborn and Nystrom, 1985]. For some particles a critical size exists at which their behavior transitions from brittle to ductile as they experience the compressing force [Roberts and Rowe, 1987]. It has been investigated which of these processes, plastic deformation or brittle deformation, is the potential cause of bonding in the powder and contributes to the formation of a coherent mass. The settled bed can be considered as a stable collection of particles that each of these particles is in point contact with its neighbors. An applied stress will be supported by these points of contact and friction between particles and the die wall. If the applied force goes beyond the critical value and material do not deform, fracture occurs. This fracture results in the creation of smaller particles and consequently number of particle contact point per unit volume increases. The breakage of larger particle to smaller particle continues until no contact point is stressed beyond its breaking point. Increasing the compaction pressure will cause more contact points to be stressed thus results in powders to be packed more densely.

3.3.1 Decompression

In the tableting industry decompression is the process that follows after the compression stage. This stage contains much information about the powders under test, which is useful to explain the routine problems that happen during formation of tablet.

3.4 Elasticity and Plasticity

There is a difference between the physical nature of a powder column and a solid body. A powder column is mostly a two-phase system (assuming there is no moisture in the column) that includes air and solid particles. Due to the presence of air in the system, a powder has the rheological behavior of a liquid. Besides, powders have the capability of being elastically or plastically compacted. The compaction process is defined as the displacement of the gaseous phase with the solid phase within the bulk as a result of the compression force that leads to the reduction of the bed volume.

Generally speaking, the powder compaction process involves a series of either reversible or irreversible stages (Figure 3.4). The former occurs as a result of material elasticity. Thus, there is a dimensional change proportional to the applied pressure. The latter stage shows the plasticity of the material [Buckner, 2009]. A powder systems behavior strongly depends on the lattice structure of the particles. When powder is subjected to an axial force, this external force brings the particles in close proximity of each other and causes the volume to reduce. This stage is generally called the particle rearrangement stage. Plastic property is the exact opposite of elasticity that is, a material possessing the property of plasticity deforms permanently. Plastic deformation in powder has both ductile and brittle behaviors. Brittle deformation occurs when larger particles fragment into a number of smaller ones. This increases the cohesiveness and the strength of the bulk which is due to the increase in the particles contact area per unit volume within the powder. Ductile deformation is the simple movement of molecules within the particles so the particles are able to flow without changing the inter-particle points of contact.

In the case of the reversible stage, different types of particle deformation occur when the compaction force goes beyond certain levels. At which, upon the

removal of the applied force, powder shows some elastic behavior by returning to its original dimension. This deformation, to a large extent, is reversible.

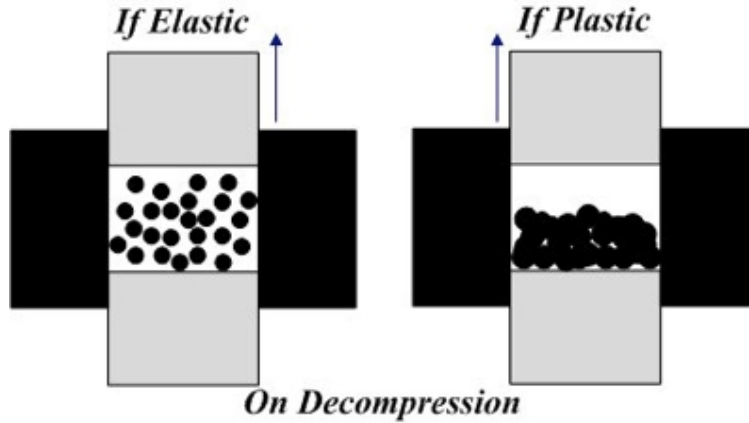


Figure 3.4: Schematic of reversible and irreversible compression

The aforementioned events, generally occur sequentially or simultaneously in a powder bed that is compressed by an axial force [Heckel, 1961b]. The strength of the final compact depends on the interaction between particles, the mechanical properties of material being compressed [Alderborn and Nystrom, 1996, Yap et al., 2008, Hersey et al., 1973] and the consolidating conditions employed [Hausner, 1967, Tousey, 2002].

Two forces axial and radial- are applied on materials that are confined within a cavity and are undergoing compression. Axial force is the main longitudinal force that causes the formation of the compact. The radial stress that is applied to the die wall from the powder occurs because of the lateral expansion of powder in the compaction process [Johnson et al., 1971].

Poissons ratio relates these two lateral and longitudinal strains:

$$Poisson'sRatio(\nu) = \frac{lateral\ strain}{longitudinal\ strain} \quad (3.10)$$

Soft materials possess a lower Poissons ratio than hard materials. According to several sources [Johnson et al., 1971, Marshall, 1963], bonding occurs by brittle fracture in powders composed of particles with a low Poissons ratio. By microscopically analyzing the transformation details of individual particles

into a single cohesive compact, a single particle must change shape significantly so that the new bonds or interactions are created between the adjacent particles. This deformation of compact is very important in predicting how material will respond to bond formation and tablet manufacturing [Buckner, 2009]. Leigh et al. [1967] and Denny [2002] proved that the difference between powders that form strong and well-intact compacts is due to the pressure cycles that occur during compression. They idealized the compaction process of powders to that of solid bodies.

When an axial load is applied on a powder during the reversible stage of compression when the powder is perfectly elastic, all of the transmitted radial forces will be in the same magnitude (in the absence of die wall friction). The relationship between the radial and axial force is on the order of $\sigma = \nu(\tau)$. Where σ is the axial force, τ is the radial force and ν is the Poissons ratio (Figure 3.5).

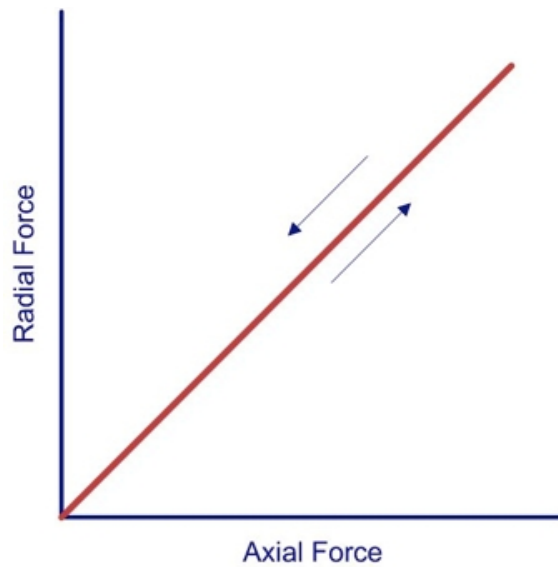


Figure 3.5: Compressional cycle of an ideal elastic body

This elastic behavior is valid when the compression pressure is lower than the yield strength or yield point of the body. If the pressure level goes beyond this yield point, the body loses its elasticity. Otherwise (in the elastic regime), when the applied force is released, all of the transmitted axial forces will be reduced proportionally, and when the force is fully removed there will no longer be any radial or axial force and the bulk can be removed (Figure 3.5).

Another scenario is when the applied force goes beyond the yield strength of a powder, during which powders do not show an immediate reaction when the force is removed from the compact. In this case when the axial force increases, its relationship with the radial force is dependent on the yield condition of the materials and is on the order of $\sigma - \tau = 2S$, where S is the yield stress in shear at which the material undergoes sliding failure, and graphically it follows the course AB in Figure 3.6. After releasing the force, point B, the body will no longer be forced to yield, and the radial force decreases at the rate of Y times the rate of the decrease of the axial force, BC. The slope of the line BC is equal to the line OA (this part will only be acquired if the maximum force is relatively high in magnitude).

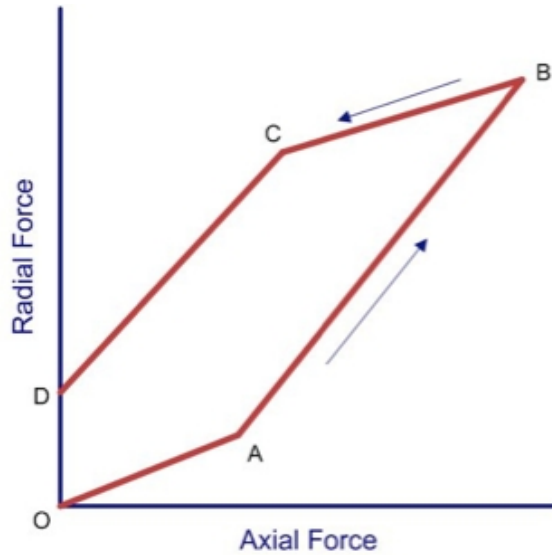


Figure 3.6: Compressed cycle of a body with constant yield stress in shear

At some point in this transitional stage, due to the difference in axial and radial forces, point C is attained when the axial force can no longer keep up with the radial force and becomes lower, i.e., the radial force is greater than the axial force by an amount equal to $2S$. At this point yield again occurs and the difference between the axial and radial forces, $\sigma - \tau$, will be constant and the course will follow the CD line. By looking at Figure 3.6, when the force is completely withdrawn from the compact, the body exerts a residual radial force with the magnitude of $2S$ on the die-wall [Weiler et al., 2010, Denny, 2002]. The above statements are based on the assumption that there is no

die-wall friction in the system, and that the difference between the axial and radial forces relies on the compression pressure whether it hits the maximum level or not; otherwise this differences would not be recognizable.

3.5 Material Compaction Behaviour

It is generally accepted that different materials have different responses to compaction. Depending on the level of compression pressure, all materials show plastic and elastic behaviors. However, the length of each course, (e.g., plasticity) depends strongly on the compression pressure and mechanical properties of the material.

Brittle materials like magnesium carbonate, calcium carbonate, sucrose and crystalline lactose consolidate by fragmentation [Roberts and Rowe, 1985, McKenna and McCafferty, 1982, Antikainen and Yliruusi, 2003]. Ductile materials such as microcrystalline cellulose, stearic acid, sodium chloride and starch consolidate by plastic deformation [Roberts and Rowe, 1986, Duberg et al., 1982]. There are other factors such as temperature, humidity, compaction rate, and particle size that influence the behavior of material under compression, (e.g. [Roberts and Rowe, 1985, 1986]). Pharmaceutical powders are compacted by more than one of these two mechanisms [Duberg and Nystrom, 1986]. Thus a general method is needed to characterize the compaction behavior of different materials.

3.6 ParticleDensity

Particle density is one of the quality control attributes for pharmaceutical powders. Density is important in determining the powder performance such as flowability, and the compaction properties. Particle density is the ratio of the particle mass over its volume. The volume may be defined differently as such, various types of density have been introduced.

3.6.1 True Density

The density of the solid object, when its volume excludes any internal or external pores (open pores) that are not a fundamental part of the molecular

packing arrangement, is called true density. This density is also known as particle density or absolute density and the correspondent volumes are called true or skeletal volumes. True density is measured by pycnometry in which a displacement fluid is used to fill the pores. Helium, air or in some cases oil can be used, depending on the type of powder. These displacement fluids penetrate between the particles voids so the true volume can be determined. Different gases may be used to avoid gas sorption by the powder.

3.6.2 Apparent Particle Density

The density of the particle when its volume includes internal (closed) pores or bubbles of gas within itself is called apparent particle density. This density can be measured using air or a liquid displacement technique, pycnometry.

3.6.3 Aerodynamic/Hydrodynamic Particle Density

The density of the particle when its volume includes both internal and external (open) pore is called aerodynamic or effective particle density. Its volume is also known as envelope or hydrodynamic volume. This density is determined by the weighted average of the solid and immobilized gas (or liquid) densities that are present within the hydrodynamic volume.

In addition to the above definitions, there are other densities that are categorized in bulk density measurement and should not be confused with particle density [Svarovsky, 1987].

3.6.4 Bulk Density

Bulk density is the mass of the powder column divided by its volume where its volume is the hydrodynamic volume of the particle plus interstitial spaces between particles. There is some confusion as to whether the moisture in the object should be included or not. To avoid confusion about this issue, the experiment conditions should be mentioned.

As the name implies, bulk density significantly depends on the state of powder, particularly on its state of compaction, due to the presence of air or

moisture (inter-or intra- particulate pores) within the bulk. Bulk density depends significantly on particle shape as well, i.e., as the particles become more spherical, the bulk density increases [Lachman et al., 1986]. The dispersity of particles in a powder bed is another factor to be considered. The definition of the term dispersity in this study is limited to describing the heterogeneity of sizes of particles in a mass of powder. A powder is called monodisperse when it is composed of particles with the same size, and polydisperse when it is composed of particles with inconsistent size. Experiments have shown that polydisperse powders possessing sphere particles with random sizes can achieve a higher packing fraction (nontrivially can get close to 1 and strongly depends on the size distribution of particles) than those consisting of monodisperse spherical particles (Their packing fraction is around 0.64-0.74). The packing fraction is the volume taken up by the solid particles in a given volume, normalized by the total volume. With the same token, powder possessing differently shaped particles can achieve higher packing fraction than those with spherical particles, i.e. depending on the shape factor and the size distribution of particles in a bulk, powders possessing irregular-shape particles can form denser compacts than what can be attained with spherical-shape particles.

Bulk density is always lower than the true density due to the fact that the bulk density of a powder is somewhere between the density of the two phases, solid and gas, involved in the bulk. The magnitude of interparticle forces that determines the flowability of the powder plays an important role in the value of bulk density. Thus a bulk of powder can have one true density but more than one bulk density, depending on the way it is compacted and the porosity level of the compact.

According to the Pharmacopeia [2011b], there are four types of bulk densities, listed as follows, in order of increasing bulk density: *aerated bulk density*, *poured bulk density*, *tapped bulk density* and *compressed bulk density*. The simplest method is to fill a container of known volume with a known mass of powder and level-off the surface with a sharp instrument. Both United States and European Pharmacopeias use different container sizes to maintain the accuracy, as the amount of powder under test may change. If the poured density is sought, powder volume is measured without disturbing the bed. If the aerated density is sought, the known amount of dry powder is poured into the container and the powder in the container is aerated by repeatedly inverting

the container. The volume is then read-off after righting the container. For the case of tapped density, the container that is filled with powder is dropped from a specific height multiple times. Depending on the standard in use, the resultant volume for each set of tapping is read.

Bulk density is an essential parameter for solid dosage manufacturing. It is used to determine the amount of powder that should be fitted into capsules, or to the blenders or hoppers on a tablet press.

Poured Density

Poured density is one of the most widely measured bulk powder properties and there are different standards for determining it. One such method is the funnel method, in which the specific amount of powder is poured freely through a funnel, solely by the force of gravity, to the graduated cylinder. The poured density can be determined, as it is the ratio of mass of powder to the occupied volume in the graduated cylinder. Some standards suggest using small rod to initiate the flowing.

Due to dominance of interparticle forces in micro-particles, none of the above methods that rely on inertia or gravity force for measuring the particle density are applicable for respiratory drugs. For those particles, the following method is applied.

3.6.5 Compressed Bulk Density

It is sometimes required to compact the powder more than what can be achieved by the tapped density technique. The reason for that is to determine the mechanical and physical properties of powder that helps in better understanding of powder quality. This can provide a useful insight into handling of powders. Obviously, powders cannot be analyzed in the same way as solid bodies can, because powders contain more than one phase. For example, powder is not linearly elastic, but mostly possesses plastic deformation; thus, it cannot simply be characterized by Young's modulus or Poisson's ratio as solid material can.

Table 3.1 shows the relationship between the useful terms commonly used

Density definitions	Symbols	Equations
Bulk density	ρ	$\frac{\text{mass, } m \text{ (kg)}}{\text{volume, } v \text{ (m}^3\text{)}}$
Specific volume	δ	$\frac{\text{volume, } v}{\text{mass, } m} = \frac{1}{\text{density, } \rho} \text{ (m}^3\text{/kg)}$
Absolute density, true density	ρ_T	$\frac{\text{mass, } m}{\text{molecular volume, } v_m}$
Apparent density	ρ_a	$\frac{\text{mass, } m}{\text{envelope volume, } e_v}$
Relative density, solid fraction	D	$\frac{\text{apparent density, } \rho_a}{\text{true density, } \rho_T}$

Table 3.1: Density definitions

in pharmaceutical powder compaction [Hancock et al., 2003];

Generally speaking, the relative density of powders increases as they undergo the compaction process. Many physical behaviors of pharmaceutical particles, powders, and compacts such as powder flow and tensile strength, can be specified by their absolute or relative densities [Abdullah and Geldart, 1999].

Chapter 4

Uniaxial Powder Compaction

4.1 Introduction

In the powder compression technique, powder that is confined within a die is compressed with small incremental movement of the punch. These small increments are recorded, along with the exact stress that they exert on the powder, at the very point of measurement. Depending on the amount of pressure that is exerted, powders show different behaviors that are useful in classifying them into groups based on their compaction levels. In other words, for some samples, the strain rate decreases after a certain compaction stress; revealing any further stress may result in particle deformation [Svarovsky, 1987].

The result of this powder compression is a very well known and useful Displacement versus Force (Stress versus Strain) profile. In the pharmaceutical industry, this plot is one of the most useful tools for studying and analyzing the compression process. This profile, which is obtained from the measurement of punch force and displacement, helps to determine the material characteristics in formulation works or to detect batch-to-batch variations in the compression properties of materials.

Many studies have suggested that the work of compression can be calculated by using the area under the strain versus stress curve [Armstrong and Morton, 1977]. However, this work also includes the work to overcome die-wall friction [Nelson et al., 1955]. Various methods have been introduced to interpret the force-displacement profile.

Figure 4.1 shows that the force exerted on the upper punch, F_A , is equal to

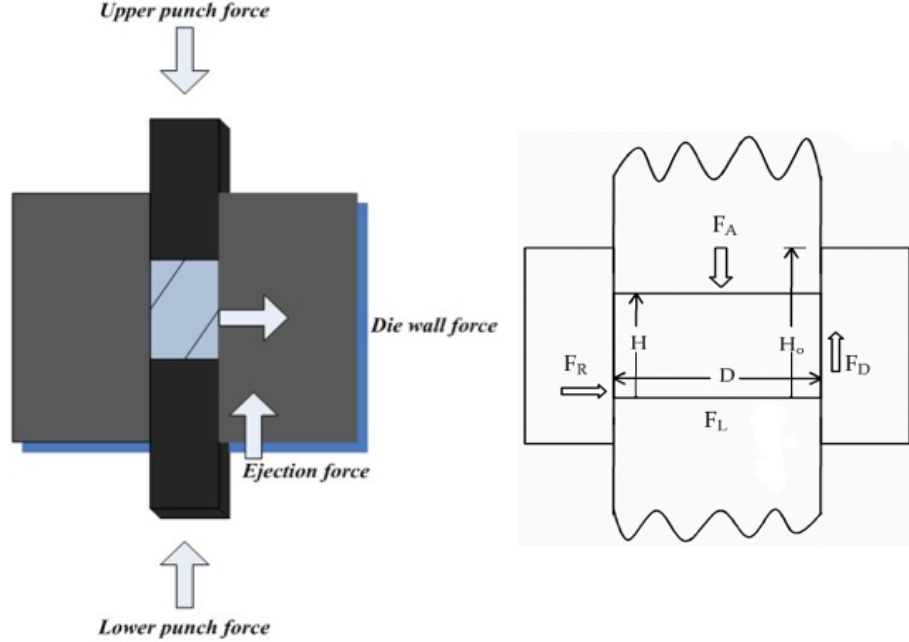


Figure 4.1: Schematic of the force being transmitted through powder bed

the sum of the both forces exerted on a lower punch, F_L , and the force needed to overcome the die wall friction, F_D . Die wall friction force occurs as a result of the radial force, F_R .

$$F_A = F_L + F_D \quad (4.1)$$

F_L is the portion of the transmitted force to the lower punch by the upper punch. By increasing the axial stress (in one direction) on a powder mass, since the materials are confined within a volume and are not free to expand, a radial force (F_R), is acting normal to the boundary between the tablet mass and die wall. Materials with higher Poissons ratio give rise to higher values of F_R . In classical friction theory, the radial force and the axial force are related to each other by the following Coulombs equation:

$$F_D = \mu F_R \quad (4.2)$$

In the above equation μ is the coefficient of friction. The radial force develops perpendicularly to the wall and consequently results in the upper punch force diminishing exponentially as the strain rate of the bulk decreases. The

relationship between the upper and lower punch forces can be expressed as [Hausner, 1967, Kikuta and Kitamori, 1983]:

$$F_L = F_A \cdot e^{-\frac{kH}{D}} \quad (4.3)$$

H and D are the height and diameter of the tablet, respectively. k is an experimentally determined material-dependent constant that includes a term for the average die-wall frictional component.

In order to better understand the value of the die-wall friction in this process, shear strength of the particles under test should also be determined. This matter is beyond the scope of this thesis.

4.2 Porosity of Packed Bed

Porosity or voidage of a powder column is defined as the ratio of the volume of the voids within the bed, i.e. the volume occupied by the air, and the overall volume of the bed. Clearly, the void volume includes the pores within the particles if they are porous. When porosity is quoted, for the sake of clarity in the description, it is important to mention whether the volume that has been measured is inclusive or exclusive of open or closed pores.

The state of compaction obviously affects the porosity of the compact and some powder can be compacted into the wide ranges of porosities. The following equation is used to relate porosity with the bulk density [Svarovsky, 1987].

$$\rho_b = \rho_p(1 - E) + \rho_a E \quad (4.4)$$

Where ρ_b is the powder bulk density, ρ_p is particle density and ρ_a is the air density. The air density in comparison to the powder density is relatively small and is neglected, thus the porosity, E , can be described as follows:

$$E = \frac{\rho_p - \rho_b}{\rho_p} = 1 - \frac{\rho_b}{\rho_p} \quad (4.5)$$

The above equation gives the porosity of a powder column. It should also be stated clearly whether or not this porosity includes pores and voids inside the

particles. In other words, the type of particle density used in this evaluation should be mentioned. It is most useful if the true density is used instead of the particle density, since the true density describes the density of the solid phase when its correspondent volume excludes both internal (closed) and external (open) pores. However, the true density cannot simply be determined.

4.3 Porosity-Pressure Function in Compaction

Porosity, E , is the function of pores and voids in a powder system. To measure the powder columns porosity, the powders dimensions and weight (bulk density or apparent density, ρ_b) and the density (true density, ρ_T) should be known. Porosity is expressed as:

$$E = \frac{\rho_b}{\rho_T} \quad (4.6)$$

The value of $\frac{\rho_b}{\rho_T}$ describes the solid fraction of a porous powder column, which is also known as relative density or the packing fraction. In the study of powder compaction, the high bulk density doesn't necessarily mean a fully packed bed with low porosity. Bulk density and true density are related to each other by the following formula:

$$\rho_b = D \cdot \rho_T \quad (4.7)$$

Where D is the relative density or packing fraction, which is a dimensionless quantity. During compression D is increased to the maximum of unity, if attainable. Powder porosity and fractional voidage can also be defined as: (usually expressed as percentage)

$$E = 1 - D \quad (4.8)$$

4.4 Porosity-Pressure Equations, Compaction Data Analysis

As long ago as 1923, Walker [1923] introduced the first compaction equation and observed a logarithmic relationship between the compacts applied pres-

sure and relative volume. Since then, more than 15 mathematical models have been proposed to describe the compaction process and to better understand how materials behave under compaction pressure. Appendix D contains a list of these models. The equations are based on the transformation of the classical stress and strain relationship as it connects the consolidation state of the powder column to the compacting pressure. The equations describe the change of relative density, porosity, volume, void ratio, and relative volume in a powder column as a function of applied pressure. Among the equations, only a few apply to pharmaceutical powders: Heckel [1961b,a], Kawakita and Lüdde [1971], Adams et al. [1994], and Cooper Jr and Eaton [1962]. However, it is unlikely for a single compaction equation to fit all of the compaction mechanisms [Alderborn and Nystrom, 1996, Odeku, 2007].

One of the main reasons for fitting the experimental data to an equation is to linearize the plots for facilitating comparisons of data sets [Grey and Beddow, 1969]. Moreover, as the density of the bulk during the powder compaction varies, these models should be able to practically allow us to extrapolate data; predicting densities at other required pressures. In addition, these empirical models should have the capability to relate the derived compression parameters to the relevant physical properties of powder and be able to differentiate between different compression mechanisms for different powders under test.

The following are brief descriptions of those mechanisms:

1. At low pressure, rearrangement or packing of particles occurs to some extent. At this stage, arches that might be formed during the die-filling process will collapse. By increasing the force, brittle material will fracture and the fractured material will fill smaller voids, thus bringing about further volume reduction. As particles become smaller further, particle breakage will become more difficult and the powder will transit to the brittle-ductile phase. At this stage, no more fragmentation occurs and the powder compresses with plastic deformation as pressure increases [Atkins and Mai, 1986].
2. Plastic deformation is one of the important stages on which most of the mathematical equations have focused. It occurs in powder columns possessing fine powders with submicron particle diameters.

3. The final mechanism is the elastic compaction of non-porous material. This compaction usually happens when the porosity of the powder bed decreases to below five to ten percent and the powder is likely to behave as a solid body.

To interpret compaction profiles using these fitting models, considerable care is needed. It is important to know which of the mechanisms are operating. Usually the use of these models should be limited to the instrument that measured the fitting parameters generated from the data. These models should be able to predict the strength of the resulting compact from the force-displacement curve. In this thesis I describe two of these models, Heckel and Kawakita, as those are two of the most common models in the pharmaceutical industry.

4.4.1 Heckel Equation

The Heckel equation, also known as Athy-Heckel, is a widely used equation in the mathematical analysis of compression curves in the pharmaceutical industry, specifically in the production of tablets.

In 1961, Heckel proposed an equation in which he correlated the densification of metallic powder to a first-order chemical reaction [Alderborn and Nystrom, 1996, Duberg and Nystrom, 1986, Heckel, 1961b,a, Celik, 1992]. In this equation he considered pores to be the reactant and densification to be the product. The equation relates the porosity changes in the powder bed to the applied pressure:

$$\frac{dD}{dP} = K(1 - D) \quad (4.9)$$

$$\frac{dD}{1 - D} = K dP \quad (4.10)$$

$$\int_{D_0}^D \frac{dD}{(1 - D)} = K \int_0^P dP \quad (4.11)$$

$$(4.12)$$

Where D_0 is the relative density of the loose powder at zero pressure.

$$\ln(1 - D_0) - \ln(1 - D) = KP \quad (4.13)$$

$$\ln\left(\frac{1}{1 - D}\right) = KP + \ln\left(\frac{1}{1 - D_0}\right) \quad (4.14)$$

$$(4.15)$$

This is the Heckel equation. A constant, A , was added to make this equation quantitatively valid (only at high pressures).

$$\ln\left(\frac{1}{1 - D}\right) = KP + A \quad (4.16)$$

K and A are constants that can be determined from the slope and the intercept of the plot, $\ln(1/(1 - D))$ versus P , by using the experimental results (Figure 4.2). A is determined by extrapolating the linear region of the plot. D is the relative density (the ratio of bulk density to true density of powder) at applied pressure P . The slope, K , is meant to give information about the plasticity of material. As such, greater slopes indicated a greater degree of plasticity [Heckel, 1961b].

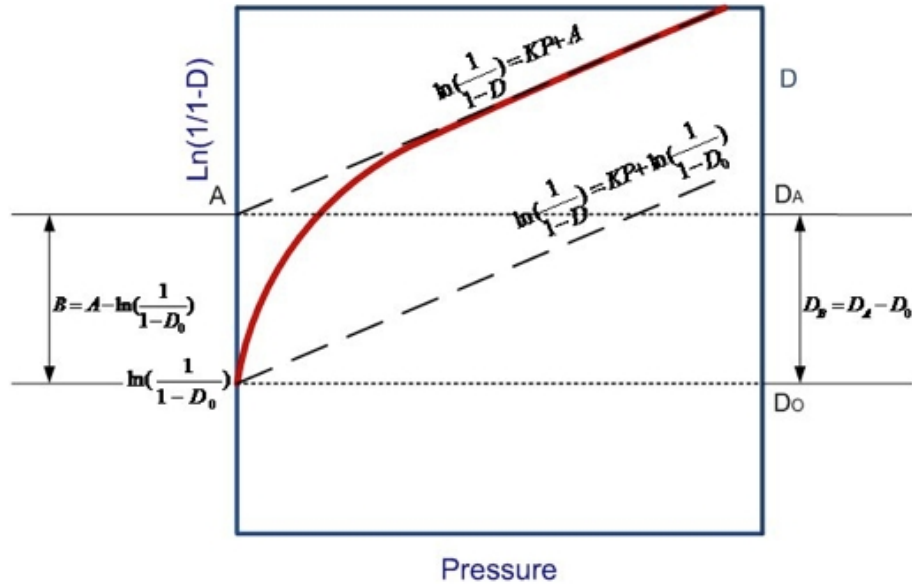


Figure 4.2: Schematic representation of the compaction behavior according to the Heckel equation [Heckel, 1961b]

In this plot, linearity exists over 65 to 80 percent of the pressure range. The nonlinear section of the plot is related to die filling and rearrangement of

particles within the powder bed during the initial process of compression. The constant A , which shows the transition from the nonlinear to the linear region, is related to the degree of pressure (low pressure) at which packing of powder occurs without the presence of any inter-particle bonding [Heckel, 1961b].

Heckel later found that there is a relationship between the constant K and the yield strength for a range of metal powders.

$$K = \frac{1}{3Y} \quad (4.17)$$

Hersey and Rees [1971] defined the reciprocal of K to be the mean yield pressure.

The ability to describe the behavior of material under compression in terms of constant A and K can first of all quantitatively describe the compaction behavior of material. Also data can be extrapolated to the degree that is unattainable experimentally.

Heckels profile has been divided into three regions (Figure 4.3).

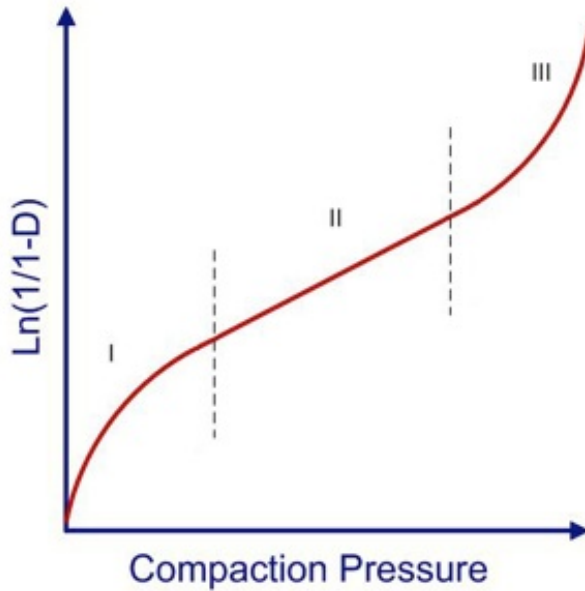


Figure 4.3: Schematic of Heckel compaction profile

Region 1 is the nonlinear region, with the decreasing slope, that is ex-

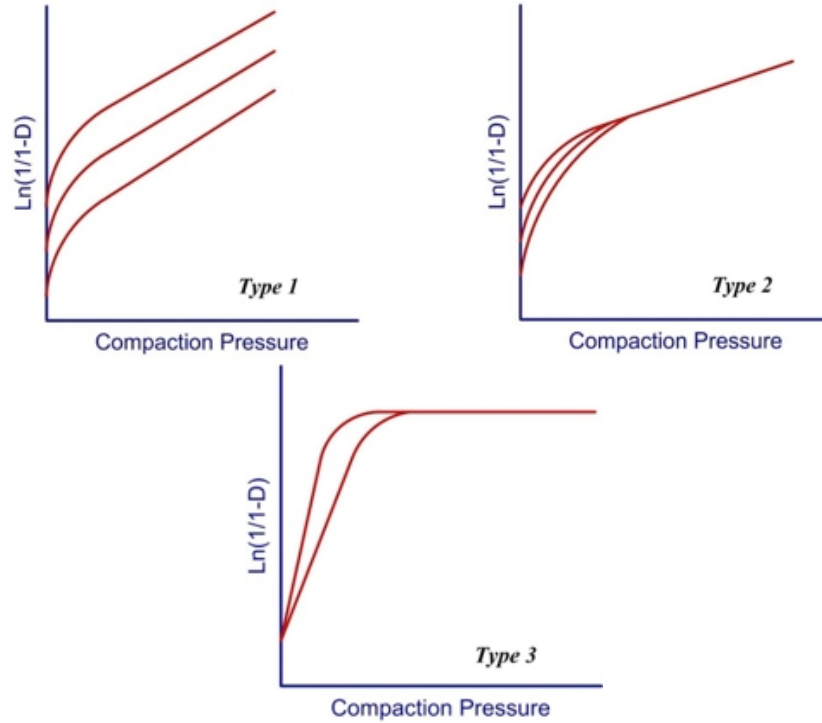


Figure 4.4: Different types of compression profile distinguished by the Heckle equation

plained by the permanent rearrangement or die filling during the initial stage of compression. Region 2 is the linear part of the plot in which irreversible or permanent particle deformation is the controlling mechanism. In this stage, many intra-particle voids are being filled, which leads to the increase in the number of contact points per unit volume and consequently increases the powder strength. Region 3 is the second non-linear part, with the increasing slope, that occurs when elastic deformation dominates the process. The third region can only be observed clearly at a very high pressure or higher than specific pressure for soft materials.

Heckel's plots were classified into three groups based on compressing different particle-size fractions of various powders by [Celik, 1992, Hersey and Rees, 1971], (Figure 4.4).

In Type 1, particles with different size fractions have different initial packing fractions and the plots remain parallel as the compaction pressure increases, indicating that the variation in initial powder bed density results in different final bed densities under any particular applied pressure. This type

of consolidation is mainly related to densification by plastic flow and later on by particle rearrangement. Type 2 powders consolidate by particle fragmentation, which can be observed by looking at the slightly curved region at the initial stage of compaction. Later, a single relationship occurs beyond a certain pressure, regardless of the initial bed density. This type is independent of particle size and is thought to be a result of the significant destruction of particles by fragmentation. The differences in initial densities have no effect on further densification as the particles during the initial stage have undergone a significant fragmentation and their subsequent compaction process is by plastic deformation. In the case of Type 3, the plots show an initial steep linear region followed by a very low volume reduction. This type can be related to the absence of rearrangement of particles at the initial stage of compaction while the densification occurs by plastic deformation.

Even though the Heckel equation is useful in analyzing the compression profile in the powder industry, its applicability in the pharmaceutical industry is questionable and has limitations in describing densification at low and very high compression pressures [Roberts and Rowe, 1985, Hersey and Rees, 1971, Sonnergaard, 1999]; e.g., at considerably high pressure the Heckles plots are often curved upward indicating the inadequacy of the function to describe volume changes in the powder column at low porosity and near to the apparent particle density of a material.

4.4.2 Kawakita Equation

In 1965, Kawakita found a relationship between the volume reduction of a powder column with respect to the applied compression pressure. This equation is based on the assumption that the confined powder in a die subjected to the pressure is in equilibrium at all stages of compression, i.e. the product of the increased applied pressure and the volume reduction is constant.

This equation is written as follows:

$$C = \frac{V_0 - V}{V_0} = \frac{abP}{1 + bP} \quad (4.18)$$

Where C is the volumetric shrinkage, V_0, V , a and b are the initial volume, the volume of a powder column under the applied pressure, P , and constant

characteristics of the powder being compressed, respectively. The determination of the initial powder volume is very important and the common method is to completely fill up the die with known dimension with powder without disturbing the powder that is already inside. After, the initial volume of the bulk is recorded at the moment of the first detected force that punch applies to the powders bed surface.

This equation can also be written by means of density and porosity as:

$$C = 1 - \left(\frac{\rho_0}{\rho_p}\right) = \left(\frac{E_0 - E_P}{1 - E_P}\right) \quad (4.19)$$

Where ρ_0, ρ_P, E_0 and E_P are initial bulk density, bulk density at pressure P , initial porosity, and porosity at pressure P , respectively. Rearranging the first equation gives us a linear form equation as:

$$\frac{P}{C} = \frac{P}{a} + \frac{1}{ab} \quad (4.20)$$

By plotting the values of $\frac{P}{C}$ versus P , the constants can be determined. The constant a represents the strain or the degree of compression and is given by the reciprocal of the slope from the linear part of the plot. It is equivalent to the value of C at infinitely high pressures, $C_\infty = \frac{V_0 - V_\infty}{V_0} = a$. The value of a describes the compressibility of a powder by indicating the maximum volume reduction in a powder under compression while the constant b describes an inclination toward volume reduction [Alderborn and Nystrom, 1996, Kawakita and Lüdde, 1971, Carneim, 2000].

Extrapolating the linear region of the plot, right at the intercept of $\frac{P}{C}$ and the vertical axis, gives a value for $\frac{1}{ab}$ (Figure 4.5). In the following graph (Figure 4.6), the plot of C versus P is shown. This plot is another interpretation of the Kawakita parameters in mathematical terms.

The mathematical models presented here are based on empirical correlations between the applied pressure and volume reduction of the material being compacted. These models carry useful information about determining the stages of compaction and the dominant mechanism taking place, although Kawakita's equation seems to be more applicable at higher pressure ranges

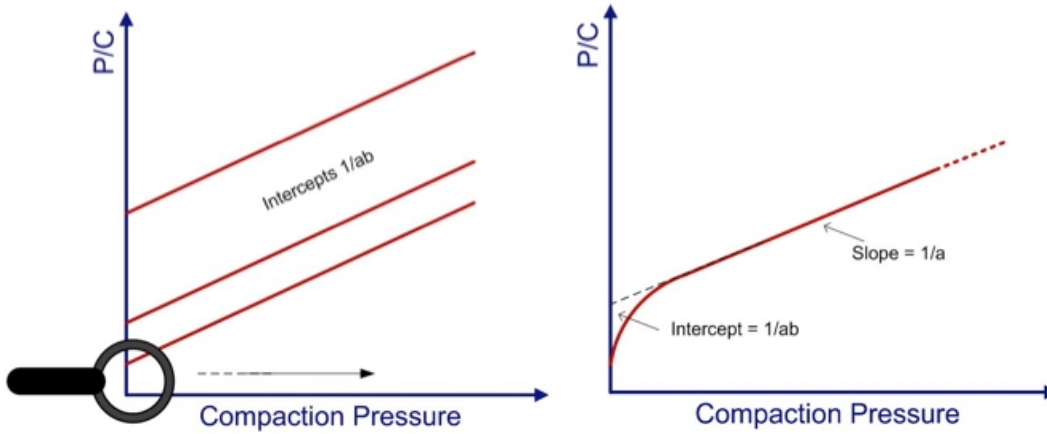


Figure 4.5: Graphical representation of Kawakita's equation

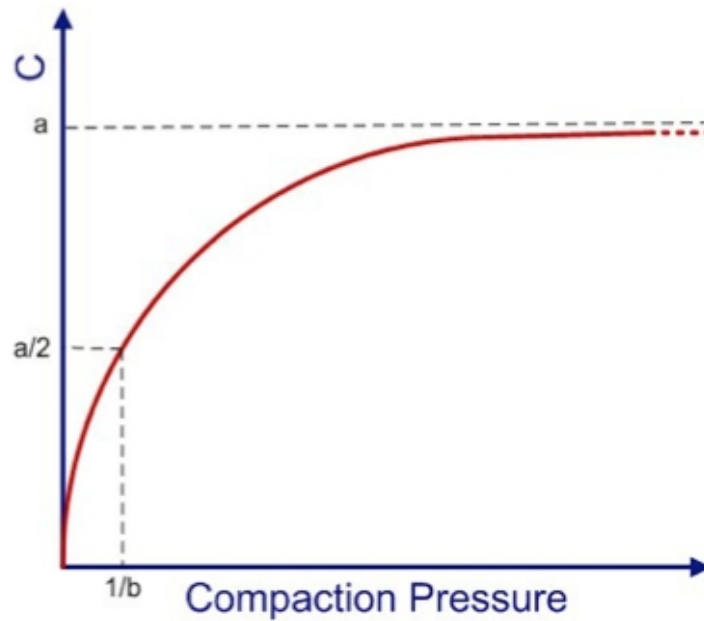


Figure 4.6: A schematic description of a typical compression pressure curve and interpretation of the Kawakita parameters

(tableting pressure). Even though Heckels and Kawakitas equations are known to be two of the most useful equations in the pharmaceutical field, there is considerable controversy over which of the two models is the best or most valid [Alderborn and Nystrom, 1996, Denny, 2002].

Compressibility Index (%)	Flowability	Hausner Ratio
≤ 10	Excellent	1.00 – 1.11
11 – 15	Good	1.12 – 1.18
16 – 20	Fair	1.19 – 1.25
21 – 25	Passable	1.26 – 1.34
26 – 31	Poor	1.35 – 1.45
32 – 37	Very poor	1.46 – 1.59
> 38	Very,very poor	> 1.60

Table 4.1: Scale of flowability [Pharmacopeia, 2011a]

4.5 On the Hausner Ratio and Compressibility Index

The *Hausner Ratio* and *Compressibility Index* are two popular and simple parameters for predicting the compressibility of powders. These methods have the potential to describe the powder handling behavior by showing the inter-particle interaction of powders at different levels of compaction. Both of these can be measured using tapped and bulk volume or density of powder [Pharmacopeia, 2011a]. The Hausner ratio, HR, was first proposed by Hausner [1967] as a characteristic of the friction condition between metal powders and it was also used to characterize the flow and compaction behaviors of powder. The compressibility index, CI, is another way of expressing the difference between the tap and aerated densities. (Aerated density is also known as apparent or poured density, which is described in section 3.6.4). In the other words, CI is the percentage increase in density. The compressibility index and Hausner ratio are calculated by the following formulas:

$$CI = 100 \frac{V_b - V_t}{V_b} = 100 \frac{\rho_t - \rho_b}{\rho_t} \quad (4.21)$$

$$HR = \frac{V_b}{V_t} = \frac{\rho_t}{\rho_b} \quad (4.22)$$

Where the subscript b represents initial bulk volume or the unsettled apparent volume prior to the initial stage of compaction and t represents tapped volume. Based on these parameters a scale of flowability can be developed [Rios, 2006], as shown in Table 4.1:

These two methods strongly depend on the methodology used. In short, HR and CI, according to the Pharmacopeia [2012], are indicators of a given powders propensity for compression. Even though the compressibility index has become very popular in evaluating the powder handling behavior, the information it provides is no more useful than that provided by the Hausner ratio [Grey and Beddow, 1969, Sørensen et al., 2006]. However, the Compressibility index is more practical in data analysis since it is used in the percentage scale.

These well-established methods and simple to measure factors seem to be very useful in characterizing powder behavior [Kostelnik and Beddow, 1971]. These methods have been proposed as the sole measure of powder flowability [Amidon et al., 2009]. Despite the usefulness of these parameters in characterizing powders, their limitation in analyzing samples with small particle diameters such as respiratory drugs and spray-dried micro particles should not be overlooked and it will be explained in section 6.9 of this thesis.

Chapter 5

Experimentation

5.1 Introduction

In the pharmaceutical industry, evaluating powder properties and their behavior is of prime importance, as it will affect the manufacturing processes and final products. Various techniques and instruments have been introduced to deal with this issue.

The main goal of the research described in this thesis is to introduce a novel technique that is an efficient alternative method for measuring the compressed bulk density of powder on a very small scale. In the pharmaceutical industry, the cost and scarcity of some valuable samples demand for a physical characterization technique that has good repeatability while needing only a very small amount of sample. For the sake of implementing the aforementioned technique, a new instrument was developed to evaluate the physical behavior of any type of powder, either respiratory or in a different solid dosage form, as only a very small amount of sample is needed (less than 50 mg, particle-size dependent). The new technique is mainly based on uniaxial lowpressure compression that was designed to introduce a cost-effective approach to determine the compaction behavior of samples at the initial stage of compaction process for powders that are going to be tableted, a process which is often overlooked by the related studies. The new setup was constructed in a way to avoid introducing random errors into the measurement made by the operator. To access the full description of the instrumentation procedure, please proceed to Appendix C.

5.2 Experimental Consideration

The following are factors that need to be considered in the development of the experimental method:

1. Uniaxial compression is a standard technique and this type of method should also be used here to allow comparison of the results with literature..
2. The way die is filled should be stated, especially when fine powders are being used, e.g. whether powder is poured freely or a funnel or vibration is used. It is important to try as much as possible to have the same initial porosity, when repeated experiments are conducted on the same sample.
3. The internal use of a lubricant, mixed within the powder bed, should be avoided because the lubricant can affect the powder beds physical behavior and its densification response. An external lubrication can be used to reduce the die-wall friction.
4. Materials under test should be characterized well, i.e. particle-size distribution, particle morphology, and the presence of aggregates within the bulk.
5. In order to minimize friction, the ratio of the height and diameter of the die should be optimized.
6. The way the data is measured should be stated, i.e., whether the measurement was obtained at pressure, in die or out of die (to be explained).
7. At high pressures, the elastic response of the instruments should be considered, calibrated and corrected.

5.3 Instrumentation

Nowadays the instrumentation of presses plays an important role in research and development and is very useful for monitoring and controlling the compaction processes in the production of solid dosage form in the pharmaceutical industry.

To plot and analyze the force-displacement curve, an accurate measurement of punch movement and the applied pressure is required. Two ways of measuring that graph are present: at pressure, in die and out of die. At-pressure measurement determines the volume reduction of the bulk of powder in a die at the time when the pressure is being exerted, while the out-of-die technique measures the volume reduction of the bulk when the compact is ejected from the die.

For the system under research, due to the viscoelastic behavior of almost all of the tested pharmaceutical powders, measurements were conducted based on the at pressure approach. We chose this method since the errors resulted by the instantaneous elastic expansion or the spring-back behavior of the compact after ejection from the die is inevitable.

5.4 UAlberta Density Tester

Formerly, a simple prototype had been introduced that was able to measure solely the compressed bulk density of pharmaceutical samples at a very small scale. It was a very simple version of the present instrument. It comprised a small cavity as the die, an analytical balance as the force-measuring component, a micrometer as a punch. The micrometer head was vertically aligned with the cavity using a custom clamping mechanism and a vertical support structure. This instrument was a manually-operated apparatus that had some limitations:

- Random errors made by the operator were inevitable.
- Placing the filled die on the balance and aligning it with the punches tip were problematic that sometimes resulted in a great deal of friction between the die-wall and the punch, which in turn affected the consistency, repeatability and accuracy of the results.
- Operating the instrument when it was placed in the environmental chamber for conducting experiment in different environmental condition was really difficult.

- Balance and the micrometers position had to be calibrated at the beginning of each experiment.
- Measurement and the data processing were really slow (sometimes it took about an hour to do one single test) and the results were inconsistent.
- The deflection rate of the analytical balance was relatively high that led to the generation of inaccurate results.

The present compressed bulk density tester is similar to a uniaxial tabletting machine that works at a very low compression force to provide the high precision that is required to determine the density of particulate material on a very small scale. In addition to the accuracy and accommodating the new approach of determining compression-derived parameters, this instrument pertains to new improvement in both design and control, which result in economy of manufacturer.

The apparatus shown in Figure 5.1 was manufactured to improve the previous setup by removing errors made by manually controlling the setup that resulted in low repeatability and inaccuracy. Moreover, after realizing the influence of humidity and temperature conditions on the results, the new instrument was developed and designed in a way to make measurements possible in any required testing conditions.

Due to the difficulties experienced with the previous setup in calibrating the position of the powder pan with respect to that of punch, the new instrument is equipped with specific means for holding and aligning the powder pan below the actuator.

5.5 Instrumentation

A non-rotary, linear actuator (Physics Instruments, M-229.26S, 25 mm), as shown in Figure 5.2, (part #6) was used as a punch to exert the axial pressure on a powder in the die. A Mercury stepper motor controller (Physics Instruments, C-663 Mercury Step) was used as an interface to control the actuator. This type of actuator was chosen because it has a threaded head to which tips with different sizes and shapes can be attached. Plus, the required advancement speed and the proper punch sizes were also considered. In this study,

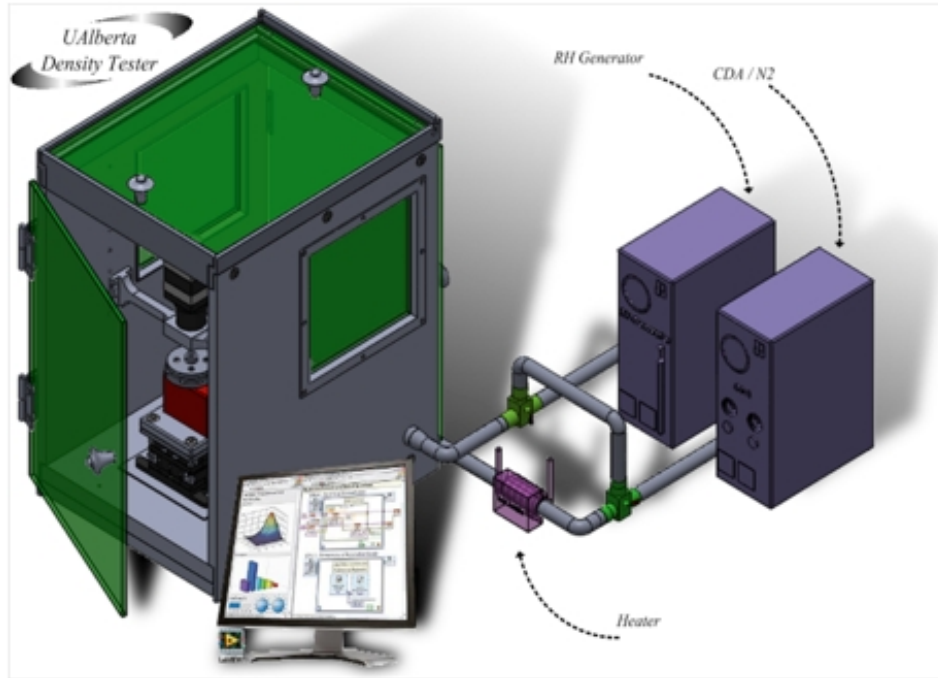


Figure 5.1: Schematic of the UAlberta Density Tester [Shamsaddini-Shahrbabak and Vehring, 2012]

the actuator may also be called a micrometer or punch.



Figure 5.2: PI Actuator and Step Motor

To record the real-time pressure being exerted on a powder under test, a load cell (FuTeK, LRF400, 10 lb.), (part #7), was used. A USB interface (FuTeK, USB220) was used to control and calibrate the loadcell (Figure 5.3).

The very small cylindrical die shown in Figure 19 was made out of stainless



Figure 5.3: FuTeK loadcell and USB Interface

steel to hold the powder. In this thesis, the words cavity and sample pan may also be used when referring to this die. Several dies (part #10) with different diameters and heights were designed and manufactured to examine the effect of wall friction so as to choose the most reliable one. However, in this study, most of the results were obtained using the die with an internal diameter and height of five and six mm, respectively (Figure 5.4).

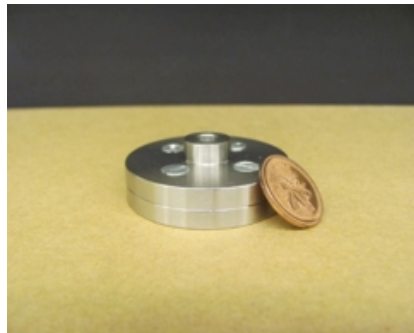


Figure 5.4: Sample pan

To increase the accuracy of the result, which is an important criterion in this instrument, the position of the punch and die should be perfectly aligned with each other. To address this issue and reduce the friction and avoid any difficulties in the punch and die alignment process during assembly, two translation stages (part #20 & 21) and a base plate (part #19), (MT1 and MT401 model, Thorlabs) were used (Figure 5.5). As the graph shows, two translation stages were placed orthogonally with respect to each other so the upper stage can be moved in x and y direction.



Figure 5.5: Thorlabs Translation Stages and Base plate

The translation stages were placed and mounted on the centre of the front side of the frame so as to provide enough room for reaching the aligning micrometers. On the frame below the centered stationary plate, enough space was considered by applying a 5 mm boss extrusion (part #16) to provide enough room to access the lower micrometer. Five threaded holes were applied on the surface of this part (part #16) for moving the stages even more than the two micrometers limit in either direction. Figure 5.6, Figure 5.7, and Figure 5.8 illustrate the front, side, and back views of the uniaxial density tester, respectively. The apparatus comprises a main frame (part #1) with a base (part #1) and side supports (part #2). The size of the frame is designed mainly for easy access to the inside for connecting cables and wires, and for replacing the micrometers tips.

The present apparatus is equipped with two front and back doors (part #3) that were pivotally (part #4) installed on the machine box to swing away. This provides easy access and easy removal of dies and punches for servicing, aligning the sample holder, cleaning/replacing punch tips (part #18), and connecting or disconnecting the interface and controller cables and wires (part #11 & 12). Doors are locked in place with two magnetic locks (part #9). Foam tape (part #5) was used to seal the box. Two windows (part #17) on either side of the frame were installed to make it possible to view the alignment process and micrometer calibration.

The drawings for the design of the present apparatus are in Appendix A.

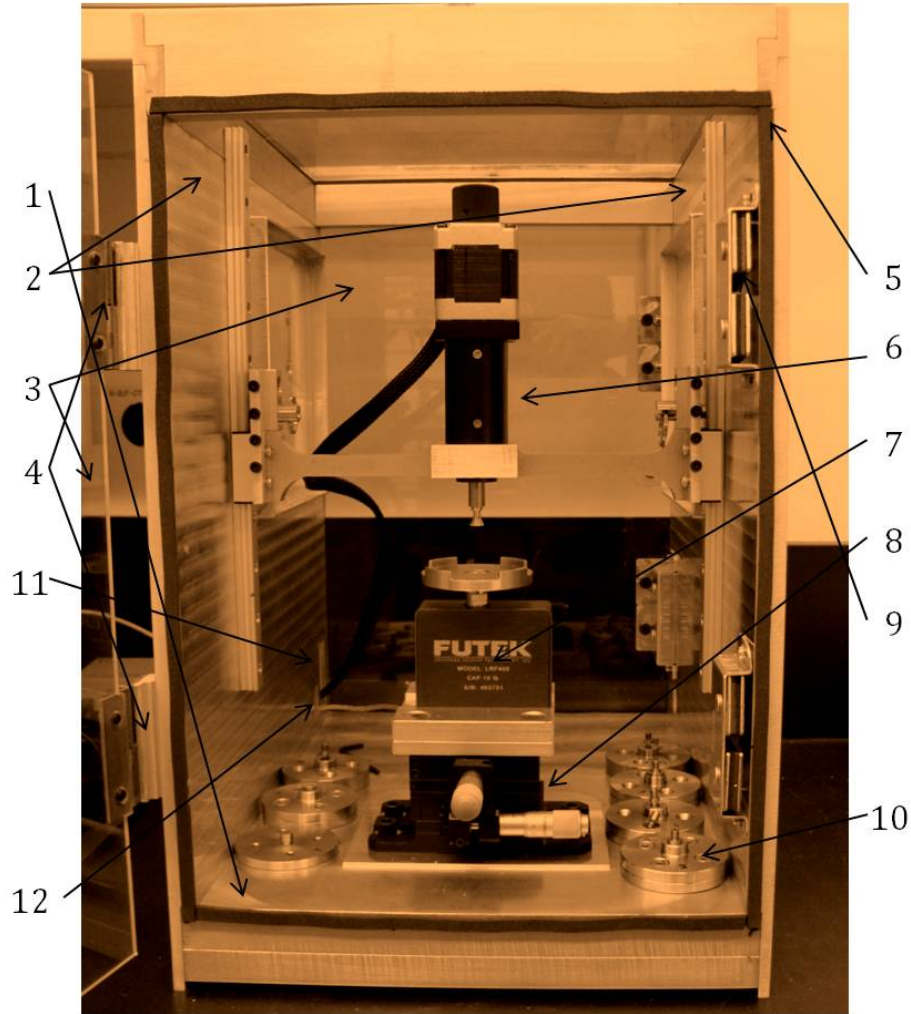


Figure 5.6: Apparatus front view photo

Two vertical guide rails (part #13) were installed and mounted on the sidewalls. Two carriages (part #14) were used to guide the actuator vertically along the guide rails, in case the actuator needs to be moved vertically farther than its movement range, e.g., for installation or cleaning purposes. The actuator is placed in a holder (part #22), which is connected from both ends to the guide rails carriages by the spring locks (part #15). Spring locks were used to facilitate driving and locking the actuator in the appropriate position.

Part #23 is the loadcell holder that was designed to mount and fix the loadcell in the translation stages. The sample pan holder (part #24) is a tray that is screwed to the top of the loadcell to hold the powder pan. To facilitate changing the testing environment conditions, the base of the apparatus is utilized to accommodate a series of piping for cryogenic fluid. Two NPT

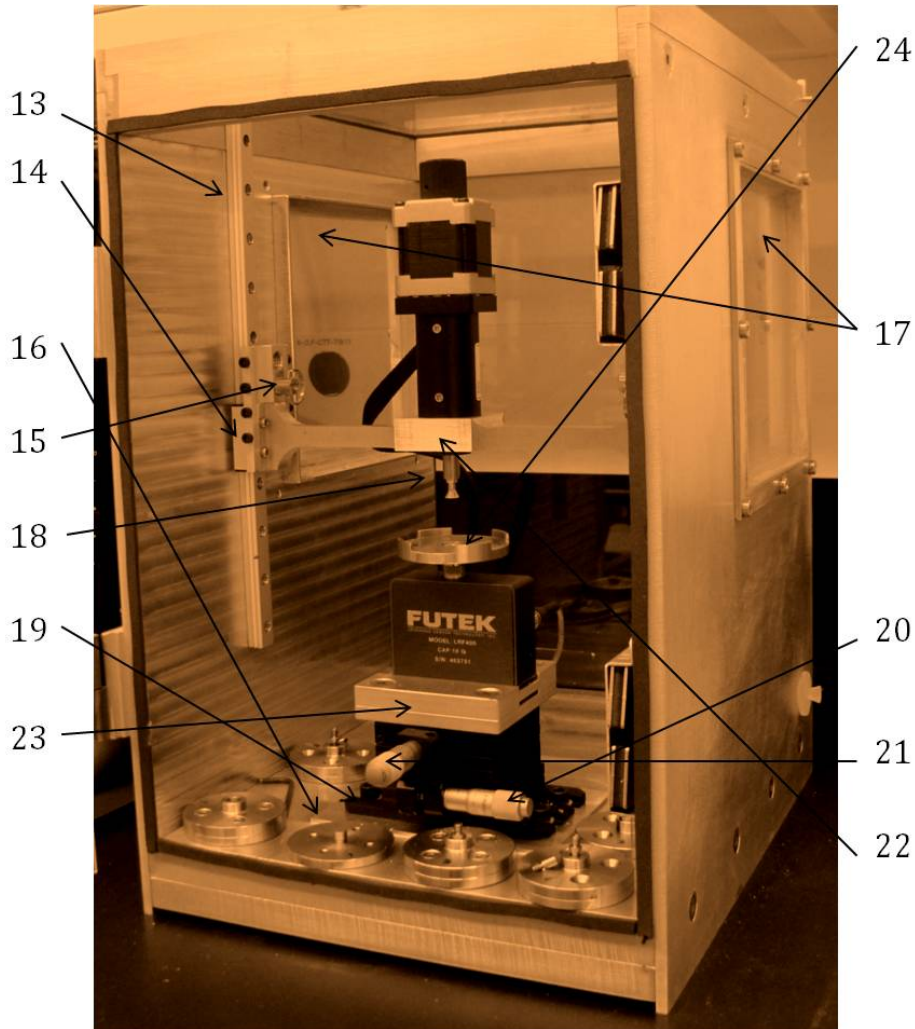


Figure 5.7: Apparatus side view photo

connecting ports (part #26) were designed as the inlet and outlet ports that can be accessed from the backside of the base.

A top glass door was built to further increase access to the equipment inside the box. The top door was hinged to the back end of the frame using two 3 mm pins (part #27) this makes it possible to remove the door completely for cleaning and maintenance.

Another port was placed on the left side of the frame (part #25) to be connected to a humidity generator, to make it possible to change the humidity inside the chamber. The base comprises two top and bottom parts that fit together using a 5 mm boss extrusion in one and a cut extrusion (part #28)

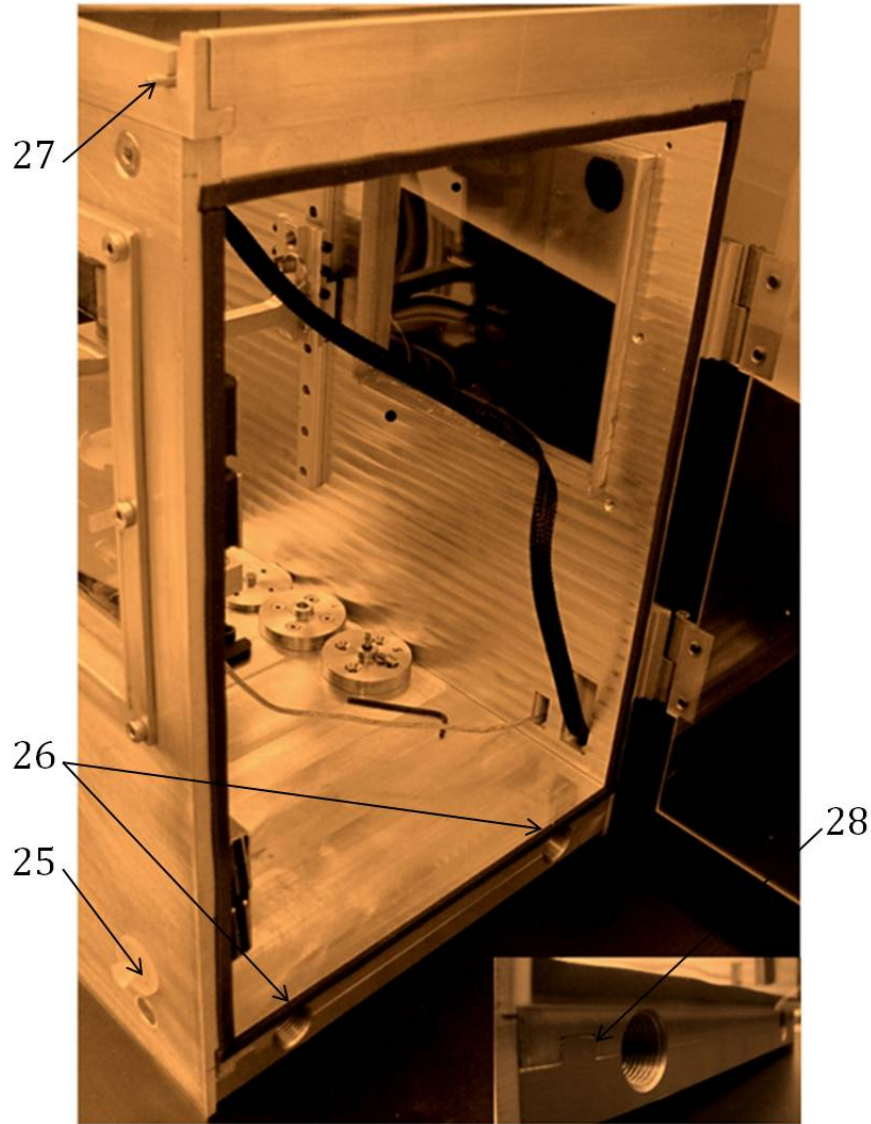


Figure 5.8: Apparatus back view photo

in the other to avoid any problems that may occur due to the expansion or contraction during heating up or cooling down. A rubber insulation sheet is also used between the two base plates to seal the piping edges and to prevent any fluid from penetrating to the base of the body.

The entire measuring equipment was installed in a box that can be sealed to accommodate any humidity conditions in the box, preventing the air currents in the room from affecting the operation of the load cell as well as preventing any dirt from entering the box from around the stage motor and the accurate loadcell. Other features are related to the economies of construction and op-

eration.

5.6 Data Acquisition Using NI LabVIEW

National Instrument LabVIEW NI 2011 software was used for data acquisition and to control the UAlberta Density Tester. LabVIEW is a visual programming language. One of the main reasons for using LabVIEW software to control the set-up was its extensive support for accessing hardware instrumentation. LabVIEW is a unique graphical programming language, which is very reliable in designing and controlling measurement systems. The loadcell and actuator were interfaced and connected to a PC using a USB connector. Each was assigned a COM port. The baud rate, data bits, parity, stop bits and flow control were set to 9600, 8, None, 1 and None, respectively. Having synchronized these five parameters in the instruments and computer, the device is ready to be controlled and executed. The general command sets from the instruments technical manual was used to receive data from both instruments. For the full description of coding procedures please proceed to Appendix B.

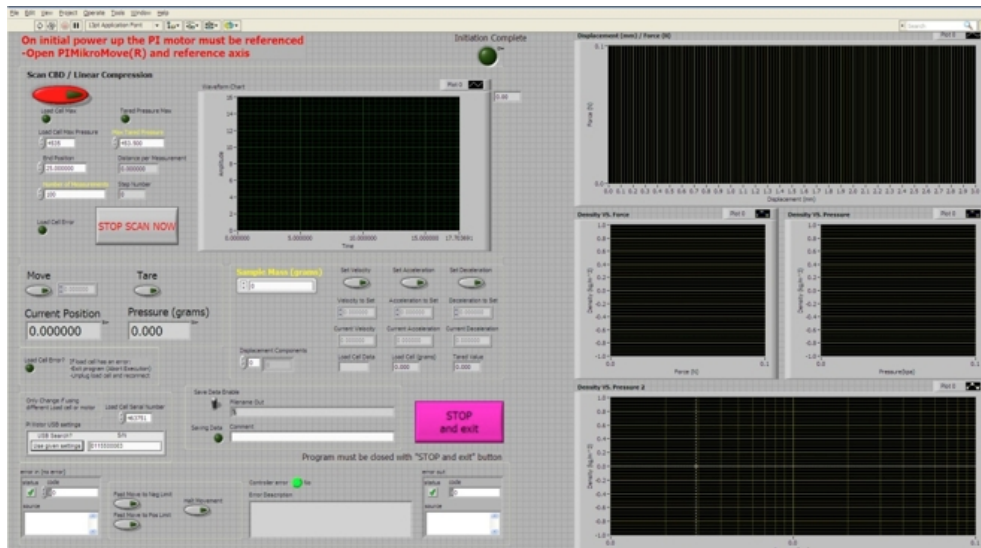


Figure 5.9: LabVIEW front panel 1

Briefly, the program is capable of simultaneously moving the punch axially into the sample pan while measuring the axial force being exerted on a loadcell. This measurement approach is called the at pressure or in die approach and it was chosen over the out of die approach to avoid any inaccuracy within

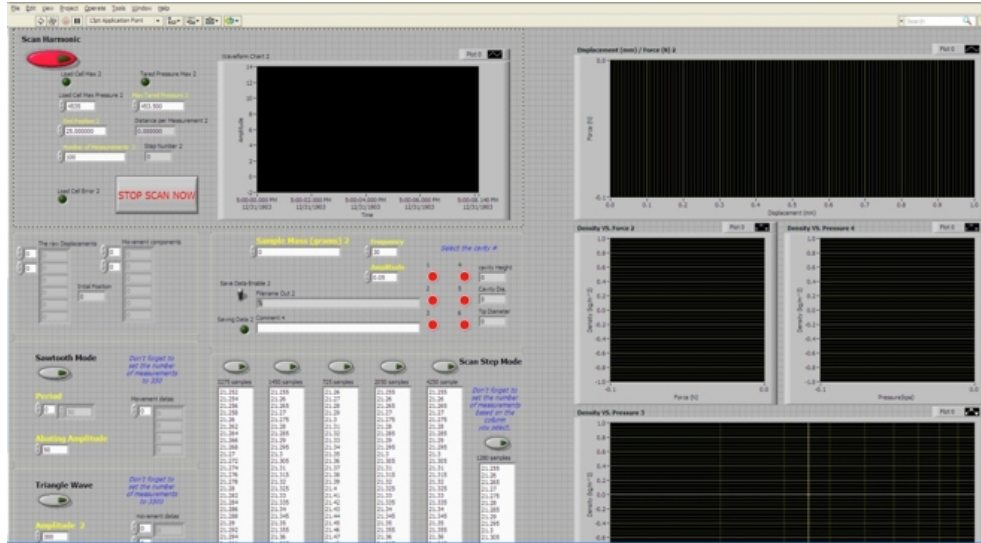


Figure 5.10: LabVIEW front panel 2

the results due to the elastic behavior of the compact after it was ejected from the die. Lab VIEW programming facilitates the controlling procedure of the apparatus by providing the front panel, Figure 5.9 and Figure 5.10, with which all of the controlling buttons would be available at the users fingertip. The numbers of controlling modes that are available include punch speed, acceleration, deceleration, maximum force and the number of measurements per test.

5.7 Measurement

Powder is gently poured, without using any funnel, into the cavity without disturbing it. A flat spatula can be used to make the surface of the powder level with the horizontal edge of the cavity. A sample pan is then placed on a balance with the repeatability of 0.01 mg accuracy (Denver Instruments, Pinnacle Series PI-225D) to determine the mass of the powder. An attempt was made to pour the same amount of powder for every measurement of every similar sample in order to keep measurements stable as much as possible. The apparent volume of the powder in the die is equal to the volume of the cavity. With this instrument there is no need to record the micrometer-zeroed position or the apparent volume, as these will be recorded automatically when the measurement begins.

The sample pan is placed on the loadcell pan. The loadcell should be tared

	A	B	C	D	E	F	G	H	I	J
1	LabVIEW Measurement									
2	Writer_Version	2								
3	Reader_Version	2								
4	Separator	Tab								
5	Decimal_Separator	.								
6	Multi_Headings	No								
7	X_Columns	No								
8	Time_Pref	Relative								
9	Operator	shamsadd								
10	Date	9/17/2012								
11	Time	56:29.7								
12	***End_of_Header***									
13	Channels	8								
14	Samples	241	241	241	241	241	241	241	500	
15	Date	9/17/2012	9/17/2012	9/17/2012	9/17/2012	9/17/2012	9/17/2012	9/17/2012	9/17/2012	9/17/2012
16	Time	56:29.7	56:29.7	56:29.7	56:29.7	56:29.7	56:29.7	56:29.7	56:29.7	56:29.7
17	X_Dimension	Time	Time	Time	Time	Time	Time	Time	Time	Time
18	X0	0.00E+00	0.00E+00	0.00E+00	0.00E+00	0.00E+00	0.00E+00	0.00E+00	0.00E+00	0.00E+00
19	Delta_X	1	1	1	1	1	1	1	1	1
20	***End_of_Header***									
21	Columns	Position	Displacement (mm)	Balance(g)	Force(N)	Volume(mm^3)	Density(kg/m^3)	Pressure(kpa)	Time (s)	Comment
22		18.75	0	0.003541	3.47E-05	167.059298	299.294924	0.001066	0	
23		18.76	0.01	0.003541	3.47E-05	166.728488	299.888763	0.001066	0.109379	
24		18.77	0.02	0.005311	5.21E-05	166.397677	300.484963	0.0016	0.218758	
25		18.78	0.03	0.005311	5.21E-05	166.066867	301.083539	0.0016	0.328136	
26		18.79	0.04	0.005311	5.21E-05	165.736056	301.684504	0.0016	0.437515	
27		18.8	0.05	0.005311	5.21E-05	165.405246	302.287873	0.0016	0.546894	
28		18.81	0.06	0.015934	0.000156	165.074435	302.893661	0.004799	0.656273	
29		18.82	0.07	0.015934	0.000156	164.743625	303.501881	0.004799	0.765652	
30		18.83	0.08	0.024785	0.000243	164.412814	304.112548	0.007465	0.875031	
31		18.84	0.09	0.024785	0.000243	164.082004	304.725679	0.007465	0.984409	
32		18.85	0.1	0.024785	0.000243	163.751193	305.341286	0.007465	1.093788	

Figure 5.11: LabVIEW output, measurement data

prior to initiating the measurement. Then the micrometer tips will be brought into close proximity of the edge of the cavity without disturbing the powder inside the cavity. The measurement is then initiated and the measurement data recorded simultaneously on the spreadsheet that will be accessible when the measurement is complete (Figure 5.11).

Care should be taken to zero the micrometer before initiating the measurement. This can be achieved by visually aligning the micrometer's tip with the horizontal edge of the cavity. Thereafter, this can be set as the zero point and is stated as the displacement in its column in the spreadsheet. Density ($\frac{kg}{m^3}$) is measured by dividing the mass, which is constant by the volume at different powder heights (i.e., the volume decreases as the micrometer advances in the cavity). Pressure is the ratio of previously determined force over the surface area of the micrometer's tip. The time column shows the elapsed time at each setpoint from the starting point of the previous micrometer's advancement. The number of samples is also shown in the header.

5.8 Errors and Uncertainties

No measurements are ever exact: there are number of factors that give rise to uncertainties and errors in a measuring system, which result in some deviations between the actual value and the measurands. The smaller this deviation, the more expensive will be the measuring system. Error is simply defined as the difference between the true value and the measured value. Generally, there is no such a value as the true value, only that we have a value that lies within a range of uncertainty [Wheeler and Ganji, 1996]. Errors in experiments fall into two categories: systematic errors, and random errors. Systematic errors are associated with a particular measuring system which gives consistent and repeatable errors. For example, a tape measure that has a 5 cm cut off, gives a consistent measurements that are 5 cm higher than the true values. One of the main sources of systematic error in a measurement system is due to the calibration as such a non calibrated system will introduce a consistent error to the measurands. Systematic errors shift all results by a significant amount in the same direction as the measurands, e.g.:

The treatment of systematic errors is very difficult and for our purpose it is suffice to recognize its existence in our results; we should mention that there are some systematic errors within our system that shift our measurands high or low, and we should also mention where these errors may be introduced into the system.

On the other hand, random errors are associated with the lack of repeatability that could happen due to the lack of experimenter precision which results in a range of random errors, Figure 5.12. Due to the randomness of these errors, there is an equal chance that these errors will be above or below the true value. The best way to interpret these errors is to take as many reading as possible and find the mean measured value. The best estimate is the mean of the repeated readings because it is impossible to know the true value [Wheeler and Ganji, 1996]. Random and systematic errors can be estimated using the following formulas:

$$\text{random error} = \text{reading} - \text{mean measured value} \quad (5.1)$$

$$\text{systematic error} = \text{mean measured value} - \text{true value} \quad (5.2)$$

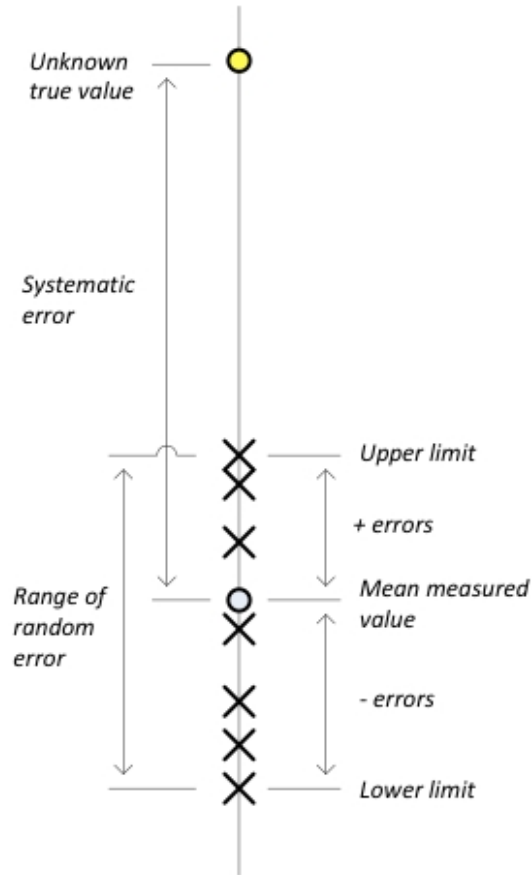


Figure 5.12: Distinction between systematic and random errors

$$\text{mean measured value} = \frac{\text{upper limit value} - \text{lower limit value}}{\text{number of repeated readings}} \quad (5.3)$$

In digital read out, the reading error is taken as the plus or minus one digit on the last readout number, e.g., if a load cell display shows 13.027 grams, the reading error would be 0.001 grams. Calibration error is associated with linearity between the input and the output that indicates how well the measuring system has been made.

5.8.1 Sources of Error

1. Experimenter-unpredictable
2. Method of measurement-unreliable experimental procedure
3. Object to be measured-non uniform thickness, edges not well defined
4. Instrument- may be faulty, not zeroed properly or out of adjustment

Instruments	Uncertainties (due to systematic errors)
Stepper-Mike linear Actuator	Unidirectional repeatability $\pm(2\mu m)$
Loadcell	Reading error 0.001 (g) (5 sps)
Loadcell	Deflection error 0.001 (mm) at high load (10 lb)
Denver Instrument (balance)	Reading error 0.00001 (g)
Actuator's holder	Deflection error
Loadcell	Calibration error
Punch's diameter (d_p)	manufacturing difficulties
Die's diameter (d_d)	Manufacturing difficulties
Die's height (h_d)	Uncertainties included in the measuring system

Table 5.1: Uncertainties associated with systematic errors involved in UAlberta density tester

The uncertainties involved in density measurement for repeated measurements using UAlberta density tester are tabulated as follows, (Tables 5.1 and 5.2):

Considering all of the above variables, compressed bulk density and compaction pressure can be written as:

$$\rho_{CBD} = f(d_d, h_p, h_d, S_i, S_r, m') \quad (5.4)$$

$$P = f(F, F_f, d_p) \quad (5.5)$$

5.8.2 Error Propagation

Having variables, each with their individual uncertainties, we need to combine these quantities to come up with a final result of our experiments. Determining uncertainties in a function of these variables can be used to combine results of our measurements. For instance, for the compressed bulk density we have:

$$\rho_{CBD} = \frac{M}{V} = \frac{M}{\frac{\pi d_d^2}{4} \cdot H} \quad (5.6)$$

Equipments	Uncertainties (due to random errors)
Friction between punch and die (F_f)	Due to misalignment
Micrometer zeroed position (S_0)	Non-uniform powder's bed surface in the die
Sample mass (m)	Non-uniform sample masses (due to cohesivity)
Sample height (h)	Non-uniform sample height (due to particle's irregular shapes)
Force exerted on the powder bed (F)	Non-monotonous response to the compaction pressure (high porosity)

Table 5.2: Uncertainties associated with random errors involved in UAlberta density tester

M is corresponded to the reading error associated with analytical balance for the initial weighing of the sample. H is correspondent to the height of the powder bed that includes terms for the actuators incremental movements and powders height, that both considering their own uncertainties can be written in the form of:

$$M = m' + dm' = m' \pm 0.00001 (g) \quad (5.7)$$

m and dm are the mass of the powder and its uncertainty, respectively.

$$H = H_p - S_a \quad (5.8)$$

H_p and S_a are powders height and actuators position, respectively.

$$\begin{aligned} H &= (h_d - h_p) - (S_i - S_r) \\ &= (h_d \pm 0.000004 m) - (S_i \pm 0.000002 m) \end{aligned} \quad (5.9)$$

$$H_p = (h_d \pm 0.000004 m) = (h' \pm dh') \quad (5.10)$$

$$S_a = (S_i \pm 0.000002 m) = (S' \pm dS') \quad (5.11)$$

h_d is the actual height of the die and the uncertainties (h_p) associated with it is corresponded to the very thin layer of powder with the thickness of $4 \mu m$

(estimated and particle size dependent) that may be above or below the horizontal edge of the die. S_i is the initial position of the punch that advances into the die and its uncertainties (S_r) is related to the unidirectional repeatability of $2 \mu m$, noted in the instruments technical manual.

$$\frac{M}{\frac{\pi d_d^2}{4} \cdot H} = \frac{m' \pm 0.00001(g)}{\frac{\pi d_d^2}{4} \cdot H[(h_d \pm 0.000004(m)) - (S_i \pm 0.000002(m))]} \quad (5.12)$$

H can be reported in the form of:

$$H = H' \pm dH' \quad (5.13)$$

where H and dH are the measured quantity and its uncertainty, respectively.

$$H' = h' + S' = h_d + S_i \quad (5.14)$$

Considering the height of the die (initial height of the powder bed) to be 5.5 mm, and the micrometer zeroed position to be 0 mm. (when the punch is horizontally aligned with the edge of the die).

$$H' = (5.5E - 3(m)) + 0 = 0.005(m) \quad (5.15)$$

Using the standard deviation to compute the overall uncertainties between these two values:

$$\begin{aligned} dH' &= \sqrt{(dh')^2 + (dS')^2} \\ &= \sqrt{0.000004^2 + 0.000002^2} \\ &= 4.47E - 6 \end{aligned} \quad (5.16)$$

Thus:

$$H = H' + dH' = 0.005 \pm 0.0000045(m) \quad (5.17)$$

The error associated with the denominator of the main equation can easily be determined after multiplying the calculated error with the constant ($\frac{\pi d_d^2}{4} = 3.3E - 5$, (considering H to be 3.1416 and d_d to be 6.5 mm).

$$\rho_{CBD} = \frac{m}{V} = \frac{M}{\frac{\pi d_d^2}{4} \cdot H} \quad (5.18)$$

$$\begin{aligned} V &= V' \pm dV' \\ &= \frac{\pi d_d^2}{4} (H') \pm \frac{\pi d_d^2}{4} \\ &= 0.000033(0.005) \pm 0.000033(0.0000045) \\ &= 0.00000016 \pm 0.00000000015(m^3) \end{aligned} \quad (5.19)$$

$$\rho_{CBD} = \frac{M}{V} = \frac{m' \pm dm'}{V' + dV'} = \frac{m' \pm 0.00000001(kg)}{0.00000016 \pm 0.00000000015} \quad (5.20)$$

Where m is the mass of the powder in kg and V is the volume of the bed of powder in m^3 .

Total error associated with the compressed bulk density can be computed as follows:

$$\rho_{CBD} == \rho' \pm d\rho' \quad (5.21)$$

$$\rho' = \frac{m'}{V'} = \frac{m'}{0.00000016} \quad (5.22)$$

Using standard deviation to determine the uncertainties associated with the above fraction:

$$\begin{aligned} \frac{d\rho'}{\rho'} &= \sqrt{\left(\frac{dm'}{m'}\right)^2 + \left(\frac{dV'}{V'}\right)^2} \\ &= \sqrt{\left(\frac{0.00000001}{m'}\right)^2 + \left(\frac{0.00000000015}{0.00000016}\right)^2} \\ &= \frac{d\rho}{\frac{m'}{0.00000016}} \end{aligned} \quad (5.23)$$

$$d\rho = \sqrt{(3.9E - 3) + (34332275.39m^2)} \quad (5.24)$$

$$\rho_{CBD} = \rho' \pm d\rho' = \frac{m'}{0.00000016} \pm \sqrt{(3.9E - 3) + (34332275.39m^2)} \quad (5.25)$$

Assuming the mass of the powder to be 50 mg, then we have:

$$d\rho' \approx 0.3(kg/m^3) \quad (5.26)$$

Thus, with the assumption of having the 50 mg powder, the overall uncertainty for the compressed bulk density is:

$$\rho_{CBD} = \rho' \pm d\rho' = 312.5 \pm 0.3(kg/m^3) \quad (5.27)$$

For the case of errors associated with the compaction pressure we have:

$$P = \frac{F}{A} \quad (5.28)$$

The uncertainties here are associated with the reading error correspondent to the loadcell (assuming that the gravitational acceleration of 9.806 m2/s to be exact).

We have:

$$P = \frac{4F}{\pi d_p^2} \quad (5.29)$$

$$F = Mg \quad (5.30)$$

F is the stress transmitted to the lower punch and include terms for friction between particles and die wall friction. There is also a reading error associated with the loadcell, which is 0.001 g. considering the gravitational acceleration to be 9.806 m^2/s and exact. We can simply multiply the measured quantity and its uncertainty with the constant, g ;

$$M = m' \pm dm' = m' \pm (0.001E - 3)(kg) \quad (5.31)$$

$$F = F' \pm dF' = m(g) \pm dm'(g) = 9.806 \pm 0.000009N \quad (5.32)$$

It must be noted that in this calculation we disregarded the uncertainties associated with the friction and levels of porosity that significantly affects the stress transmitted to the lower punch and sensed by the loadcell.

Using the multiplication rule for multiplying a constant with the uncertainties, we have:

$$P = P' \pm dP' = \left(\frac{4}{\pi d_p^2}\right).F' \pm \left(\frac{4}{\pi d_p^2}\right).dF' \quad (5.33)$$

$$P = 32594.93F' \pm 32594dF' \quad (5.34)$$

$$P = 319625.88m \pm 0.3(kPa) \quad (5.35)$$

m in this equation is the mass shown on the loadcells sensor meaning that it changes with compaction pressure and the uncertainties associated with it becomes very minimal and insignificant as the compaction pressure increases.

Comparing the obtained estimates for the uncertainties in the computation of compressed bulk density and compaction pressure, the uncertainties correlated with the former can be neglected while the errors associated with the non-uniform response of powder to the compaction pressure, friction between individual particles, and friction between particles and the die wall play a role. However, their calculations are burdensome. The above calculations showed that the high variation of data in the lower pressure region (in the plot of CBD versus compaction pressure) is because of the high porosity within the bulk. This high porosity causes a significant variation of stress sensed by the loadcell at the low-pressure region, until by increasing the compaction pressure, the uncertainties associated with the changes in the porosity of the powder bed becomes very small.

Chapter 6

Low-Pressure Compaction, Results and Discussion

6.1 Introduction

The low-pressure compression method is able to quantify the mechanical properties of pharmaceutical powders precisely, which is very important in evaluating the final quality of either excipients or active ingredients powder.

6.2 Applicability of Tapped Density Measurement

Tapped density measurement, in brief, is a traditional method used to indirectly show the morphology and flowability of powder. The apparatus is made up of a graduated cylinder that falls vertically from a specific height a particular number of times or vibrates for a certain amount of time. The volume of a powder after each vibration is recorded until no further changes in powder bulk volume are noted and a steady-state density is reached. Based on the recorded apparent and tapped volumes, correspondent densities are calculated. The specification of the settling apparatus and the applied method for determining the tapped and poured densities are included in both: United States Pharmacopeia [2004b], and European Pharmacopeia [2004a] with only minor differences.

According to the United States Pharmacopeia, the major drawback of tapped density measurement is that it cannot be applied to small sample

masses, because its sample consumption is relatively high [Pharmacopeia, 2010, 2011b]. This high sample consumption rate makes many bulk-characterizing studies such as determining the flow-related properties impossible. In modern pharmaceutical development, only a few grams of a pharmaceutical sample are often synthesized. Samples are becoming increasingly expensive and rare [Sørensen et al., 2005].

In tapped density measurements, powders are subjected to a constant force of gravity that leads to a volume reduction by tapping the cylinder. With that in mind, what should be done if the powder being tested is from the category of a respiratory drug with a significantly smaller size, for which inter-particle forces are larger than inertial forces? In such cases, the applicability of the classical tapped density measurement for powder with a respirable size range appears to be questionable. Because these powders do not fully compact under external forces comparable to those present in the tapped density method, it is not well suited for respiratory powders. The classical tapped density method was developed for larger particle sizes. In addition, difficulties in visually reading the sample surface due to not having the horizontal surface after each tapping, introduce inaccuracy into the results.

Thusly motivated, a fast, efficient, and reliable method needs to be introduced, along with an instrument that requires only a small amount of sample without compromising the accuracy of the results.

6.3 Method

Compressed Bulk Density (CBD) can determine the highest bulk density that a bulk of powder possesses. For the purpose of our research, and to increase the accuracy of the measurement, a very accurate and stiff load cell with the capacity of 44.5 N was chosen. According to the supplier (www.FuTek.com), the load cell deflection at its maximum capacity is 0.116 mm. The elastic deformation of the load cell sensor when subjected to the compression force was rectified by moving the punch in an empty die to allow an accurate measurement of the true displacement. CBD measurement is based on uniaxially compressing the powder and measuring its density under defined pressure. This instrument is similar to the commercially available instrument (Geopyc

1360, Micromeritics) for larger sample masses.

A cylindrical cavity is loosely filled with a known mass of powder and then placed on the load cell. A mating actuator with a non-rotating spindle is used as a punch. After zeroing the micrometer, it starts advancing in the cavity in small increments and compresses the powder. The amount of force being exerted on the load cell at each step and the correlated micrometer advancement is accurately measured and recorded. The measured force versus displacement data was processed into a graph that shows density as a function of pressure on the powder bed.

The instruments parameters for the density measurement were fixed at 0.25 mm/s for the punch advancement speed, 25 mm/s^2 for the acceleration and deceleration rate and 500 samples per measurement. These parameters were decided based on the effects of the compression rate (will be discussed in detail) on the compression curves to increase the consistency of the results. The punches diameter in this study was manufactured on a cut-and-try basis to acquire the desire engineering fit (i.e., sliding fit). The clearance applied between the sliding parts was 0.1 mm to reduce the die wall friction as much as possible without having the powder to flow out of cavity when subjected to the pressure. This variation between the punch and die diameter caused a negligible inaccuracy in the measurement. An attempt was made to replicate measurements with the same sample masses. However, there are some inevitable variations in the measurement results since the exact sample masses can never be achieved trivially.

The compressed bulk density measurement was determined by the following formula:

$$\rho = \frac{m}{V} \tag{6.1}$$

Where m is the mass of the powder column in the cavity and V is the volume of the powder at different pressures or micrometer advancement. From these values the correlation between density and pressure can be obtained. An example of the measurement data is shown in Figure 6.1. Below is an example plot of density versus pressure (units are in kg/m^3 and kPa). In as much as single value density measurements are not sufficient to describe the packing

behavior of a powder with small particles, the entire compression curve should be considered. However, in order to give a value for the CBD of different samples, solely for comparison purposes, based on a previously published correlation, [Klevan et al., 2009, Holman and Leuenberger, 1989], the density at a pressure of 35.3 kPa is used. The density at this pressure was found to be equivalent to the density of the same sample in a tapped density measurement. Horizontal error bars show how much variation exists from the mean values of compaction pressure (i.e., standard deviation of uncertainty for triplicate density measurements). As it is shown, the variation of pressure is high in the rearrangement or at low-pressure region.

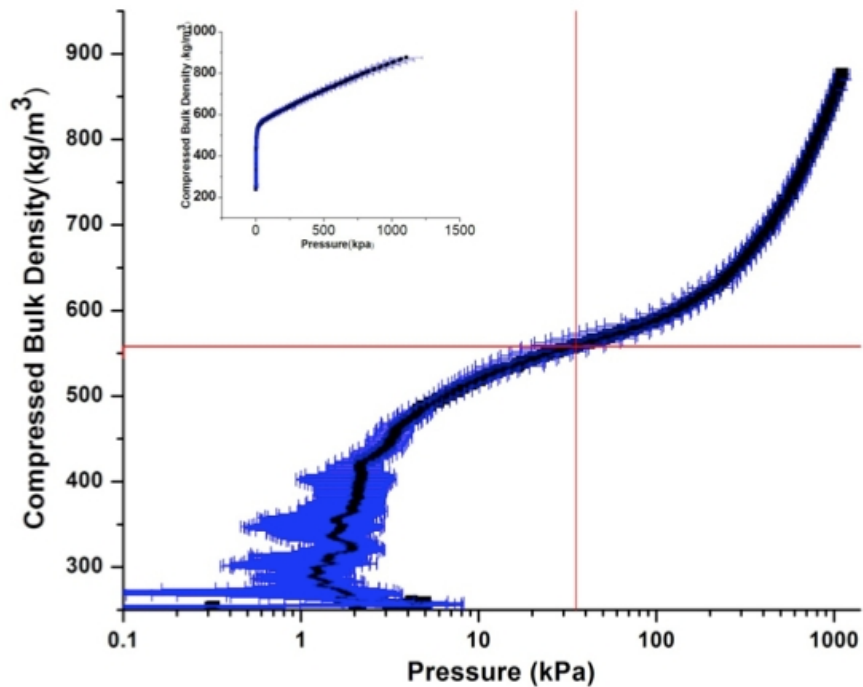


Figure 6.1: Compressed bulk density profile for Crystalline Leucine

During the initial filling of the die with powder, prior to the compression process, the only forces that exist between the particles are related to the packing characteristics of particles in the die: particle density, and powder mass. When the compaction process is initiated, volume reduction occurs that is the main mechanism in the close packing process. As the compaction force increases, the particle rearrangement becomes more difficult until any further increase in pressure would lead to the particle deformation.

6.4 Materials

Several pharmaceutical samples were tested in this research, most of which are commercially available. Samples with various consolidation behaviors were chosen including both substances that have been characterized as mainly brittle and substances with plastically deforming behavior. Samples were chosen based on their assumed compression mechanics to create a wide range of mechanical properties.

All of the samples were stored at constant humidity and temperature conditions in a desiccator for three days prior to initiating the experiment. The table that is shown below (Table 6.1) lists materials that were compressed during this study.

Substance	Supplier	Particle Size, Size Distribution ²	Remarks	True Density ¹
Crystalline L-leucine (flowable L-leucine)	Sigma Aldrich Cat # L8000	MMAD=8.19 μm GSD=1.75	Highly flowable raw material, irregular plate-like shape	1293 kg/m^3
Crystalline L-leucine	Acros Organic Cat# 125121000	MMAD=10.4 μm GSD=1.84	Crystalline raw material	1262 kg/m^3
Micronized Paracetamol	PCCA ³ Canada	MMAD=6.34 μm GSD=1.80	Active ingredient in traditional respirable dosage form	1285 kg/m^3
Sodium Chloride	MP Biomedicals Cat# 102892	ND	Ductile, granular with irregular shape	2152 kg/m^3
Cellulose, NF Microcrystalline	Medisca Canada	MMAD=12 μm GSD=1.68	Avicel PH102	1541 kg/m^3
Magnesium Stearate, $Mg(C_{18}H_{35}O_2)_2$	Across Organic Cat# 240760250	MMAD=3.67 μm GSD=1.99	Lubricant	1020 kg/m^3

Talc	Medisca Canada	MMAD=9.09 μm GSD=1.93	Lubricant	Not available
Ibuprofen	PCCA Canada	MMAD=9.48 μm GSD=1.82	Needle-like shape	1234 kg/m^3
Spray Dried D-leucine /Trehalose	Particle Engineering Lab	MMAD=3.48 μm GSD=1.63	In a 0.8/0.2 w/w formulation ratio	Not available
Spray Dried L-leucine	Particle Engineering Lab	$d_a \approx 4\mu m$	low particle density, respirable dosage form	Not available
Spray Dried Trehalose	Particle Engineering Lab	$d_a \approx 4\mu m$	High particle density, cohesive, respirable powder	Not available
Sucrose	Sigma Aldrich Cat# S93378	ND	Hard material	1590 kg/m^3
Crystalline Trehalose Dihydrate	Fisher Bioreagent, Cat# BP2687	$d_F^4 \approx 65\mu m$	Crystalline raw material with large particle size	1580 kg/m^3
Spray Dried L-leucine /Trehalose	Particle Engineering Lab	MMAD=3.91 μm GSD=1.84	In a 0.8/0.2 w/w formulation ratio, core shell structure	Not available
Dextrometh- orphan	PCCA Canada	MMAD=8.37 μm GSD=1.68	Crystalline powder with sharp, roughly polyhedral shape	Not available

Table 6.1: Materials used for compression test

Leucine is one of the well-known pharmaceutical excipients because of its ability to improve aerosol dispersibility and release active pharmaceuticals to the lungs when dealing with pulmonary drug delivery. Trehalose is another excipient known for being a stabilizing agent for bio-pharmaceutical actives

[Feng et al., 2011]. Microparticles composed of L-Leucine, Trehalose and D-leucine were manufactured. Samples were spray-dried using a Büchi Nano Spray Dryer B-90 (Büchi Labortechnik AG, Flawil, Switzerland). The target aerodynamic diameter of particles made with this spray dryer is $4 \mu m$ corresponding to an atomized droplet diameter of $7 \mu m$. Aerodynamic diameter is defined as the diameter of spherical particle with the density of $1 g/cm^3$ that has the same settling velocity in air as the irregular particle in question [Vehring, 2008]. More details about the spray drying procedures for these samples can be found in Vehring [2008], Matinkhoo et al. [2011]. Microcrystalline cellulose is a white, odorless, tasteless, and crystalline powder, which is known as one of the best filler-binders in the tableting industry due to its cost, solubility and compactibility. Paracetamol is a high-dose drug that has a very poor flowability. This powder is soft and fragments intensively. Sucrose is considered to be a relatively hard powder that fragments under high compaction pressure.

This powder shows limited deformation during compression [Alderborn and Nystrom, 1996].

Aerodynamic diameter distribution of the samples was determined using *TSI Aerodynamic Particle Sizer Spectrometer 3321*. The particle sizer was used in tandem with the *TSI Small-Scale Particle Disperser 3433* to disperse the powder prior to sizing. MMAD stands for Mass Median Aerodynamic Diameter and is the median of the distribution of airborne particle mass with respect to the aerodynamic diameter. Geometric Standard Deviation or GSD is a measure of the spread of an aerodynamic particle size distribution which typically calculated as follows:

$$GSD = \sqrt{\frac{d_{84}}{d_{16}}} \quad (6.2)$$

Where d_{84} and d_{16} represent the diameters at which 84% and 16% of the aerosol mass are contained, respectively, in diameters less than these diameters.

6.5 Compaction Data Analysis

Due to the extensive pressure ranges in the compression process, it is obvious that it is better to plot the pressure axis logarithmically to spread out the data in a distinguishable form (Figure 6.1). It should be noted that a good compaction curve should be able to indicate the changes in the compression mechanism. The application of low-pressure compaction requires very accurate equipment and thus the accurate load cell and actuator give us this opportunity to fully understand and interpret the compaction profiles.

Figure 6.2 illustrates the plot of compression pressure vs. compressed bulk density for a variety of samples. Generally, the density of the powder bulk increases during different compaction phases, as expected. Plotting the pressure axis of the graph in a logarithmic scale reveals the experimental scatter at the initial stage of compaction, indicating the presence of a rearrangement stage in the powder bed. The rationale behind this phase goes as follows: at first, when powder is poured into the cavity, the porosity of the powder bed is relatively high. During the initial stage of compression, the porosity of the powder system decreases as its volume reduces and solid particles replace the other phase (air or mixture of humidity and air) in the bulk. Generally speaking, by applying the compression pressure, solid particles move around and tend to fill the interstitial spaces between particles in a powder bed. Thus, the continuous changes in the contact area between the particles in the powder bed that are subjected to the compaction pressure result in such a variation in the force that the loadcells sensor senses the change. In other words, the scatter data at low pressure is explained as follows; certain amount of force is needed to overcome a certain threshold to break the existing structure in the powder, for example bridges or agglomerates within the powder. However, the powder does not yield in a simple monotonous fashion but rather in a discontinuous fashion. At low pressure regions, where rearrangement of particles in the powder bed are observed, as the compaction pressure increases, this rearrangement of particles continues until the interstitial spaces in the absence of agglomerates in the bulk become smaller than the particles themselves. At higher pressure, particle fracture will occur and is accompanied by a greater reduction in the volume of the bulk as the fractured particles continue to fill up the external pores within the bulk, leading to the formation of a stronger compact with lower porosity.

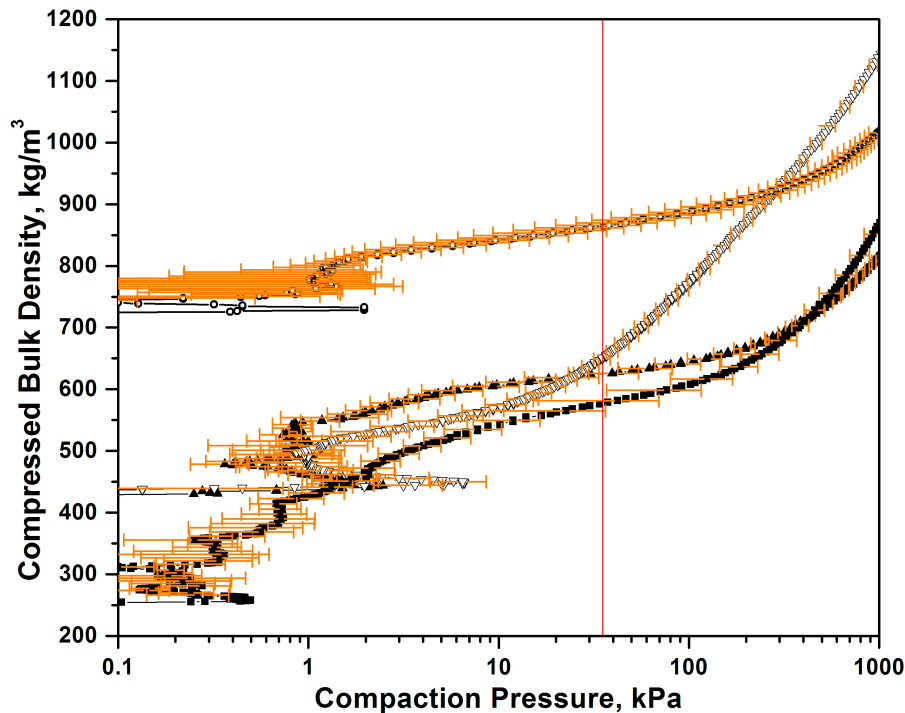


Figure 6.2: Density profile for some samples, open Circle=Crystalline Trehalose; closed square= Crystalline L-Leucine; close triangle= Dextromethorphan; open triangle=flowable L-Leucine

It is easily distinguishable by looking at the above graph (Figure 6.2) that the duration and extension of the rearrangement stage differ from sample to sample and depend on some factors such as particle size, shape and hardness. This phenomenon has been observed for more than 60 samples tested so far. However, it is very clear that the crystalline Trehalose that has a large particle size shows little rearrangement during the initial stage of compaction and has a very stiff response to the compression. In contrast with other samples, crystalline Trehalose is already compacted to a large extent when poured into the sample pan and does not compact much. One reason that crystalline Trehalose has less of a particle rearrangement in its bed during the initial stage of compaction is because it has coarse particles that are relatively large. Larger particles pack better because they are less cohesive. However, they create more porosity in the powder bed when compared to the bulk of smaller particles poured in a pan with a constant volume. Similar results were achieved with Sucrose Figure 6.10 and NaCl (not shown).

The colorful error bars in each plot show the variation from the mean value measurement of pressure or in other word, the standard deviation of uncertainty of the pressure when the experiment was done in quintuplicate for each sample. This variability is at its maximum at low pressure and decreases as the pressure increases. The high uncertainty of pressure at low pressure region results in the compression parameters such as the Hausner ratio and Carr index to seem inapplicable. (This will be covered in more detail in the following section).

6.6 Compact Porosity

The rate of change of porosity provides an estimate of material compressibility. In this study, consolidation models are based on the applied pressure. Generally speaking, materials are considered compressible when their porosity changes are relatively high when subjected to compressive pressure.

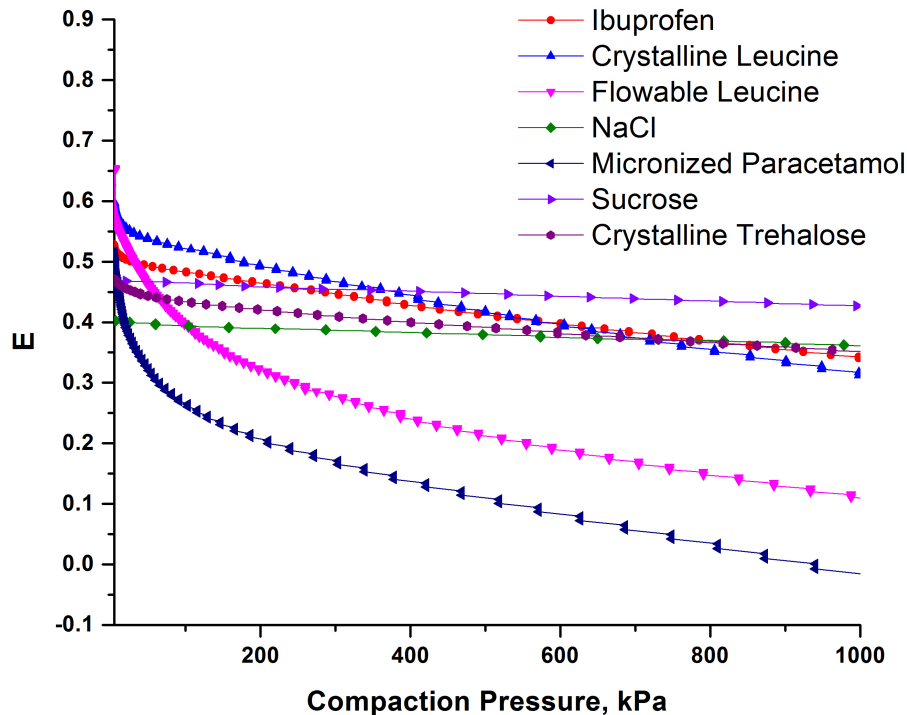


Figure 6.3: Plots of Porosity versus compaction pressure

Porosity reflects the extent of consolidation. The above graph (Figure 6.3) shows the changes in the porosity of different samples when subjected to

pressure this graph is calculated based on the equation presented in section 4.3:

$$E = 1 - D \quad (6.3)$$

$$D = \frac{\rho_b}{\rho_T} \quad (6.4)$$

Ture density (ρ_T) of each sample was taken from the Table 4. Bulk density at different pressures (ρ_b) were calculated based on the experimental results and the graph of porosity versus compaction pressure is plotted.

Among these samples, micronized Paracetamol shows a great deal of plastic deformation in its powder bed that could be due to either the brittle or ductile behavior of materials. However, Paracetamol possesses a very soft material that creates agglomerates when poured into the cavity and is considered a fragmenting material. It will be also shown in the following section that this powder starts its significant plastic deformation mechanism at a pressure of well below 400 kPa, beyond which particle fracture occurs and powder starts to show its significant elastic response. Paracetamol, after the pressure of 1 MPa, obtains negative tablet porosity. The logical explanation is the change of particle density at high pressures associated with particle elastic deformation. This explanation is also supported by the results reported in the last section of this thesis. This result is also seen by the work of Sun and Grant [2001] for some brittle powder at high compaction pressure [Klevan et al., 2009]. By the same token, flowable Leucine has a tendency to reduce its porosity. Sucrose is also considered as a fragmenting material but this particle needs higher pressure to undergo fracture; thus, we only see a limited change in porosity. Compared to other softer materials, Sodium Chloride and Trehalose show the lowest compressibility over a range of applied pressure. The line of reasoning seems to break down when Ibuprofen and crystalline Leucine are considered. These materials show greater resistance to the applied pressure. The rationale behind this behavior can be attributed to the shape of these two particles. The needle shape of Ibuprofen particles and the plate shape of crystalline Leucine (the SEM images are shown in Appendix E) cause a great number of particle-particle contact points that result in greater compact strength. Both of these materials undergo ductile-/plastic deformation with minor fracture in the bulk; thus, the result of a lower change in the porosity of the bulks.

6.7 Moisture Constant Influences on CBD

Theoretically, the compressed bulk density of powder for a given compressive load should remain unchanged at all moisture contents; i.e., the mass and volume of the bulk should be independent of the amount of moisture, assuming the powder does not take up any moisture and water is only held within the empty pores. However, it was found that the particle density changes slightly with increasing moisture. For some samples, moisture uptake results in particles swelling and subsequently increases the bulk volume, thus causing an overall decrease in particle density. In other cases, the particle structure may be weakened, which will result in the particle collapsing, and consequently decreasing the particle volume and increasing the overall particle density.

The presence of moisture in the bulk may compromise the compactibility of powders. Exceeding the critical RH, which depends on the moisture uptake of each sample, will result in the involvement of the water phase in the powder system that dissolves the interparticulate bonding, decreases the strength and consequently affects the density of the powder [Antikainen and Yliruusi, 2003].

A variety of respirable powders containing Trehalose and L-Leucine (Sigma Aldrich, Cat #L8000) were analyzed. The samples shown here represent two very different powders. One sample, spray-dried Leucine, represents a respirable dosage form with an aerodynamic diameter of $2 \mu\text{m}$ and a very low particle density. As a control for a powder with a large particle diameter, Trehalose dehydrate crystals (Fisher Bioreagents Cat #BP2687) with a Ferret diameter of approximately 0.5 mm were chosen. Samples were stored at $< 5\%$ RH and $20 \pm 2^\circ \text{C}$ in a desiccator cabinet prior to initiating the experiment. For tests in humid conditions, samples were exposed to lab conditions at 23.5°C and $30.8 \pm 5\%$ RH.

The compressed bulk density shows a strong dependence on relative humidity (Figure 6.4). The compressed bulk density of spray-dried Leucine in dry conditions increases about fourfold in the pressure test range compared to only a twofold increase for the test at ambient humidity. The equivalent tapped densities for the spray-dried Leucine powder were 115 kg/m^3 and 39 kg/m^3 for the dry and ambient humidity cases, respectively. This effect is lower on crystalline Leucine that has a larger particle size than that of spray-

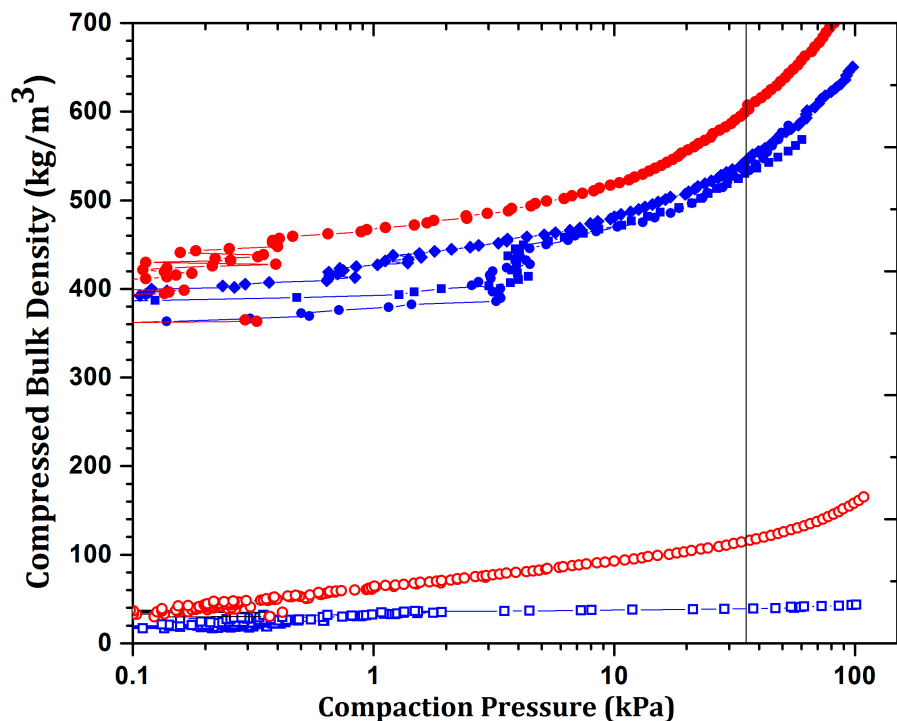


Figure 6.4: Effect of ambient humidity on spray-dried Leucine (open symbols) and crystalline Leucine (closed symbols), (red=dry condition, blue=humid condition)

dried Leucine.

Similarly, humidity did not have a significant influence on the crystalline Trehalose CBD (Figure 6.5); the CBD increased by a factor of about 1.2 in the test range. Similar equivalent tapped densities of 800 kg/m^3 and 825 kg/m^3 were found for the dry and ambient humidity cases, respectively [Shamsaddini-Shahrbabak and Vehring, 2012].

Generally speaking, bulk density is affected by several factors such as particle size, particle shape, hardness, surface roughness, powder handling history, sample preparing conditions, testing environment and the state of powder compaction. Among all of the mentioned factors, an often overlooked factor is the moisture content of powder, in spite of the fact that moisture content has been shown to play a significant role in densification and consolidation of powder [Pharmacopeia, 2011b, Svarovsky, 1987].

The moisture uptake of samples depends upon the solid/water interaction

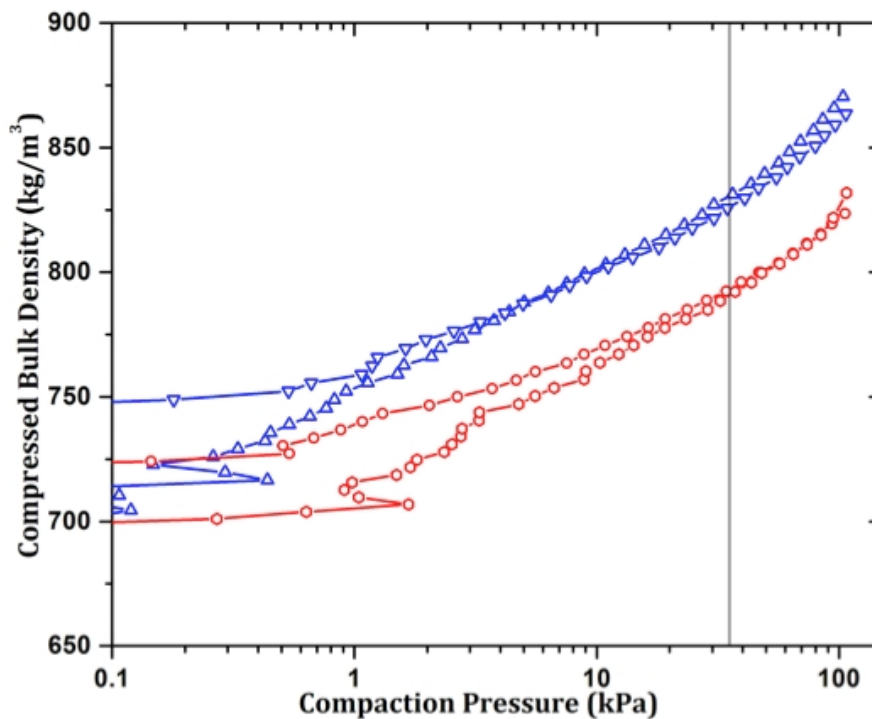


Figure 6.5: Effect of humidity on CBD for crystalline Trehalose (red=dry condition, blue=humid condition)

that refines the interparticulate or intermolecular bond formation that varies from sample to sample due to the solid particles chemical nature (hydrophobic nature) and mechanical properties (strength of the crystal lattice) [McKenna and McCafferty, 1982].

6.8 Data Fitting

Most of the fitting models such as Heckel, Kawakita and Walker are applied at the pressures higher than 1 MPa, i.e., the pressure required for tableting. Thus, using those models for low-pressure compression should be done with caution. However, the models can be useful for understanding the compression data at low pressure [Sørensen et al., 2005]. By using the Heckel and Kawakita models, we assess whether low-pressure compression can be considered as an alternative method to pharmacopeia methods for evaluating bulk densities and compressibility.

6.8.1 Heckel's Profile

The Heckels profiles (described in detail in section 4.4.1), which have been categorized into three profiles based on the effect of original particle size, can be explained by a new categorization, proposed by Klevan et al. [2009]. In this categorization, the bending of the compaction profile in region I, shown in the Heckels profile (Figure 6.6) can be classified into three types with associated mechanistic explanation, as illustrated in the graph below. Figure 6.6 shows the Heckels profile for three different powders that each of which has different shape in region I.

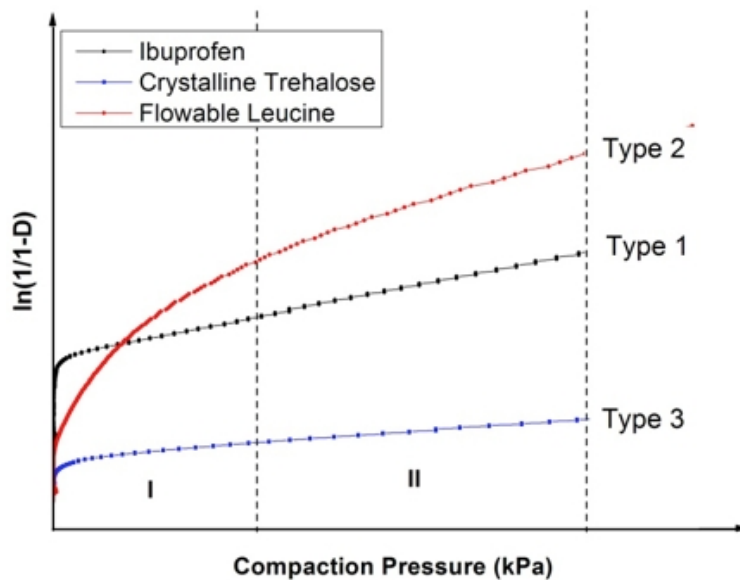


Figure 6.6: A schematic illustration of three different types of Heckel's profile

The shape of region I for the first type can be described by the significant particle rearrangement in combination with slight particle fragmentation. The second type shows an extended and smoother change of slope that was seen for flowable Leucine. Because of its low cohesion, particles tend to slip over each other easily. This extensive bending region is due to the ductile behavior or particle fragmentation and with very little particle rearrangement. In the case of type 3, a very slight linearity is seen in region I, indicating limited particle rearrangement and fragmentation. For all the three types of powder, region II shows an approximately linear response to the compaction, revealing relatively high plastic deformation and pore-filling step. The Region III, which is not shown, is associated with elastic deformation in the system of powder under

test. The presence of this region (region III) depends on the range of compression pressure used. Thus, due to our low-pressure compression experiment, this region was only observed for some powder whose mechanical strength and properties caused them to undergo elastic deformation.

Influence of Elastic Deformation on Heckel Plots

In Figure 6.7, the Heckel compression profiles are shown for some powders investigated in this study. The overall shape of the compaction profile depends on the particle size and the material being tested.

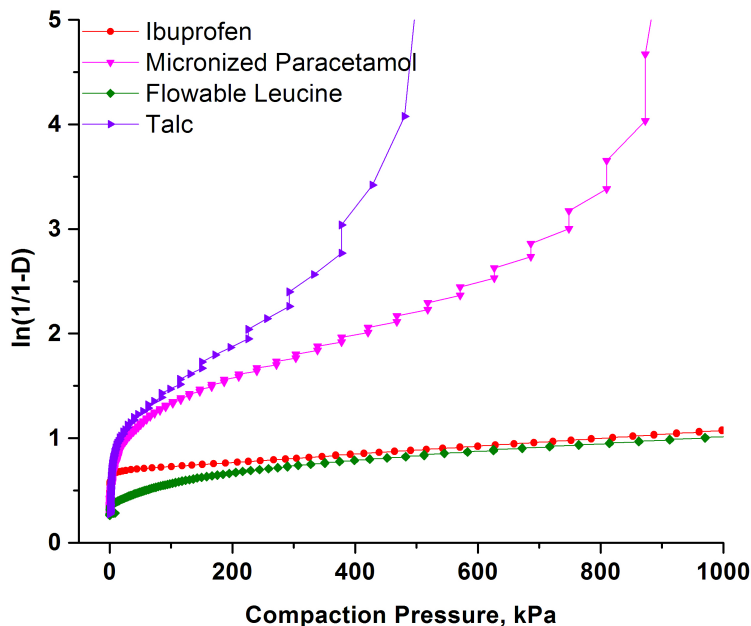


Figure 6.7: Heckel compression profile for four samples in the pressure range of 0-1 MPa

At low pressure, all powders show a decreasing slope followed by the linear region as the compaction pressure increases. Hence, all of the powders express a compression behavior associated with regions I and II. Comparatively, two of the powders shown have increasing slope at higher pressures, which is associated with region III. The compaction pressure at which the transition from different regions of the compression profile occurs is different depending on the powder in question, i.e., only some of the powders expressed all three compression regions in the pressure range used in this study. However, higher

compaction pressure is needed to completely categorize a powder by its compression behavior.

6.8.2 Kawakita's profile

The fundamental idea behind the Kawakita equation (described in detail in section 4.4.1) is that the particles subjected to the compressive force are in equilibrium at all stages of compression; i.e. the product of pressure term and volume term is constant [Patel et al., 2007]. Among Kawakita's parameters, the inverted b , b^{-1} represents the pressure needed to achieve a strain of $a/2$. Thus the constant a describes the total compressibility of a powder while the constant b explains the initial compressibility of the powder system.

When performing a compression test, the accurate determination of the initial bulk volume is practically impossible. The imprecise measurement of the initial volume affects Kawakita's compression parameter. To show the effect of initial volume on Kawakita's parameter, two different initial volumes were recorded and analyzed: first, the poured volume from the undisturbed bulk of powder and second, the volume recorded at an applied force of 5 N. Results are shown in Figure 6.8.

The degree of compression varies among four samples shown in Figure 6.8. The Kawakita equation seems to be more reliable at the very high compaction pressure. It is shown in [Nordström et al., 2009] that the Kawakita's compaction profile at high pressure (in the range of tableting pressure, ≈ 500 MPa) becomes completely horizontal meaning a significant resistance of powder to compression force while no further volume reduction occurs. However, we can easily observe the powders proclivity for reaching that region in our results. Particle size is an important factor in this kind of behavior. Another interpretation from the above graphs, which is also supported by the work of Nordström et al. [2009] is the influence of the initial volume on C_{max} and the derived Kawakita parameter, a . A higher strain is the poured volume is used as an initial volume, compared to when the volume at the certain pressure, 5 N in this case, is taken. This indicates that a significant degree of powder compression was already achieved at low compression pressure. Thus, the use of poured volume as an initial volume is the preferred procedure in order to

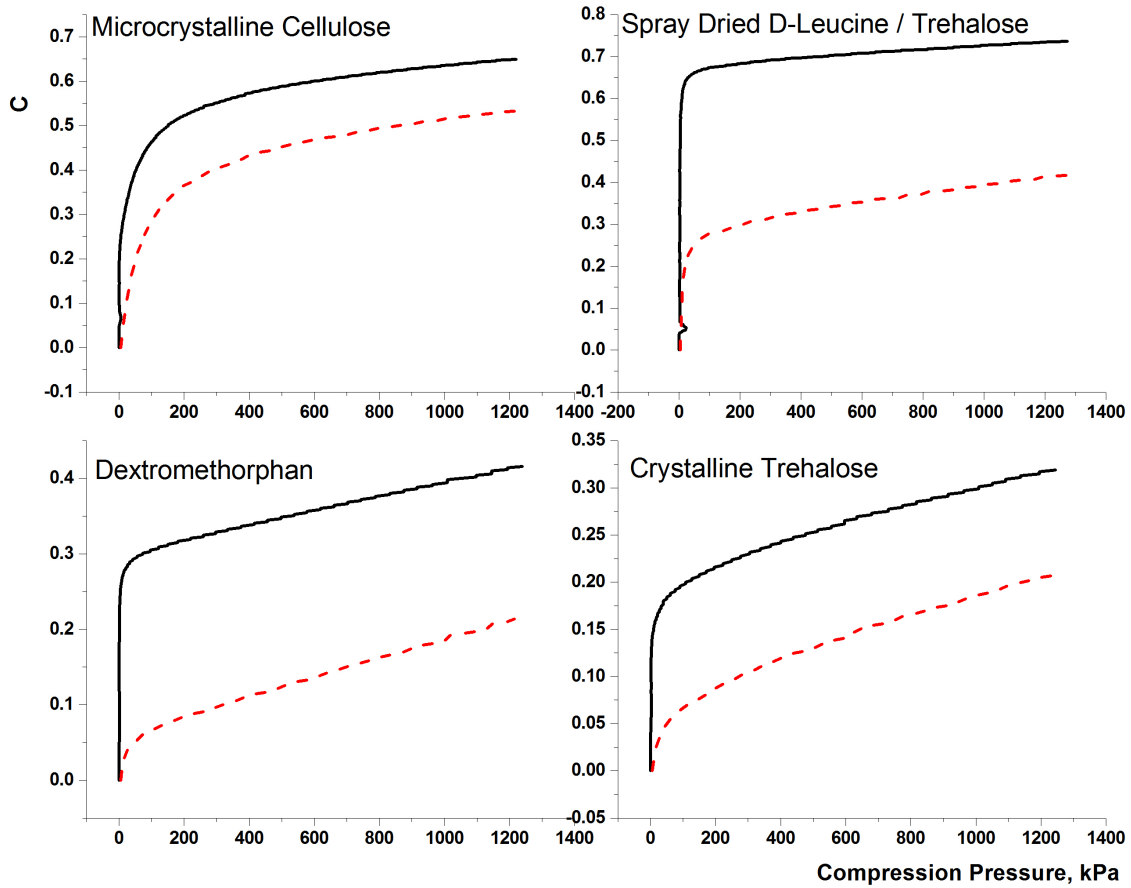


Figure 6.8: Plot of strain versus compression pressure for four different samples: line= compaction curve when C , Kawakita parameter, was determined at the poured pressure, dashed line = compaction curve when C , Kawakita parameter was determined at the initial volume recorded at the pressure of 5N

get a good interpretation of the compression profiles.

Disregarding the effects of initial volume on the Kawakita compression profiles, graphs show a sudden and significant initial compression with increasing compression pressure for all of the samples tested above. The curves then experience a marked bent followed by a linear region that tends to level off at higher pressure and reach a plateau. Due to the limited pressure range, the third region cannot be seen completely in these results, although different slopes for samples are present and noticeable, and reveal how powders react differently to consolidation pressure.

Both of these empirical methods, Heckel and Kawakita models, explain

the fact that compaction behavior cannot be described by assuming a single compaction mechanism-either filling of large voids by particle rearrangement or filling of small void by particle fracture or plastic flow, but rather a combination of these two mechanisms occurring at different stages of compaction [Carneim, 2000].

The compression properties of material under compression give a basic understanding of the tableability of material, introducing a relationship between the compact formation and the volume reduction properties of powders, which may make it possible to predict formulation properties.

6.9 Hausner Ratio and Compressibility Index

The flowability rate of various samples is different and depends on particle size, shape and some other mechanical properties. The HR and CI of some of the samples are calculated (equations were described in detail in section 4.5) and tabulated below (Table 6.2). In order to calculate the HR and CI for each sample, the density at pressure which the slightest force on the powder is noticed was recorded as an apparent density and for the case of tapped density, the density at the pressure of 35.3 kPa is taken.

Among all of the samples tested for flowability, paracetamol and the spray-dried powder, as shown in Table 6.2, have the lowest flowability. This fact has also been noticed when attempting to fill the sample pan, as the powder does not pass easily through the sample vial and a spatula was used. These powders were forming arches and agglomerates during the filling process. This behavior has also been observed with spray-dried powders and with paracetamol as well, since both tend to form large and irregular aggregates with a low density as a result of the dominance of the surface forces such as Van-der-Waals in comparison to the initial forces, gravity. In contrast, it was much easier to fill the sample pan with powder having larger particles such as flowable Leucine, Trehalose and Sucrose. In other words, particles of upper micron size range or larger are usually more influenced by gravity than cohesion forces [Tousey, 2002]. Experimentally speaking, the finer the powder the less flowable the particle, although the crystal lattice and chemical nature of the material also play a role in flowability. As for the flowable Leucine, particles were observed to slip

Substance	CI %	HR	Flow Character
Paracetamol	40.74 ± 2.6	1.68 ± 0.23	Very, very poor
Crystalline Trehalose	16.86 ± 0.7	1.20 ± 0.01	Fair
Sucrose	1.46 ± 0.6	1.03 ± 0.335	Excellent
Crystalline L-leucine	35.08 ± 0.7	1.58 ± 0.044	Very poor
Flowable Leucine	23.25 ± 0.6	1.32 ± 0.014	Passable
Spray dried D-leucine /Trehalose	65.46	2.89	Very, very poor

Table 6.2: Hausner Ratio and Carr Index for different samples

over each other at the slightest bed disturbance. Determining the flowability of the respirable powders is very important as it helps determining the energy needed for particle dispersion for inhalation.

It was found that the sample history significantly affects the initial state of compaction for respirable powders. This results in large variability at low pressures, and consequently a wide range of Hausner ratios and Carr indices were observed, (e.g. Figure 6.9).

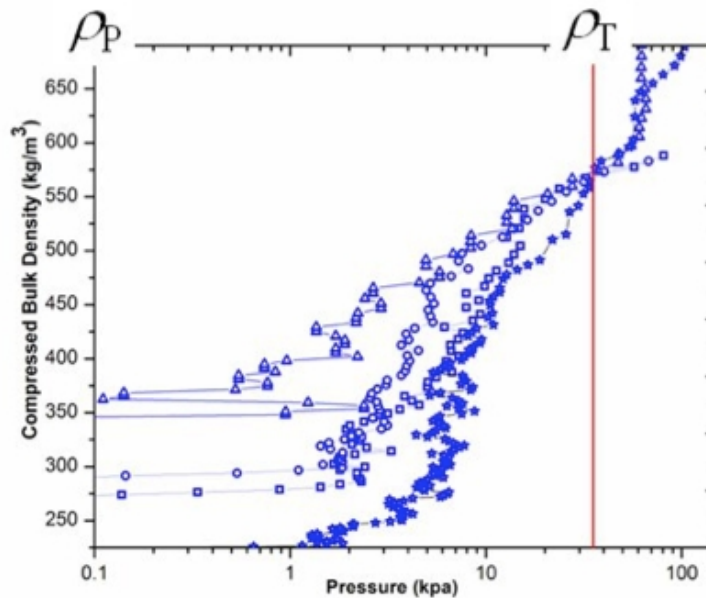


Figure 6.9: Sample history causes large variability at low pressure and wide range of HR and CI for the same powder [Shamsaddini-Shahrbabak and Vehring, 2012]

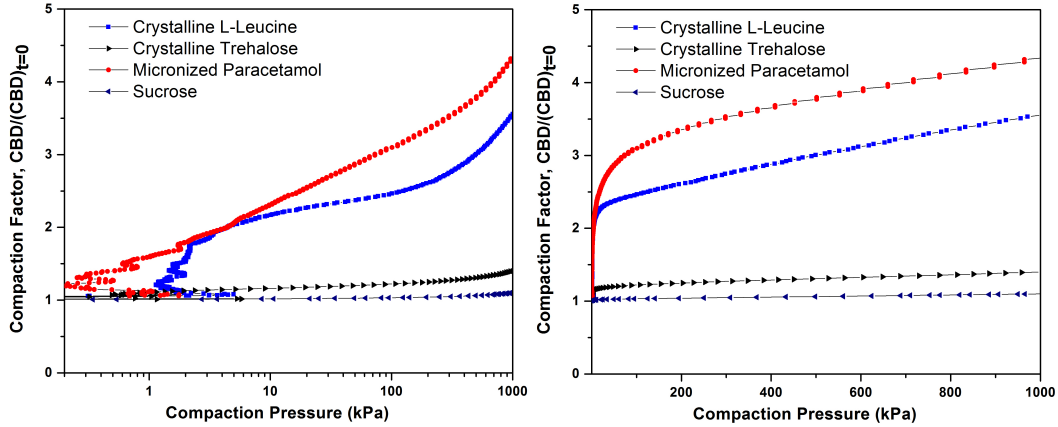


Figure 6.10: Compressibility of four different samples as a function of axial pressure, axis is in log scale for the left graph

For this reason, the usefulness of these two compression-derived parameters, the Hausner ratio and Compressibility Index is questionable for spray-dried samples with small particle diameters.

6.10 Compressibility and Compaction Factor

In general, powders are compressible when there is a volume reduction in their bulk whenever they are subjected to a compressive force. A graph was introduced to show the compressibility of different samples being tested.

These graphs (Figure 6.10) show the relationship between the compaction pressure and compressed bulk densities of powders normalized by compressed bulk densities at zero compaction pressures. This graph is a good tool to determine the cohesivity or compressibility of the pharmaceutical powder. The right graph in Figure 6.10 highlights two important facts; first, the higher the slope the more cohesive the powder is or, in the other words, cohesive powder tends to reduce its volume when it is subjected to increasing compacting pressure. For instance, Trehalose and Sucrose, which possess coarse particles with larger particles, do not undergo a significant volume reduction. Comparatively, for the case of Paracetamol and L-Leucine, which possess smaller and softer particles, the rate of volume reduction is far higher than that of the two former samples. Second and more important is the point of transition from the

particle rearrangement region to the consolidation region. At this point, the linear region of the plot starts to grow, indicating the plasticity of substances. Comparing these two graphs, we see that the initial region can be described as a rearrangement stage of compaction. We also see that the duration of this process is different for every sample and depends on the physical properties of particles such as particle size and shape.

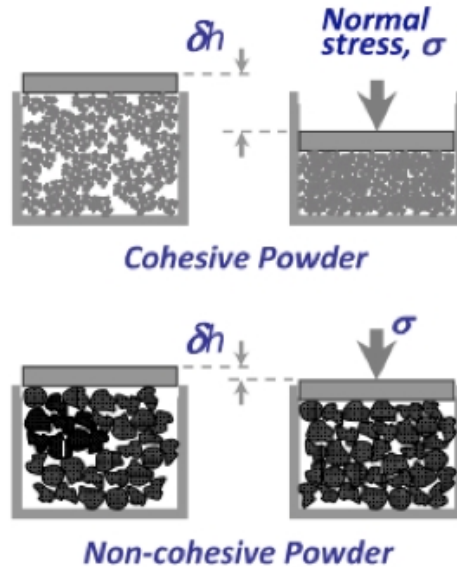


Figure 6.11: Schematic of Powder cohesivity [Freeman, 2012]

The graph shown above (Figure 6.11) illustrates the difference between the two samples with respect to their cohesiveness. Generally, coarse particles like Sucrose and crystalline Trehalose were already compacted to a large extent when poured into the sample pan. We see a very minor rearrangement at the initial stage of compaction. It is clearly shown in the right graph of Figure 6.10 that the compaction mechanism of Trehalose and sucrose has started respectively with small and no particle rearrangement followed by the stiff response to the compression pressure, respectively. The low slope of the linear region indicates a very small volume reduction in the compression of these two samples.

In comparison, the curved region in the Paracetamol plot indicates the relatively high rearrangement region that accompanies its plastic densification. Basically, when poured to the sample pan, Paracetamol powder creates agglomerates. Thus, the high void ratio in the powder column is reduced by

collapses of those arches in the bulk resulting in a very noticeable curved region at the transition point.

6.11 Compression Speed

Various studies have shown the effect of the compaction rate on the compactibility of pharmaceutical powders [Holman and Leuenberger, 1989, Ruegger and Celick, 2000, Armstrong and Palfrey, 1987, 1989]. Powders with plastic or viscoelastic deformation under compression are compacted more and form a stronger compact as the compaction rate decreases. In other words, they are compacted more densely and thus possess higher density at a specific compaction pressure. On the other hand, powders with brittle characteristics are not affected that significantly when the compaction speed changes, because fragmentation in powder under compression occurs quickly [Ruegger and Celick, 2000]. Figure 6.12 shows compaction graphs for four different samples with various physical characteristics being compacted at different rates.

Graph a shows the density profile for microcrystalline cellulose at four different compaction speeds. This powder is compacted with plastic deformation. Clearly, the compact becomes denser as the compaction rate decreases, meaning that the decrease in compression rate can prevent capping or lamination. Capping is the result of air entrapment within a powder compact during compression, which makes the compact (tablet) to separate horizontally, either partially or completely from the main body of the compact. In lamination, compact separates into two or more distinct horizontal layers [Tousey, 2002]. By looking closely at the initial rearrangement stage of the graph, it is clear that powders that have been compacted by the faster rate did not experience as much rearrangement as those compacted at a lower rate. This variation stays the same for crystalline Trehalose that has coarser and larger particles. Generally, crystalline Trehalose particles are considered to undergo fragmentation during compression but in-as-much-as we compress powder with relatively low pressure, we did not observe any fragmentation in the compact after the experiment and it is slightly compacted by the plastic deformation. Again, the rearrangement section shows particle rearrangement to varying degree during the initial stage of compaction for samples compressed at different rates. Appendix E shows SEM images for powder under test before and after the

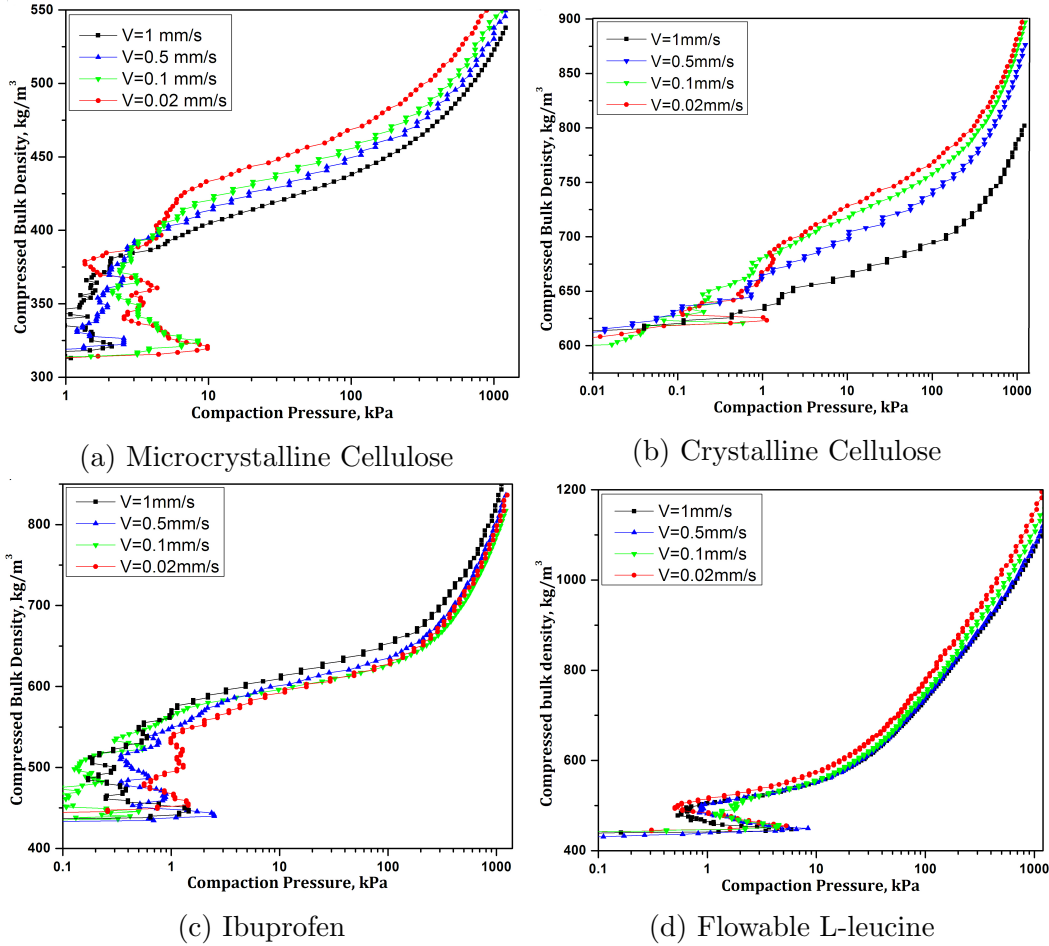


Figure 6.12: Compaction profiles at different compaction rate

compression test.

Graph c, which shows the density profiles for Ibuprofen, reveals negligible changes in the density of the compact, when compacted at different rates. As the SEM micrographs show, Ibuprofen underwent fragmentation during compression. As for the powder with brittle deformation, compact strength seems to be unaffected by the compaction rate. In addition, the rearrangement extension in the graph indicates a very small difference, as particles fracture at any speed and slip over each other to fill up the voids. For the case of flowable Leucine, a very similar result was observed for different compaction rate even at the initial stage of compaction. The high flowability of this powder seems to play an important role in obtaining such a similar compaction profile at different compaction rate. The particles of flowable Leucine slip over each other

very easily at any compaction rate. However, the influence of flow property for crystalline Trehalose in achieving different compression profile at various compression rates seems to be affected by its shape. When powders are compressed at a high rate, they do not find enough time to rearrange and fill the voids as they will be compressed on each other without filling any voids and will show stiffer response to the compaction.

The compaction rate has been shown to influence the compaction efficiency to some extent. It was observed that consolidation became more difficult with increasing compaction rate in the tested range (0.02-1 mm/s). In other words, greater stress was required to reach a desirable density. In addition, materials with elastic deformation during high-speed compression are more susceptible to capping and lamination, which mostly occur at real tableting pressure, which is by far more than the pressure in this research.

In general, most pharmaceutical powders behave like viscoelastic materials to some extent. However, they cannot be strictly categorized as exhibiting specific types of deformation since during powder compression a combination of deformation mechanisms exist.

The effects of compaction rate on the compaction curves have been shown. However, for the sake of consistency in the results of density measurement, it is attempted to use the standard compaction rate of 0.25 mm/s which is slow enough to avoid capping of fine powders or sharp response of irregular particles to the compaction pressure and fast enough to avoid plastic flow of highly flowable particles.

6.12 Modulated Compression Profile

In the pharmaceutical industry, there are times when the compression parameters of a powder need to be determined without destroying the particles, which is of paramount importance in modern pharmaceuticals when dealing with scarce or expensive powders.

Using the NI LabVIEW software as an interface to control the setup gives us the capability to control the actuators movement and the measurement

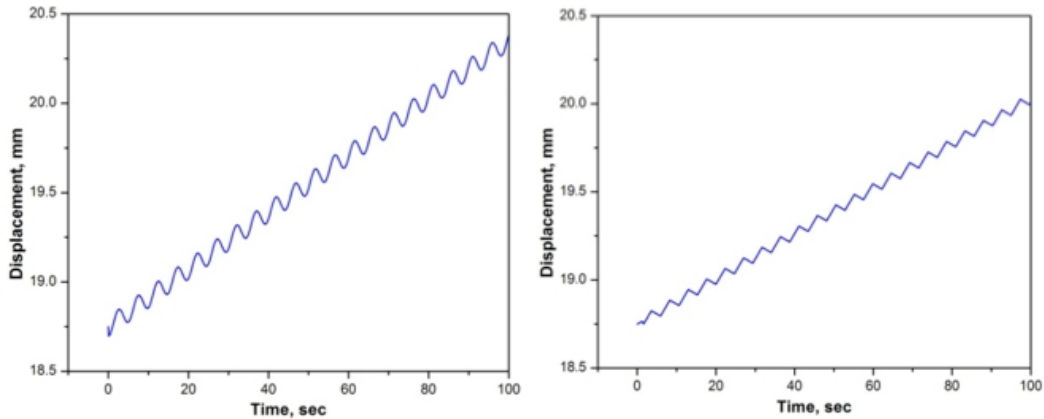


Figure 6.13: Schematic of the modulated compression profile, harmonic (sinusoidal) and triangle wave

criteria. Present control modes for the actuator are constant rate compression, harmonic wave, saw tooth wave, triangle wave and step mode. Profiles for two of these modes are shown in Figure 6.13. In these modes, different amplitude, frequency and advancement speed can be set. Using these modes helps differentiating between the elastic and plastic behavior of the material that are being tested, which can be useful in further describing the materials physical properties. Additionally, it can determine the exact point of a packed bed, beyond which the likelihood of the occurrence of the breakage or ductile deformation of particles increases.

Although the low-pressure compaction test does not state the real fragmentation location in the bulk as for that to occur, a relatively higher pressure in the range of tableting pressure is required.

The modes shown in Figure 6.13 are based on the subsequent compression and decompression of powder. These modes are not available in any commercial instruments. In our study with low-pressure compaction, almost all of the obtained compression graphs show the linear region indicating plastic deformation of powder or more precisely irreversible consolidation, because of the porosity that decreases either by rearrangement of particles or filling of the voids by smaller particles.

Table 6.3 shows the functions used to program the three modes of the ac-

Modes	Formula
Triangle wave	$x(t) = \frac{I}{p}(t - p \lfloor \frac{t}{p} + \frac{1}{2} \rfloor)(-1)^{\lfloor \frac{t}{p} - \frac{1}{2} \rfloor}$
Sawtooth wave	$x(t) = I(\frac{t}{p} - \lfloor \frac{1}{2} + \frac{t}{p} \rfloor)$
Sinuousoidal wave	$x(t) = I \sin f(t)$

Table 6.3: Different wave functions of actuator movement

tuator's movement:

Where p , I and f are the required parameters to plot the desired wave. The parameter p controls the time during which the wave is formed (set to 40), I controls the amplitude of each cycle (set to 40) and f controls the number of cycles in one experiment (set to 50).

This experiment is performed in a way that for instance during one cycle; the advancement of the punch into the die compresses the powder and then, by having the punch withdrawn from the powders surface, due to the viscoelastic feature of powder (if any), there will be a change in the porosity of the bulk. This phenomenon can only be observed when punch proceeds back again into the already compacted powder bed. During the start of the next cycle, as the punches tip reaches its original lift-off position at the previous cycle, no load is noticed until the punches tip hits the powder bed surface again. It is said that the powder has undergone creep deformation if there is any changes in the strain rate of the compact, i.e. the lift-off position of the punch may be different from the position that the powder surface is subjected to the load in the next compression cycle. The amount of creep deformation depends on the time the powder is given to rest and elasticity of the materials. We used the same approach to differentiate the elastic and plastic regions of the powder on a very small scale.

Implementing this technique provides information about the pressure at which powder is fully compacted and the porosity is at its lowest over the range of the applied pressure. When powder is being compressed, porosity within the bulk decreases as the bulk volume decreases. During the initial

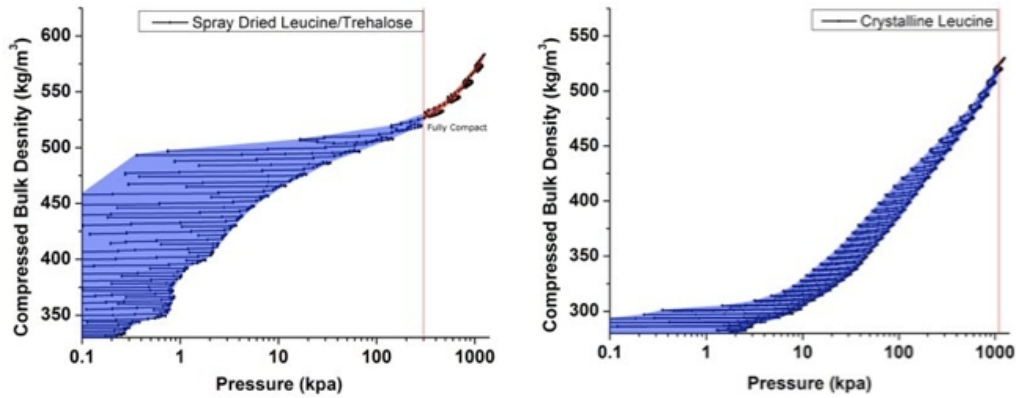


Figure 6.14: Modulated compression profile differentiating the elastic and plastic region of the powder bed, Triangular wave mode is used

stage of compression, due to the high void ratio in the bulk, the lowest number of contact points between the particles results in low compaction strength and the powder will be compacted easily. As the pressure increases, the porosity decreases quickly and the results are reflected in the steep response (graphically) of powder consolidation to the compression force because the number of contact points increases significantly. This behavior can be explained by the extensive distribution of the applied force on the surface area of particles in close proximity of each other; i.e., as long as the surface area is small, the total work of compression is expended on moving particles to the external pores between the particles. This step continues until the surface areas of the voids in the bulk become lower than surface areas of solid particles that are in true contact and are subjected to the applied force. For the same reason, powder under compression during the primary stage of compression shows the plastic response as the force is removed from the powder bed. However, when the increase in the compaction pressure begins to reduce the porosity, the powder starts to show its elastic behavior. This is clearly shown in the graphs, that the excess input of energy in the form of compression is utilized as an elastic recovery during decompression. However, this elastic recovery in pharmaceutical powder is stress dependent and with this technique we can determine for the first time the point (pressure) at which particles in a powder bed may be fractured or undergo permanent deformation.

The powders shown in Figure 6.14 are two different samples: spray-dried Leucine / Trehalose and flowable Leucine. The spray-dried sample possesses very fine particles and creates arches and agglomerates with high porosity as it is poured into the die. Thus, the work of the compression is put into reducing the porosity of the bulk. During the compression and decompression cycles, the powder proves the presence only of plastic deformation, which is accompanied by the collapses of the arches formed previously within the powder bed. The powder starts to show reversible, i.e., elastic behavior at pressure of about 300 kPa, beyond which most of the work that was needed to deform the new elastic material is recovered during the decompression phase. It must be noted that some of this compression work is expended on overcoming the friction between bulk of powder and the die wall due to the radial strain, and between the particles.

In the case of flowable Leucine, due to its chemical nature, particles rearrange very easily. Thus, the pore-filling process within this bulk of powder occurs faster than with that of other samples. For the same reason, flowable Leucine already starts showing some elastic behaviors when the compaction pressure exceeds 10 kPa. However, this spring-like behavior of flowable Leucine at this low pressure was observed for all of the samples being tested but with relatively smaller magnitudes (showed less elastic response at low pressures). The graph indicates that Leucine powder is very compactable, which is evident by its being fully packed at the pressure of above 1000 kPa i.e., the powder starts its elastic response to the compaction pressure at the pressure of 1000 kPa. Being fully compacted at this pressure may also be an indication of no fracture in the particles, since if there were any particle fragmentation within the bulk; the powders elastic response would begin earlier.

Another reason that the modulated compression profile is useful is that it can validate the Heckel profile for better interpretation of the compaction mechanisms. Comparing the Heckel compaction and modulated compression profiles based on the experimental results can be a very reliable way to help understand the underlying compression mechanism at each region in the compaction profiles.

The following set of figures compares both; the Heckel plot and modulated compression profile for five different samples.

For the above results, the same batch for every sample was used to plot both: the Heckels and modulated compaction profiles. We attempted to keep the mass of powder constant for every batch. The compression and decompression rate was set to 0.25 mm/s for all of the tests. Samples were tested in ambient laboratory conditions, $RH = 28 \pm 4\% \mid T = 22 \pm 1.5^\circ C$. A triangular wave mode was applied and period, and amplitude were set to 5 (s), $2E - 5$ (m), respectively, for all of the above tests (which are equivalent to the values assigned to each parameter in the wave equations mentioned above). The frequency depends on the number of samples per measurement. With high frequency and lower amplitude, the elastic deformation starting point can be determined accurately, although for some samples a load cell with a higher capacity is needed to extend the pressure range and to locate the exact pressure at which the powder is fully compacted without having any particle fragmentation or ductile deformation in the fully packed bed.

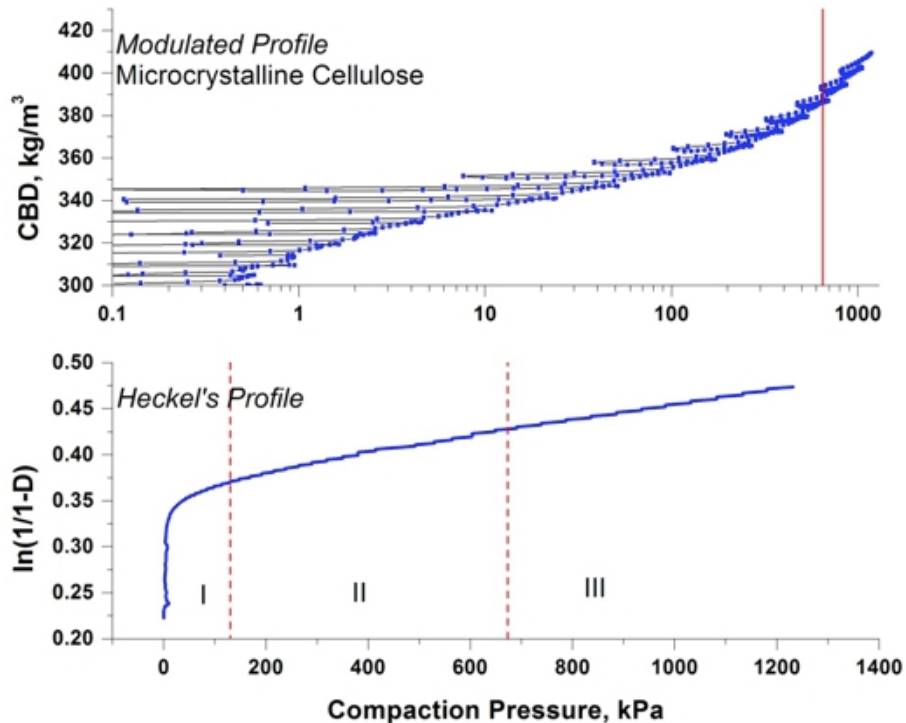


Figure 6.15: Modulated compression and Heckel profiles for microcrystalline Cellulose representing three different regions in the compression mechanism

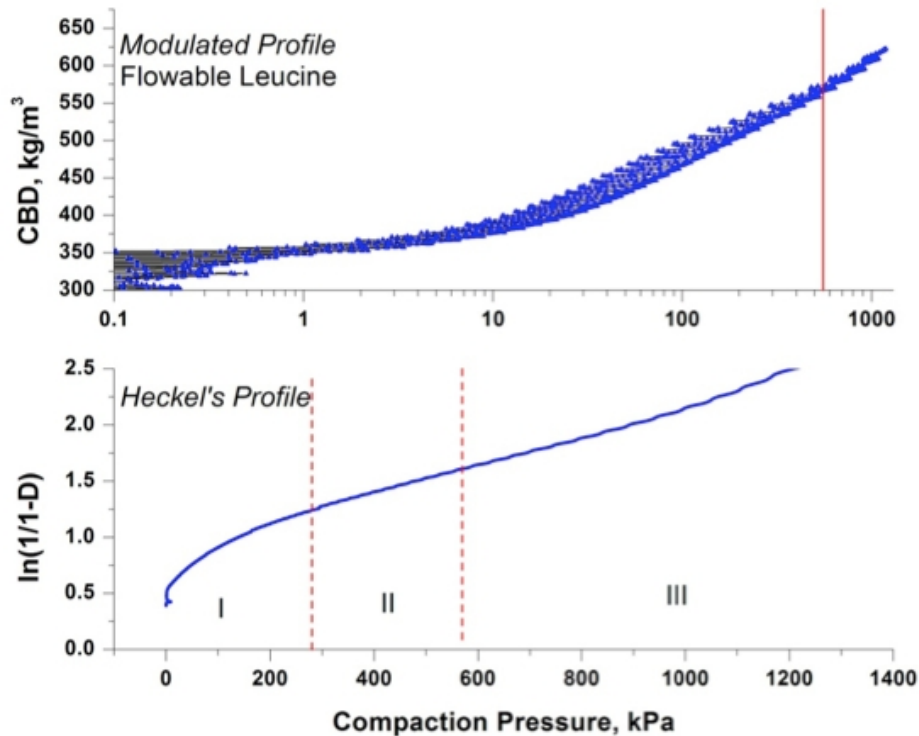


Figure 6.16: Modulated compression and Heckel profiles for flowable Leucine representing different regions in the compression mechanism

In the first graph (Figure 6.15), the modulated compaction profile of microcrystalline cellulose is compared with its Heckel profile. Avicel PH102 (also known as microcrystalline cellulose) as its SEM image (in Appendix E) shows, possesses fine powders that undergo plastic deformation easily. As the graphs indicate, cellulose reaches its packed-bed state at the compaction pressure of higher than 600 kPa, where the powder starts experiencing its first elastic behavior. The inflection point shown in the Heckels profile also proves the presence of this elastic deformation, i.e., a clear bending of the upper part of the Heckels profile was obtained as the powder starts resisting to the compacting pressure. The point at which elastic deformation starts, is where a powder shows its first large elastic response to the compacting pressure (with respect to the pressure range) which graphically is the point of intersection between the two: linear compression and modulated compression profiles (red line in Figure 40). The elastic deformation of cellulose powder starts at high pressures, where the powder bed is fully packed that increases the contact area between particles, thus, results in the higher friction or cohesion force between particles.

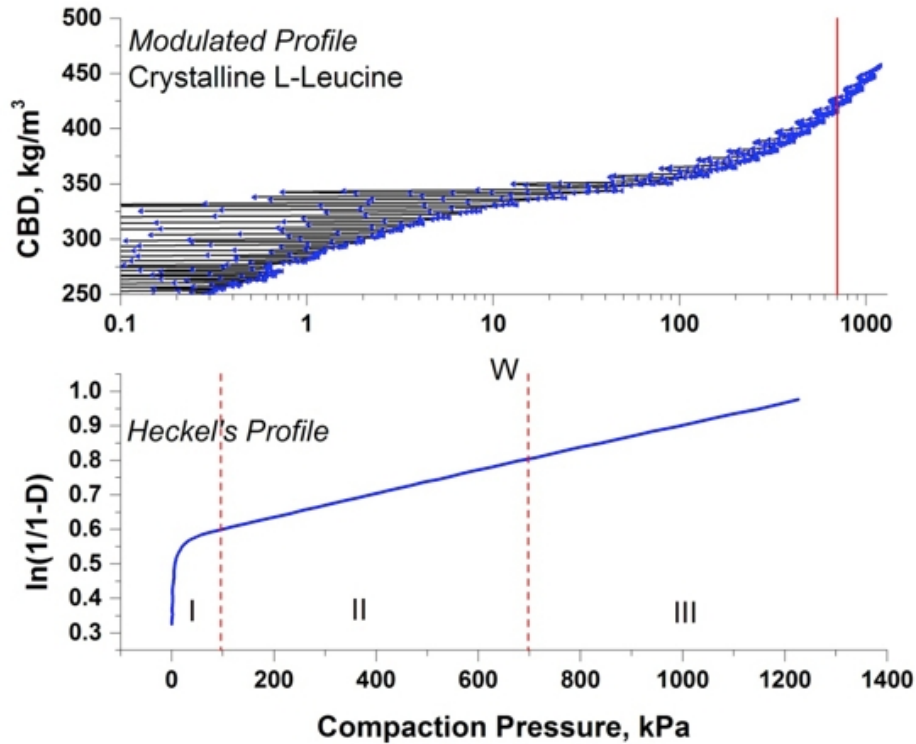


Figure 6.17: Modulated compression and Heckel profiles for crystalline Leucine representing different regions in the compression mechanism

For the case of flowable Leucine powder that possesses small plate-like shape particles, Figure 6.16 indicates some overlap of plastic and elastic deformation in the bulk as the powder undergoes compression. Flowable Leucine powder due to having non-cohesive particles with ductile property tends to compact easily under stress and the slope of the linear region in the Heckel profile shows the degree of consolidation by the plastic flow. At around the pressure of 600 kPa powder starts showing its elastic response. At this pressure, the porosity of the bed has been reduced to the lowest achievable porosity without having any broken particles or particles that have undergone permanent deformation in the bulk, with respect to the applied pressure range. Flowable Leucine powder shows an extensive rate of spring-back behavior at each compression and decompression cycles, when the load is removed from the surface of the bed. Even though the slope of the linear section of the Heckel plot is an indication of the high rate of densification by plastic deformation but in general, the correspondent region to the plastic deformation in the Heckel plot (region II), points out that most of the compression force

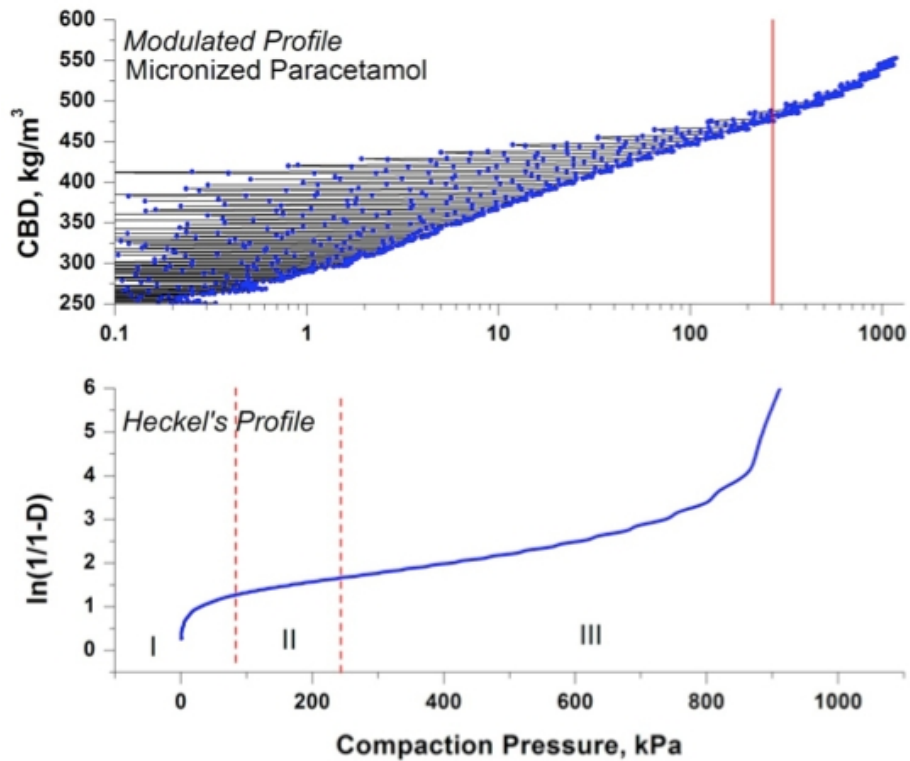


Figure 6.18: Modulated compression and Heckel profiles for micronized Paracetamol representing different regions in the compression mechanism

was used for rearrangement and the elastic deformation, which are the main mechanisms in compacting this powder. This type of behavior is likely caused by the plate-like shape of these particles that results in a large contact area per unit volume. Thus, this powder shows more resistance to the compaction. However, the ductility of this powder allows the powder to be compacted well enough as long as the force is applied; thus, this powder experiences the elasto-plastic behavior.

In the third graph (Figure 6.17), the Heckel profile for crystalline Leucine shows less plastic deformation than what flowable Leucine does. Its first elastic response is detected at the pressure of higher than 700 kPa. Considering the slope of the Heckel plot in its second region indicates that this type of Leucine powder is compressed less than the flowable leucine. This is likely caused by the presence of small asperities around its particles that increases the friction between particles, which leads to showing the higher strength to the compaction stress. Consequently, due to the rough surfaces of these particles that result in interlocking of neighboring particles, this powder tends to show less

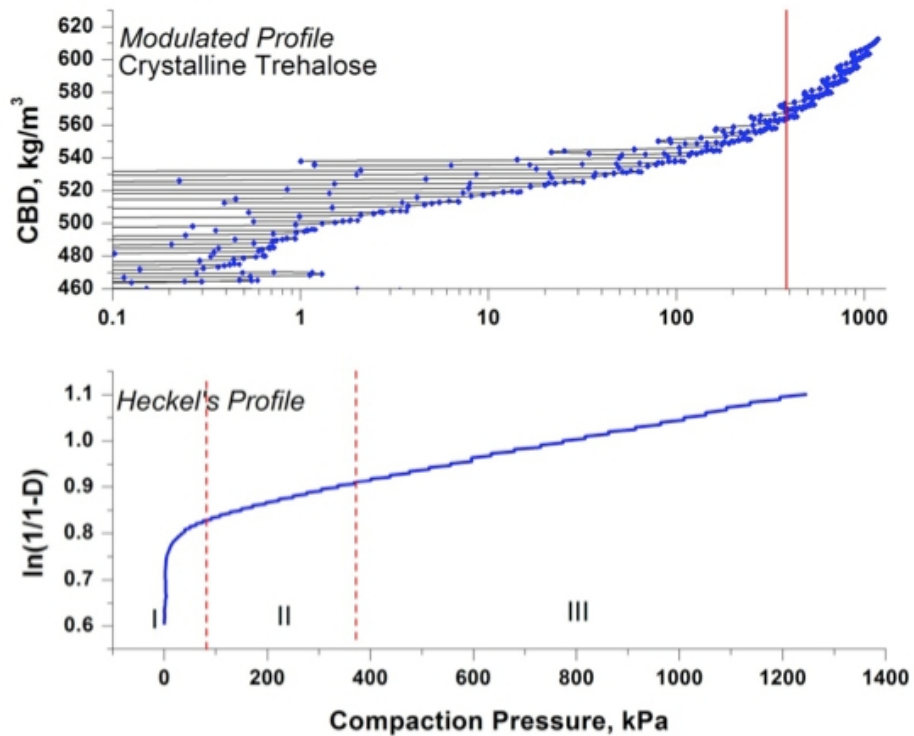


Figure 6.19: Modulated compression and Heckel profiles for crystalline Trehalose representing different regions in the compression mechanism

spring-back behavior than what flowable Leucine does. Comparing both; the Heckel and modulated compaction profiles, the plastic region is clearly noticeable, indicating the plastic deformation to be the main mechanism of the compaction for this powder in this pressure range. However, the internal pores (shown in the SEM graph) in the particles of this powder results in having a high porosity even at the highest compaction pressure in these experiments.

Figure 6.18 shows the modulated compaction and Heckel profiles for micronized Paracetamol. This powder shows a very high porosity within its powder bed due to formation of arches and agglomerates when it is poured into the cavity. Hence, as it is shown in the modulated compaction profile, an extensive plastic region (which is accompanied by the particle rearrangement) is seen until the porosity reaches to the point where the contact area of particle increases and starts to show some resistance to the load. Paracetamol powder possesses fragmenting materials that undergo significant fragmentation when subjected to compaction force. Thus, during consolidation, its porosity decreases to a large extent when the powder is almost fully packed. Paracetamol

starts showing its first elastic behavior at a pressure of above 300 kPa.

In the case of crystalline Trehalose (Figure 6.19), which possesses large and hard particles with brittle deformation, the large contact area between its large particles results in the increased frictional force that opposes the dense packing. Although, the Trehalose powder shows its first elastic response at the pressure of around 400 kPa, the porosity within its bulk is still relatively high. SEM image of this particle shows the creation of small cracks in some particles indicating that this pressure range is not enough for full compaction of this powder.

Different materials have different responses to the harmonic compression profile. The above figures clearly show different elasto-plastic deformations of materials under compression and decompression forces. In short, initially particles in a powder bed undergo rearrangement. The extension of this rearrangement behavior depends on the frictional and the cohesive forces between particles that are close together. As the compression pressure increases, particles can no longer hold together and material with brittle properties undergo fragmentation while others that have ductile properties may deform. The fragmentation of larger particles produces small particles, which serve a void-filling role and results in a powder with a lower porosity and higher density. An important factor to consider is the applied pressure, as such; some hard materials may not experience fragmentation and consequently respond stiffly to the compaction pressure. The modulated compaction profile helps determining the point at which powder shows its first elastic response which means; the powder bed is either relatively packed or the frictional and cohesive forces between particles are larger than the compaction pressure and the application of any force beyond that level may cause particles to fracture.

Notes

¹O'Neil [2006]

²GSD and MMAD, explained in Chapter 6.4

³Pharmacy Compounding Centre of America

⁴Feret diameter, Average distance between pairs (horizontal and vertical) of parallel tangent lines to the particle's projected outline

Chapter 7

Conclusion

A novel technique has been introduced to determine compression-derived parameters for powders. The method, which is based on low-pressure, uniaxial, confined compaction within the range of 0-1200 kPa, is a very efficient method that requires only milligram quantities of sample rather than the several grams needed for the conventional compression techniques or tapped density measurements. A suitable instrument has been manufactured and interfaced with a computer for data acquisition in LabVIEW to reduce operator-introduced errors. A series of pharmaceutical powders with different particle sizes and physical properties was tested. The test samples were different batches of spray-dried powders with particle diameters in the respirable range and additional pharmaceutical powders with larger particles. Different plots of compressed bulk density vs. compaction pressure were analyzed.

It was determined that classical powder density tests that were developed for samples with large particle sizes are not well suited for respirable powders, because the interparticle forces rather than inertial forces dominate the compaction behavior of respirable powders. Tests also showed that the relative humidity during the compaction test impacts the results and should be controlled. It was found that the sample history can influence the initial state of compaction reduces the usefulness of the Carr index and Hausner ratio for respirable powders. However, a new graph has been proposed to demonstrate the compressibility with which the compaction factor can be determined.

Different method settings had different effects on the low-pressure compression curves. For example, different geometries of punches and dies were tested in the optimization of the design. The compression rate did not have a

significant effect on the compressed bulk density within the investigated speed ranges from 0.02 to 1mm/s, but due to the low-pressure compaction, noticeable differences in the compaction curves were observed. The compression of a bed of agglomerates in a confined space gives a good estimation of the powder strength used to measure applied stress and strain. The effect of particle size in the compacts porosity has also been analyzed.

Two common mathematical models, Heckel, and Kawakita were used to further evaluate and predict the compressibility of powders with different properties using the experimental results. The Heckel model has been shown to be very good at differentiating different stages of compaction, while the Kawakita model shows a very promising applicability in determining compression parameters for the low-pressure compaction technique. These two models showed that different compaction mechanisms such as; particle rearrangement, particle fragmentation, and viscoelastic deformation are involved in powder compaction.

The new instrument is also capable of compressing powders with harmonic, sawtooth, and triangle wave compression profiles, a mode that is not available in any commercial instrument. The modulated compression profiles were used to determine the elastic and plastic behavior of powders without destroying the particles. The results of powder compression that used modulated profile were compared and validated with experimental results when fitted to the Heckel model.

Several aspects of the uniaxial compression of pharmaceutical powder at low-pressure compaction were addressed. The low-pressure compaction approach seems to be very sensitive to any changes that occur in the system, as it significantly responds to any changes in either the powders that are being tested or the method being used. The instrument and technique provides the capability to easily control the compression procedure. The investigation on the modulated compaction profile also showed that the critical assessment of the in-die and out-of-die measurements, by considering the fundamental deformation behavior of the materials under question, is possible.

Due to the excellent repeatability of the low-pressure compaction technique, it is possible to differentiate between materials that are different, chem-

ically and physically. In addition to that, this technique is a very efficient and sensitive method to characterize very small sample masses. Thus, it provides an alternative method that is cost-effective and superior to other commercially available instruments and, particularly, the traditional tapped-density measurement that requires several grams of sample, which is a very critical issue for expensive and rare powders.

Bibliography

- E. C. Abdullah and D. Geldart. The use of bulk density measurements as flowability indicators. *Powder Technology*, 102(2):151–165, 1999.
- M. J. Adams, M. A. Mullier, and J. P. K. Seville. Agglomerate strength measurement using a uniaxial confined compression test. *Powder Technology*, 78(1):5–13, 1994.
- C. Ahlneck and G. Alderborn. Moisture adsorption and tableting. i. effect on volume reduction properties and tablet strength for some crystalline materials. *International Journal of Pharmaceutics*, 54(2):131 – 141, 1989.
- G. Alderborn and C. Nystrom. Studies on direct compression of tablets xiv. the effect of powder fineness on the relation between tablet permeametry surface area and compaction pressure. *Powder Technology*, 44(1):37 – 42, 1985.
- G. Alderborn and C. Nystrom. *Pharmaceutical Powder Compaction Technology*. Marcel Dekker, Inc., 1996.
- G. E. Amidon, P. J. Secreast, and D. Mudie. *Developing Solid Oral Dosage Forms: Pharmaceutical Theory and Practice*, chapter Particle, powder, and compact characterization, pages 163–186. Elsevier, 2009.
- O. Antikainen and J. Yliruusi. Determining the compression behaviour of pharmaceutical powders from the force–distance compression profile. *International journal of pharmaceutics*, 252(1):253–261, 2003.
- S. J. Antony, W. Hoyle, Y. Ding, and J. Zhu. *Granular material: Fundamental and Applications*, chapter Fluidization of Fine Powder. The Royal Society of Chemistry, 2004.

- N. Armstrong and L. P. Palfrey. The effect of machine speed on the consolidation of four directly compressible tablet diluents. *Journal of pharmacy and pharmacology*, 41(3):149–151, 1989.
- N. A. Armstrong and F. S. S. Morton. The effect of granulating agents on the elasticity and plasticity of powders. *J. Powder Bulk Solids*, 1:32–35, 1977.
- N. A. Armstrong and L. P. Palfrey. Punch velocities during the compaction process. *Journal of pharmacy and pharmacology*, 39(7):497–501, 1987.
- A. G. Atkins and Y-W. Mai. Deformation transitions. *Journal of materials science*, 21(4):1093–1110, 1986.
- M. Baerns. Effect of interparticle adhesive forces on fluidization of fine particles. *Industrial and Engineering Chemistry Fundamentals*, 5(4):508–516, 1966.
- I. S. Buckner. *Compression calorimetry, powder compaction thermodynamics and deformation mechanisms*. PhD thesis, The University of Iowa, 2009.
- R. D. Carneim. *Characterization of Uniaxial Compaction in Spray Dired Ceramic Powder*. PhD thesis, The Pennsylvania State University, 2000.
- R. L. Carr. Evaluating flow properties of solids. *Chem. Eng*, 72(2):163–168, 1965.
- M. Celik. Overview of compaction data analysis techniques. *Drug development and industrial pharmacy*, 18(6-7):767–810, 1992.
- D. P. Coffin-Beach and R. G. Hollenbeck. Determination of the energy of tablet formation during compression of selected pharmaceutical powders. *International Journal of Pharmaceutics*, 17(2-3):313 – 324, 1983.
- A. R. Cooper Jr and L. E. Eaton. Compaction behavior of several ceramic powders. *Journal of the American Ceramic Society*, 45(3):97–101, 1962.
- A. H. De Boer, G. K. Bolhuis, and C. F. Lerk. Bonding characteristics by scanning electron microscopy of powders mixed with magnesium stearate. *Powder Technology*, 20(1):75 – 82, 1978.
- P. J. Denny. Compaction equations: a comparison of the heckel and kawakita equations. *Powder Technology*, 127(2):162–172, 2002.

- B. V. Derjaguin. The force between molecules. *Scientific American*, 203(1):47–53, 1960.
- B. V. Derjaguin, V. M. Muller, and Y. P. Toporov. Effect of contact deformations on the adhesion of particles. *Journal of Colloid and Interface Science*, 53(2):314 – 326, 1975.
- M. Duberg and C. Nystrom. Studies on direct compression of tablets xvii. porosity-pressure curves for the characterization of volume reduction mechanisms in powder compression. *Powder Technology*, 46(1):67 – 75, 1986.
- M. Duberg, C. Nyström, et al. Studies on direct compression of tablets. vi. evaluation of methods for the estimation of particle fragmentation during compaction. *Acta Pharmaceutica Suecica*, 19(6):421, 1982.
- A. L. Feng, M. A. Boraey, M. A. Gwin, P. R. Finlay, P. J. Kuehl, and R. Vehring. Mechanistic models facilitate efficient development of leucine containing microparticles for pulmonary drug delivery. *International journal of pharmaceutics*, 409(1):156–163, 2011.
- W. H. Finlay. *The mechanics of inhaled pharmaceutical aerosols: an introduction*. Academic Press, 2001.
- T. Freeman. Ft4 powder rheometer methodology,. Technical report, Freeman Technology, 2012.
- D. Geldart. Types of gas fluidization. *Powder Technology*, 7(5):285 – 292, 1973.
- R. O. Grey and J. K. Beddow. On the hausner ratio and its relationship to some properties of metal powders. *Powder Technology*, 2(6):323–326, 1969.
- B. C. Hancock, J. T. Colvin, M. P. Mullarney, and A. V. Zinchuk. Pharmaceutical powders, blends, dry granulations, and immediate-release tablets. *Pharmaceutical technology*, 2003.
- J. S. Hardman, B. A. Lilley, J. S. Hardman, and B. A. Lilley. Mechanisms of compaction of powdered materials. In *Proceedings of the Royal Society of London. A. Mathematical and Physical Sciences*, volume 333, pages 183–199. the Royal Society of London, 1973.

- H. H. Hausner. Friction conditions in a mass of metal powder. *Int. J. Powder Met.*, 3(4):7–13, 1967.
- R. W. Heckel. An analysis of powder compaction phenomena. *Trans. Metall. Soc. AIME*, 221(1001-1008), 1961a.
- R. W. Heckel. Density-pressure relationship in powder compaction. *Transaction of the Metallurgical Society of AIME*, 221(4):671–675, 1961b.
- J. A. Hersey and J. E. Rees. Deformation of particles during briquetting. *Nature*, 230(12):96–96, 1971.
- J. A. Hersey, J. E. Rees, and E. T. Cole. Density changes in lactose tablets. *Journal of Pharmaceutical Sciences*, 62(12):2060–2060, 1973.
- T. Higuchi, A. Narsimha Rao, J. W. Busse, and J. V. Swintosky. The physics of tablet compression. ii. the influence of degree of compression on properties of table. *Journal of the American Pharmaceutical Association*, 42(4):194–200, 1953. ISSN 1930-2304.
- W. C. Hinds. *Aerosol Technology: Properties, Behavior, and Measurement of Airborne Particle*. Wiley-Interscience, New York, 1982.
- L. E. Holman and H. Leuenberger. Effect of compression speed on the relationship between normalised solid fraction and mechanical properties of compacts. *International journal of pharmaceutics*, 57(1):R1–R5, 1989.
- Q. Huang. *Flow and fluidization properties of fine powders*. PhD thesis, University of Western Ontario, London, ON, Canada, 2009.
- K. L. Johnson, K. Kendall, and A. D. Roberts. Surface energy and the contact of elastic solids. *Proceedings of the Royal Society of London. A. Mathematical and Physical Sciences*, 324(1558):301–313, 1971.
- T. M. Jones. The physicochemical properties of starting materials used in tablet formulation. *Int. J. Pharm. Tech. Prod. Manu.*, 2:17–24, 1981.
- K. Kawakita and K-H. Lüdde. Some considerations on powder compression equations. *Powder technology*, 4(2):61–68, 1971.
- K. Kawakita and Y. Tsutsumi. An empirical equation of state for powder compression. *Japanese journal of applied physics*, 4(1):56–63, jan 1965.

- J. Kikuta and N. Kitamori. Evaluation of the die wall friction during tablet ejection. *Powder Technology*, 35(2):195–200, 1983.
- I. Klevan, J. Nordström, A. Bauer-Brandl, and G. Alderborn. On the physical interpretation of the initial bending of a shapiro–konopicky–heckel compression profile. *European journal of pharmaceutics and biopharmaceutics*, 71(2):395–401, 2009.
- I. Klevan, J. Nordstram, I. Tho, and G. Alderborn. A statistical approach to evaluate the potential use of compression parameters for classification of pharmaceutical powder materials. *European Journal of Pharmaceutics and Biopharmaceutics*, 75(3):425 – 435, 2010.
- M. C. Kostelnik and J. K. Beddow. New techniques for tap density. *Modern Developments in Powder Metallurgy; Proceedings. Editor: Henry H. Hausner*, 4:29, 1971.
- L. Lachman, H. A. Lieberman, and J. L. Kanig. *The theory and practice of industrial pharmacy*. Lea and Febiger Philadelphia, 1986.
- S. Leigh, J. E. Carless, and B. W. Burt. Compression characteristics of some pharmaceutical materials. *Journal of Pharmaceutical Sciences*, 56(7):888–892, 1967.
- Q. Li, V. Rudolph, B. Weigl, and A. Earl. Interparticle van der waals force in powder flowability and compactibility. *International Journal of Pharmaceutics*, 280(1):77 – 93, 2004.
- M. Luangtana-Anan and J. T. Fell. Bonding mechanisms in tableting. *International Journal of Pharmaceutics*, 60(3):197 – 202, 1990.
- K. Marshall. A new technique for investigating the process of tablet compression: A preliminary report. *Journal of Pharmacy and Pharmacology*, 15(1):413–421, 1963.
- S. Matinkhoo, K. H. Lynch, J. J. Dennis, W. H. Finlay, and R. Vehring. Spray-dried respirable powders containing bacteriophages for the treatment of pulmonary infections. *Journal of pharmaceutical sciences*, 100(12):5197–5205, 2011.
- S. Mattsson. *Pharmaceutical binders and their function in directly compressed tablets: Mechanistic studies on the effect of dry binders on mechanical*

- strength, pore structure and disintegration of tablets*. PhD thesis, Uppsala University, Department of Pharmacy, 2000.
- A. McKenna and D. F. McCafferty. Effect of particle size on the compaction mechanism and tensile strength of tablets. *Journal of Pharmacy and Pharmacology*, 34(6):347–351, 1982.
- R. M. Nedderman. *Statics and kinematics of granular materials*. Cambridge University Press, 1992.
- E. Nelson, L. W. Busse, and T. Higuchi. The physics of tablet compression. vii. determination of energy expenditure in the tablet compression process. *Journal of the American Pharmaceutical Association*, 44(4):223–225, 1955.
- J. Nordström, I. Klevan, and G. Alderborn. A particle rearrangement index based on the kawakita powder compression equation. *Journal of pharmaceutical sciences*, 98(3):1053–1063, 2009.
- O. A. Odeku. The compaction of pharmaceutical powders. *Pharmaceutical Reviews*, 5, 2007.
- S. Patel, A. M. Kaushal, and A. K. Bansal. Effect of particle size and compression force on compaction behavior and derived mathematical parameters of compressibility. *Pharmaceutical research*, 24(1):111–124, 2007.
- Euro. Pharmacopeia. *5th Edition, European Pharmacopeia*. Strasbourg, France, 2004a.
- Euro. Pharmacopeia. *Bulk Density and Tapped Density of Powders*. European Pharmacopeia, suppliment of 6.8 to european pharmacopeia edition, 2010.
- US. Pharmacopeia. *The National Formulary*. Rockville, MD, 2004b.
- US Pharmacopeia. *Powder Flow (1174)*. United States Pharmacopeia, Rockville, MD, usp 29-nf 24 (us pharmacopeia convention) edition, 2011a.
- US Pharmacopeia. *Bulk Density and Tapped Density of Powders (616)*. United States Pharmacopeia, stage 6 harmonization edition, 2011b.
- US Pharmacopeia. *Bulk Density and Tapped Density of Powders*. United States Pharmacopeia, 2012.

- V. M. Puri. Introduction to flowability via powder mechanics. Powder Characterization Short Course Note, 2001.
- P. J. Ramsey. *Physical Evaluation of Compressed Powder Systems: The Effect of Particle Size and Porosity Variation on Hiestand Compaction Indices*. PhD thesis, University of Iowa, 1996.
- K. Rietema. Powders, what are they? *Powder Technology*, 37(1):5–23, 1984.
- K. Rietema. *The Dynamics of Fine Powders*. Elsevier Applied Science, 1991.
- K. Rietema, J. Boonstra, G. Schenk, and A. H. M. Verkooijen. The interaction between gas and dispersed solids and its effect on handling operations of solid. In *Proceeding of the European Symposium on Particle Technology*, Amsterdam, The Netherlands, 1980. European Symposium on Particle Technology.
- M. Rios. Developments in powder flow testing. Technical report, Advanstar Communications Inc., 2006.
- R. J. Roberts and R. C. Rowe. The effect of punch velocity on the compaction of a variety of materials. *Journal of pharmacy and pharmacology*, 37(6):377–384, 1985.
- R. J. Roberts and R. C. Rowe. The effect of the relationship between punch velocity and particle size on the compaction behaviour of materials with varying deformation mechanisms. *Journal of pharmacy and pharmacology*, 38(8):567–571, 1986.
- R. J. Roberts and R. C. Rowe. Brittle/ductile behaviour in pharmaceutical materials used in tableting. *International Journal of Pharmaceutics*, 36(2-3):205 – 209, 1987.
- C. E. Rowlings, D. E. Wurster, and P. J. Ramsey. Calorimetric analysis of powder compression: Ii. the relationship between energy terms measured with a compression calorimeter and tableting behavior. *International Journal of Pharmaceutics*, 116(2):191 – 200, 1995.
- C. E. Ruegger and M. Celick. The effect of compression and decompression speed on the mechanical strength of compacts. *Pharmaceutical development and technology*, 5(4):485–494, 2000.

- S. Sayyar Roudsari. *Pressure Distribution Evaluation of Different Filling Methods for Deposition of Powders in Dies: Measurement and Modeling*. PhD thesis, The Pennsylvania State University, 2007.
- A. Shamsaddini-Shahrbabak and R. Vehring. The compression behavior of respirable powders at different relative humidity measured by a compressed bulk density tester for small sample masses. In *Proceeding of Respiratory Drug Delivery*, Phoneix, AZ, 2012. Respiratory Drug Delivery.
- J. M. Sonnergaard. A critical evaluation of the heckel equation. *International journal of pharmaceutics*, 193(1):63–71, 1999.
- J. M. Sonnergaard. Investigation of a new mathematical model for compression of pharmaceutical powders. *European Journal of Pharmaceutical Sciences*, 14(2):149 – 157, 2001.
- A. H. Sørensen, J. M. Sonnergaard, and L. Hovgaard. Bulk characterization of pharmaceutical powders by low-pressure compression. *Pharmaceutical development and technology*, 10(2):197–209, 2005.
- A. H. Sørensen, J. M. Sonnergaard, and L. Hovgaard. Bulk characterization of pharmaceutical powders by low-pressure compression ii: Effect of method settings and particle size. *Pharmaceutical development and technology*, 11(2):235–241, 2006.
- J. N. Staniforth and M. E. Aulton. Powder flow. *Pharmaceutics: the science of dosage form design*, pages 197–210, 2002.
- C. Sun and D. J. W. Grant. Influence of elastic deformation of particles on heckel analysis. *Pharmaceutical development and technology*, 6(2):193–200, 2001.
- L. Svarovsky. *Powder testing guide: methods of measuring the physical properties of bulk powders*. Elsevier Applied Science, New York, 1987.
- D. Tabor et al. *The friction and lubrication of solids*, volume 1. Oxford University Press, USA, 2001.
- M. D. Tousey. The granulation process 101. *Pharm Tech*, pages 8–13, 2002.
- R. Vehring. Pharmaceutical particle engineering via spray drying. *Pharmaceutical research*, 25(5):999–1022, 2008.

- E. E. Walker. The properties of powders. part vi. the compressibility of powders. *Transactions of the Faraday Society*, 19(July):73–82, 1923.
- C. Weiler, M. Egen, M. Trunk, and P. Langguth. Force control and powder dispersibility of spray dried particles for inhalation. *Journal of Pharmaceutical Sciences*, 99(1):303–316, 2010.
- A. J. Wheeler and A. R. Ganji. *Introduction to engineering experimentation*. Prentice Hall Englewood Cliffs, NJ, 1996.
- S. F. Yap, M. J. Adams, J. P. K. Seville, and Z. Zhang. Single and bulk compression of pharmaceutical excipients: Evaluation of mechanical properties. *Powder Technology*, 185(1):1–10, 2008.
- P. York. Particle slippage and rearrangement during compression of pharmaceutical powders. *Journal of Pharmacy and Pharmacology*, 30(1):6–10, 1978. ISSN 2042-7158. doi: 10.1111/j.2042-7158.1978.tb13144.x.
- J. Zhao, H. M. Burt, and R. A. Miller. The gurnham equation in characterizing the compressibility of pharmaceutical materials. *International Journal of Pharmaceutics*, 317(2):109 – 113, 2006.

Appendix A

SolidWorks Drawings

© by Abouzar Shamsaddini 2013

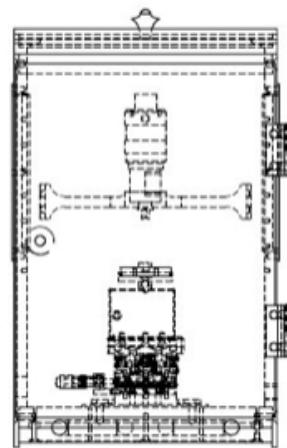
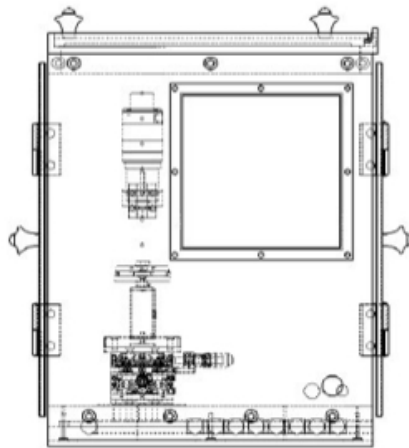
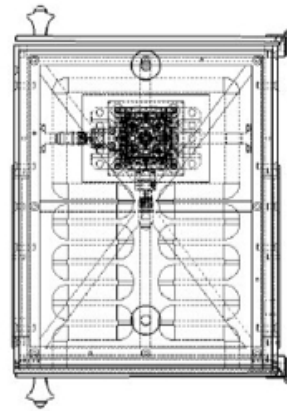
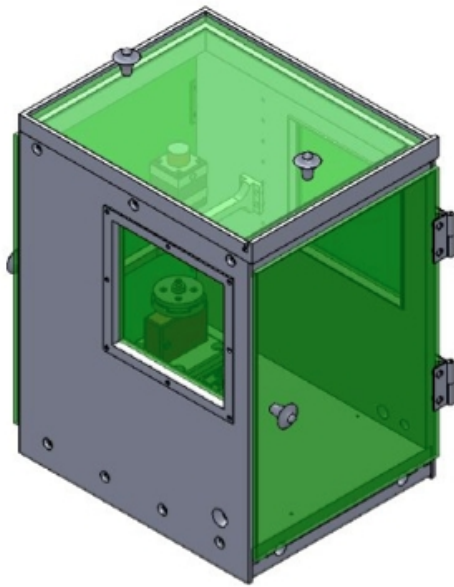
A.1 Tolerances and Fits

Two extreme permissible variations of a size between which the actual size is contained is called tolerance while fit is the relationship that exists between two parts which are to be assembled with respect to the difference on their sizes before assembly. There are three types of fit between the mating parts; Clearance fit is applied when it is needed that the two mating parts to rotate and slide freely with respect to each other. Interference fit is applied when it is needed that the mating parts to be securely held. Transition fit is applied when it is needed that the mating parts to be securely held yet not so securely that it cannot be disassembled.

The below table contains information that needs to be considered during manufacturing of the parts of the UAlberta density tester that are to be assembled together.

Parts	Types of Fits	Tolerances
Punch	Clearance fit	$6.00^{+0.00}_{-0.01}$ (mm)
Sample Pan, part 2 (die)		$6.45^{+0.01}_{-0.00}$ (mm)
Sample pan, part 1(die filler)	Transition fit	$6.426^{+0.00}_{-0.002}$ (mm)
		$6.451^{+0.02}_{-0.00}$ (mm)
Sample pan holder (inner dia.)	Transition fit	$50.00^{+0.00}_{-0.05}$ (mm)
Sample pan, part1 (outer dia.)		$50.00^{+0.05}_{-0.00}$ (mm)
Base, bottom plate (boss extrusion)	Interference fit	$10.00^{+0.00}_{-0.02}$ (mm)
Base, top plate (cut extrusion)		$10.00^{+0.02}_{-0.00}$ (mm)
Pins, and pin holes	Transition fit	$3.00^{+0.00}_{-0.025}$ (mm)
Window	Interference fit	$160.250^{+0.00}_{-0.02}$ (mm)
Window pane		$156.250^{+0.02}_{-0.00}$ (mm)
Actuator holder, and actuator	Transition fit	$30.00^{+0.05}_{-0.00}$ (mm)

Table A.1: Tollerances and fits in UAlberta density tester instrument



NOTE : (Unless otherwise sepcified)

- * All Dimensions in milimeters**
- * Parts have to be clean and burr free**

PARTICLE ENGINEERING / VEHRING

TITLE: **UAlberta
Density Tester**

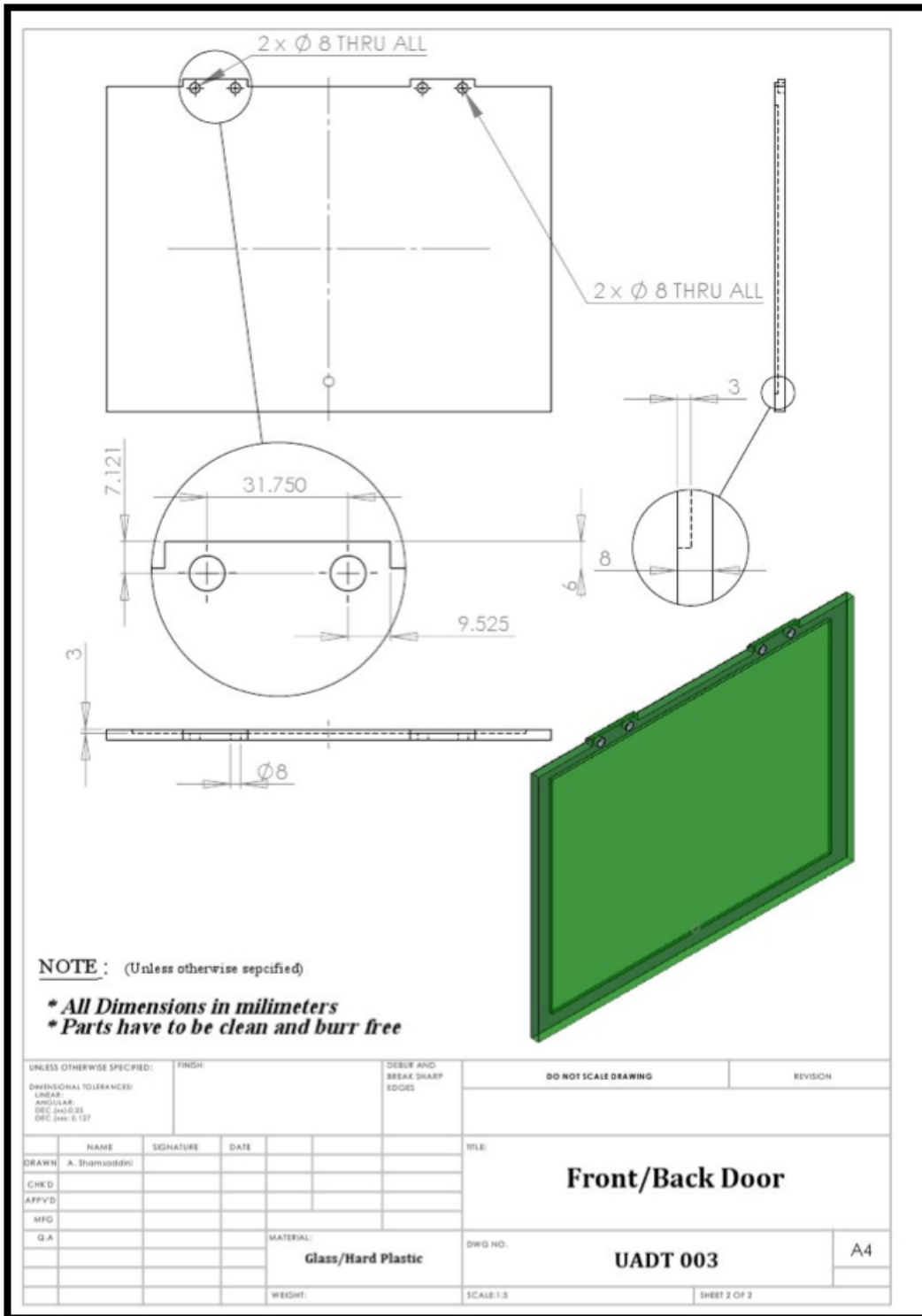
DRAWN	NAME	DATE	
CHKD	<i>A. Shamsaddini</i>	<i>14/Dec/2011</i>	
APPVD			
MFG			
Q.A			
	MATERIAL:		
	6061 Aluminum/Stainless Steel/ Glass/ Hard Plastic (RP)		
	WEIGHT:		

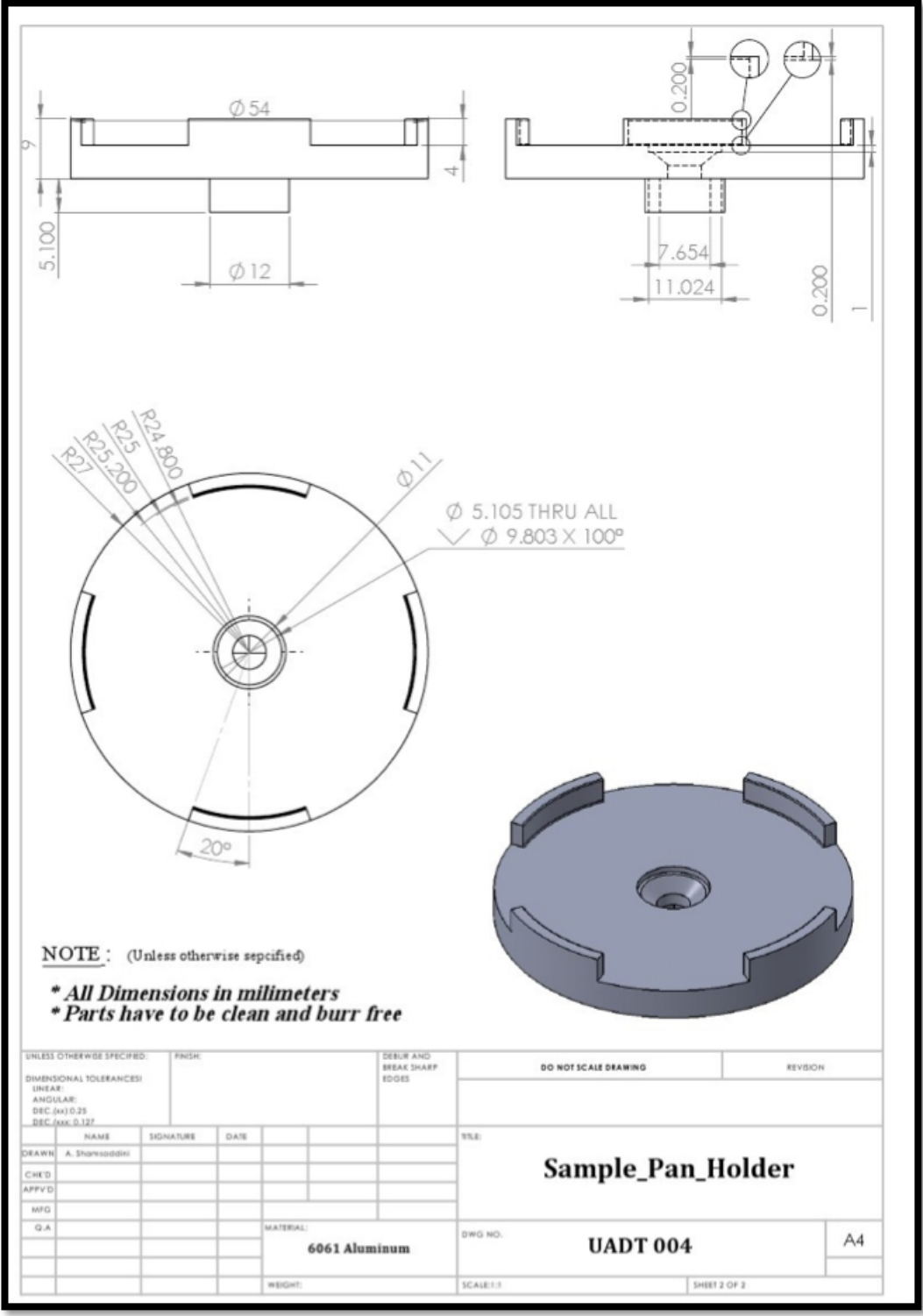
DO NOT SCALE DRAWING

A4

SCALE: 1:10

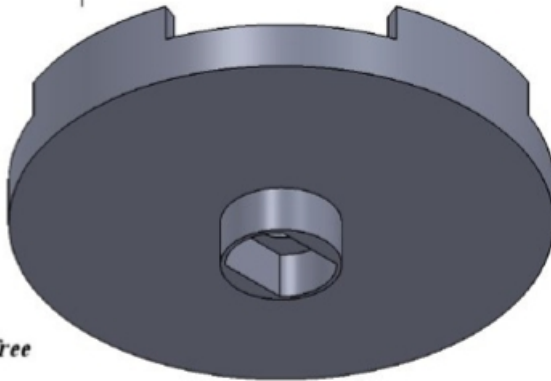
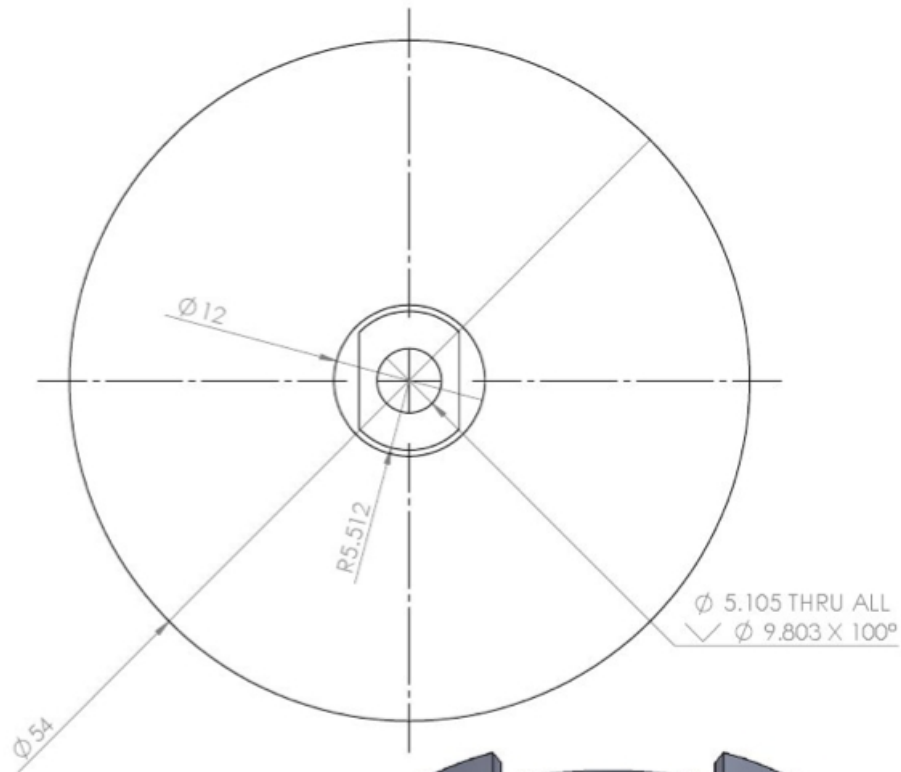
SHEET 1 OF 45





NOTE : (Unless otherwise specified)
*** All Dimensions in millimeters**
*** Parts have to be clean and burr free**

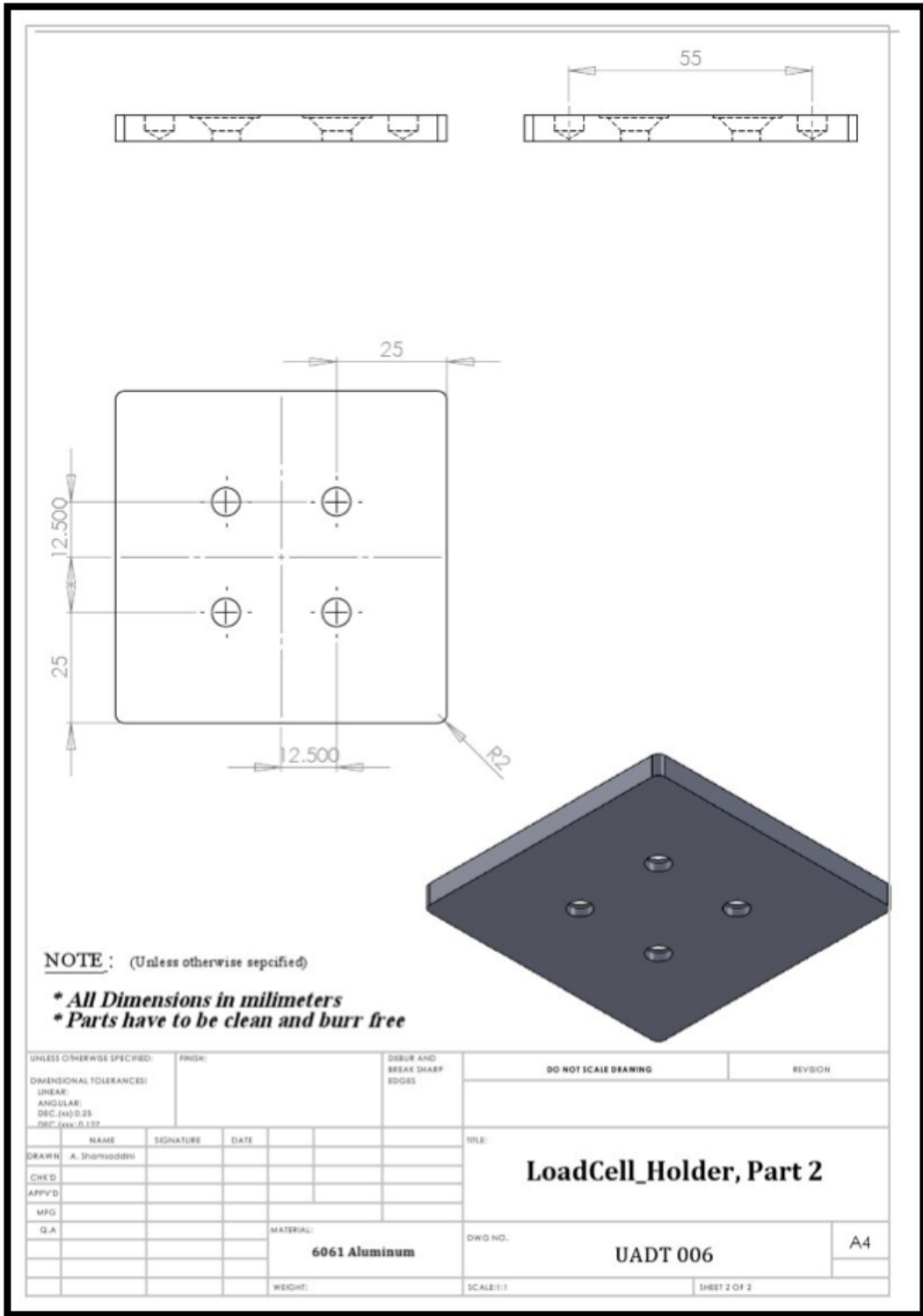
UNLESS OTHERWISE SPECIFIED:		FINISH:		DEBUR AND BREAK SHARP EDGES		DO NOT SCALE DRAWING		REVISION	
DIMENSIONAL TOLERANCES:									
LINEAR:									
ANGULAR:									
DEC (ASD.35)									
DEC (XXX.5.127)									
	NAME	SIGNATURE	DATE			TITLE:			
DRAWN	A. Sharifuddin					Sample_Pan_Holder			
CHECKED									
APPROVED									
MFG									
QA									
		MATERIAL:		DWG NO.		UADT 004		A4	
		6061 Aluminum							
		WEIGHT:		SCALE:1:1		SHEET 2 OF 2			

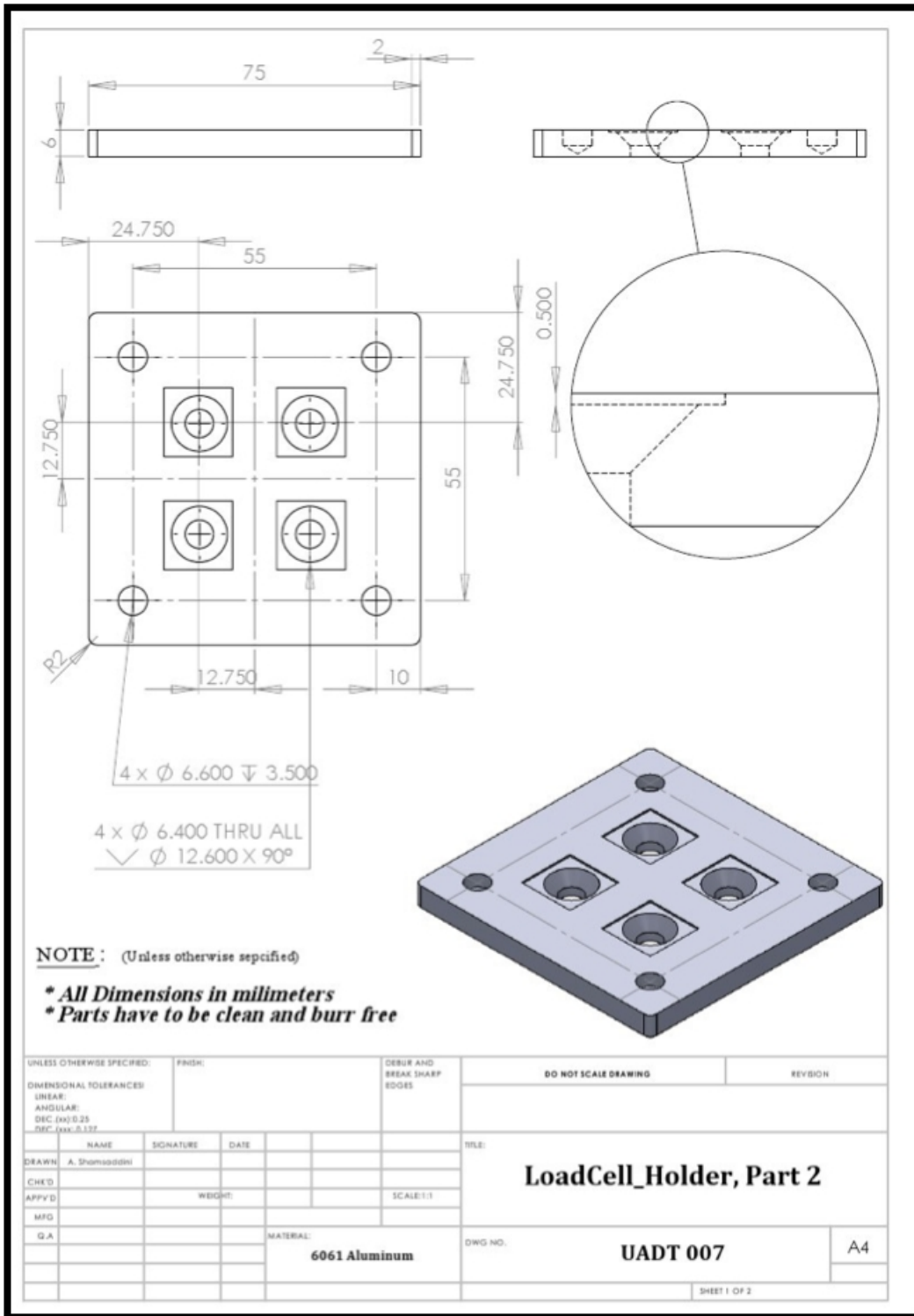


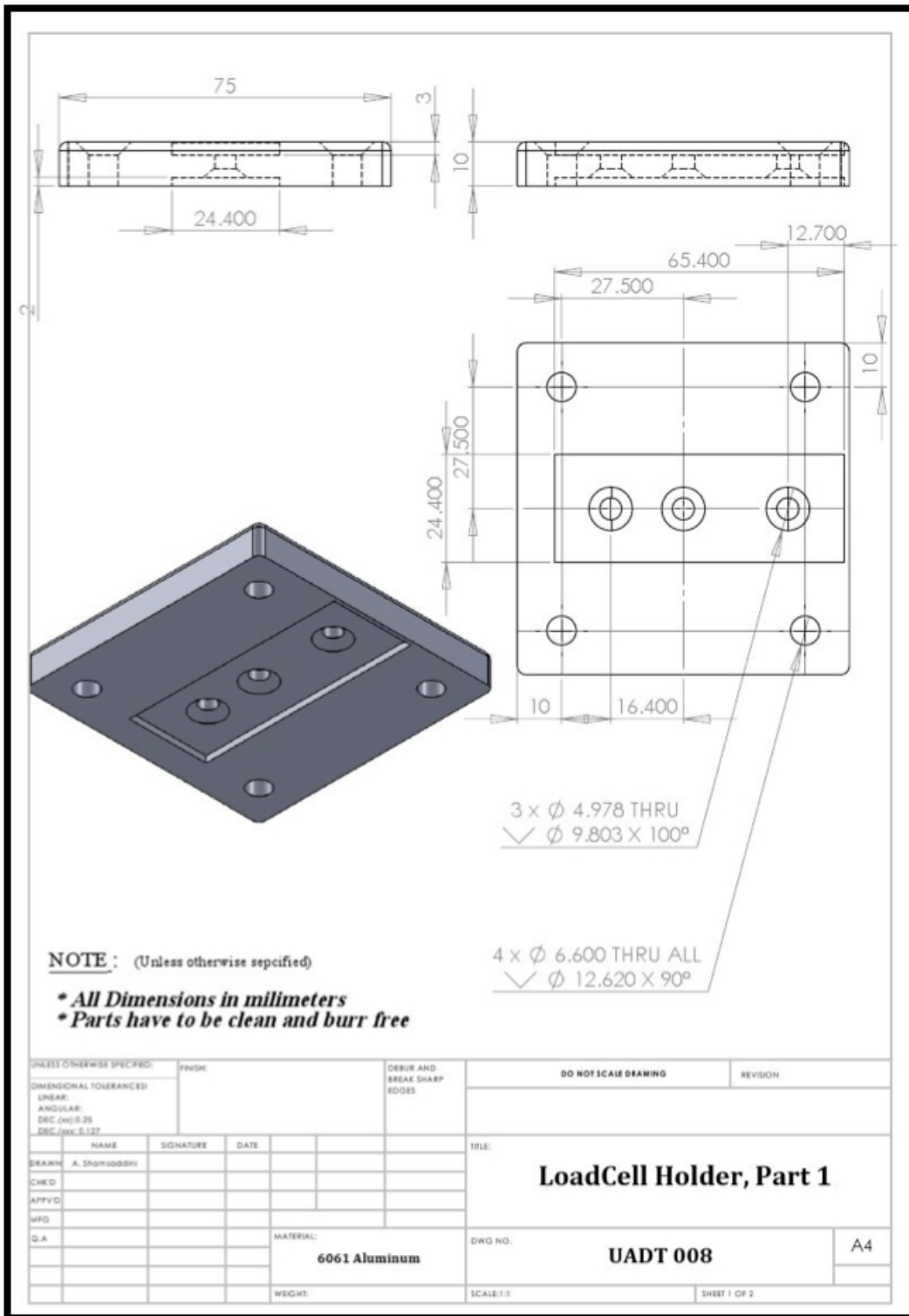
NOTE : (Unless otherwise specified)

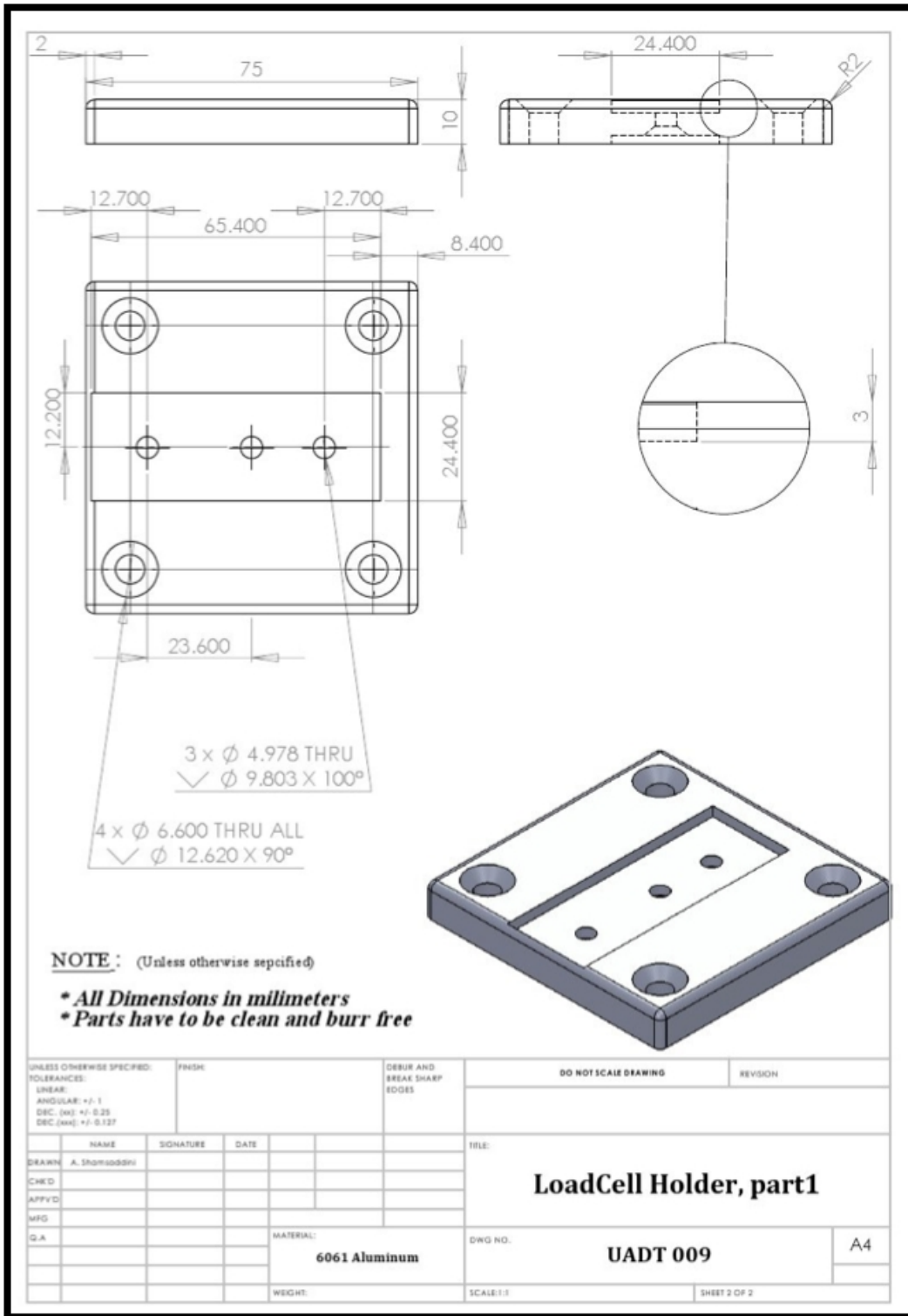
- * All Dimensions in millimeters
- * Parts have to be clean and burr free

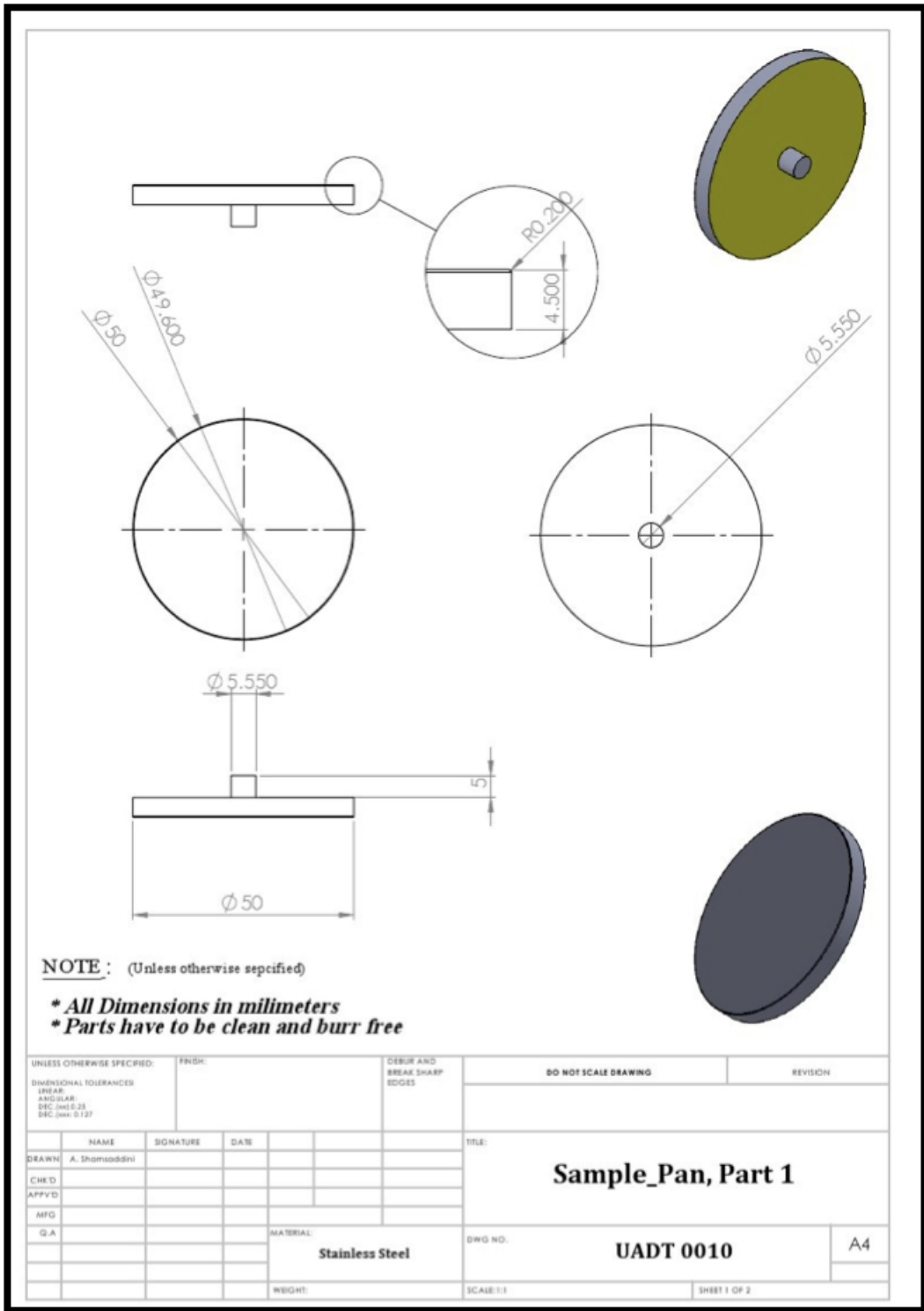
UNLESS OTHERWISE SPECIFIED:		FINISH:		ISSUE AND BREAK SHARP EDGES		DO NOT SCALE DRAWING		REVISION	
DIMENSIONAL TOLERANCES:									
LINEAR:									
ANGULAR:									
DEC (XXX.D.DD)									
DEC (XXX.D.DD)									
DRAWN: A. Shamsuddin		SIGNATURE		DATE		TITLE:			
CHK'D:						Sample_Pan_Holder			
APP'VD:									
MFG:						MATERIAL:		DWG NO. UADT 005	
QA:						6061 Aluminum		A4	
						WEIGHT:		SCALE: 1:1	
								SHEET 2 OF 2	

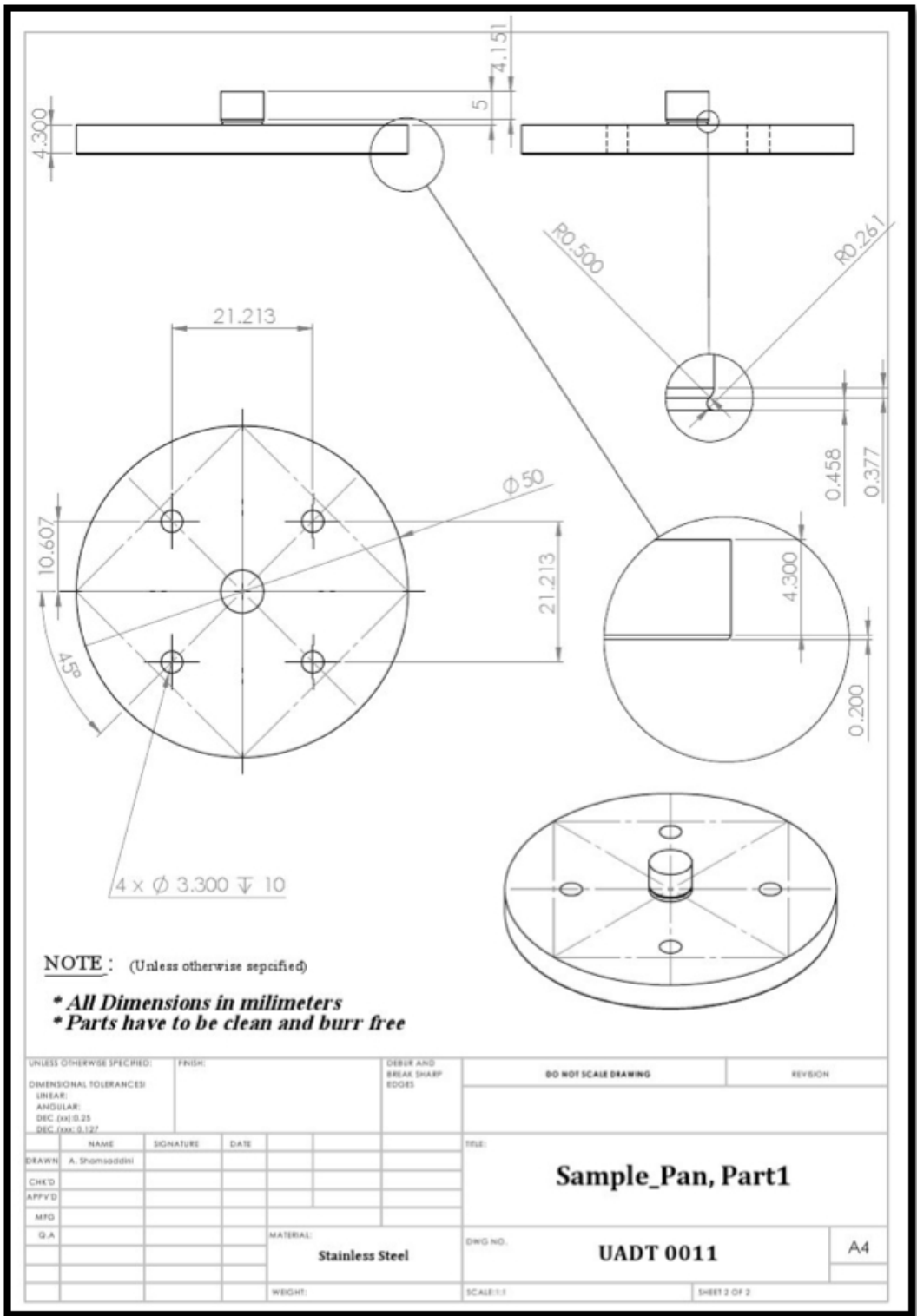








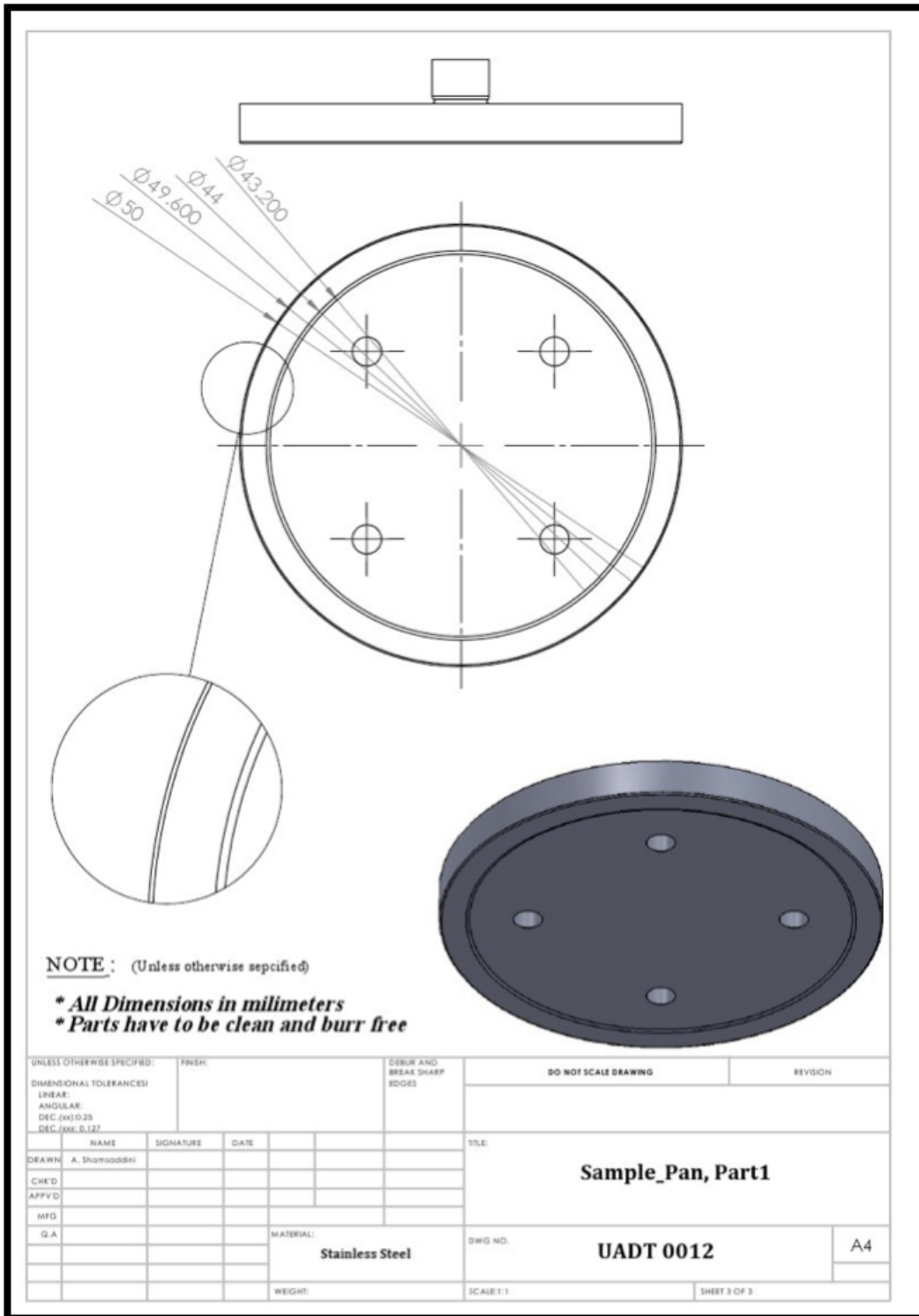


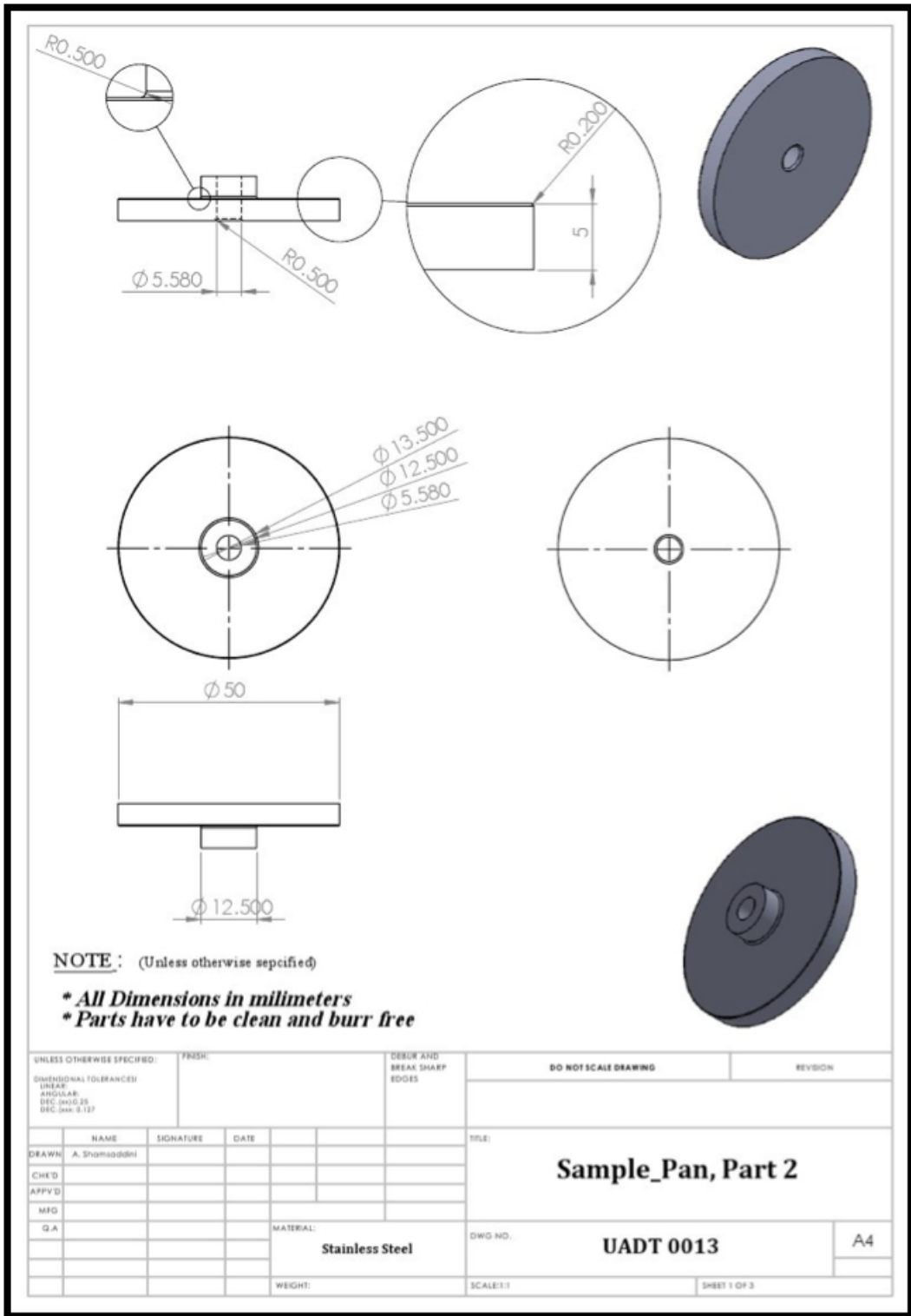


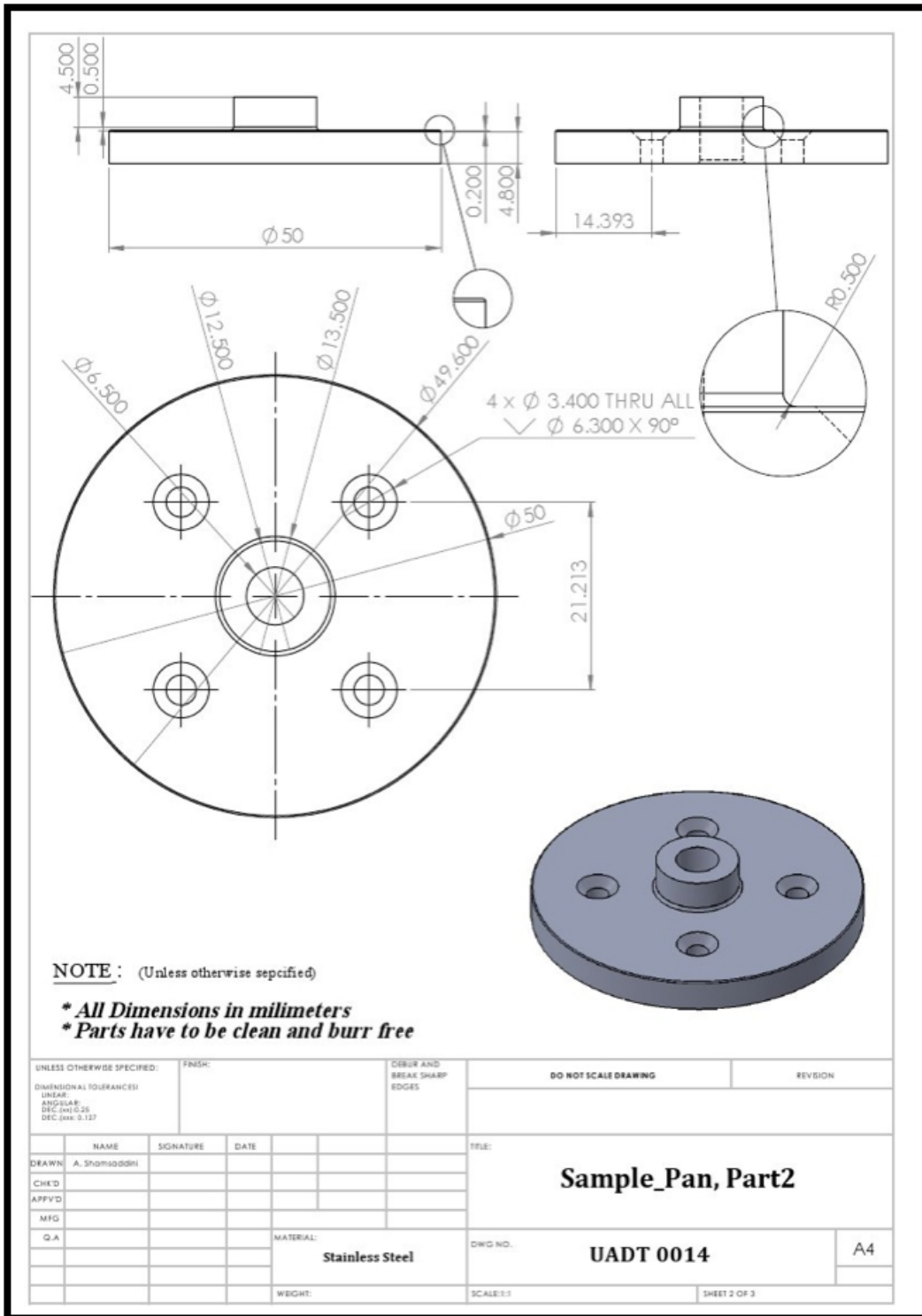
NOTE : (Unless otherwise sepcified)

- * All Dimensions in millimeters
- * Parts have to be clean and burr free

UNLESS OTHERWISE SPECIFIED:		FINISH:		DEBUR AND BREAK SHARP EDGES		DO NOT SCALE DRAWING		REVISION	
DIMENSIONAL TOLERANCES:									
LINEAR:									
ANGULAR:									
DEC (xx) 0.25									
DEC (xxx) 0.127									
DRAWN		NAME		SIGNATURE		DATE		TITLE:	
A. Shamsiddin								Sample_Pan, Part1	
CHKD									
APPVD									
MFG									
QA								MATERIAL:	
								Stainless Steel	
								DWG NO. UADT 0011	
								A4	
								SCALE: 1:1	
								SHEET 2 OF 2	



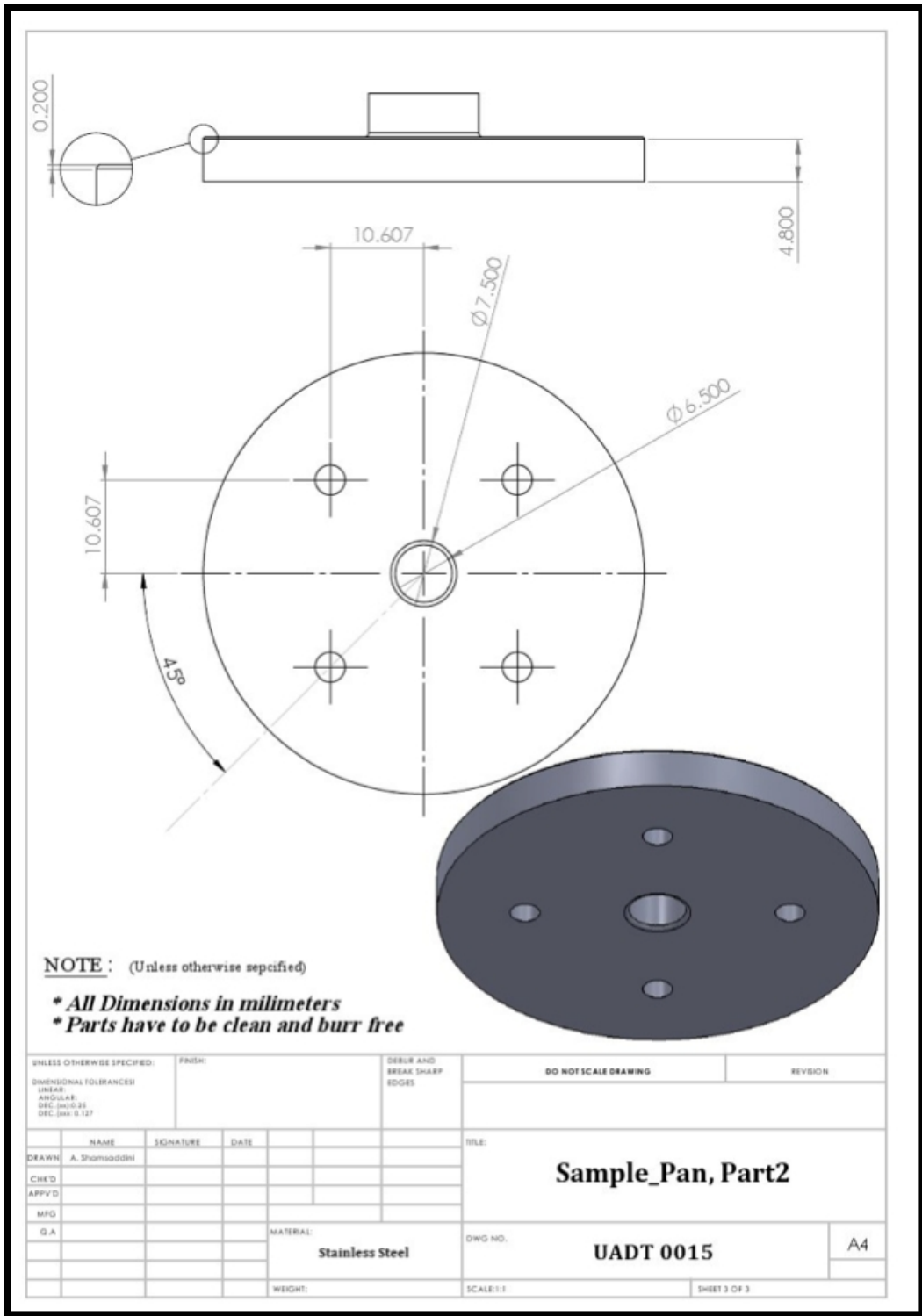


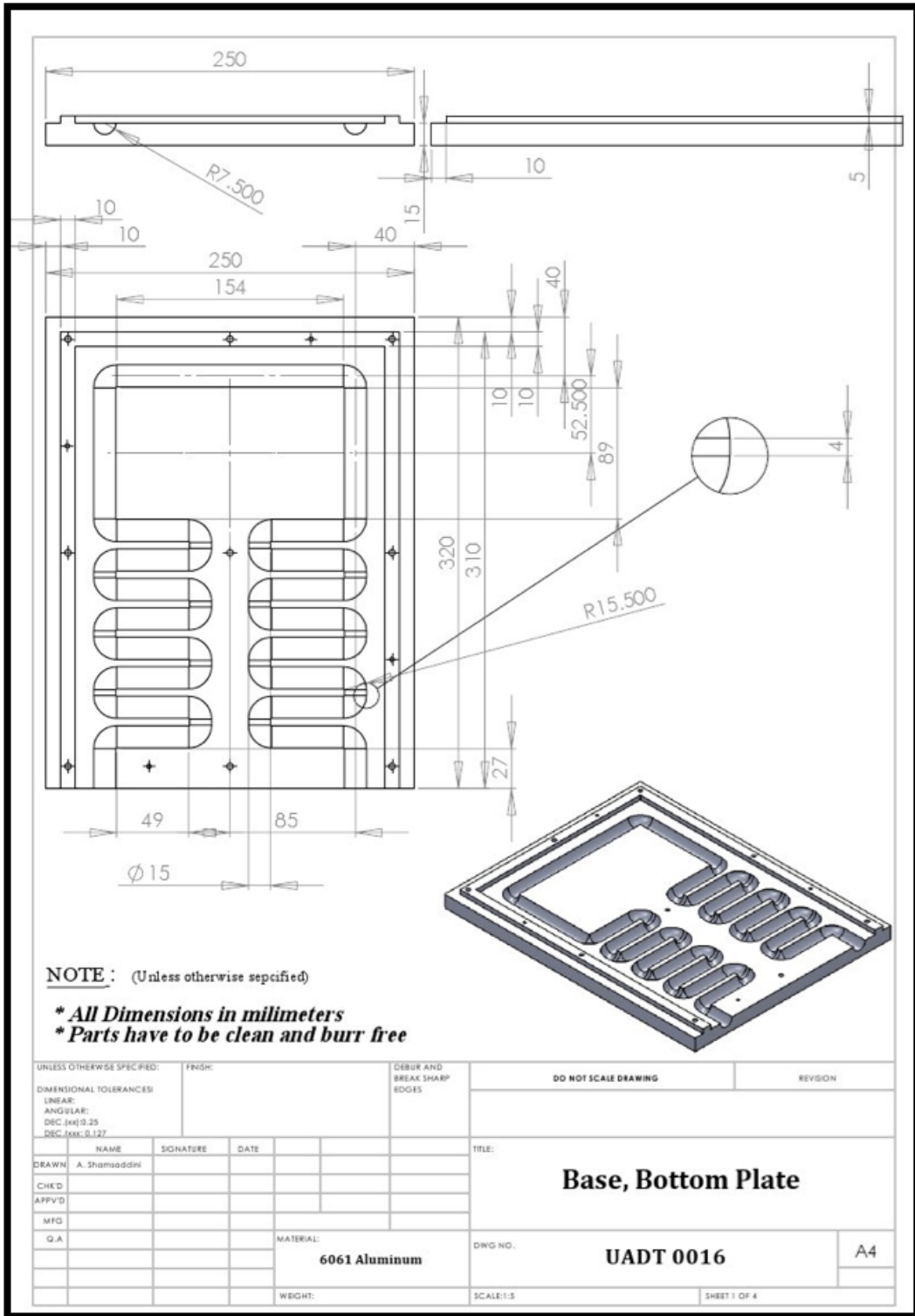


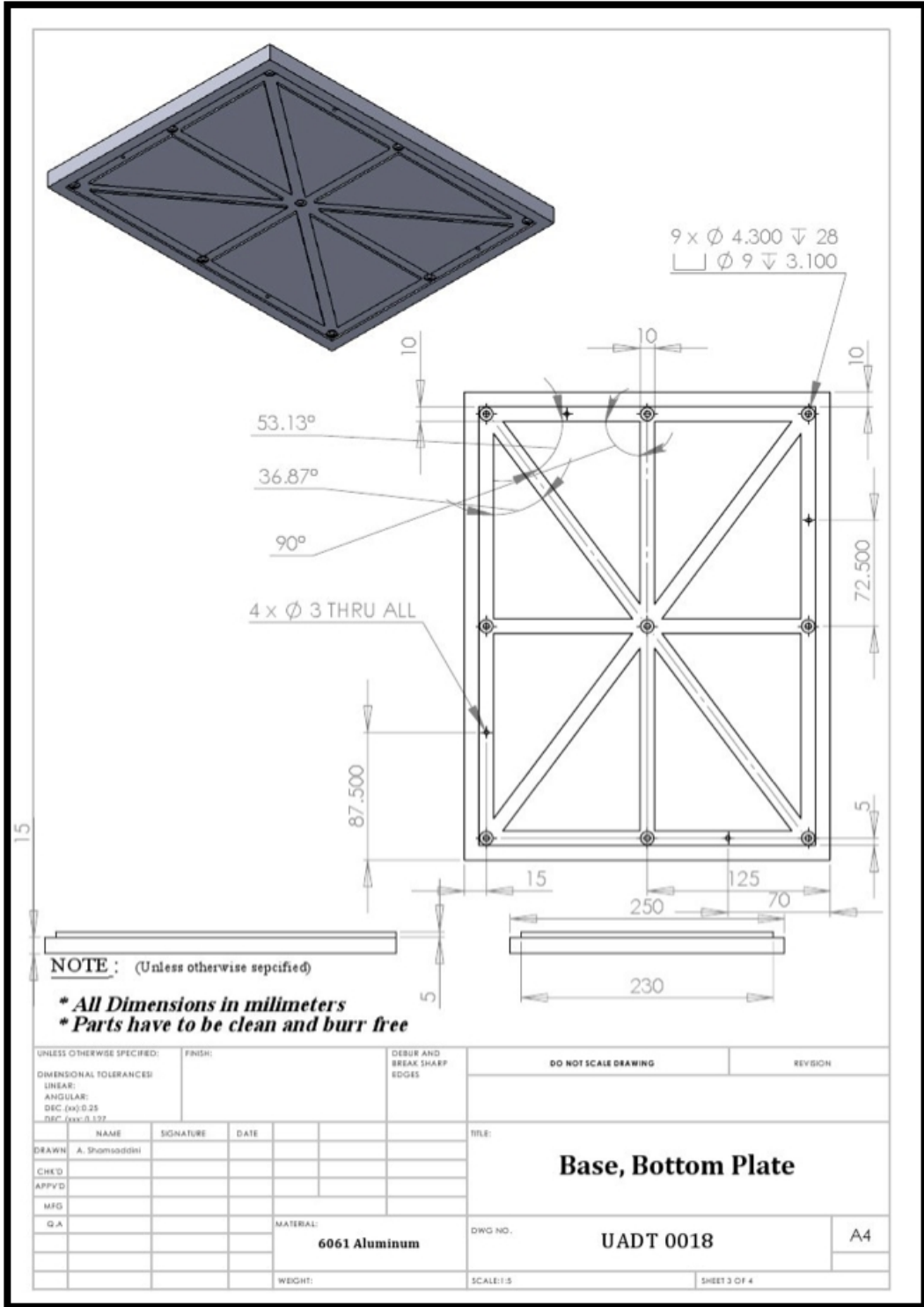
NOTE : (Unless otherwise specified)

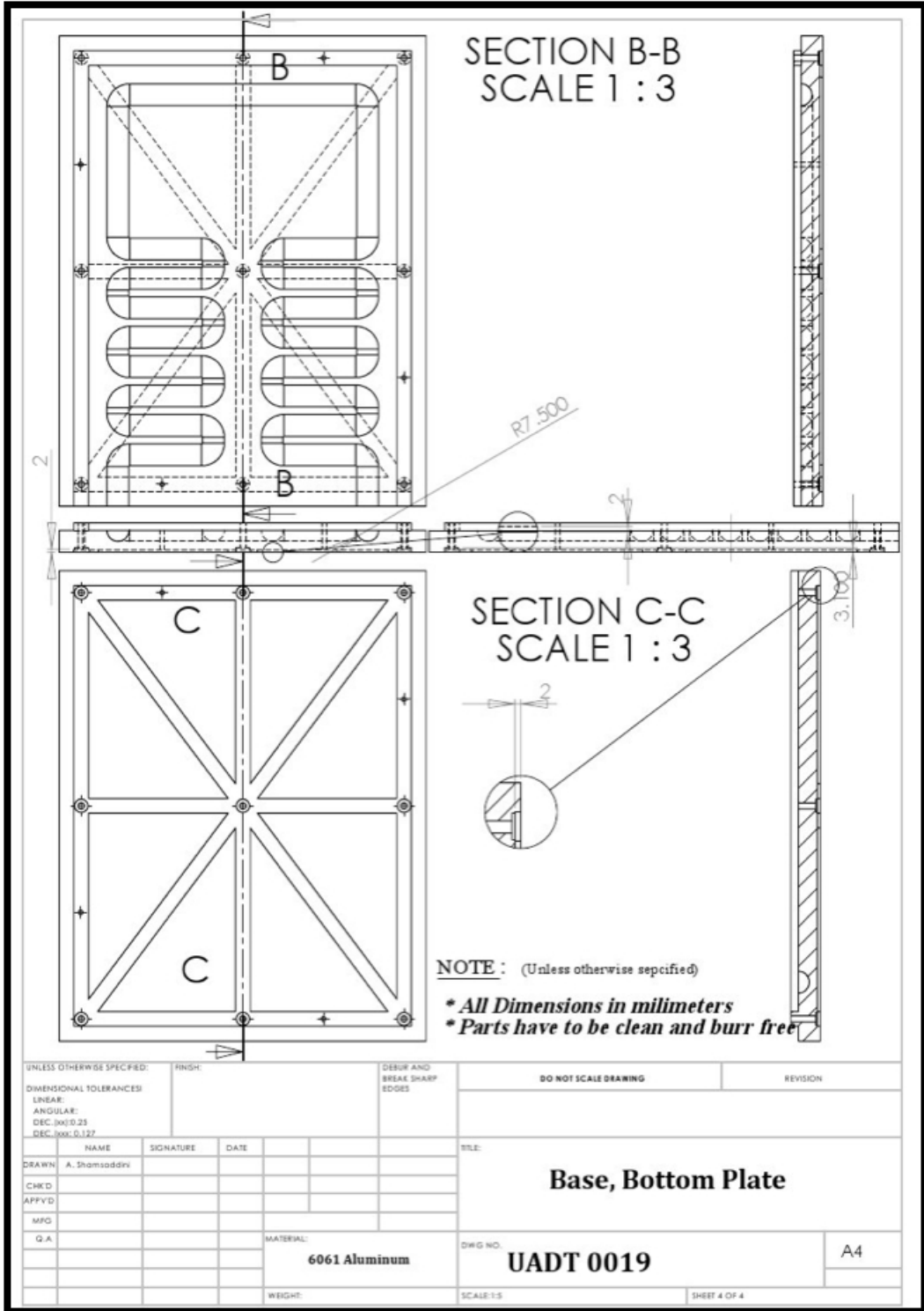
- * All Dimensions in millimeters**
- * Parts have to be clean and burr free**

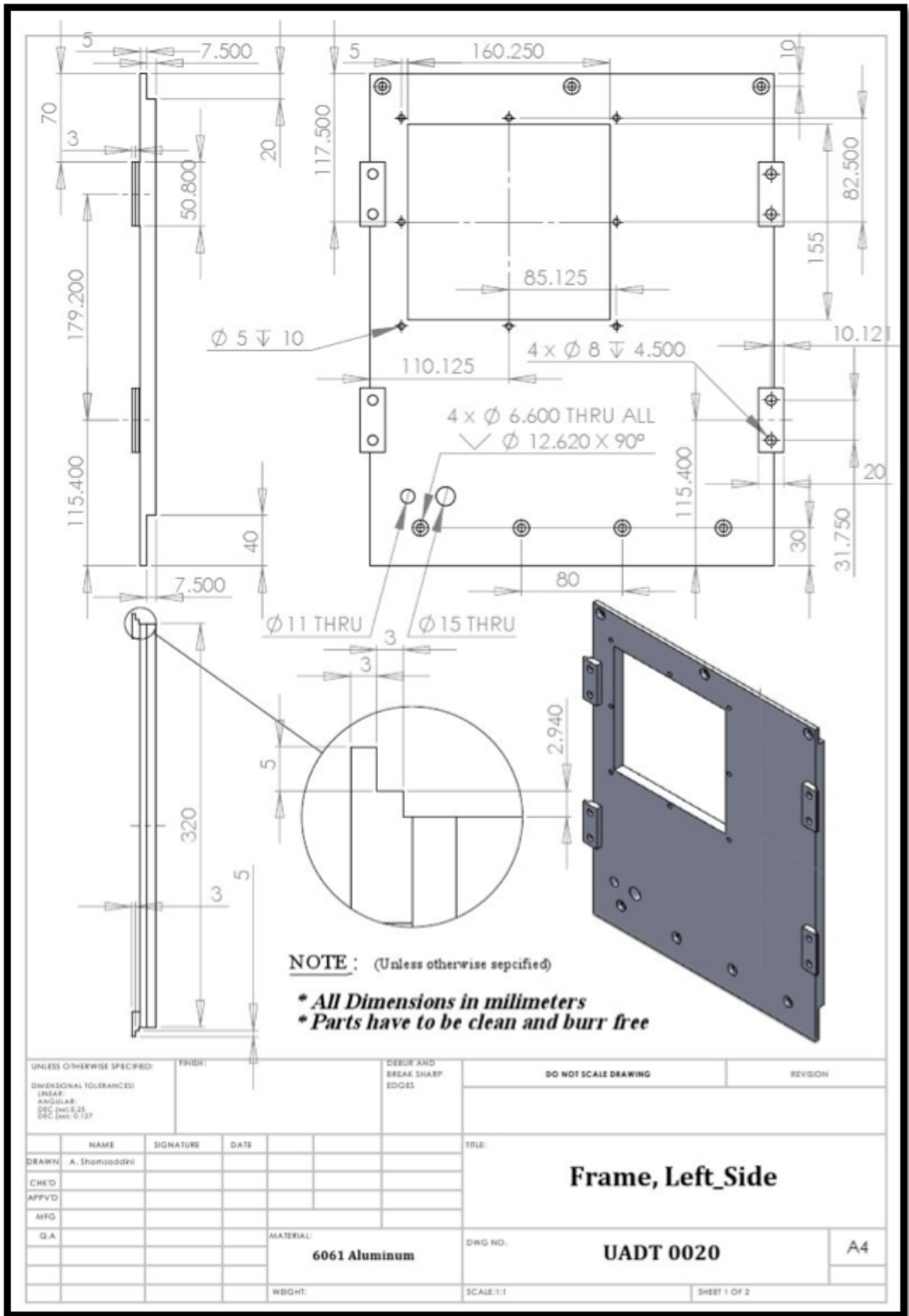
UNLESS OTHERWISE SPECIFIED:		FINISH:		DEBUR AND BREAK SHARP EDGES		DO NOT SCALE DRAWING		REVISION		
DIMENSIONAL TOLERANCES:										
LINEAR:										
ANGULAR:										
DEC: (MIL) 0.25										
DEC: (MM) 0.127										
NAME	SIGNATURE	DATE				TRUE:				
DRAWN	A. Shamsoddini					Sample_Pan, Part2				
CHK'D										
APP'VD										
MTG										
Q.A										
MATERIAL:			Stainless Steel			DWG NO.:		UADT 0014		A4
WEIGHT:						SCALE: 1:1		SHEET 2 OF 3		

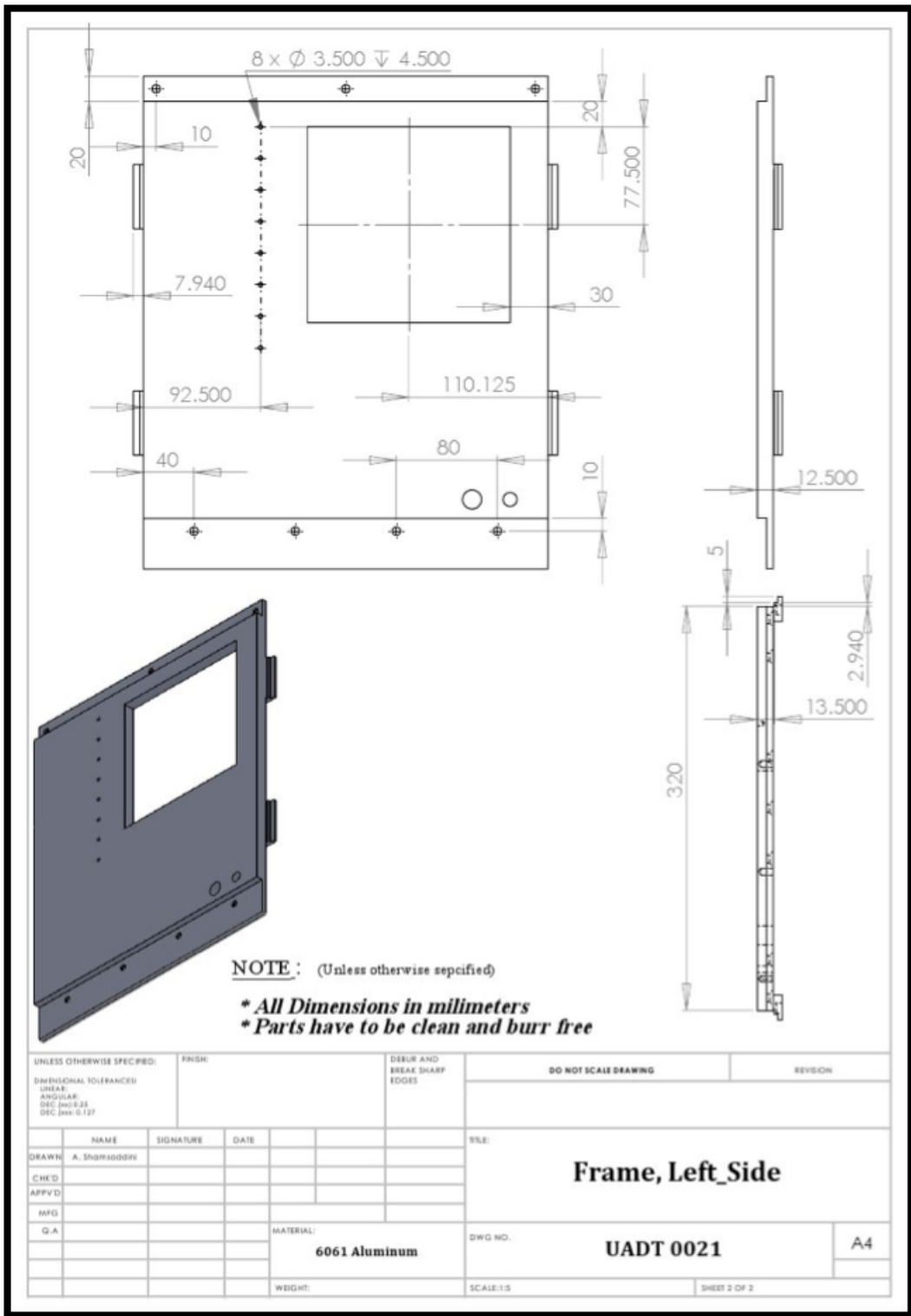








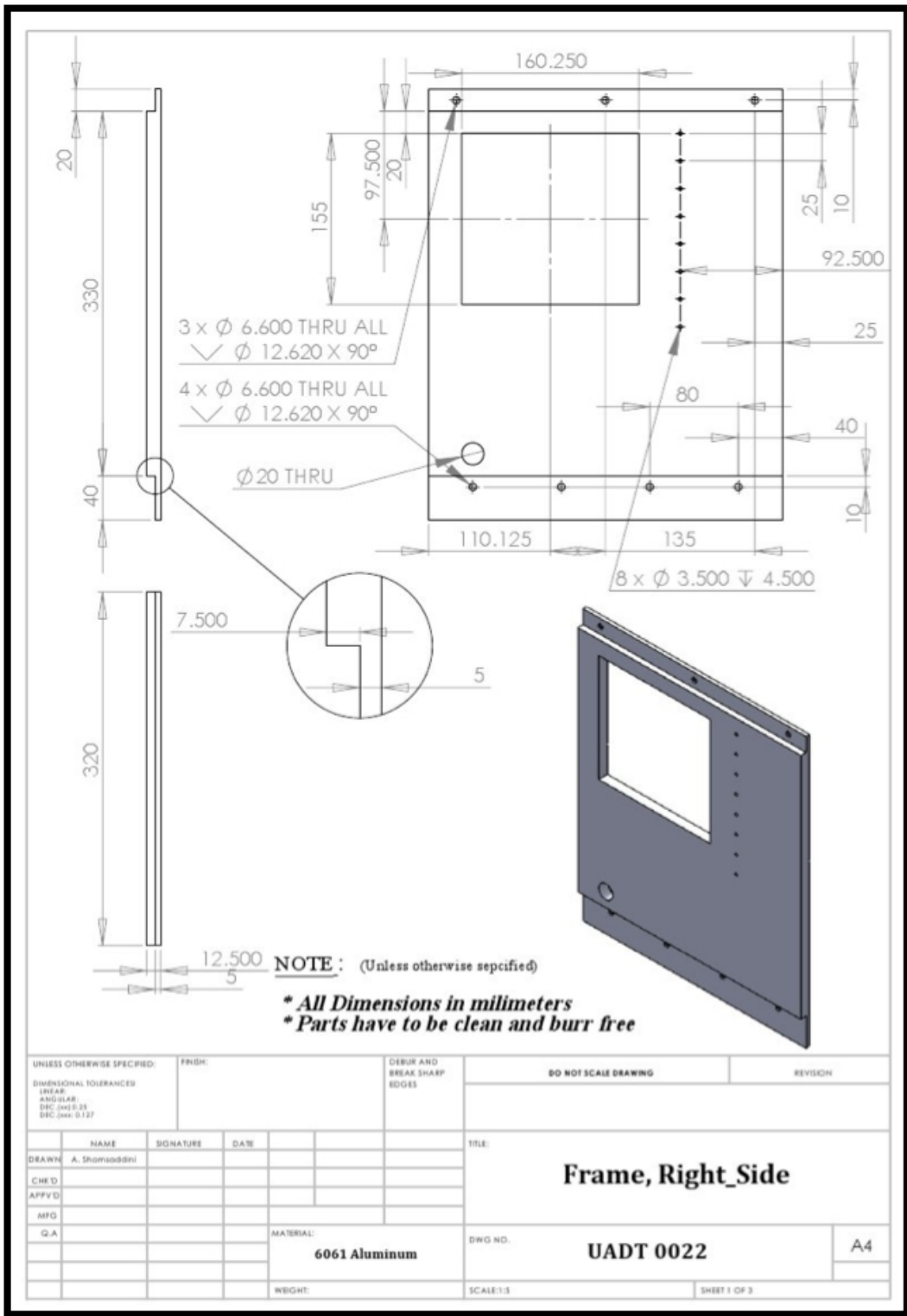


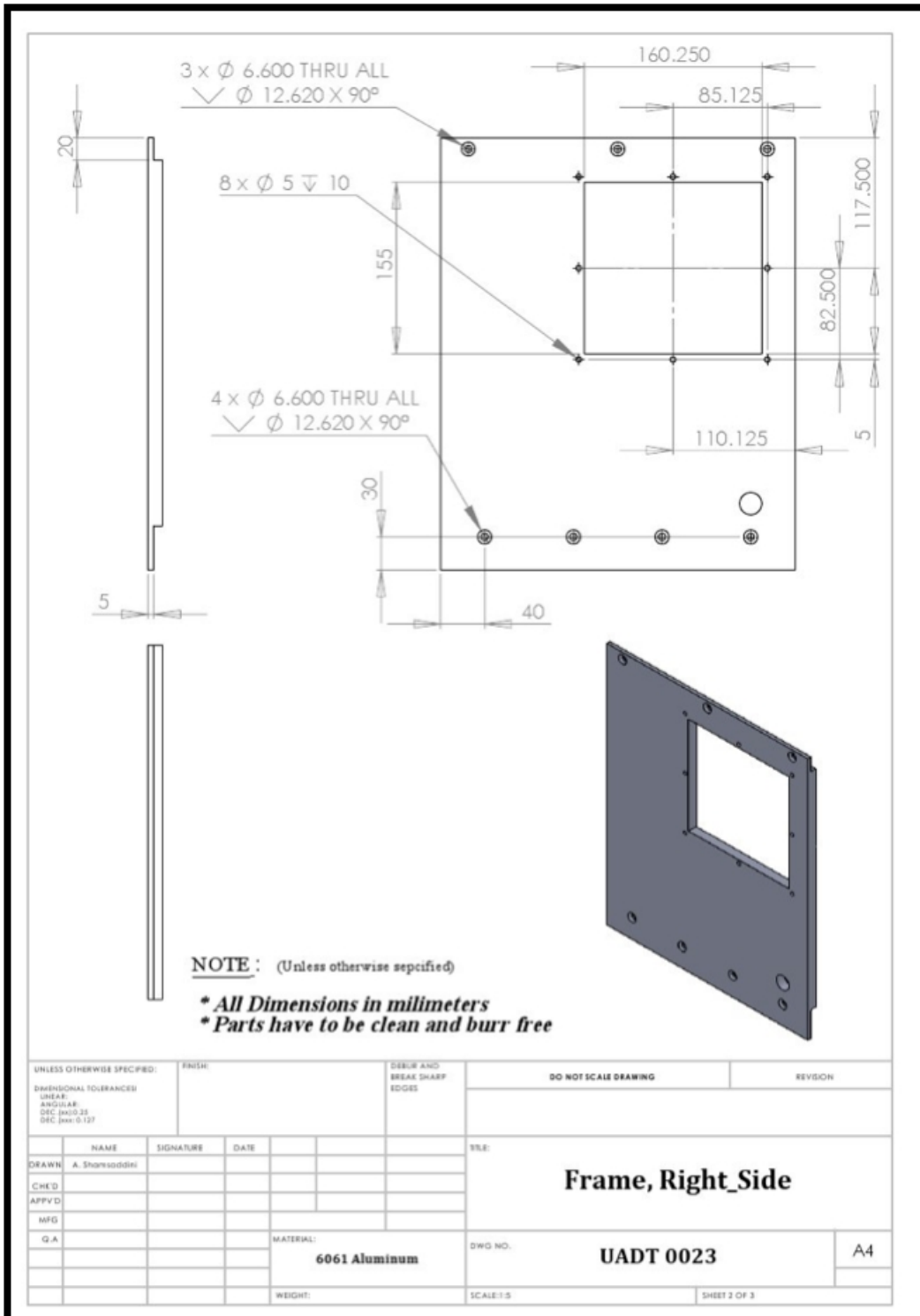


NOTE : (Unless otherwise specified)

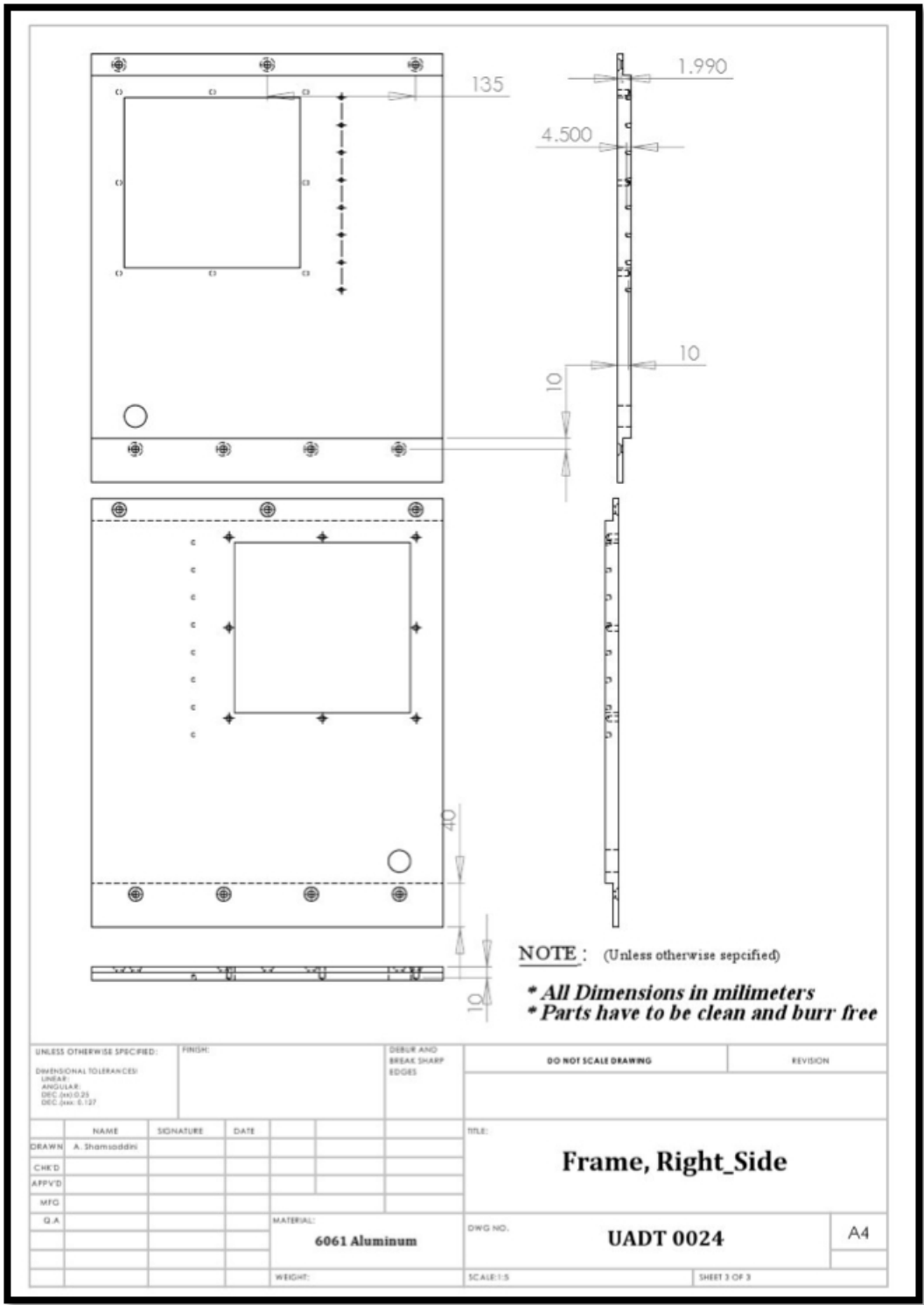
*** All Dimensions in millimeters**
*** Parts have to be clean and burr free**

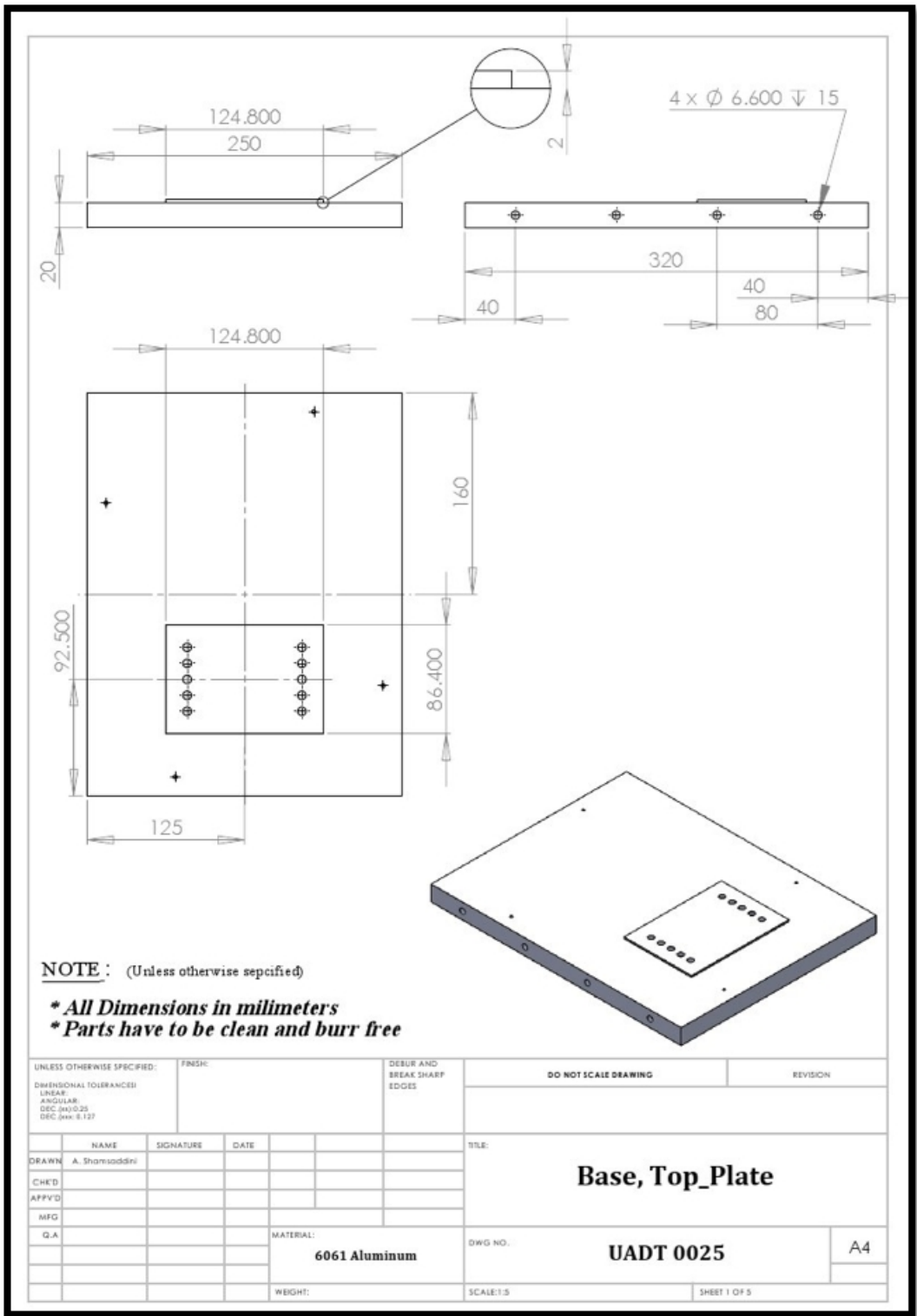
UNLESS OTHERWISE SPECIFIED:		FINISH:		DEBUR AND BREAK SHARP EDGES:		DO NOT SCALE DRAWING		REVISION:	
DIMENSIONAL TOLERANCES:									
LINEAR:									
ANGULAR:									
DEC: (MILS):									
INC: (MILS):									
SEC: (MILS):									
DRAWN:		SIGNATURE:		DATE:		TITLE:			
A. Shor-oddoy						Frame, Left_Side			
CHECKED:									
APPVED:									
MFG:									
Q.A:									
		MATERIAL:		DWG NO.:		SCALE: 1:5		SHEET 2 OF 2	
		6061 Aluminum		UADT 0021				A4	
		WEIGHT:							





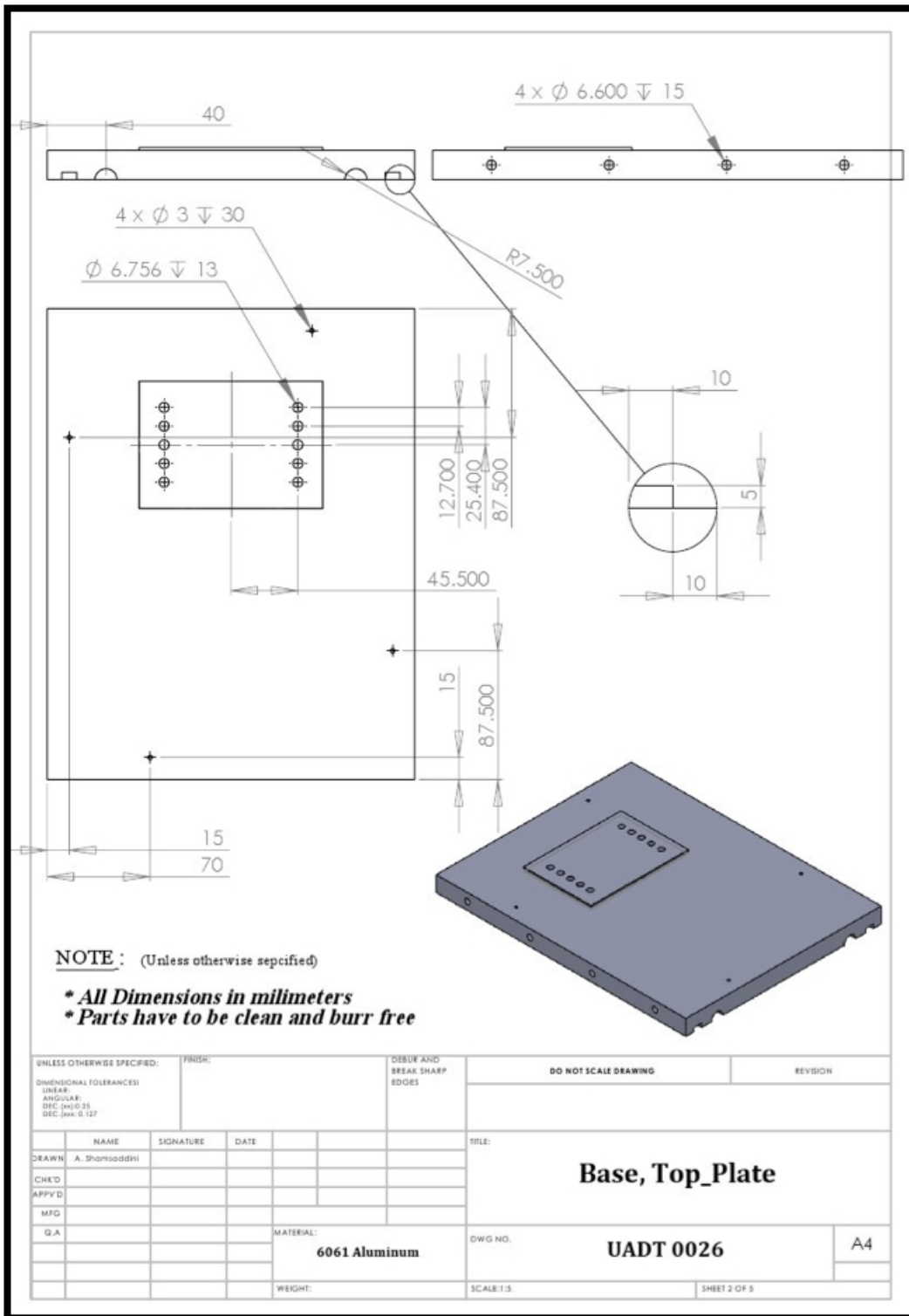
UNLESS OTHERWISE SPECIFIED:		FINISH:		DEBUR AND BREAK SHARP EDGES		DO NOT SCALE DRAWING		REVISION	
DIMENSIONAL TOLERANCES									
LINEAR:									
ANGULAR:									
DEC (MILS):									
SEC (MILS):									
DRAWN		SIGNATURE		DATE		TITLE:			
A. Shamsoddini						Frame, Right_Side			
CHECKED									
APPROVED									
MFG									
Q.A									
				MATERIAL:		DWG. NO.		A4	
				6061 Aluminum		UADT 0023			
				WEIGHT:		SCALE: 1:5		SHEET 2 OF 3	

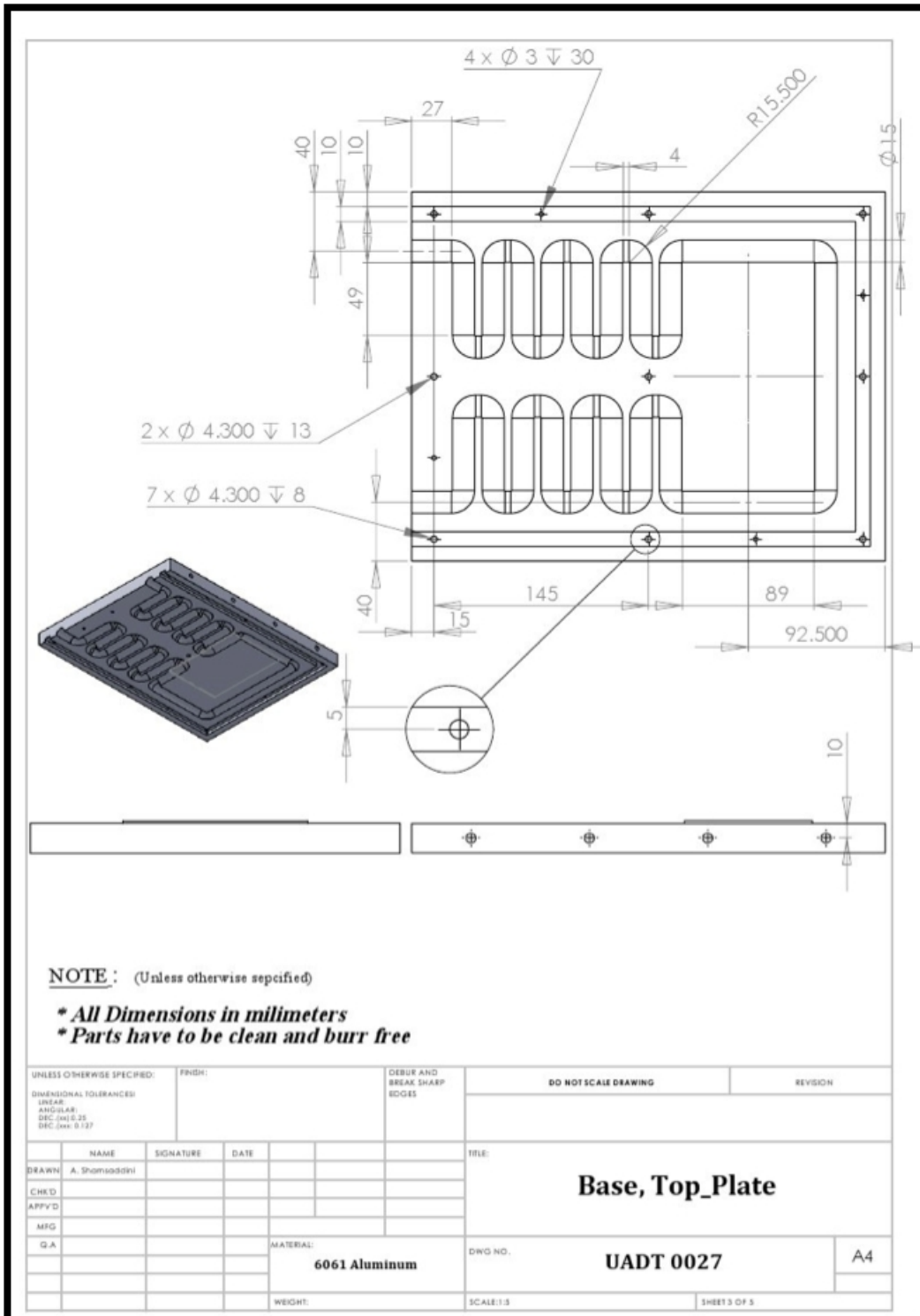


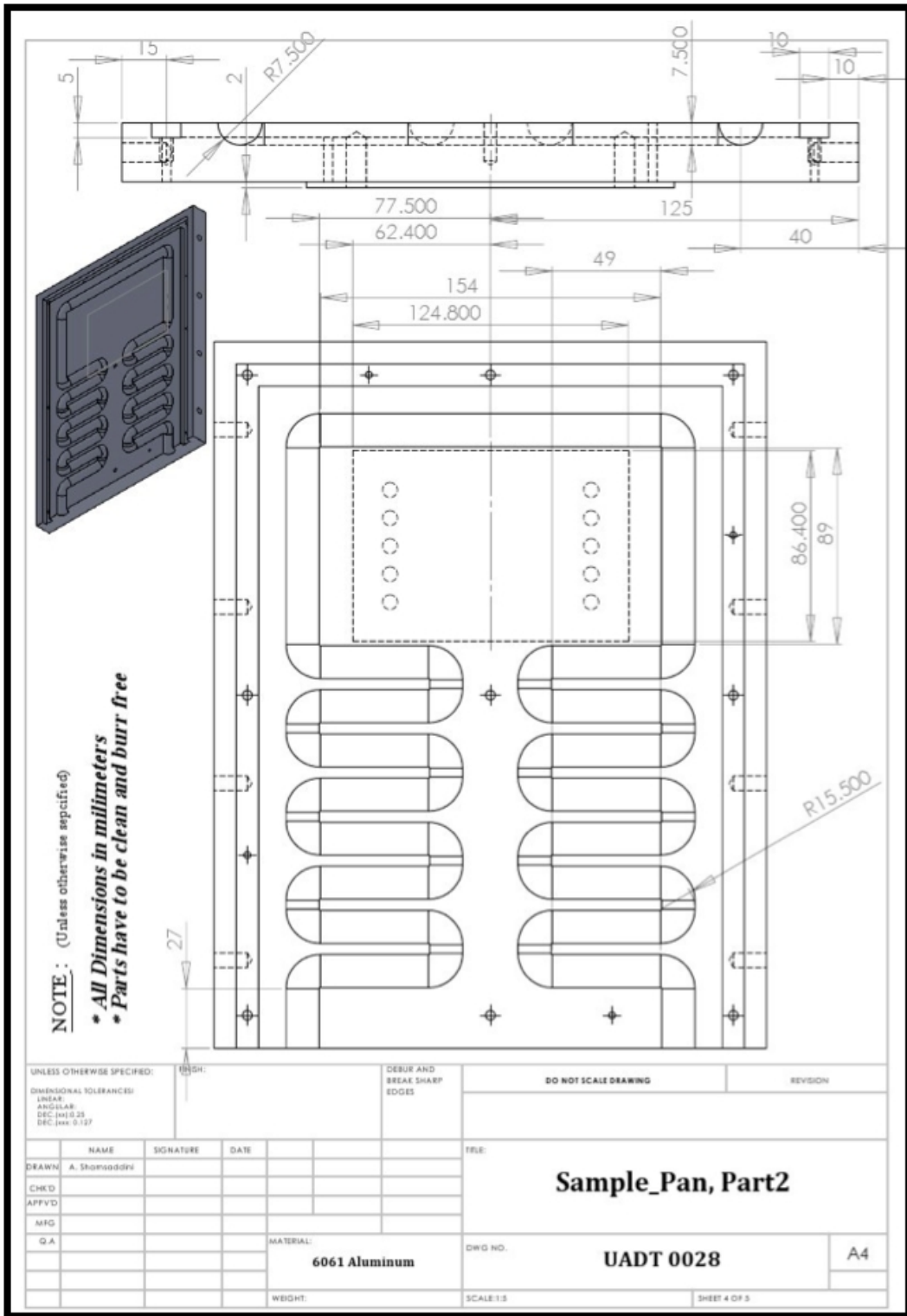


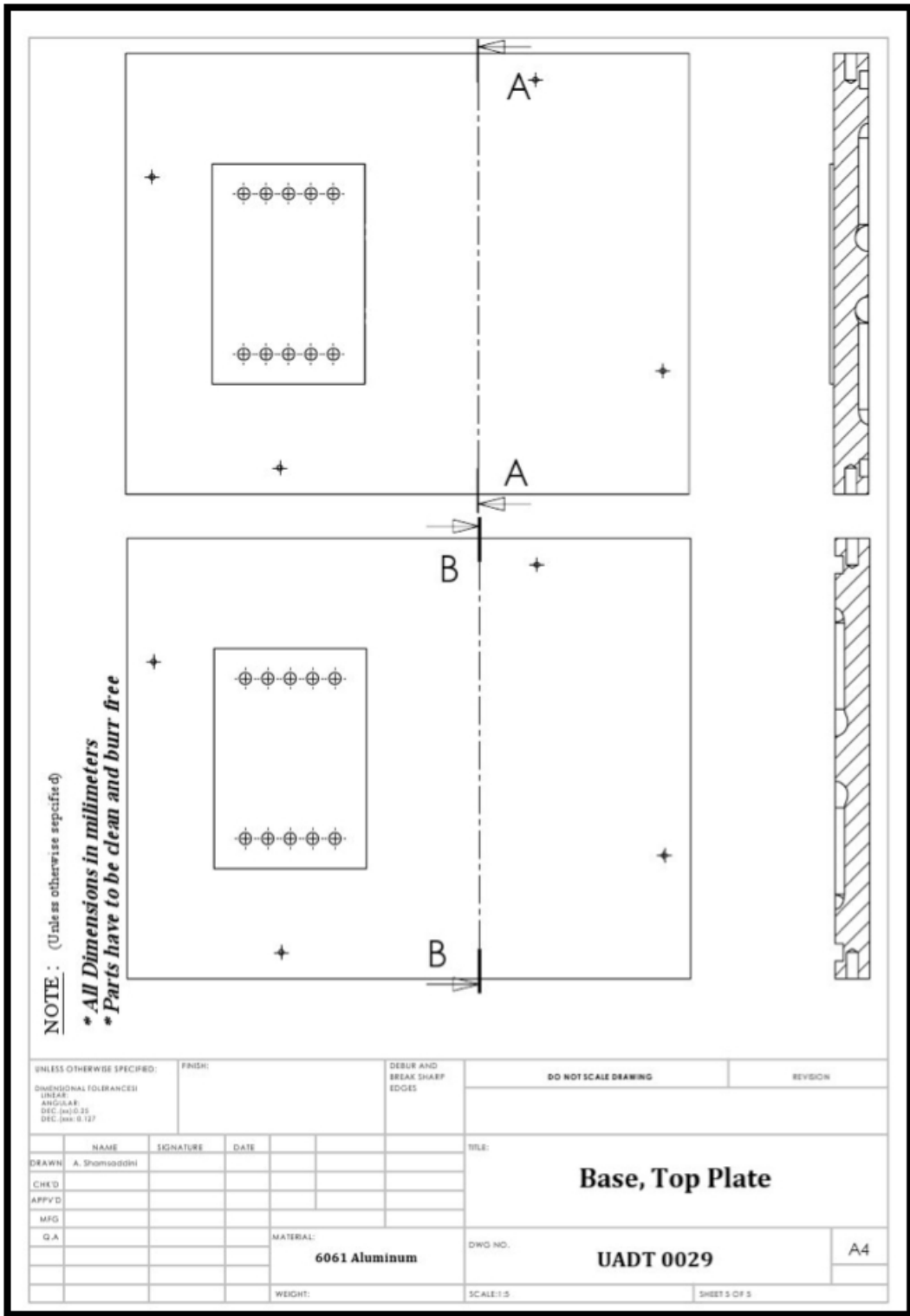
NOTE : (Unless otherwise sepcified)
*** All Dimensons in millimeters**
*** Parts have to be clean and burr free**

UNLESS OTHERWISE SPECIFIED:		FINISH:		DEBUR AND BREAK SHARP EDGES		DO NOT SCALE DRAWING		REVISION	
DIMENSIONAL TOLERANCES: LINEAR ANGULAR DEC (MM) 0.25 DEC (MM) 0.127									
DRAWN: A. Shamsoddini		SIGNATURE:		DATE:		TITLE:			
CHECKED:						Base, Top_Plate			
APPROVED:									
MFG:									
Q.A:									
		MATERIAL:		DWG NO.:		UADT 0025		A4	
		6061 Aluminum							
		WEIGHT:		SCALE:1:5		SHEET 1 OF 5			

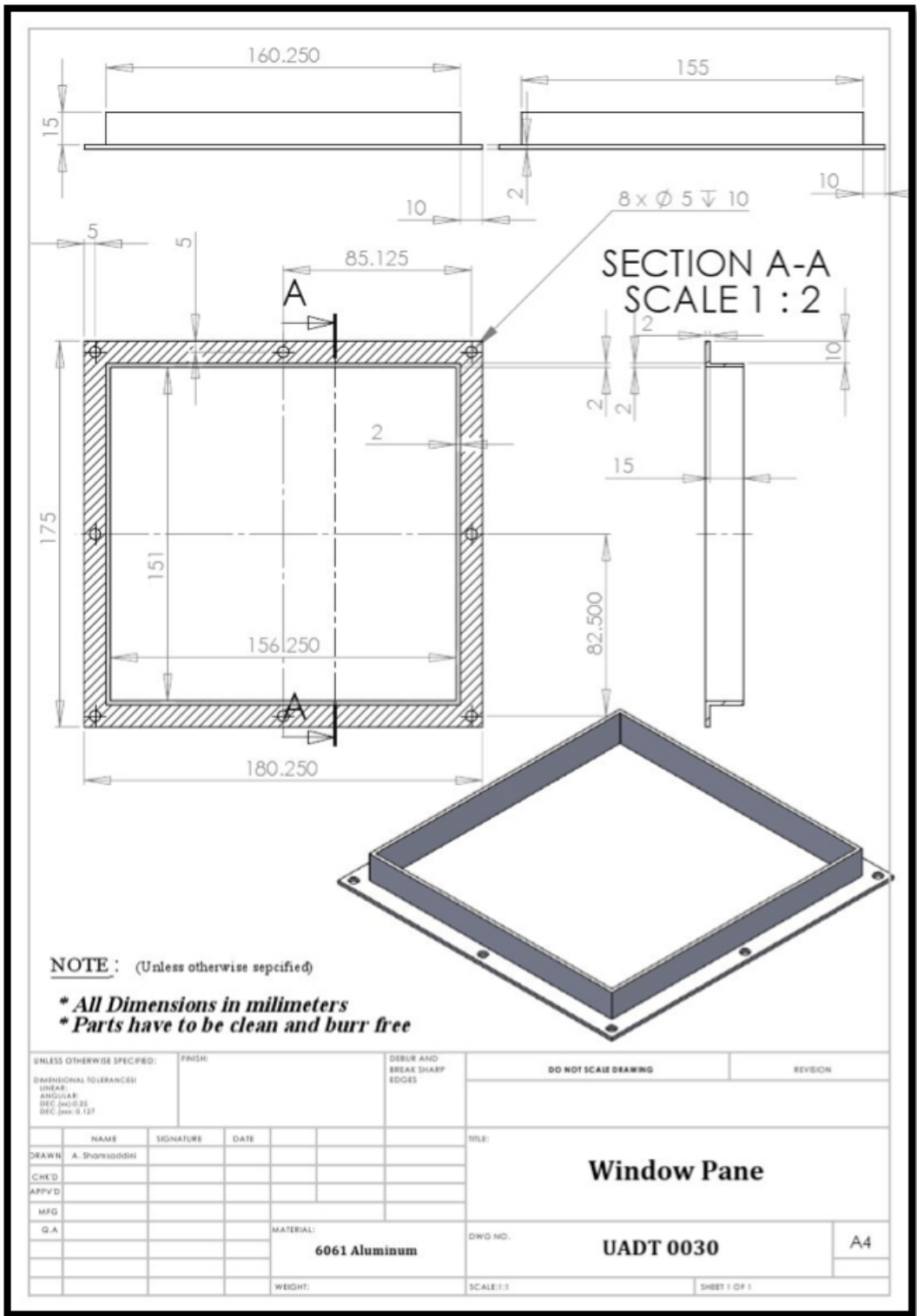








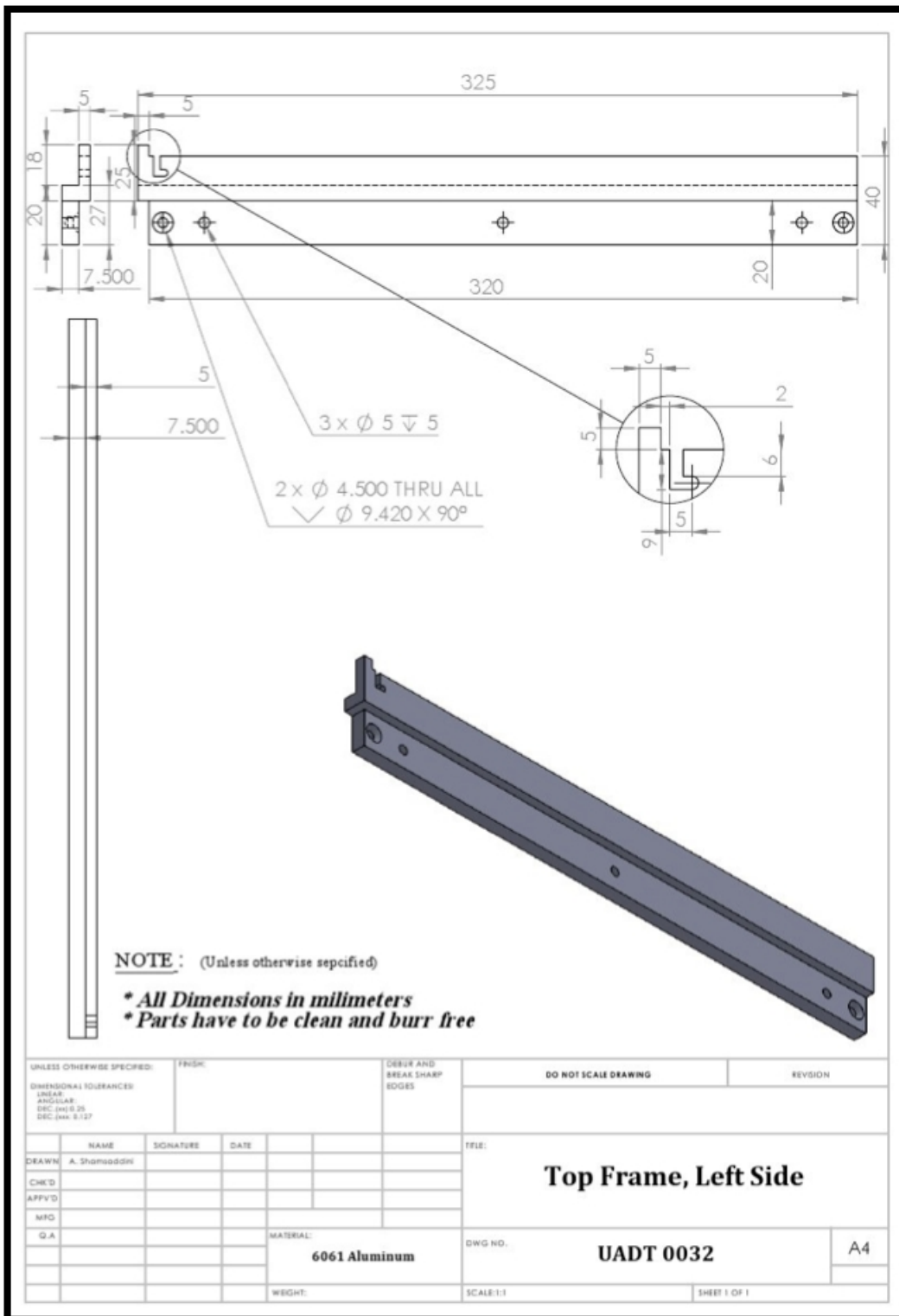
UNLESS OTHERWISE SPECIFIED:		FINISH:		DEBUR AND BREAK SHARP EDGES		DO NOT SCALE DRAWING		REVISION	
DIMENSIONAL TOLERANCES: LINEAR ANGULAR DEC: (MSS) 35 DEC: (MIL) 8, 127									
NAME	SIGNATURE	DATE				TITLE:			
DRAWN	A. Shamsoddini					Base, Top Plate			
CHK'D									
APP'VD									
MFG									
QA									
		MATERIAL:		DWO NO.		UADT 0029		A4	
		6061 Aluminum							
		WEIGHT:		SCALE:1:3		SHEET 5 OF 5			



NOTE : (Unless otherwise specified)

- * All Dimensions in millimeters
- * Parts have to be clean and burr free

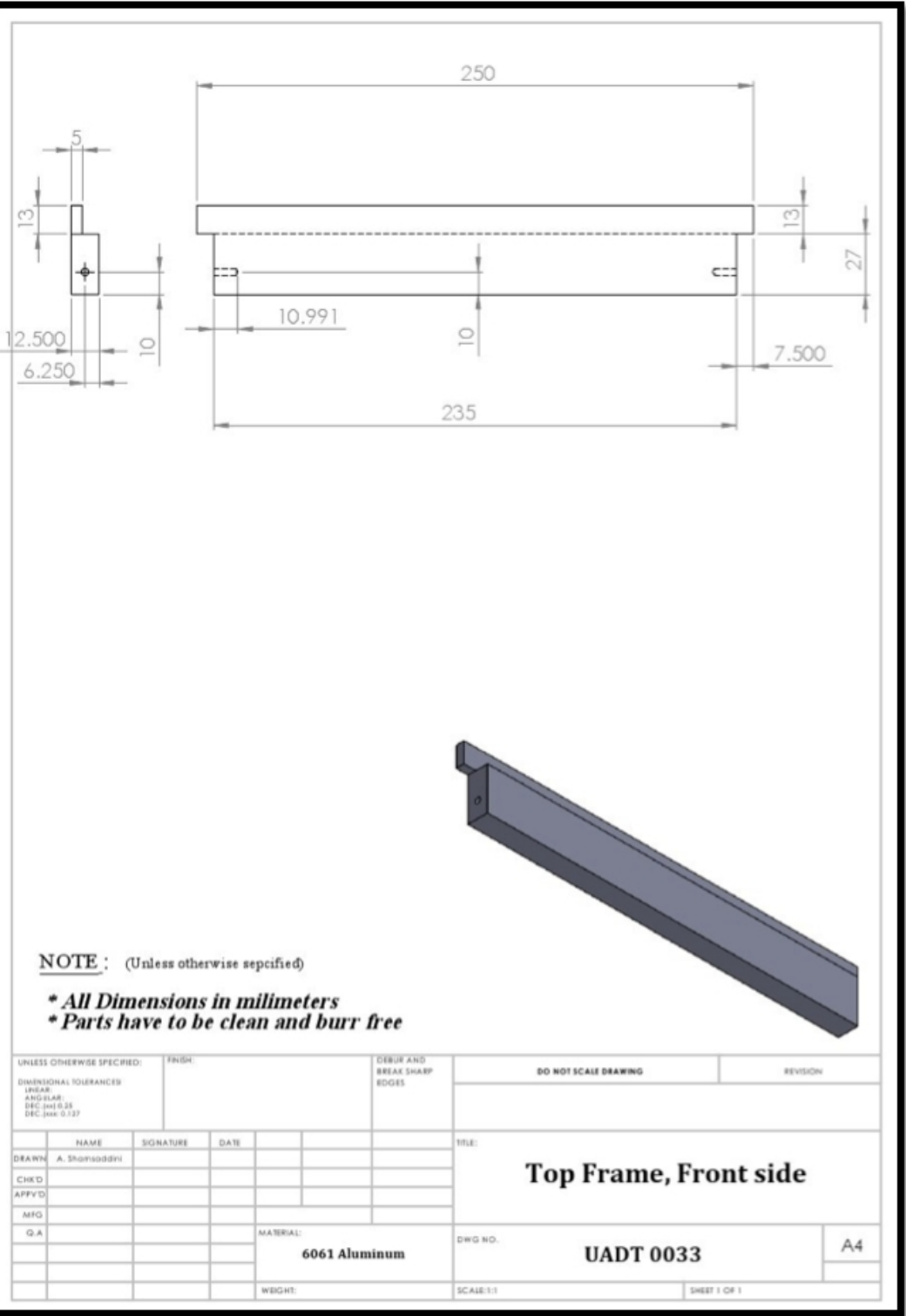
UNLESS OTHERWISE SPECIFIED:		FINISH:		DEBUR AND BREAK SHARP EDGES		DO NOT SCALE DRAWING		REVISION	
DIMENSIONAL TOLERANCES: LINEAR: ANGULAR: DEC (M) 0.25 SEC (M) 0.127									
NAME	SIGNATURE	DATE				TITLE:			
DRAWN	A. Shorshoddin					Window Pane			
CHK'D									
APP'VD									
MFG									
Q.A									
		MATERIAL:		DWG NO.		UADT 0030		A4	
		6061 Aluminum		SCALE: 1:1		SHEET 1 OF 1			
		WEIGHT:							



NOTE: (Unless otherwise specified)

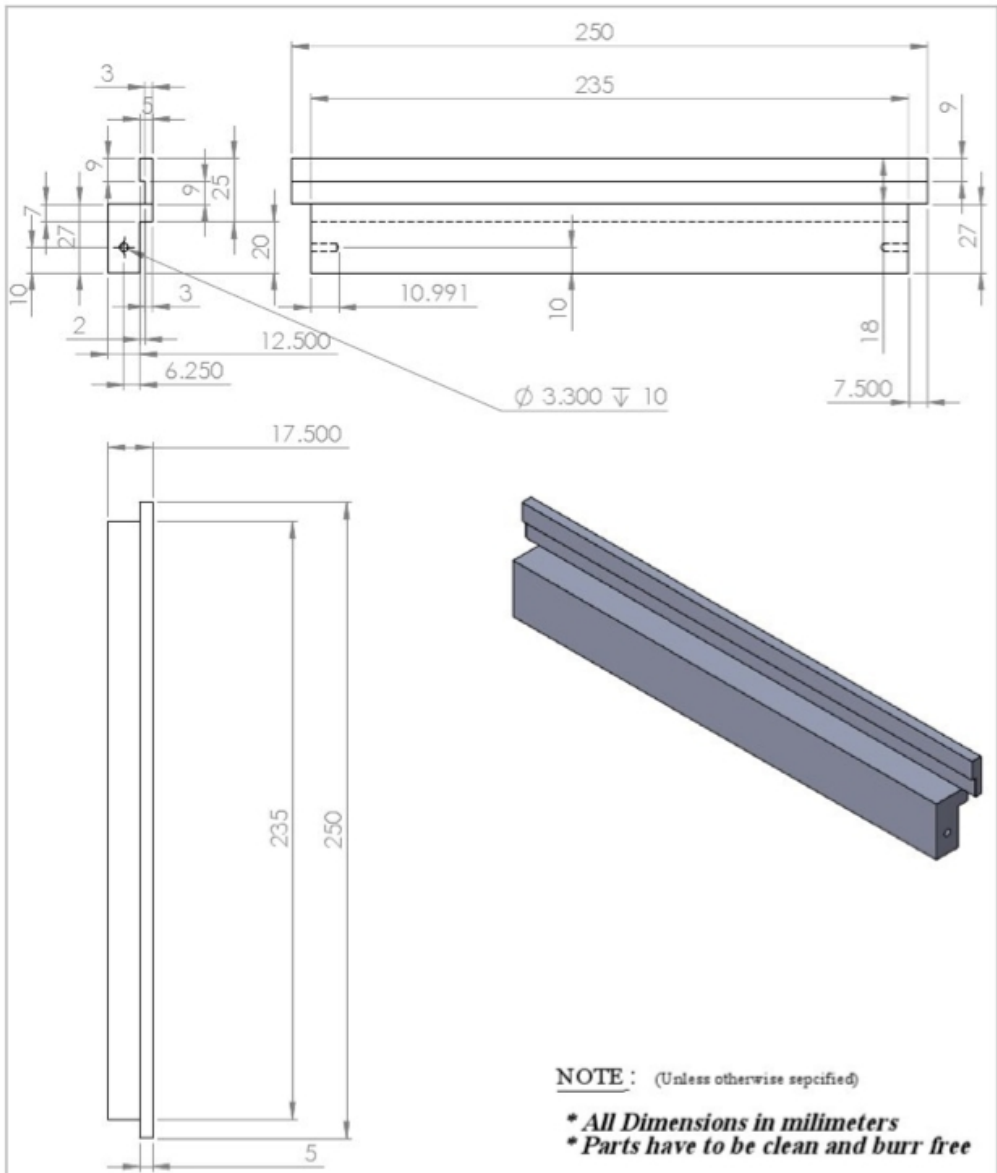
- * All Dimensions in millimeters
- * Parts have to be clean and burr free

UNLESS OTHERWISE SPECIFIED:		FINISH:		DRESS AND BREAK SHARP EDGES		DO NOT SCALE DRAWING		REVISION		
DIMENSIONAL TOLERANCES										
LINEAR										
ANGULAR										
DEC (MKS 25)										
DEC (MKS 5.127)										
NAME	SIGNATURE	DATE				TITLE:				
DEAWN	A. Shamsoddin					Top Frame, Left Side				
CHK'D										
APP'VD										
MFG										
Q.A										
MATERIAL:			6061 Aluminum			DWG NO.		UADT 0032		A4
WEIGHT:						SCALE:1:1		SHEET 1 OF 1		

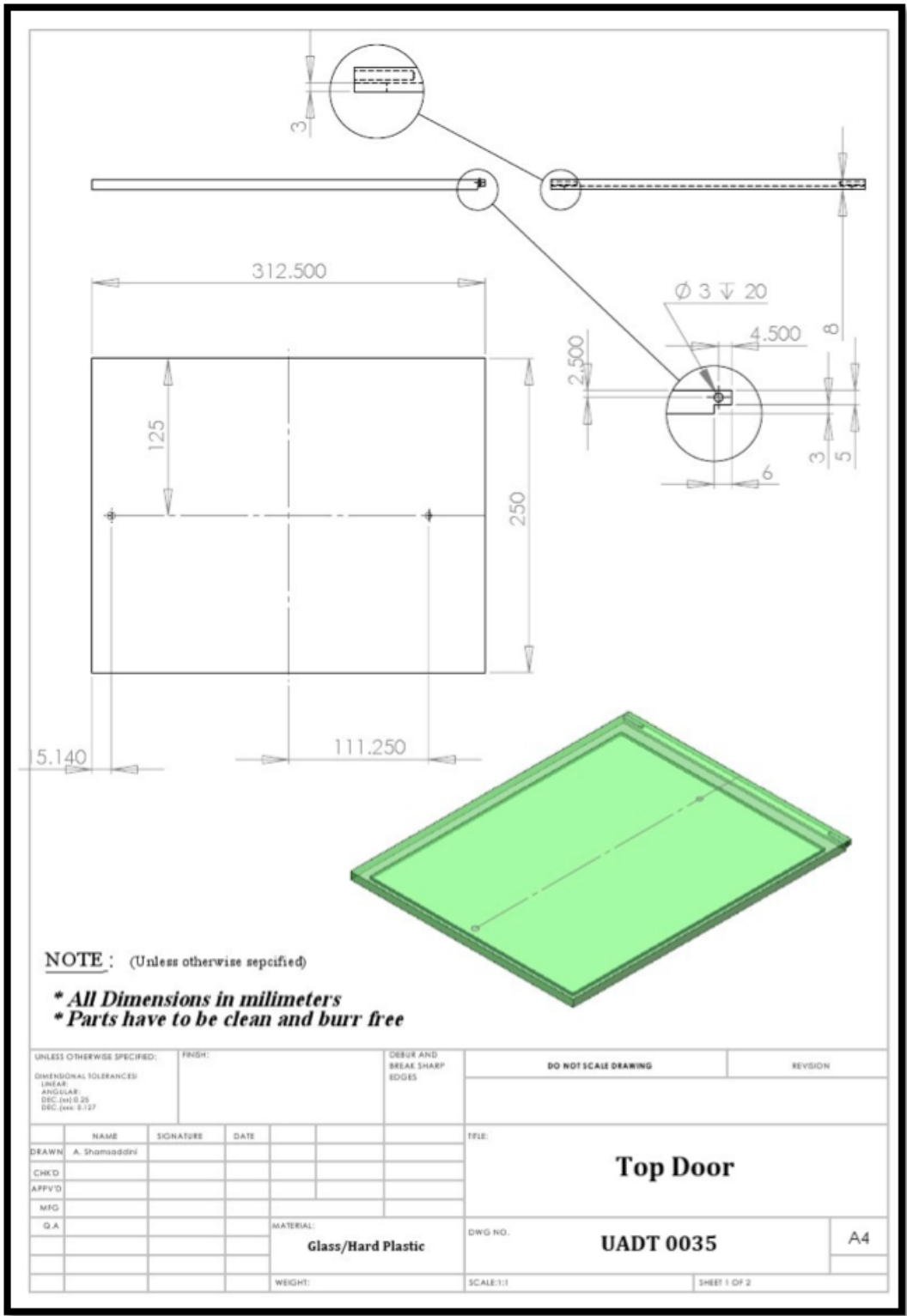


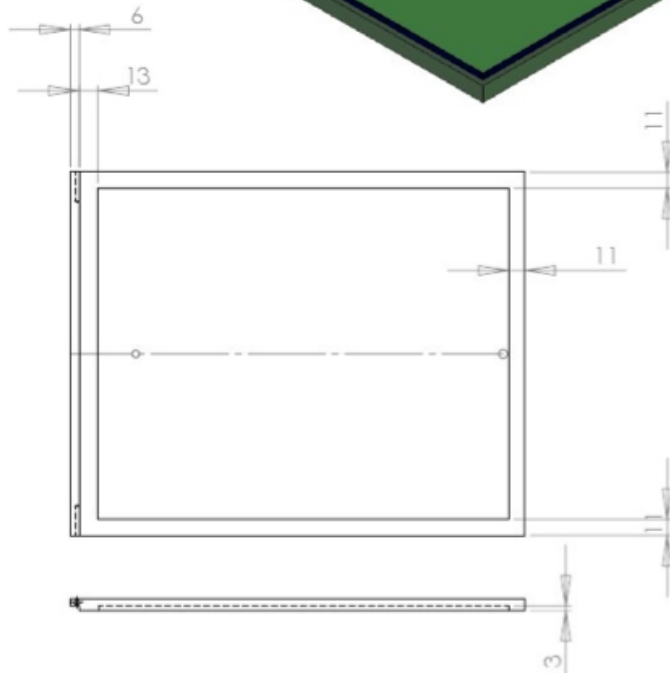
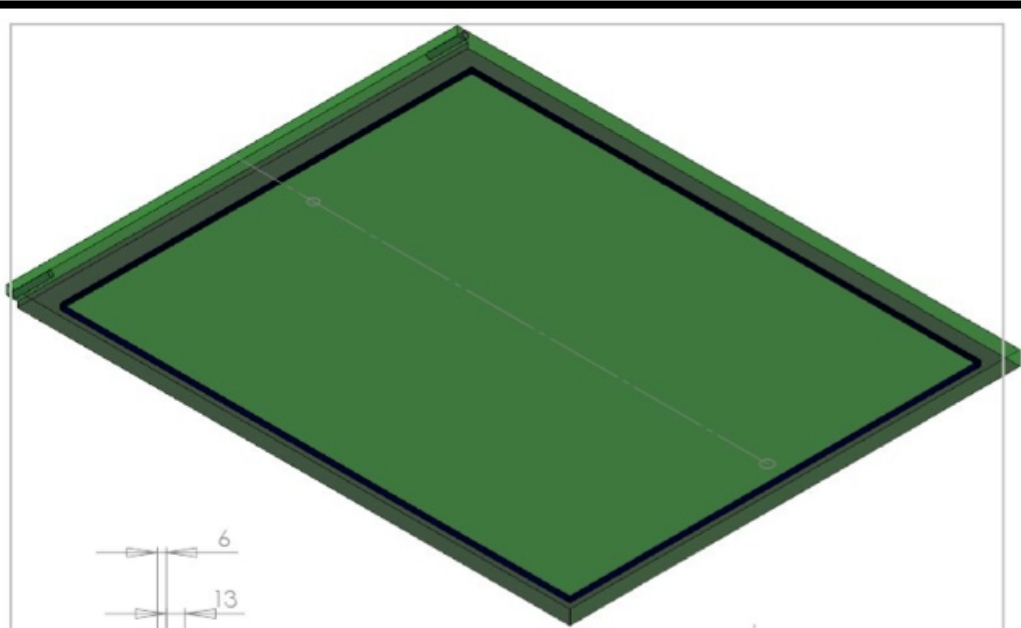
NOTE : (Unless otherwise specified)
** All Dimensions in millimeters*
** Parts have to be clean and burr free*

UNLESS OTHERWISE SPECIFIED:		FINISH:		DEBUR AND BREAK SHARP EDGES		DO NOT SCALE DRAWING		REVISION:	
DIMENSIONAL TOLERANCES LINEAR ANGULAR DEC: (MIL) 0.25 DEC: (MM) 0.127									
NAME	SIGNATURE	DATE				TITLE:			
DRAWN: A. Shamsoddini						Top Frame, Front side			
CHKD:									
APPVD:									
MFG:									
Q.A:									
		MATERIAL:		6061 Aluminum		DWG NO. UADT 0033		A4	
		WEIGHT:				SCALE: 1:1		SHEET 1 OF 1	



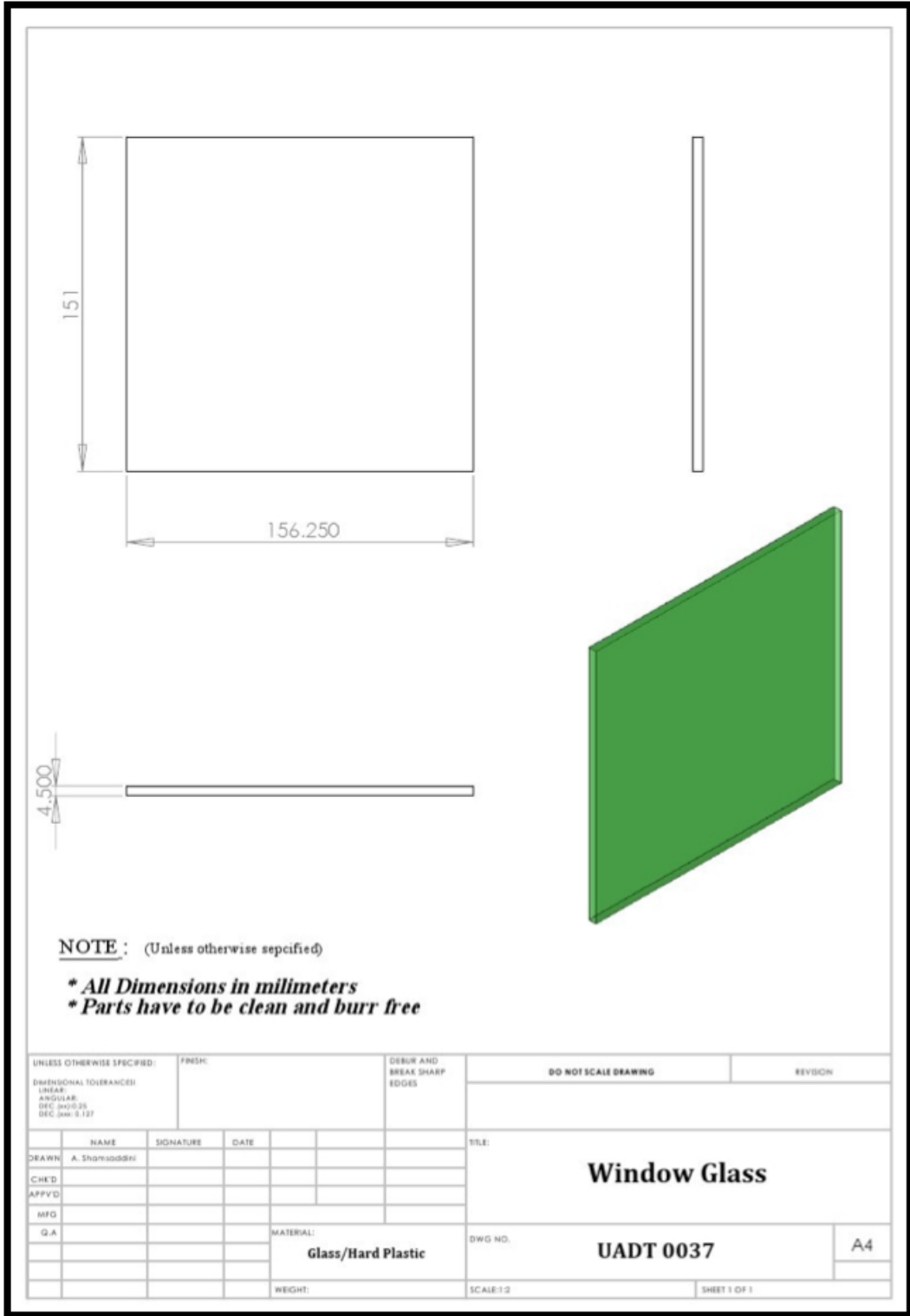
UNLESS OTHERWISE SPECIFIED:		FINISH:		DEBUR AND BREAK SHARP EDGES		DO NOT SCALE DRAWING		REVISION	
DIMENSIONAL TOLERANCES:									
LINEAR:									
ANGULAR:									
DEC (MM): ±0.25									
DEC (IN): 0.127									
	NAME	SIGNATURE	DATE			TITLE:			
DRAWN	A. Shamsoddini					Top Frame, Back Side			
CHECKED									
APPROVED									
MFG									
Q.A.									
				MATERIAL:		DWG NO.	UADT 0034		A4
				6061 Aluminum					
				WEIGHT:		SCALE: 1:1	SHEET 1 OF 1		





NOTE : (Unless otherwise specified)
 * All Dimensions in millimeters
 * Parts have to be clean and burr free

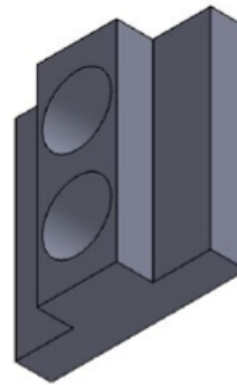
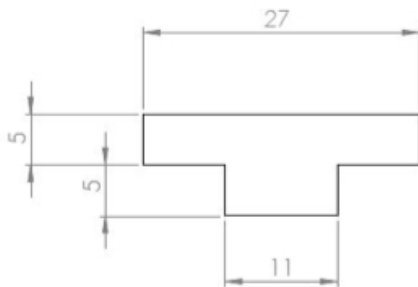
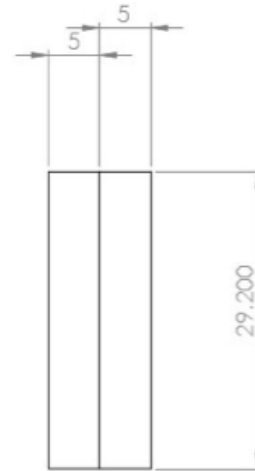
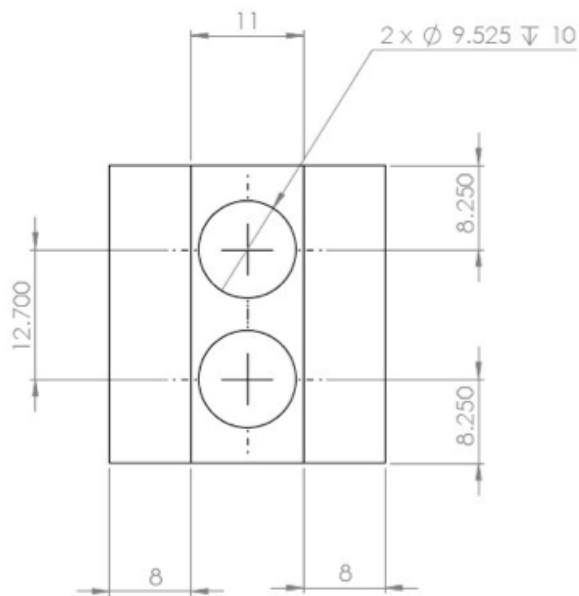
UNLESS OTHERWISE SPECIFIED:		FINISH:		DEBUR AND BREAK SHARP EDGES		DO NOT SCALE DRAWING		REVISION	
DIMENSIONAL TOLERANCES:									
LINEAR:									
ANGULAR:									
DEC (MIL): 0.25									
DEC (MM): 0.127									
DRAWN:		NAME	SIGNATURE	DATE		TITLE:			
CHK'D:		A. Shamsiddin				Top Door			
APP'D:									
MFG:									
Q.A:									
		MATERIAL:				DWD NO.		A4	
		Glass/ Hard Plastic				UADT 0036			
		WEIGHT:				SCALE: 1:5		SHEET 2 OF 2	



NOTE : (Unless otherwise sepcified)

- * All Dimensions in millimeters*
- * Parts have to be clean and burr free*

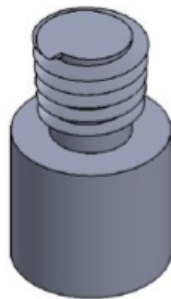
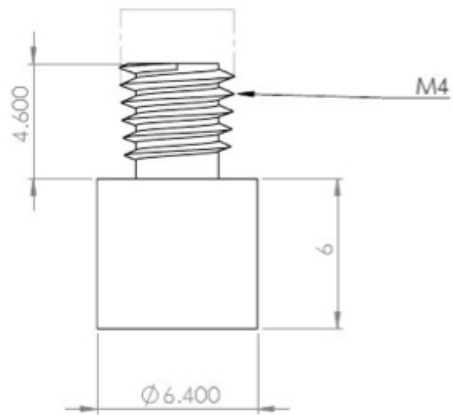
UNLESS OTHERWISE SPECIFIED:		FINISH:		DEBUR AND BREAK SHARP EDGES		DO NOT SCALE DRAWING		REVISION	
DIMENSIONAL TOLERANCES:									
LINEAR									
ANGULAR									
DEC 3/40.25									
DEC 3/40.127									
NAME		SIGNATURE		DATE		TITLE:			
DRAWN		A. Shamsoddini				Window Glass			
CHKD									
APPVD									
MFG									
QA									
				MATERIAL:		DWG NO.		A4	
				Glass/Hard Plastic		UADT 0037			
				WEIGHT:		SCALE:1:2		SHEET 1 OF 1	



NOTE : (Unless otherwise specified)

- * All Dimensions in millimeters
- * Parts have to be clean and burr free

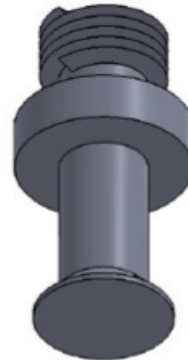
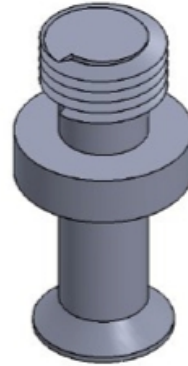
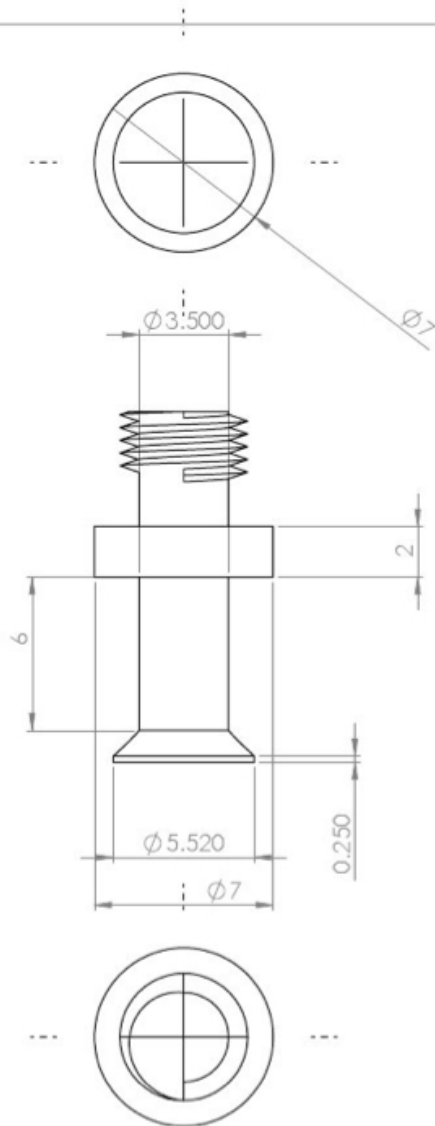
UNLESS OTHERWISE SPECIFIED:		FINISH:		DEBUR AND BREAK SHARP EDGES		DO NOT SCALE DRAWING		REVISION	
DIMENSIONAL TOLERANCES: LINEAR ANGULAR DEC (MILS) DEC (MM) 3/32									
NAME	SIGNATURE	DATE				TITLE:			
DRAWN: A. SHAMSODDINI						Spring-Lock Holder			
CHKD:									
APPVD:									
MFG:									
QA:									
		MATERIAL:		DWG NO.		A4			
		6061 Aluminum		UADT 0038					
		WEIGHT:		SCALE:2:1		SHEET 1 OF 1			



NOTE : (Unless otherwise specified)

- * All Dimensions in millimeters
- * Parts have to be clean and burr free

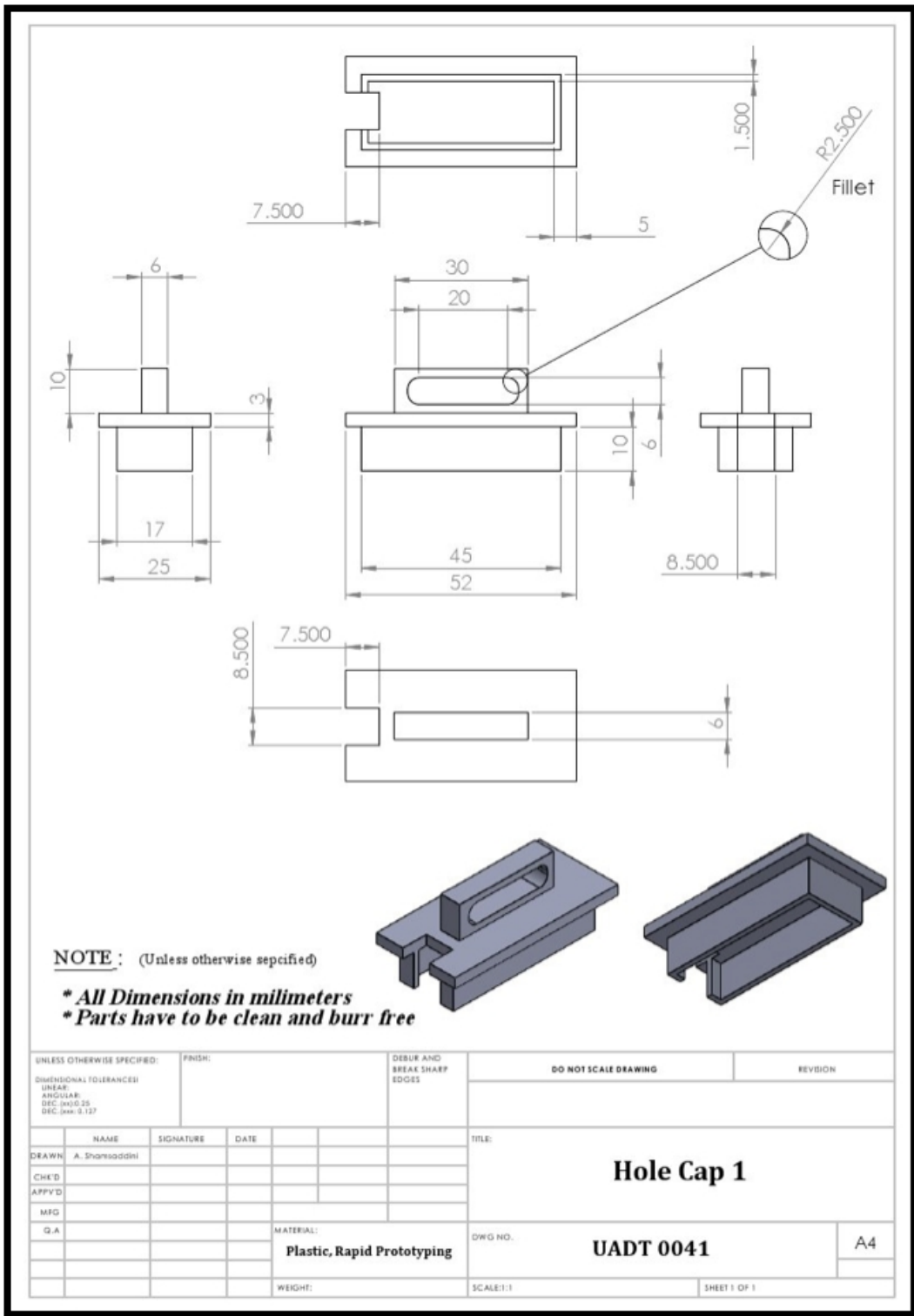
UNLESS OTHERWISE SPECIFIED:		FINISH:		DEBUR AND BREAK SHARP EDGES		DO NOT SCALE DRAWING		REVISION	
DIMENSIONAL TOLERANCES: LINEAR: ANGULAR: DEC: (MKS) 33 DEC: (MM) 0.127									
DRAWN: A. Shqrisiddiqi		SIGNATURE:		DATE:		TITLE:			
CHECKED:						Cylindrical Punch Tip			
APPROVED:									
MFG:				MATERIAL:		DWG NO.:		A4	
Q.A:				StainLess Steel		UADT 0039			
				WEIGHT:		SCALE: 1:1		SHEET 1 OF 1	



NOTE : (Unless otherwise specified)

- * All Dimensions in millimeters
- * Parts have to be clean and burr free

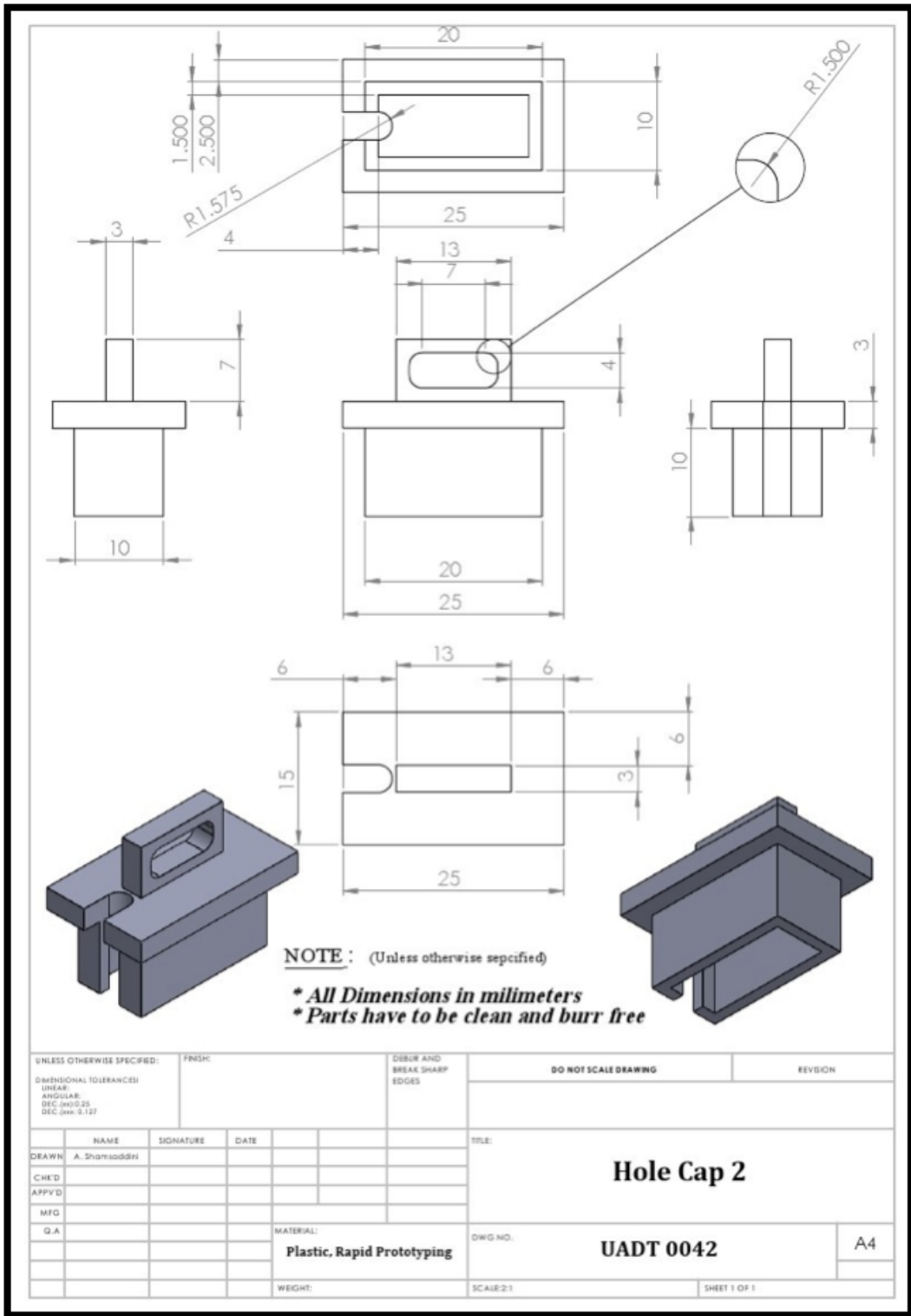
UNLESS OTHERWISE SPECIFIED:		FINISH:		DEBUR AND BREAK SHARP EDGES		DO NOT SCALE DRAWING		REVISION	
DIMENSIONAL TOLERANCES: LINEAR: ANGULAR: SEC. 341.0.35 DEC. 341.0.127									
DRAWN	NAME	SIGNATURE	DATE			TITLE:			
CHK'D	A. Shamsiddini					Disk-Shape Punch Tip			
APP'VD									
MFG									
Q.A									
				MATERIAL:		DWG NO.	UADT 0040		A4
				Stainless Steel					
				WEIGHT:		SCALE:1:1	SHEET 1 OF 1		

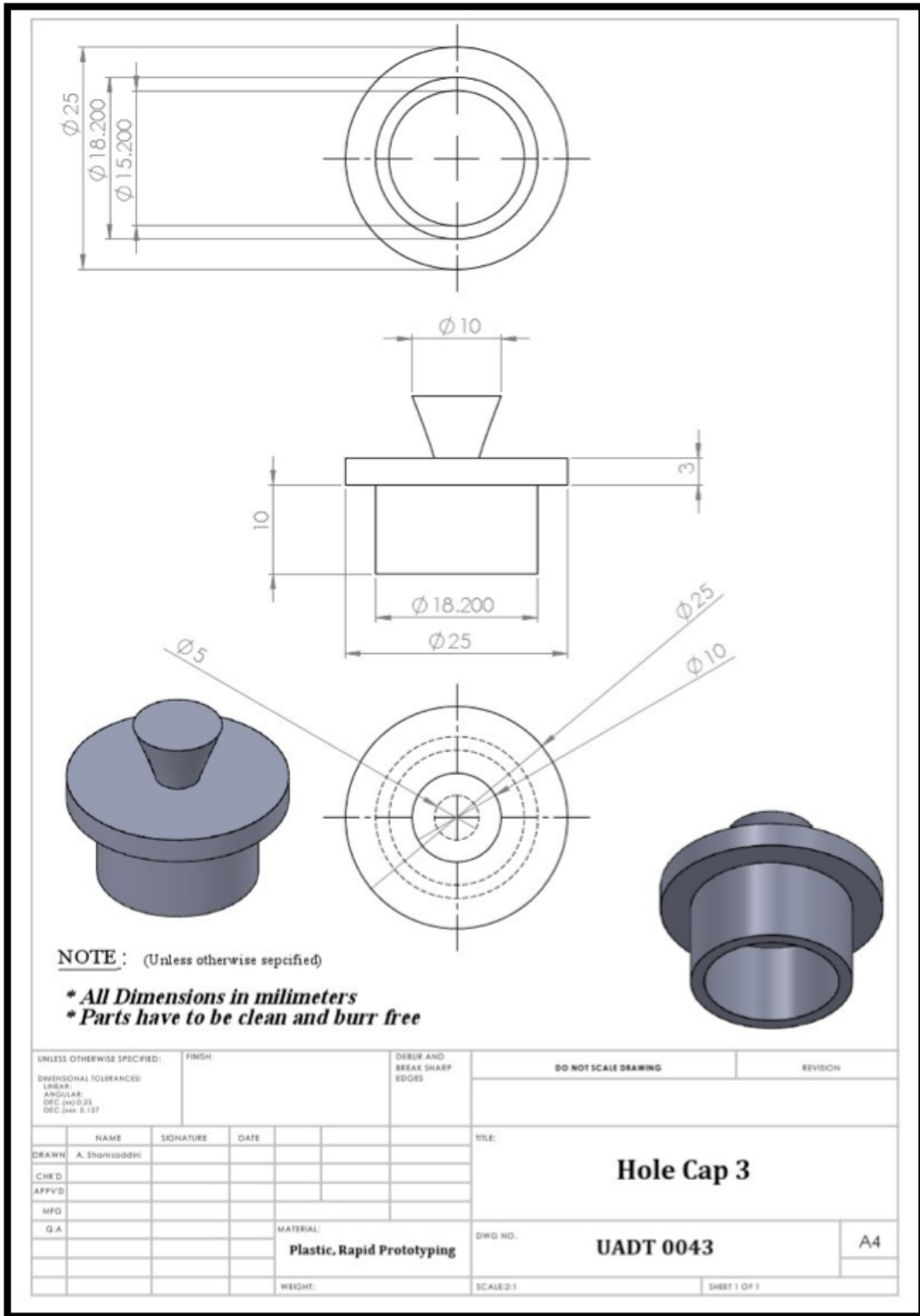


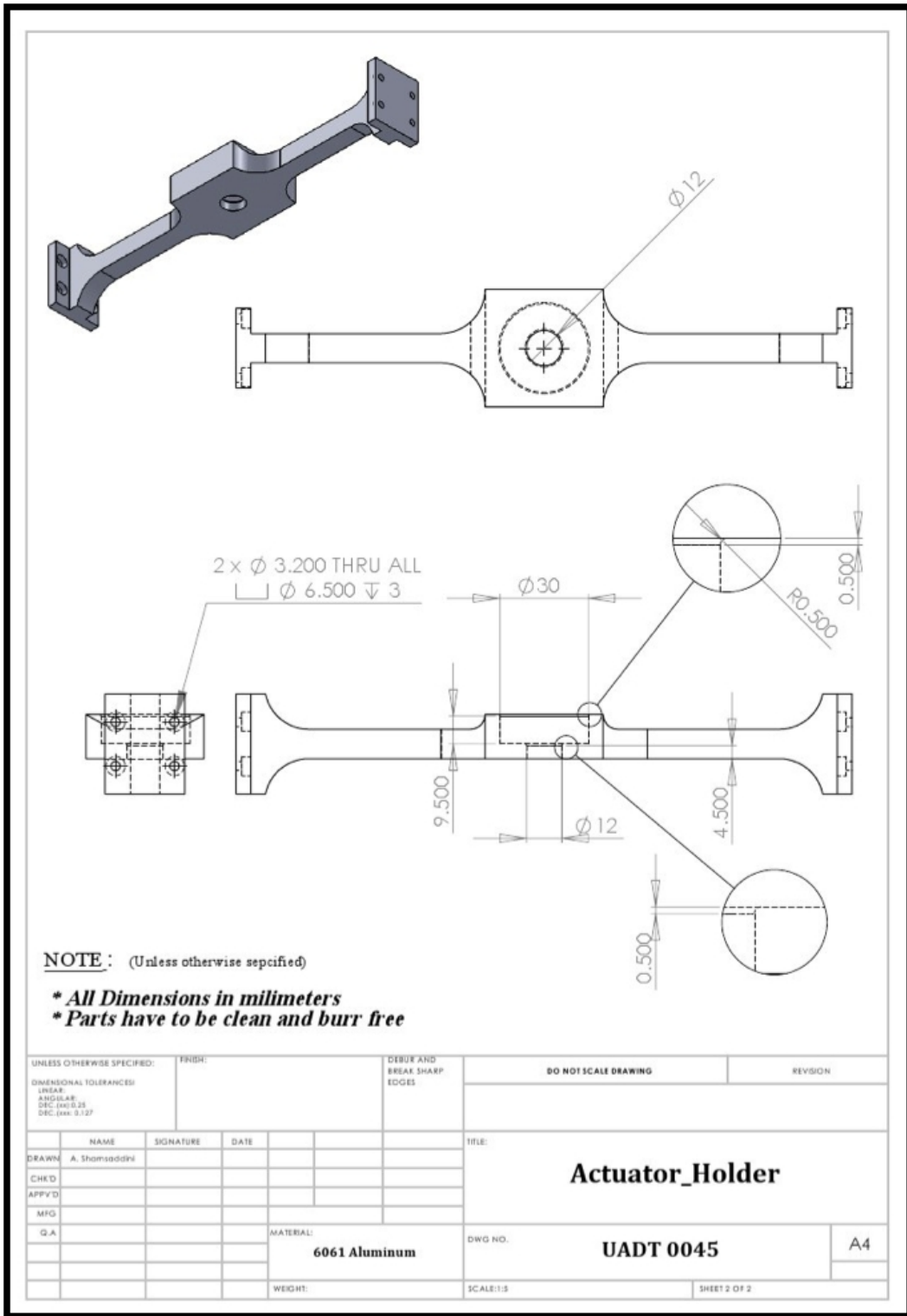
NOTE : (Unless otherwise specified)

- * All Dimensions in millimeters*
- * Parts have to be clean and burr free*

UNLESS OTHERWISE SPECIFIED:		FINISH:		DEBUR AND BREAK SHARP EDGES		DO NOT SCALE DRAWING		REVISION	
DIMENSIONAL TOLERANCES:									
LINEAR:									
ANGULAR:									
DEC: (ISO: IS:									
DEC: (mm: 0.127									
DRAWN:		NAME	SIGNATURE	DATE		TITLE:			
CHK'D:		A. Shamsoddini				Hole Cap 1			
APPVED:									
MFG:									
Q.A:									
		MATERIAL:		DWG NO.:		UADT 0041		A4	
		Plastic, Rapid Prototyping		SCALE: 1:1		SHEET 1 OF 1			
		WEIGHT:							



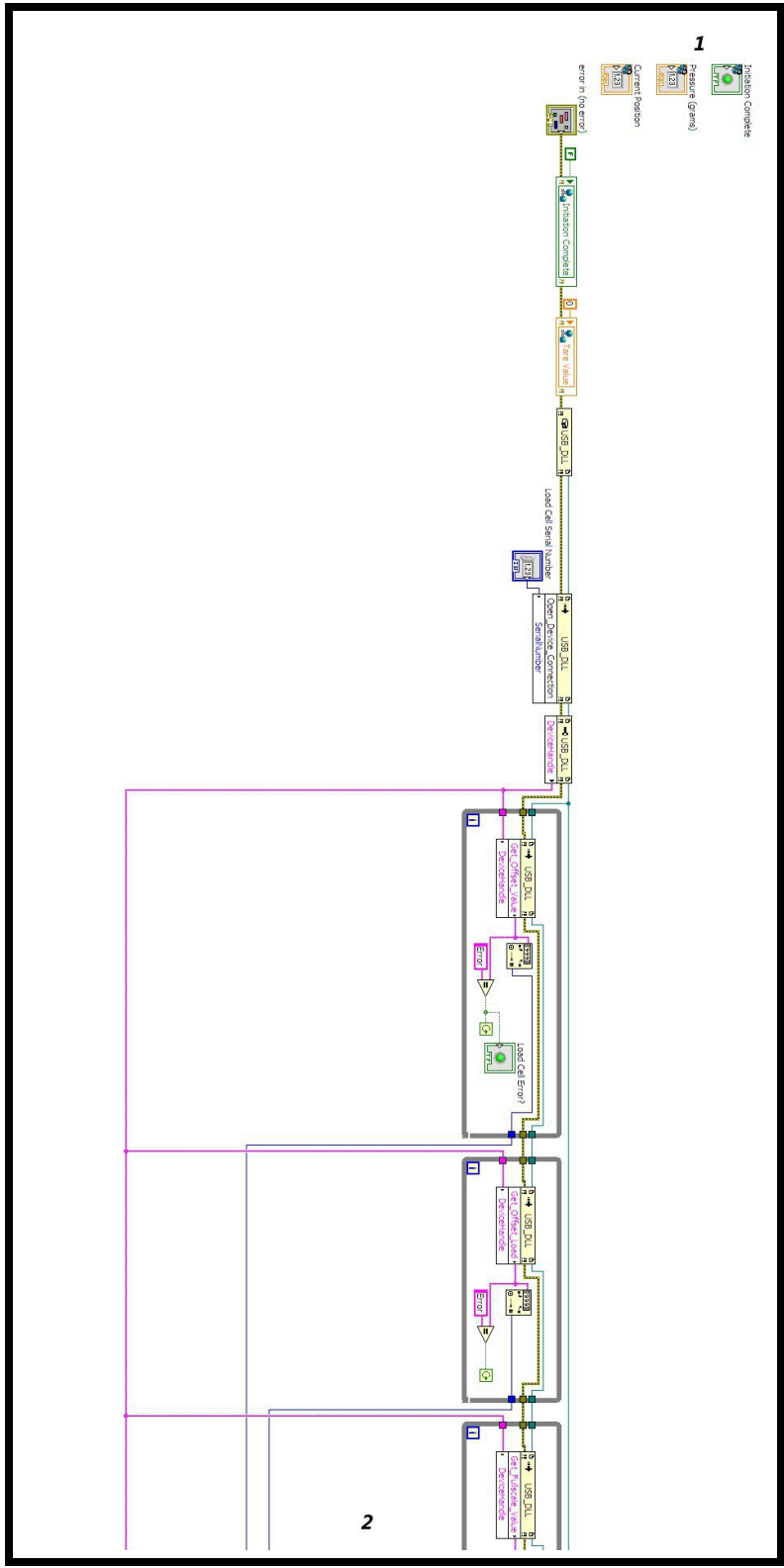


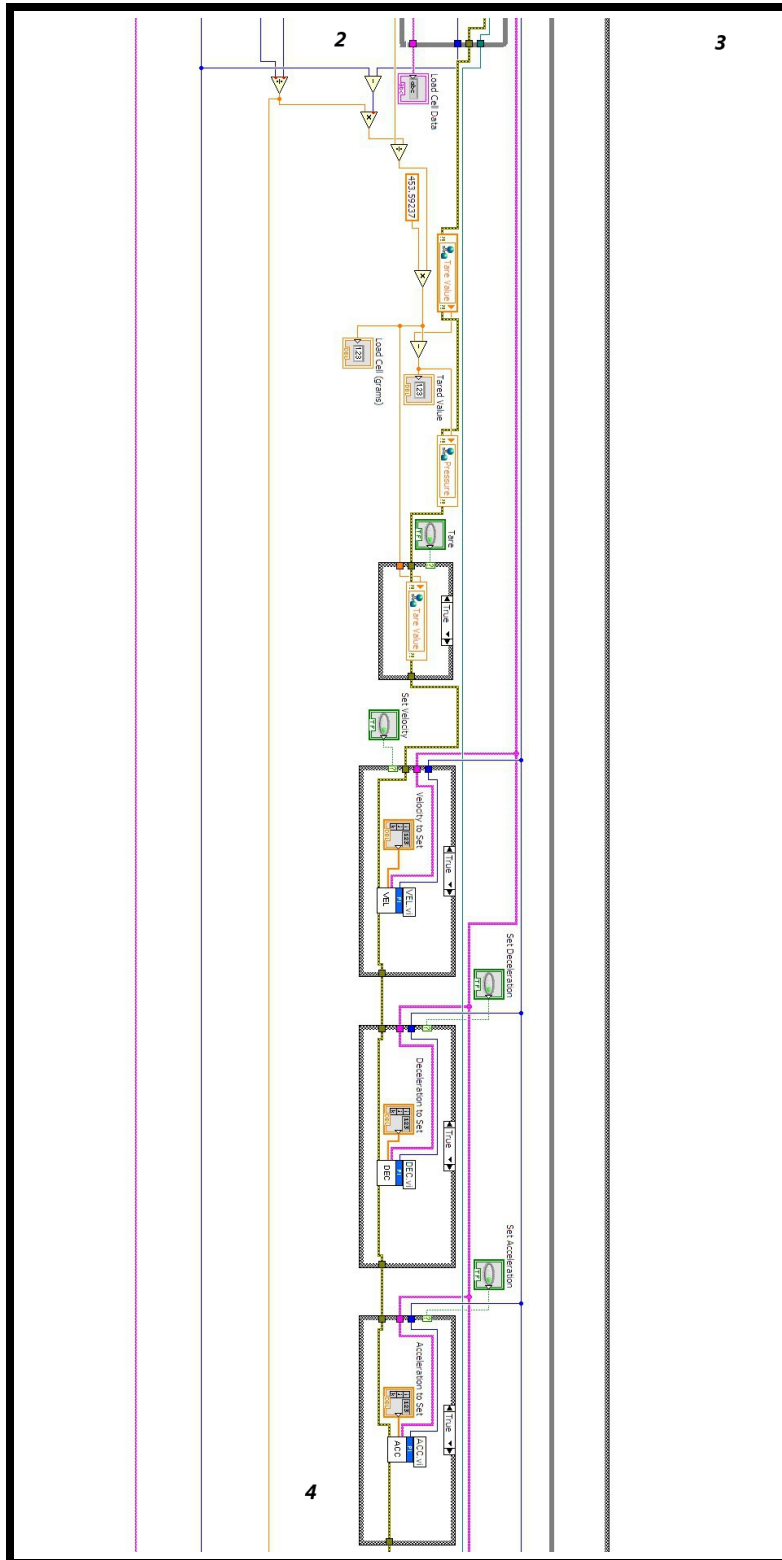


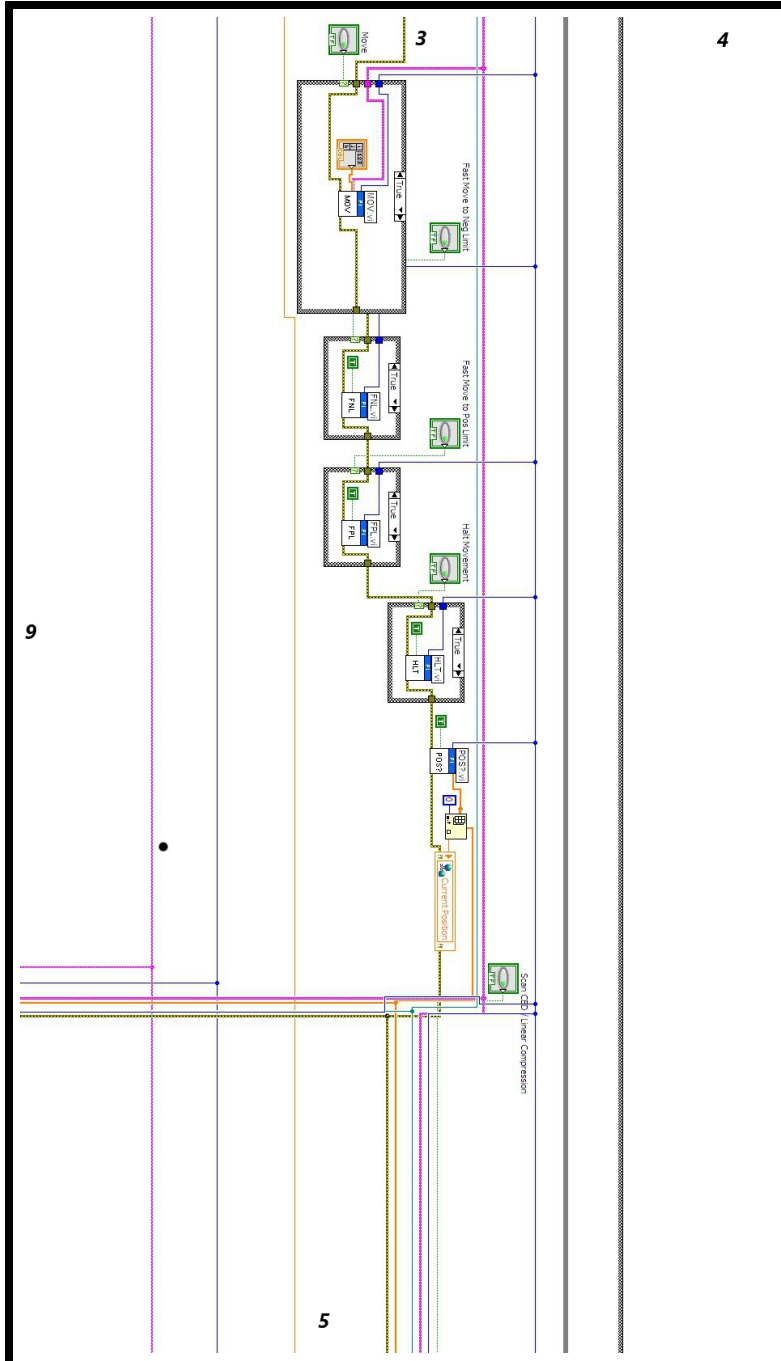
Appendix B

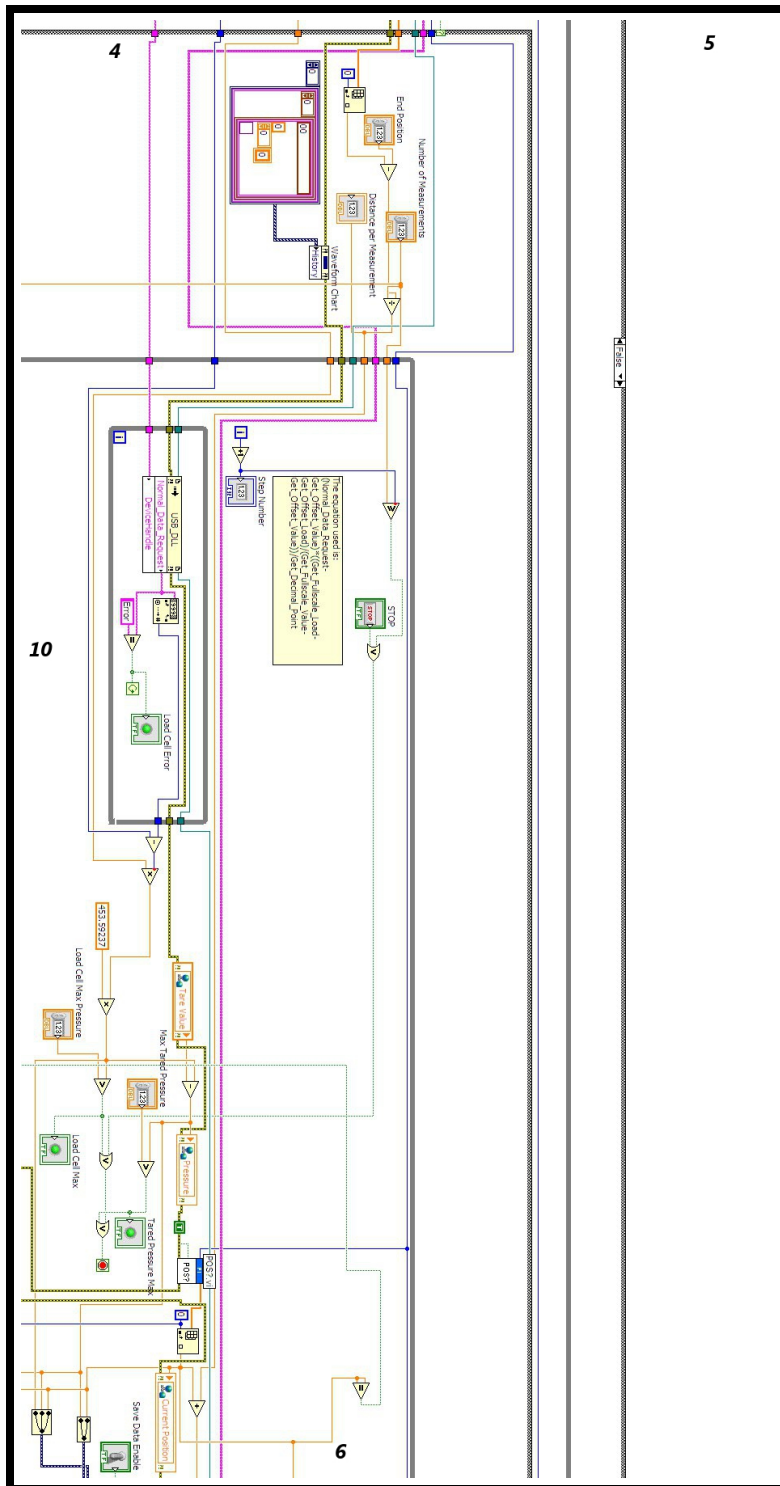
LabVIEW Code

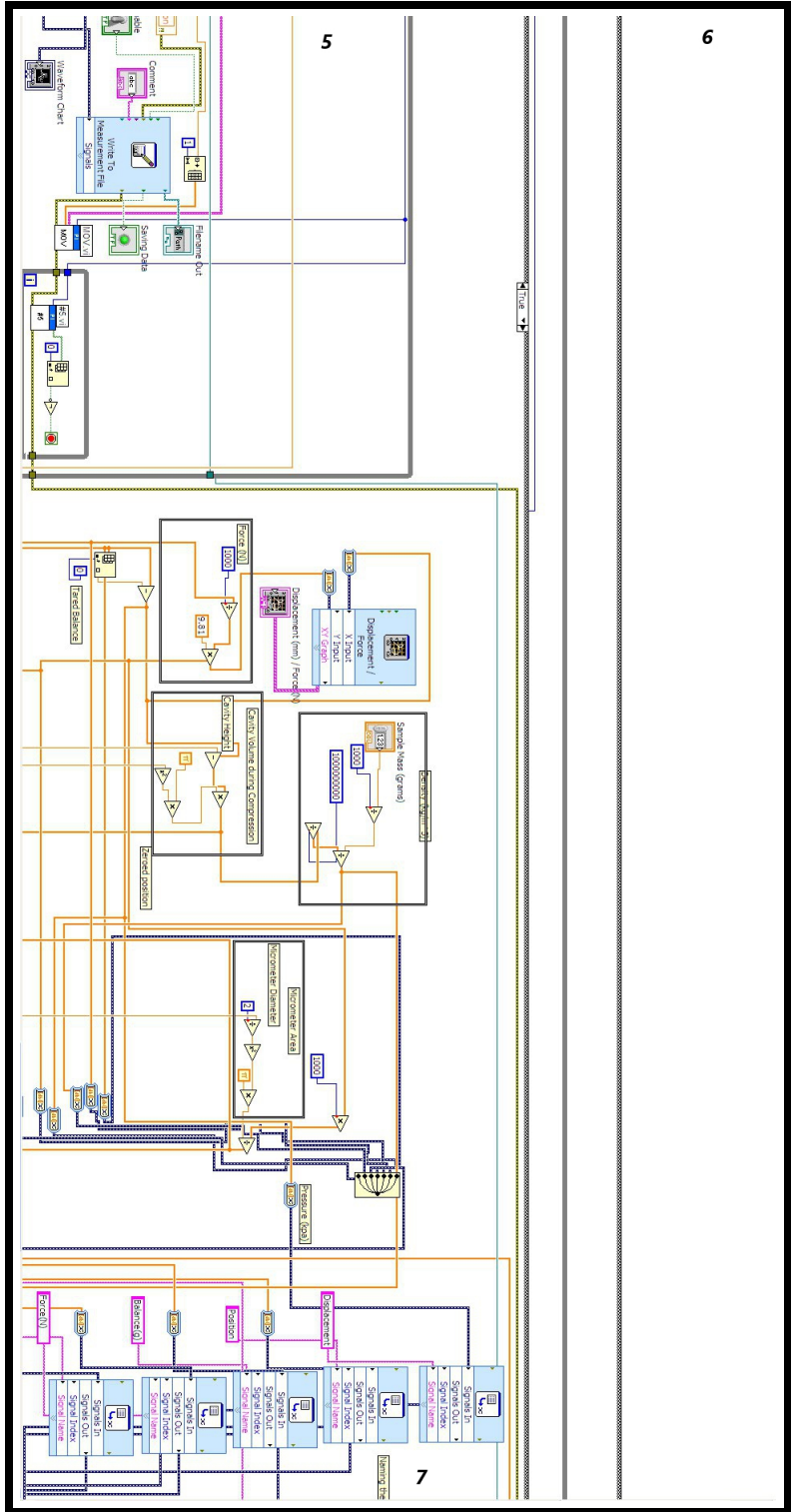
© by Abouzar Shamsaddini 2013

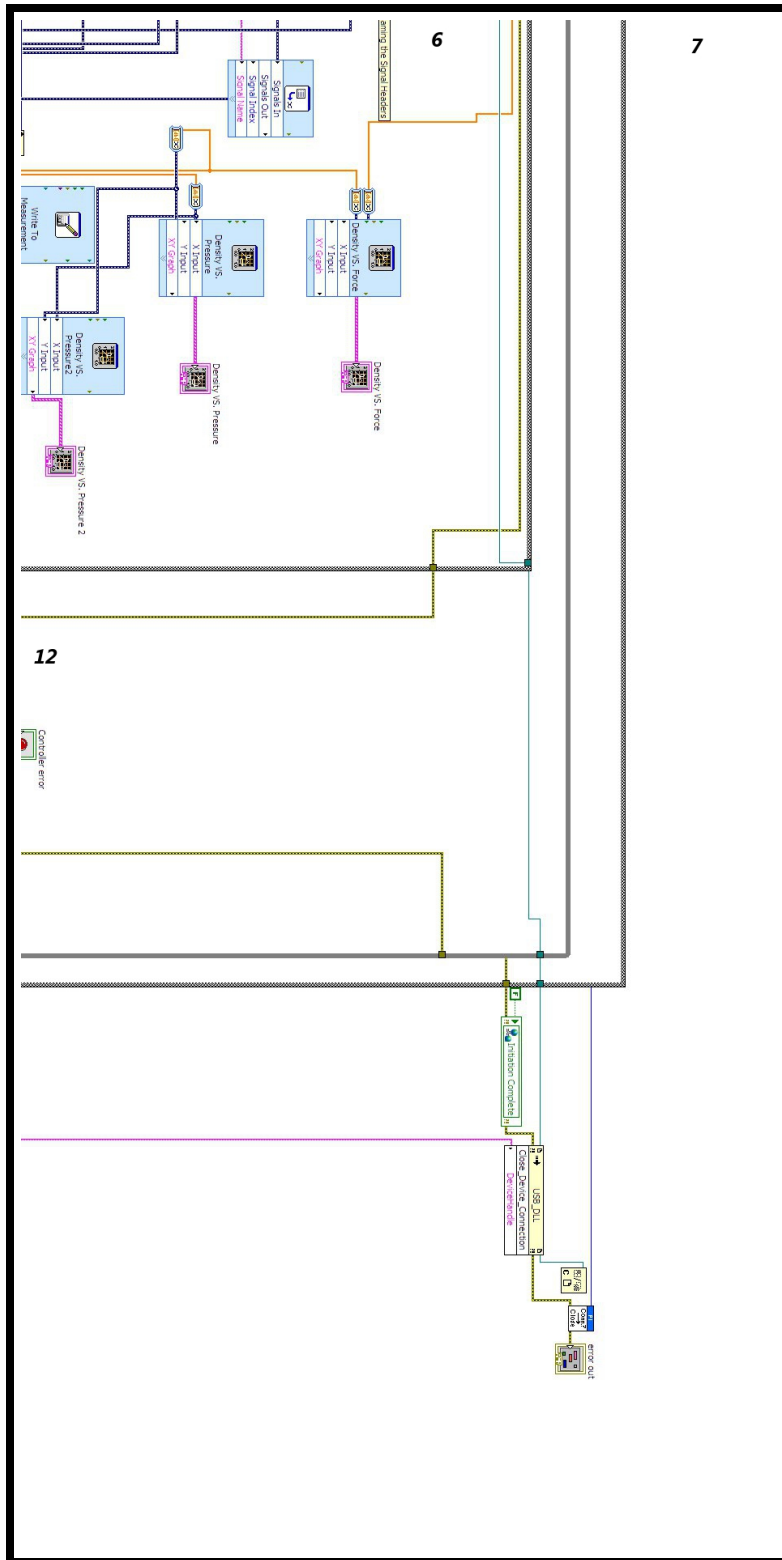


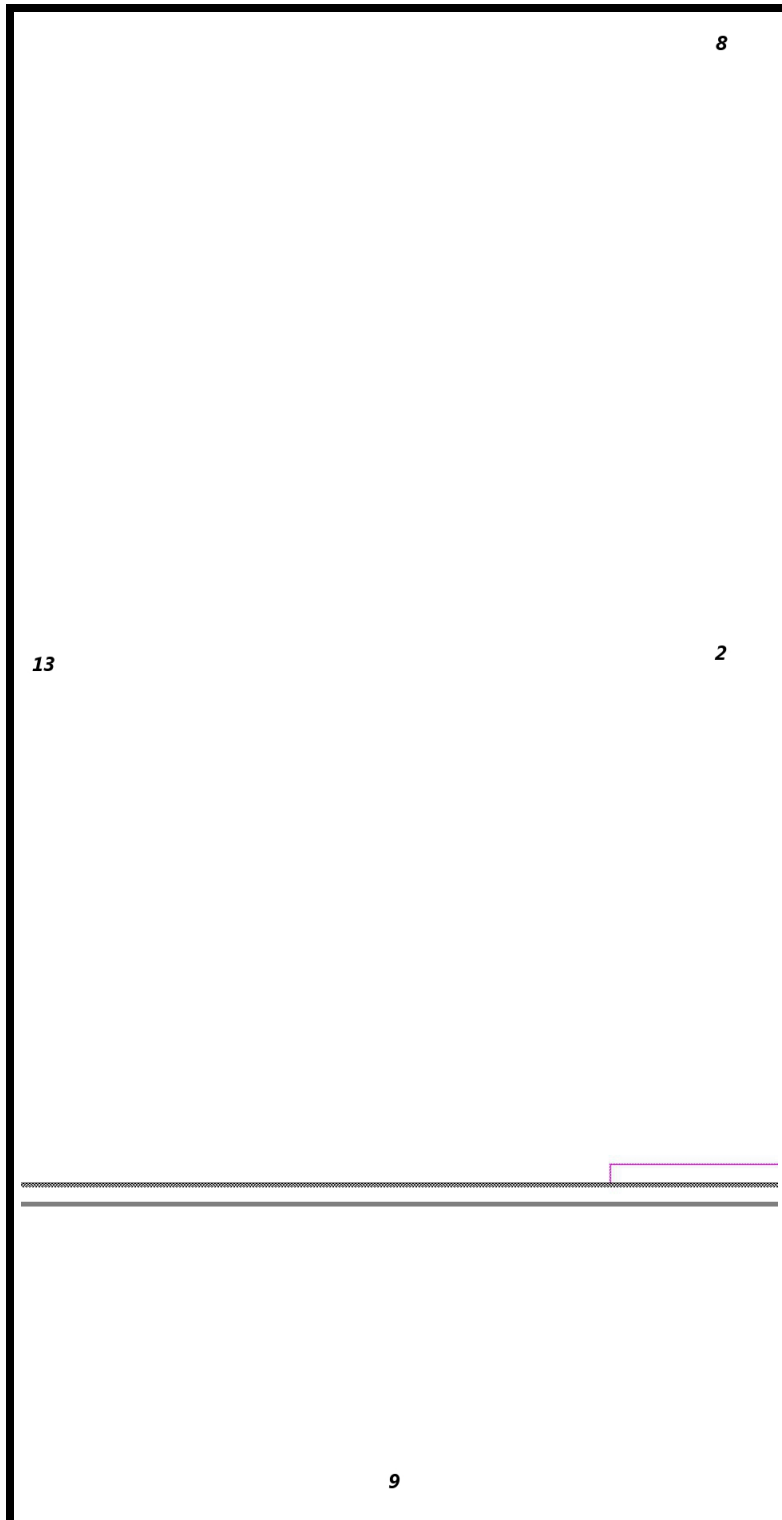


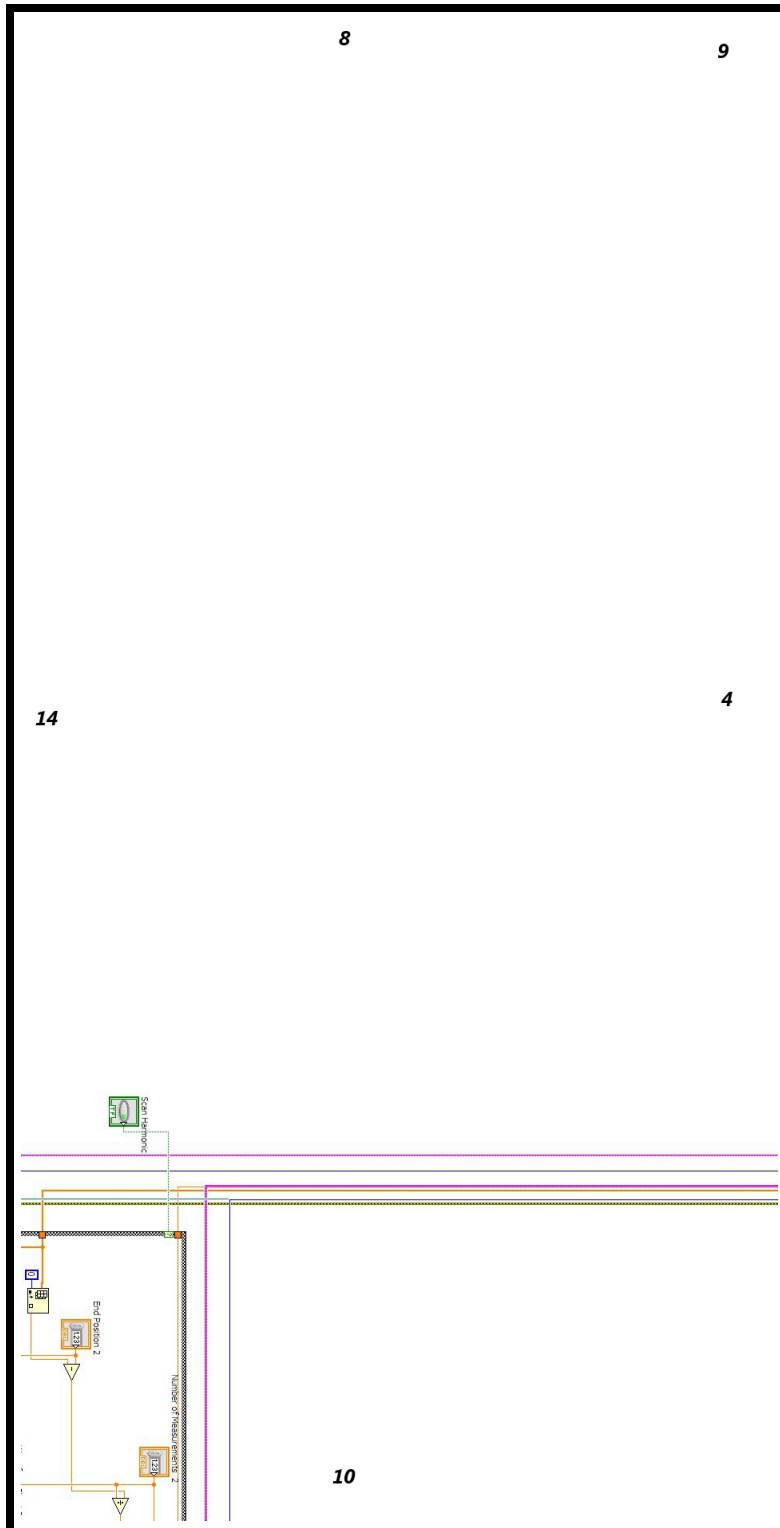


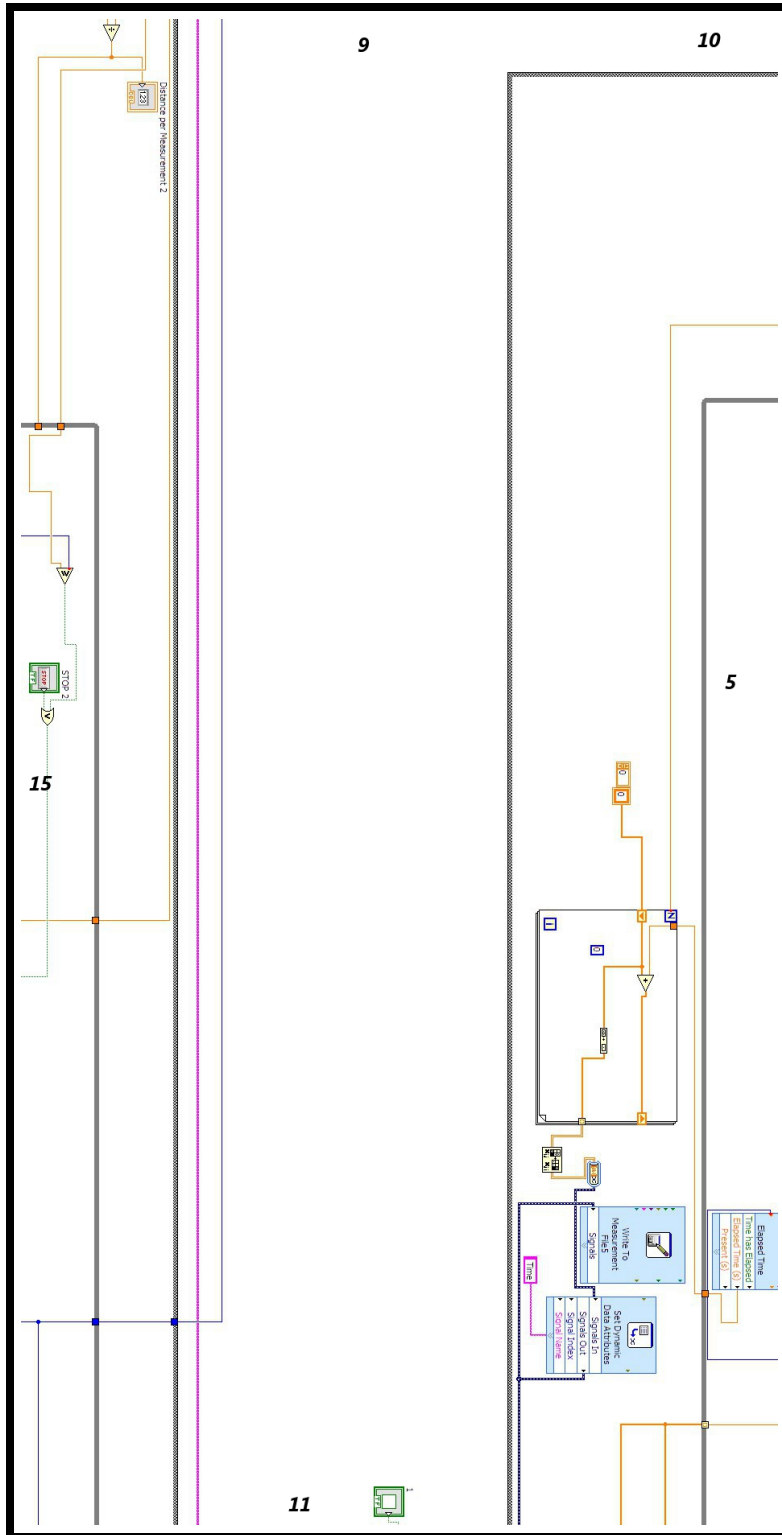


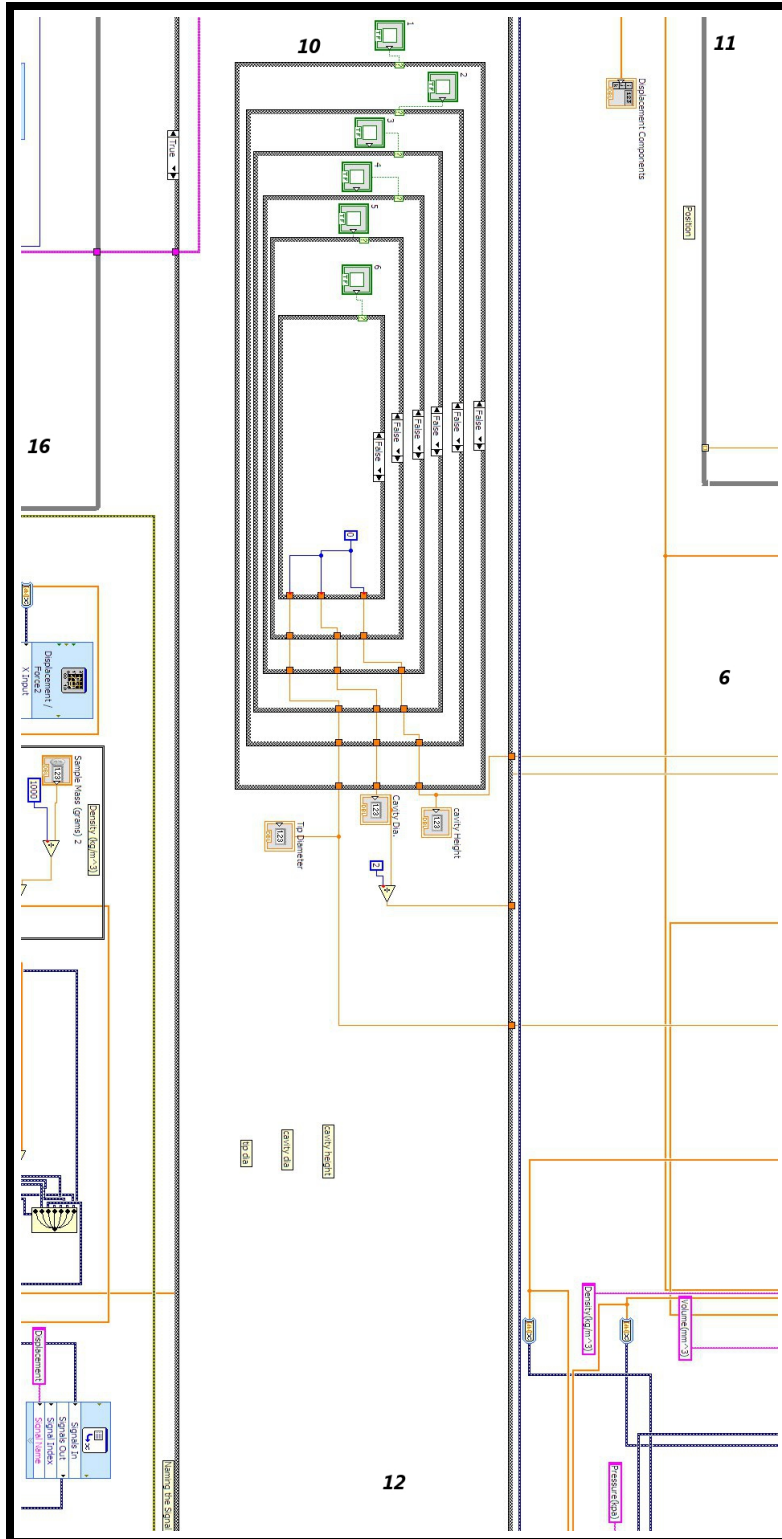


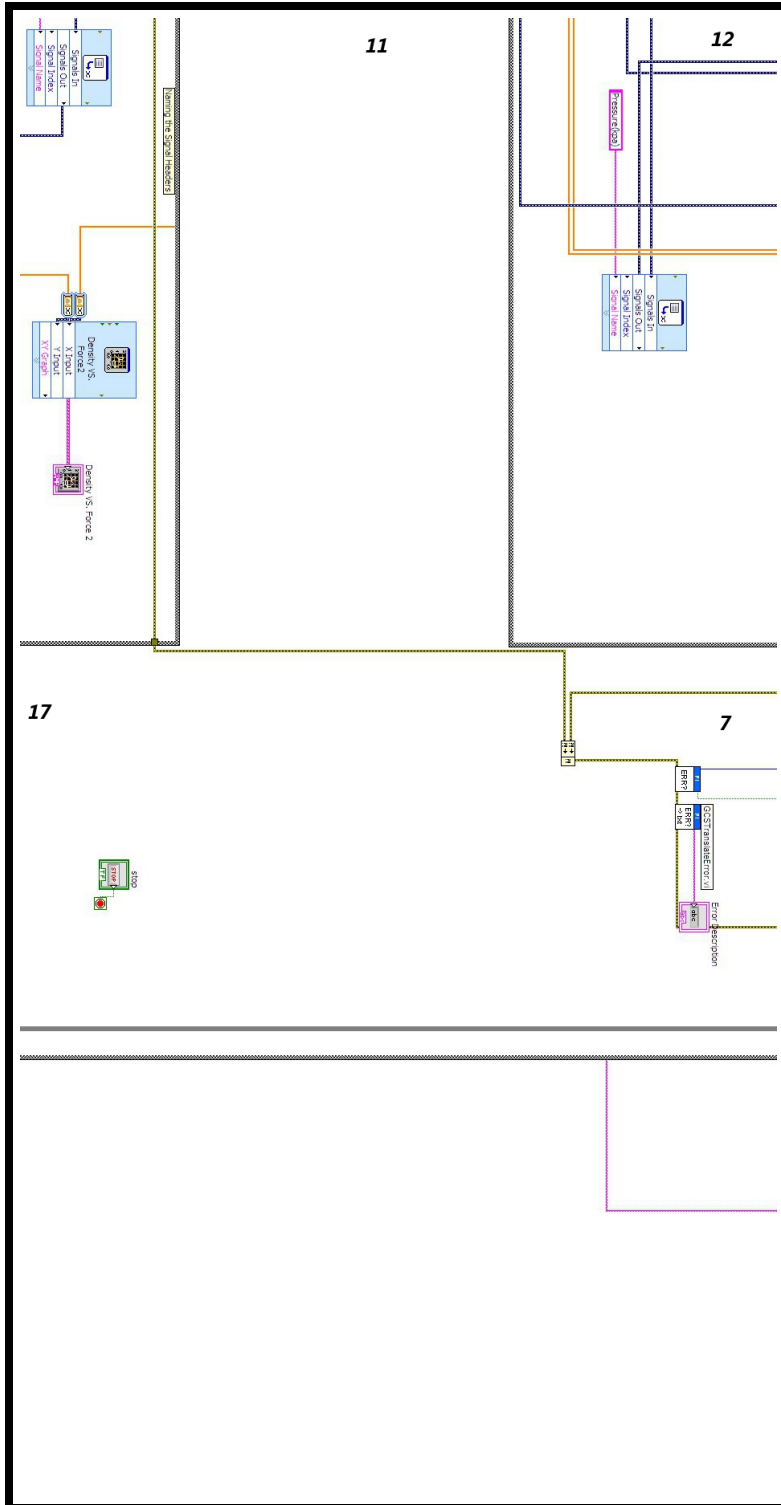




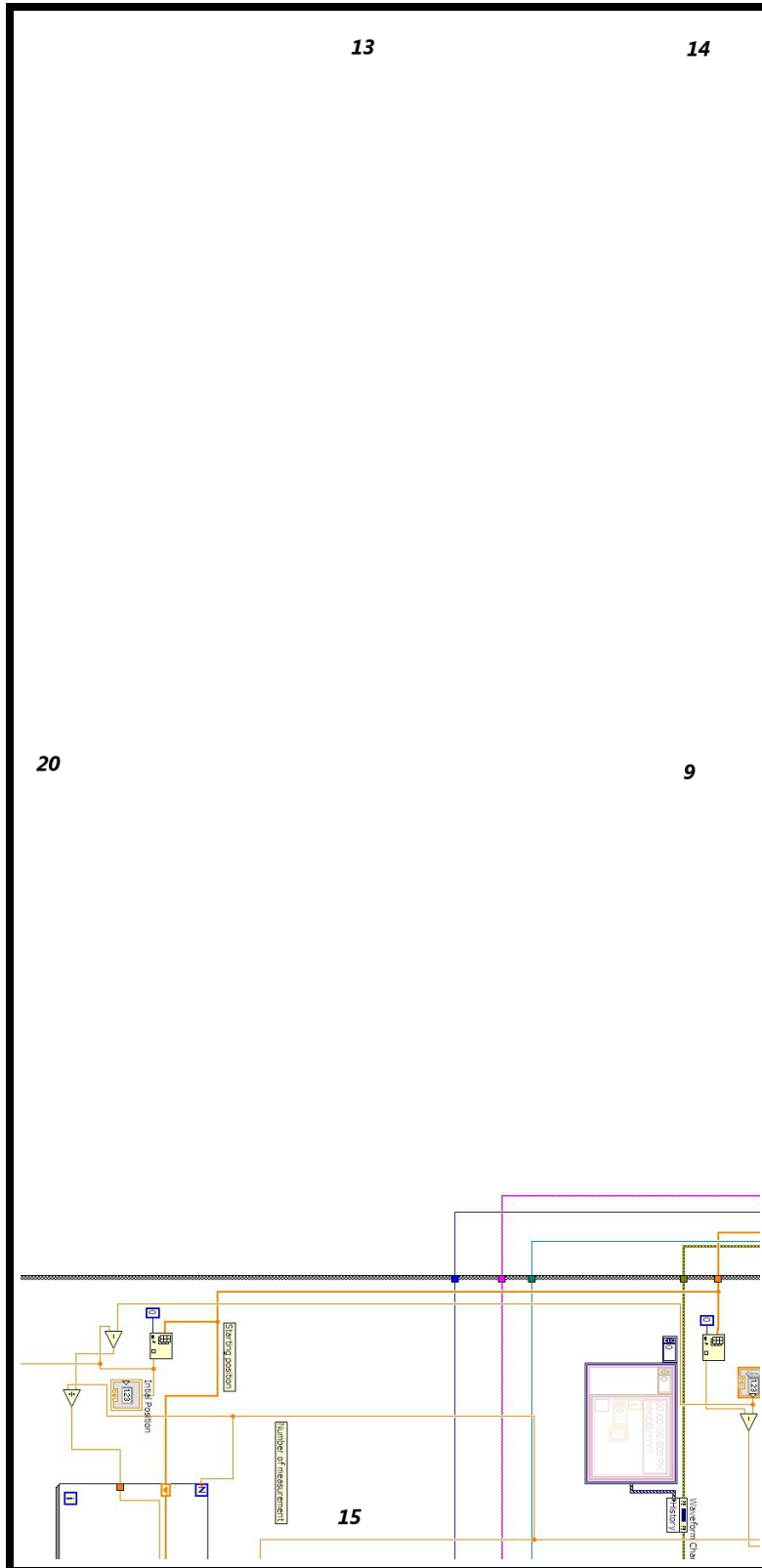


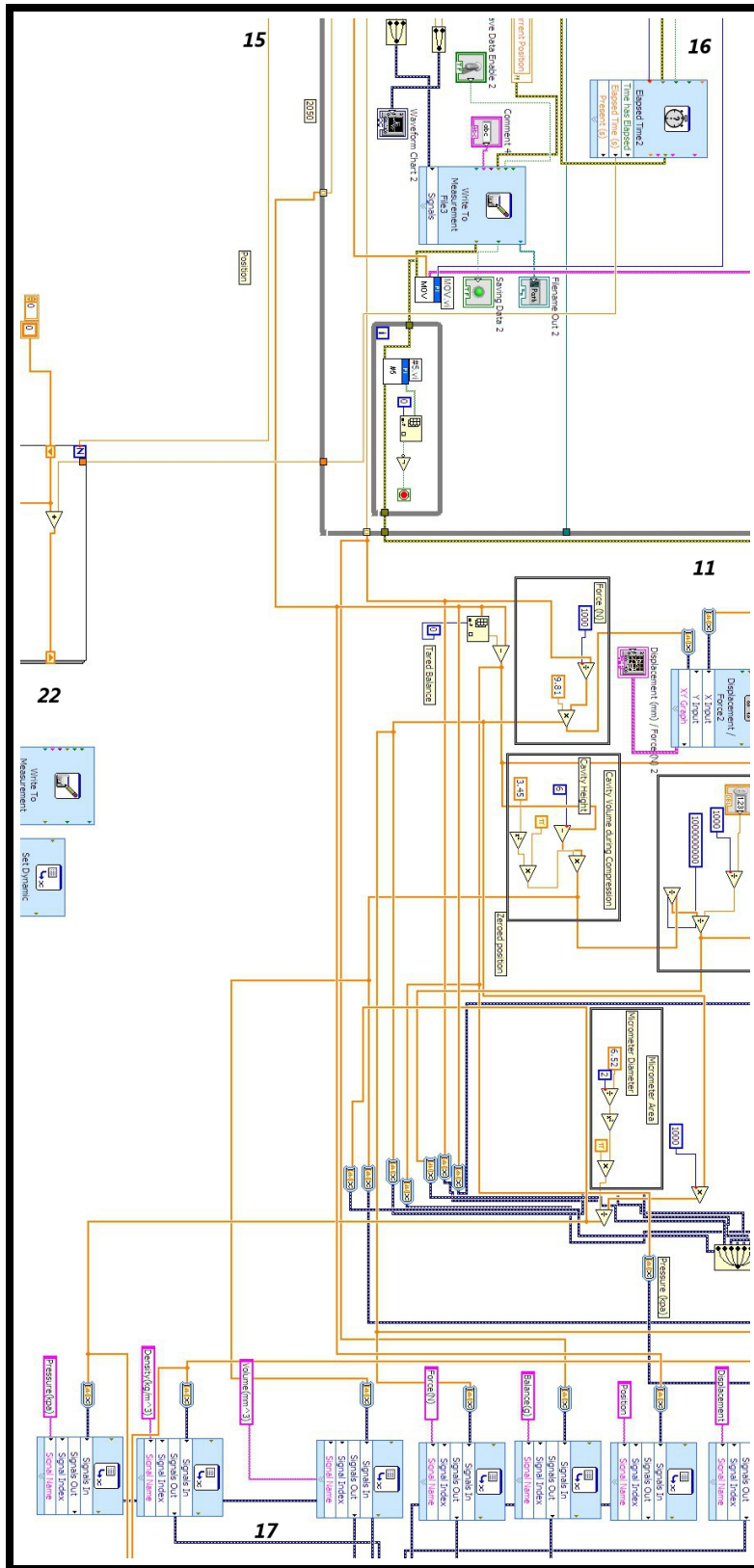






	13
18	8
<hr/> <hr/>	
	14





18

13

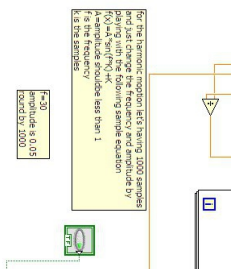
19

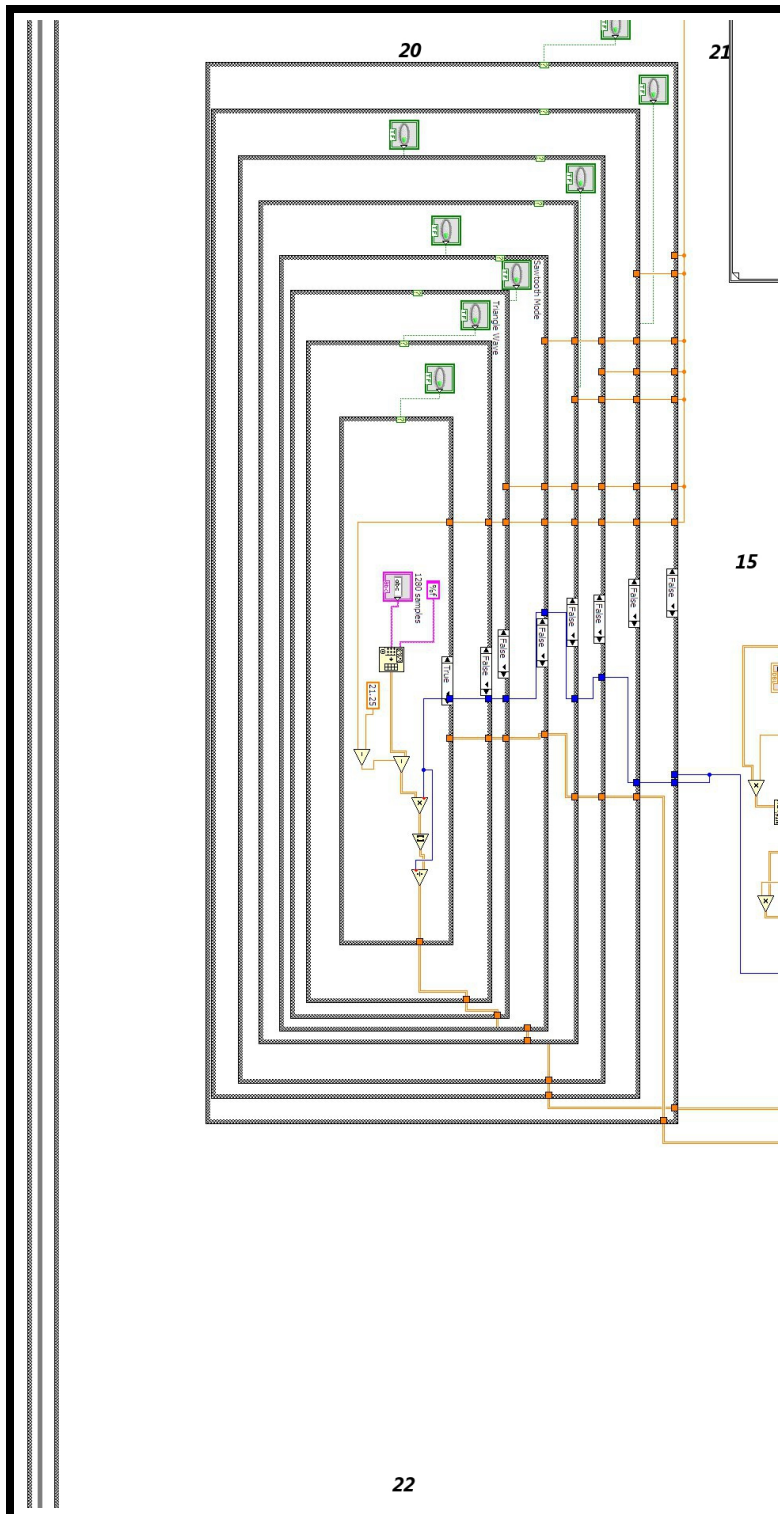
19

20

14

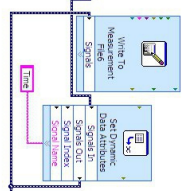
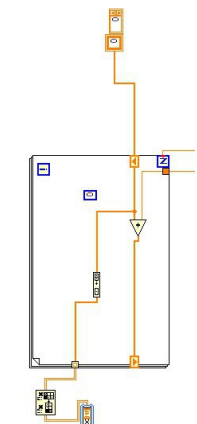
21



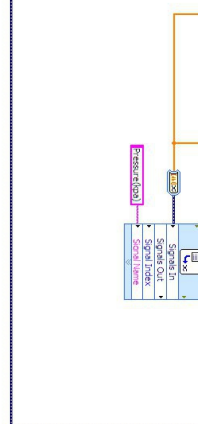


21

22



16



23

22

23

17

Appendix C

Instrument Implementation, Code Compilation and Control

C.1 Sample Preparation

Six different sample pans with different dimensions along with 10 actuator tips with different size and shape have been manufactured to evaluate the effects of friction. Cavity Number 1 is chosen to be the best cavity to be used that introduces the lowest die wall friction in to the results. Punch number 1, disk shape, should be used for that cavity. For all of the measurement it is better to keep the samples for three days in the desiccator prior to initiating the measurement. For sample preparation please follow the below steps:

1. Tare the scale (*Scale should be calibrated. For the calibration please use the instruments instruction manual*)
2. Assemble the top and bottom plates of the sample pan (i.e. put the screws in)
3. Weigh the assembled apparatus (sample pan) and record

If you need to avoid exposing the powder to the atmosphere and do the dry measurement, do the following in the dry box and make sure the relative humidity is quite low (i.e. it has been flushed for quite some time)

4. Start to add powder to the hole in the sample pan you have assembled. Be careful not to spill outside of the hole. Level off the top with the small metal spatula that has flat edges. Clean off any powder that is not in the hole, but do not disturb the powder that is in the hole. (A tiny brush can be used to clean the powders spilled outside of the hole.

5. Weigh the filled sample pan and record
6. Carefully place the sample pan on the sample pan holder on the top of the loadcell in the UAlberta Density Tester. (be noted that translation stages have been calibrated before)
7. Sample pan is ready for measurement (please proceed to the start up section to the measurement)

C.2 Cavity Position Calibration

Sample pan position on the load cell can be changed to align the cavity with the actuator in order to reduce the influence of wall friction in the system. Two Thorlab Translation stages have been diagonally placed below the load cell, attached to the load cells holder plate, and are to displace the load cell in X and Y direction using two micrometer with 25 mm displacement range. Two precision dowel pins have been designed that allow for left-right handed configuration. To calibrate the cavity position follow the below procedures.

1. Unscrew both of the lock screws from the back side of each translation stage.
2. Use micrometers to displace stages to the proper position.
3. Start up the controlling system, by pressing the run button from the LabVIEW toolbar (*Please proceed to the startup section for the code compilation procedure and follow it precisely before moving on to the next step*)
4. Move the tip of the actuator (incrementally) and near it to the cavity with having it slightly touching its horizontal edge. The changes in the load cell indicator indicates that the load cell sensor has been touched
5. Visually align the cavity with the actuators tip.
6. Try to incrementally move the tip into the cavity while you are calibrating the stages simultaneously to keep as low load on the loadcell as possible. The lower the load the better. However as you move the actuator farther down the hole it gets harder.

7. When the proper position of translation stages is determined, use the corresponding Allen/Hex key to tighten the calibrating micrometers at their own place.
8. The cavity position is now calibrated

C.3 Instrument Startup

PI M-229-26S Stepper-Mike Linear Actuator, its C-663 Stepper Motor Controller and FUTEK LRF400 load cell with its USB220 interface are connected through the USB port to the computer. For the installation procedure of these devices, use their instruction manual. SENSIT Test and Measurement, and PI MicroMove are to be installed at first.

PI software, PI MicroMove, should be used to connect the controller with which the actuator can be referenced and calibrated whenever the PC is rebooted. In order to start up the controller connection please follows these steps:

1. Run the PI MicroMove
2. From the startup controller page choose the USB tab as the connecting port
3. From the same page select the controller that is being used (C-663)
4. Click Connect button
5. From the next page (Select Connected Stages) find and select the actuator that is being connected to the controller (M-229-26S)
6. Click Assign button
7. From the next page (Start Up Axes), select the actuator from the list and click Ref. Switch
8. The above procedure will calibrate and reference the actuator and it will move the actuator to its home position which is at 12.5 mm
9. Actuator is perfectly referenced and is ready to work (this procedure is only needed to be done whenever the PC is restarted or otherwise it wont be recognized by the LabVIEWs referencing VIs)

****Futek loadcell is very sensitive to its connectors and it should be treated gently, (Please and Thank you!)**

*****Forgetting/skipping any of the following steps will result in 4-6 weeks delay while it is gone to be recalibrated by the supplier company. Please carefully follow the below steps:**

1. Connect the USB220 to the front USB port of the PC
2. Run the SENSIT Test and Measurement 2.2
3. Click on Trial version
4. Click OK
5. On the next page, you see device number 1 with its serial number, 463751, is connected. Click Load.
6. From the next page you can see the real time reading from the loadcell and the unit should be shown only in lb. (Although it can be changed to kg, g and), Which means that the device is already calibrated and is ready to use*. If the unit is not shown in lb. and is in V/mV , please follow the steps stated in the troubleshooting section.
7. Now close the program by clicking on the exit button from the file tab.
8. Loadcell is now ready to be used and called by the LabVIEW program

C.4 Troubleshooting and Important Remarks

- **DO NOT OPEN THE LABVIEW CODE BEFORE CALIBRATING THE INSTRUMENTS**
- **ALWAYS USE USB SAFETY REMOVE SOFTWARE TO DISCONNECT THE USB PORTS FROM THE SYSTEM OR OTHERWISE THE LOAD CELL WILL LOSE ITS CALIBRATION DATA**
- **AFTER THE EXPERIMENT, STOP AND EXIT THE PROGRAM, CLOSE THE LABVIEW SOFTWARE AND SAFELY REMOVE THE USBS USING THE USB SAFELY REMOVE SOFTWARE. DISCONNECT THE USB220 FROM THE PC WHEN ITS CONNECTION LIGHT TURNED OFF**

- FUTEK LOADCELL IS VERY SENSITIVE TO ITS CONNECTORS AND IT SHOULD BE TREATED GENTLY
- IN THE CASE OF ANY INTERRUPTION OF ANY KIND, POWER OUTAGE OR HAVING ANY ERROR LIGHTS IN THE CODE ILLUMINATED, THE ENTIRE PROGRAM SHOULD BE CLOSED AND INITIATED AGAIN BY FOLLOWING PROCEDURES STATED IN THE CALIBRATION STAGE. THIS TYPE OF ERROR HANDLING FALLS WITHIN GENTLY TREATING THE INSTRUMENTS

C.4.1 Restoring Loadcell Calibration Data

If in any case, load cell showed the units in V/mV or it cannot be recognized by the SENSIT software, it means that it lost its calibration and should be recalibrated again. Base on the type of the error occurs in the load cell library, it may/may not clear the main memory. In which case un-uniformed reading will be shown that is not correlated to the Load cell at use. The calibration points may be lost or corrupted. Calibration data can be restored depends on how much of it has been wiped out. To restore the calibration data Restore Backup Utility software can be used. To restore the data follow the steps below:

1. Connect the USB220
2. Run Restore Backup Utility
3. Enter the serial number in the appropriate box
4. Put number 2 for the page number *(DO NOT RESTORE FROM PAGE 1 AS IT FORMATS THE CALIBRATION HISTORY)
5. Select Restore Backup and confirm
6. Put number 3 for the page number this time *(DO NOT RESTORE FROM PAGE 1 AS IT FORMATS THE CALIBRATION HISTORY)
7. Select Restore Backup and Confirm
8. Disconnect the USB220 using USB Safety Remove** (Important)
9. Connect it back again and run SENSIT Test and Measurement software

10. Check to see if the unit is shown in lb. this time or not
11. If not, do the same thing again.
12. If the problem still occurs, youre done !!!, pack it and send it to the company for recalibration (please contact; Alex Friedman, Tel: (416) 617-0918, email: sales@a-kast.ca , Futek Representative, for calibration)

C.5 Code Compilation

PI_motor3.vi is used to control the setup and acquire measurement data. In addition to the linearly moving the actuator, the code was built in a way to be able to move the actuator with different modes. Harmonic, Step mode, Triangle wave mode and Saw tooth wave mode. Before initiating the code, please make sure the instruments are connected and calibrated.

*****AFTER THE EXPERIMENT, STOP AND EXIT THE PROGRAM, CLOSE THE LABVIEW SOFTWARE AND SAFELY REMOVE THE USBS USING THE USB SAFETY REMOVE SOFTWARE. DISCONNECT THE USB220 FROM THE PC WHEN ITS BLUE LIGHT TURNED OFF*****

C.5.1 Compressed Bulk Density Measurement

For CBD density measurement please use the top part of the front panel

1. Open the PI_motor3.vi
2. Run the code by pressing the arrow shape button on the main toolbar
3. Press the run button.
4. Few seconds after pressing the run button, *Initiation light* at the top of the page is illuminated and load cell starts to show the read time weight on it
5. Place the filled sample pan in the sample pan holder on the top of the load cell
6. Please enter the mass (in grams) of the into the designated place Sample Mass (grams)

7. Put the value of 4000 in the Max Tared Pressure, meaning the highest pressure beyond which loadcell stops working. *(it is the safety button to donot allow the pressure on the loadcell to exceed its real capacity i.e. 4535 g)
8. Go to the second part of the code, lower panel, and select the cavity # corresponding to the cavity number you are using (Number 1 is the common one)
9. By selecting the cavity # buttons, cavity height, cavity diameter and the tip diameter is shown
10. Use the cavity height to put the proper number for the End Position, (as not to let the actuator move more than what is needed and not to let the loadcell capacity being exceeded, it is to be 23.75 for cavity #1)
11. Set the number of measurement which 500 would be enough for CBD measurement
12. Bring the actuator tip near cavity and visually align it with the horizontal edge of the cavity (for the cavity #1, the micrometer zeroed position is 18.75)
13. Set the velocity (use 0.25 or 0.2 mm/s for density measurement)
14. Tare the loadcell (although it keeps changing)
15. Press the Big Red Button, Scan CBD/Linear Compression, to start the measurement
16. The measurement will be done when the pressure exceeds the Max Tared Pressed that has been set at the start or the set number of measurement has been reached.
17. Youll be asked to select the destination to save the recorded file. (note pad file with "lvm" format) (this will happen every time you stop the code and rerun it again, otherwise continuous measurement will be over-written to the same file, that can also be categorized by writing a comment in comment empty bar)
18. Plots will be graphed automatically

19. Measurement is done and you can stop the code by pressing STOP and exit button

C.6 Actuator's Harmonic Advancement, Modulated Compaction Profile

For producing modulated profiles, second part (lower section) of the front panel should be used. And button for every section to be compiled should be pressed before pressing the main executing button, Scan Harmonic.

C.6.1 Sawtooth Mode

In this mode the measurement data point are not consistent, (i.e. there are only data two points at the top and bottom of each cycle when it is on its abating region.

1. Open the PI_motor3.vi
2. Run the code by pressing the arrow shape button on the main toolbar
3. Press the run button.
4. Few seconds after pressing the run button, Initiation light at the top of the page is illuminated and ;oadcell starts to show the read time weight on it
5. Place the filled sample pan in the sample pan holder on the top of the loadcell
6. Please enter the mass (in grams) of the into the designated place Sample Mass (grams) 2
7. Put the value of 4000 in the Max Tared Pressure 2, meaning the highest pressure beyond which loadcell stops working. *(it is the safety button to donot allow the pressure on the loadcell to exceed its real capacity i.e. 4535 g)
8. Go to the second part of the code, lower panel, and select the cavity # corresponding to the cavity number you are using (Number 1 is the common one)

9. By selecting the cavity # buttons, cavity height, cavity diameter and the tip diameter is shown
10. Use the cavity height to put the proper number for the End Position 2, (as not to let the actuator move more than what is needed and not to let the loadcell capacity being exceeded, it is to be 23.75 for cavity #1)
11. Set number of measurement, it is preferred for the saw tooth movement to have 350 number of measurement
12. Both period and amplitude can be set (50 for both would be the value of preference for this mode)
13. Bring the actuator tip near cavity by pressing the Move button and visually align it with the horizontal edge of the cavity (for the cavity #1, the micrometer zeroed position is 18.75)
14. Set the velocity (use 0.25 or 0.2 mm/s for density measurement)
15. Tare the loadcell (although it keeps changing)
16. Push the Sawtooth Mode button
17. Press the Big Red Button, Scan Harmonic, to start the measurement
18. The measurement will be done when the pressure exceeds the Max Tared Pressed that has been set at the start or the set number of measurement has been reached.
19. Youll be asked to select the destination to save the recorded file. (note pad file with lvm format) (this will happen every time you stop the code and rerun it again, otherwise continues measurement will be overwritten to the same file, that can also be categorized by writing a comment in comment empty bar)
20. Plots will be graphed automatically
21. Measurement is done and you can stop the code by pressing STOP and exit button in the upper part of the front panel

C.6.2 Triangle Wave Mode

In this mode the measurement data points are consistent meaning the same number of data points will be set on any region of the cycle.

1. Open the PI_motor3.vi
2. Run the code by pressing the arrow shape button on the main toolbar
3. Press the run button.
4. Few seconds after pressing the run button, Initiation light at the top of the page is illuminated and loadcell starts to show the read time weight on it
5. Place the filled sample pan in the sample pan holder on the top of the loadcell
6. Please enter the mass (in grams) of the into the designated place Sample Mass (grams) 2
7. Put the value of 4000 in the Max Tared Pressure 2, meaning the highest pressure beyond which loadcell stops working. *(it is the safety button to donot allow the pressure on the loadcell to exceed its real capacity i.e. 4535 g)
8. Go to the second part of the code, lower panel, and select the cavity # corresponding to the cavity number you are using (Number 1 is the common one)
9. By selecting the cavity # buttons, cavity height, cavity diameter and the tip diameter is shown
10. Use the cavity height to put the proper number for the End Position 2, (as not to let the actuator move more than what is needed and not to let the loadcell capacity being exceeded, it is to be 23.75 for cavity #1)
11. Set number of measurement, it is preferred for the Triangle wave movement to have 4000 number of measurements
12. Both period and amplitude should be set *(Period should always be an even number otherwise a fuzzy graph will be generated, period 40 and amplitude 80 would be good values to have enough number of cycles,

if period and amplitude have the same number, the step mode will be formed)

13. Bring the actuator tip near cavity by pressing the Move button and visually align it with the horizontal edge of the cavity (for the cavity #1, the micrometer zeroed position is 18.75)
14. Set the velocity (use 0.25 or 0.2 mm/s for density measurement)
15. Tare the loadcell (although it keeps changing)
16. Push the Triangle Wave Mode button
17. Press the Big Red Button, Scan Harmonic, to start the measurement
18. The measurement will be done when the pressure exceeds the Max Tared Pressed that has been set at the start or the set number of measurement has been reached.
19. Youll be asked to select the destination to save the recorded file. (note pad file with lvm format) (this will happen every time you stop the code and rerun it again, otherwise continues measurement will be overwritten to the same file, that can also be categorized by writing a comment in comment empty bar)
20. Plots will be graphed automatically
21. Measurement is done and you can stop the code by pressing STOP and exit button in the upper part of the front panel

C.6.3 Sinusoidal Mode

1. Open the PI_motor3.vi
2. Run the code by pressing the arrow shape button on the main toolbar
3. Press the run button.
4. Few seconds after pressing the run button, Initiation light at the top of the page is illuminated and loadcell starts to show the read time weight on it
5. Place the filled sample pan in the sample pan holder on the top of the loadcell

6. Please enter the mass (in grams) of the into the designated place Sample Mass (grams) 2
7. Put the value of 4000 in the Max Tared Pressure 2, meaning the highest pressure beyond which loadcell stops working. *(it is the safety button to donot allow the pressure on the loadcell to exceed its real capacity i.e. 4535 g)
8. Go to the second part of the code, lower panel, and select the cavity # corresponding to the cavity number you are using (Number 1 is the common one)
9. By selecting the cavity # buttons, cavity height, cavity diameter and the tip diameter is shown
10. Use the cavity height to put the proper number for the End Position 2, (as not to let the actuator move more than what is needed and not to let the loadcell capacity being exceeded, it is to be 23.75 for cavity #1)
11. Set number of measurement, it is preferred for the Triangle wave movement to have 4000 number of measurements
12. Both frequency and amplitude should be set *(frequency 30 and amplitude 0.05 would be good values to have enough number of cycles)
13. Bring the actuator tip near cavity by pressing the Move button and visually align it with the horizontal edge of the cavity (for the cavity #1, the micrometer zeroed position is 18.75)
14. Set the velocity (use 0.25 or 0.2 mm/s for density measurement)
15. Tare the loadcell (although it keeps changing)
16. Press the Big Red Button, Scan Harmonic, to start the measurement
17. The measurement will be done when the pressure exceeds the Max Tared Pressed that has been set at the start or the set number of measurement has been reached.
18. Youll be asked to select the destination to save the recorded file. (note pad file with lvm format) (this will happen every time you stop the code and rerun it again, otherwise continues measurement will be overwritten

to the same file, that can also be categorized by writing a comment in comment empty bar)

19. Plots will be graphed automatically
20. Measurement is done and you can stop the code by pressing STOP and exit button in the upper part of the front panel

C.6.4 Step Mode

Six different types of step like wave have been used to fulfill the need for step like movement of the actuator. For each of them, number of samples per measurement which should be set on the proper place is written on the top of each column. To select either of the columns, push button placed on the top of each column should be pressed. The shape of the plot is somewhat prescribed by the numbers written below each column. e.g. for the first column, 125 up, 100 flat and (0.002) means; 125 points for rise up, 100 points for the width of the pulse and 0.002 is the length of each data point.

C.7 Assembling and Disassembling

The apparatus may need to be disassembled for different purposes such as cleaning, maintenance or taking the loadcell apart in order to send it to the company for recalibration. In order to disassemble the setup, follow the steps below;

1. Disconnect the cables and wires from the computer, electric outlets and loadcell
2. Disassemble the top door using two pins
3. Release the spring lock that are holding the actuator holder and bring it up while it is still placed in it. (actuator can be released from its holder by loosening the small screw from around the actuator)
4. Take the sample pan from its holder
5. Open the single screw connecting the sample pan holder to the loadcell sensor (gently)
6. Open the four screws connecting the loadcell to it holder

7. Remove the loadcell and open three screw located under it
8. Stages can be removed by opening their screws

DO NOT OPEN THE LABVIEW CODE BEFORE CALIBRATING THE INSTRUMENTS

ALWAYS USE USB SAFETY REMOVE SOFTWARE TO DISCONNECT THE USB PORTS FROM THE SYSTEM OR OTHERWISE THE LOAD CELL LOSES ITS CALIBRATION DATA

****AFTER THE EXPERIMENT, STOP AND EXIT THE PROGRAM, CLOSE THE LABVIEW SOFTWARE AND SAFELY REMOVE THE USBS USING THE USB SAFETY REMOVE SOFTWARE. DISCONNECT THE USB220 FROM THE PC WHEN ITS BLUE LIGHT TURNED OFF****

Appendix D

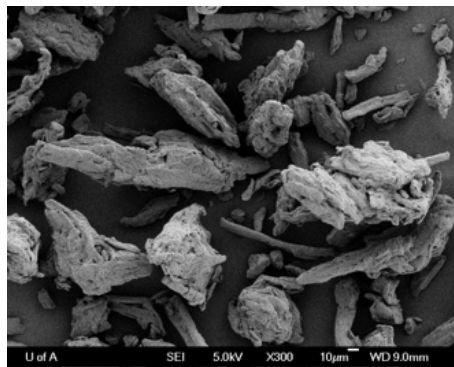
List of the Compression Models

Model's Name , [Sonnergaard, 2001], [Weiler et al., 2010, Walker, 1923], [Kawakita and Lüdde, 1971]	Equation
Balshin	$\ln F = -c_1\left(\frac{V}{V_\infty}\right) + c_2$
Smith	$\frac{1}{V} = \frac{1}{V_0} = c_3 P^{\frac{1}{3}}$
Murray	$\ln\left(\frac{V}{V-V_\infty}\right) = c_4\left(\frac{V_\infty}{V-V_\infty}\right)^{\frac{1}{3}} - c_5 P$
BallHausen	$\ln\left(\frac{V_\infty}{V-V_\infty}\right) = c_6 P + \ln c_7$
Konopicky	$\ln\left(\frac{V}{V_0-V_\infty}\right) = c_8 P + \ln\left(\frac{V_0}{V_0-V_\infty}\right)$
Jones	$\ln P = -c_9\left(\frac{V}{V_\infty}\right)^2 + C_{10}$
Athy	$\frac{V-V_\infty}{V} = \frac{V_0-V_\infty}{V_0} e^{-c_{11} P}$
Nutting	$\ln\left(\frac{V_0}{V}\right) = c_{12} P^{c_{13}}$
Tanimoto	$\frac{V_0-V}{V_0} = \frac{c_{14} P}{V_0} + \frac{c_{16} P}{P+c_{15}}$
Terzaghi	$\frac{V-V_\infty}{V_\infty} = -c_{17} \ln(P + c_{18}) - c_{19}(P + c_{20}) - c_{21} P + c_{22}$
Cooper	$\frac{V_0-V}{V_0-V_\infty} = c_{23} e^{-\frac{c_{24}}{P}} + c_{25} e^{-\frac{c_{26}}{P}}$
Gurnham, [Zhao et al., 2006]	$P = c_{27} e^{\frac{c_{28}}{V}}$
Nishihara	$\ln\left(\frac{V_0}{V}\right) = -\left(\frac{P}{c_{29}}\right)^{\frac{1}{c_{30}}}$
Tsuwa	$\frac{V_0-V}{V_0} = \frac{V_0-V_\infty}{V_0} \cdot \frac{\left(\frac{1}{c_{31}}\right)^P}{1+\left(\frac{1}{c_{32}}\right)^P}$
Kawakita	$\frac{V_0-V}{V_0} = \frac{c_{32} c_{33} P}{1+c_{33} P}$
Sonnergaard(log-exp)	$V = V_1 - w \log(P) + V_P e^{-\frac{P}{P_m}}$
Shapiro	$\ln E = \ln E_0 - c_{34} P - c_{35} P^{0.5}$
Walker	$V = c_{36} - c_{37} \ln P$

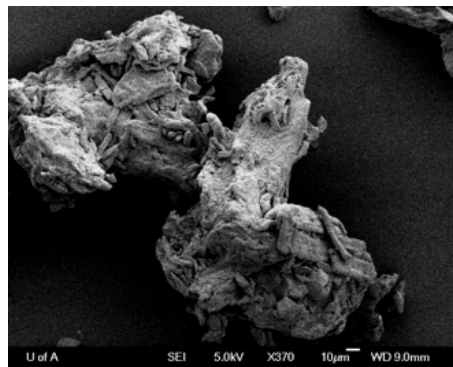
Table D.1: Various equations describing the compaction of powders, V_0 =initial apparent volume of powder, V = volume of powder under the applied pressure P , V_∞ =net volume of powder, $c_1 \dots c_{37}$ = constants, E_0 =initial porosity, P_m = mean pressure, V_1 = pressure at 1 MPa

Appendix E

Scanning Electron Microscopy (SEM) Images

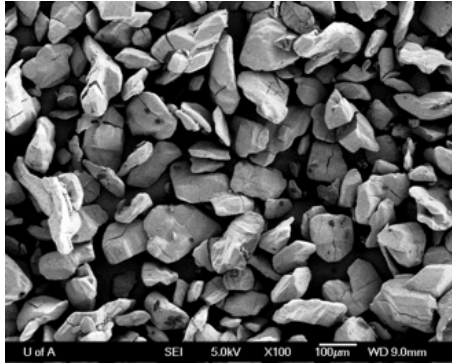


(a) Before the Compaction

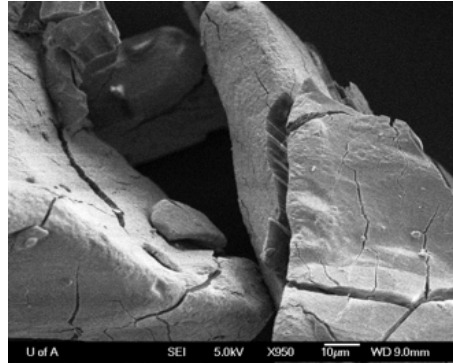


(b) After the Compaction

Figure E.1: SEM images of Microcrystalline Cellulose

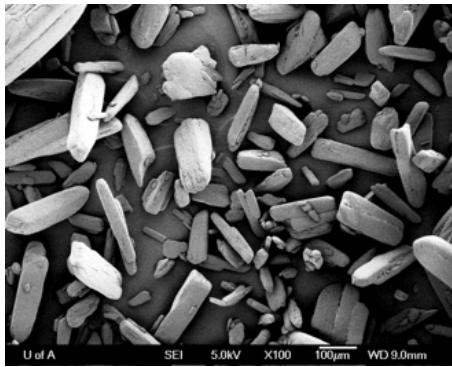


(a) After the Compaction

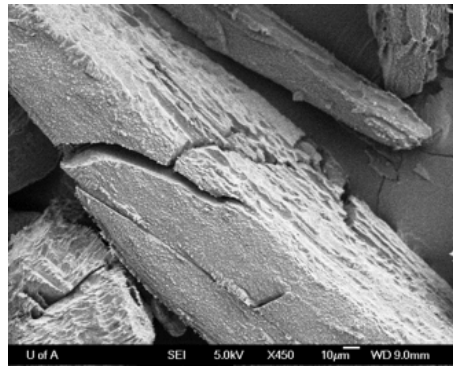


(b) After the Compaction

Figure E.2: SEM images of Dextromethorphan

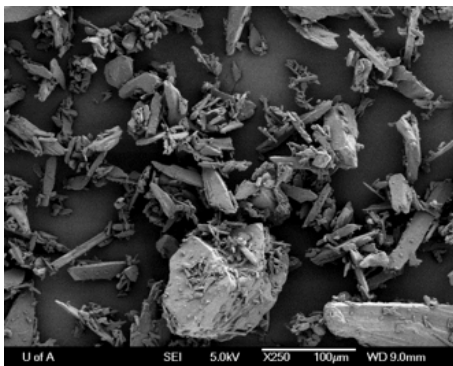


(a) After the Compaction

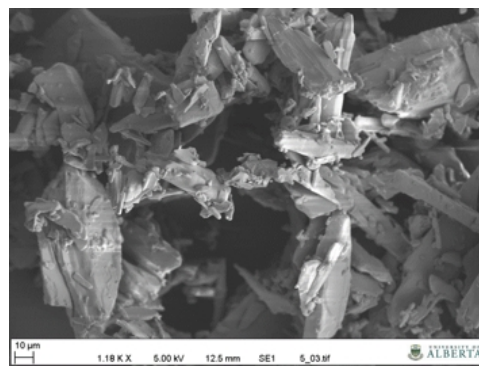


(b) After the Compaction

Figure E.3: SEM images of Ibuprofen



(a) After the Compaction

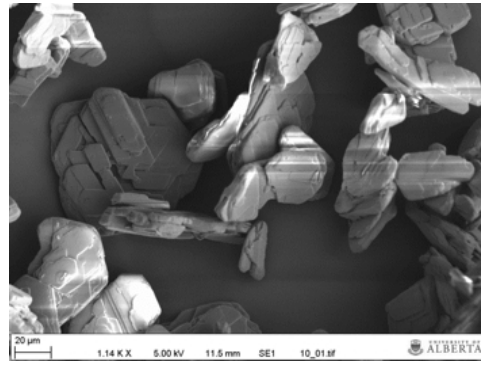


(b) After the Compaction

Figure E.4: SEM images of Micronized Paracetamol

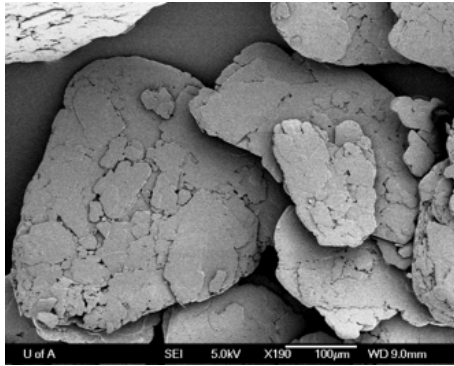


(a) After the Compaction

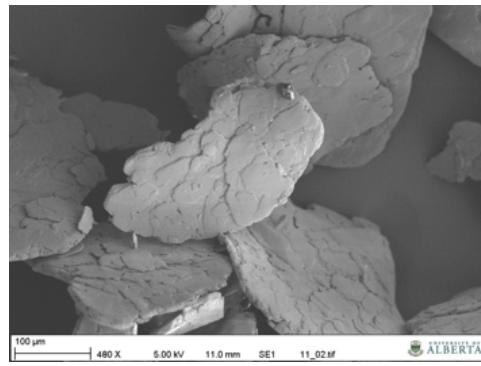


(b) After the Compaction

Figure E.5: SEM images of Crystalline Leucine

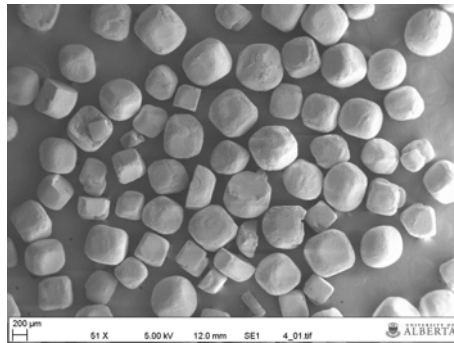


(a) After the Compaction

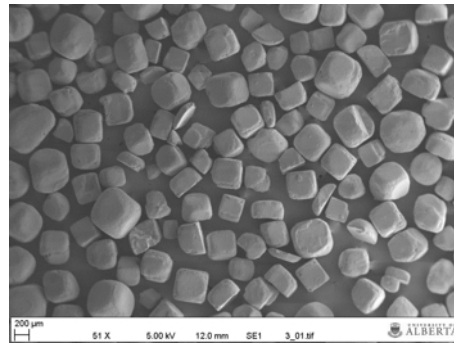


(b) After the Compaction

Figure E.6: SEM images of Crystalline Flowable Leucine

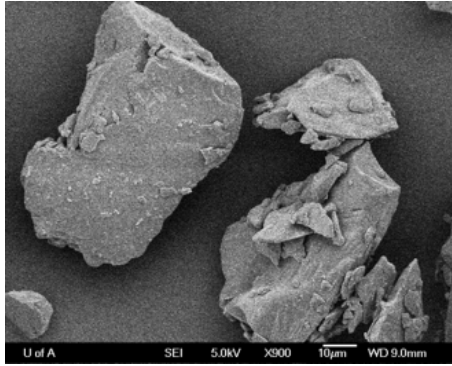


(a) After the Compaction

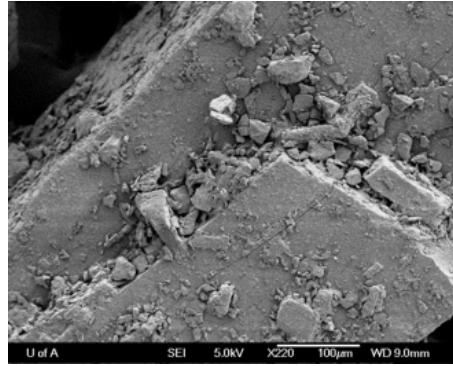


(b) After the Compaction

Figure E.7: SEM images of NaCl

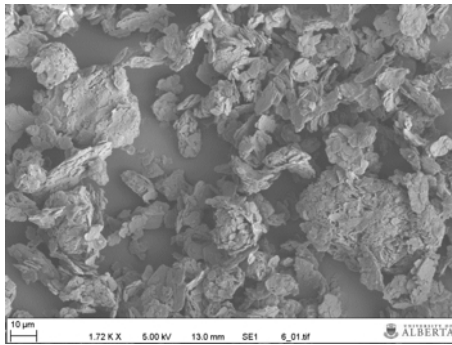


(a) After the Compaction

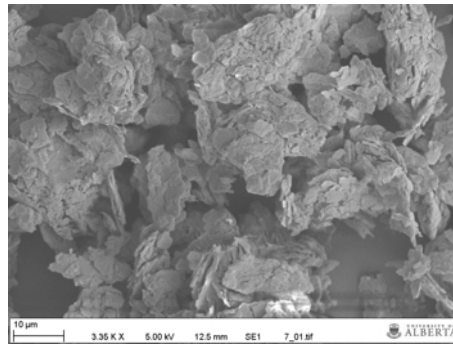


(b) After the Compaction

Figure E.8: SEM images of Crystalline Trehalose

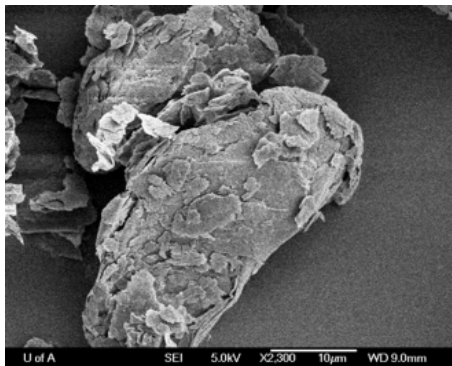


(a) After the Compaction

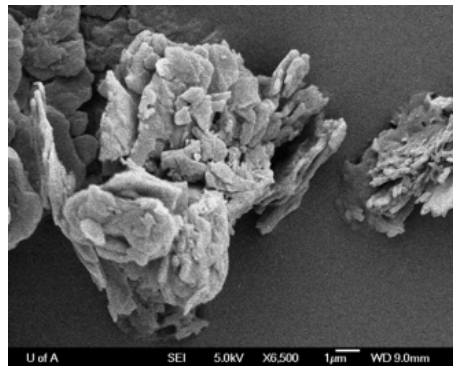


(b) After the Compaction

Figure E.9: SEM images of Magnesium Stearate

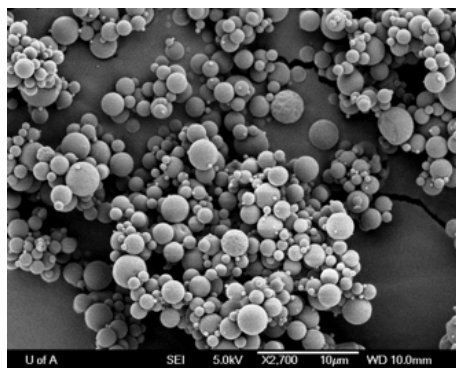


(a) After the Compaction

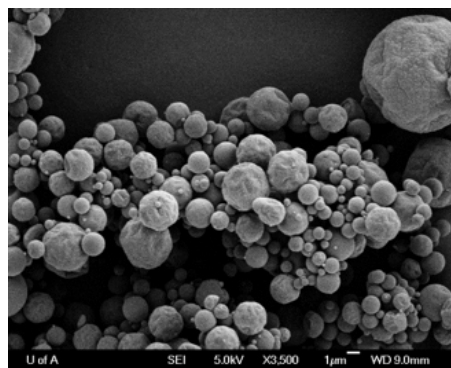


(b) After the Compaction

Figure E.10: SEM images of Talc



(a) After the Compaction



(b) After the Compaction

Figure E.11: SEM images of Spray Dried L-leucine/Trehalose